Characterisation of the glioblastoma perivascular niche and the role of DOCK4 in blood vessels and tumour invasion

Teklu Feyissa Egnuni

Submitted in accordance with the requirements for the degree of Doctor of Philosophy (PhD)

Leeds Institute of Medical Research at St James's Campus
School of Medicine
The University of Leeds

May 2019

The candidate confirms that appropriate credit has been given within the thesis where reference has been made to the work of others.

I dedicate this piece of work to my beloved late mother Ayelech Gedefa whom I painfully lost to cancer and those who are dearly affected by this challenging problem in our modern time.

Acknowledgments

First and foremost, as a Christian, I would really like to express my gratitude to God for helping me to materialise my goals. I believe that this could not have happened without His help and the sincere faith and trust I have in Him. The contribution of my family to successful completion of my study has been immense. When I was down you encouraged me, when I became busy and kept your time to myself you understood me. My beautiful wife Netsanet Ali and my lovely daughters Hamerti, Katie and Becky, I would like to simply say thank you and I love you, as there are no better words to reciprocate your love, patience and support.

I would like to sincerely thank my supervisors Dr Georgia Mavria and Prof Susan Short. Dr Mavria, you are an amazing supervisor, colleague and close friend. I have learned a lot working with you over the past three years and I hope that our collaboration will continue in the future. Your continuous advice, discussions and suggestions encouraged me to achieve the maximum threshold of the learning curve. Likewise, the encouragement, guidance and comments received from Prof Susan Short over the course of this study were paramount. From the beginning you showed me direction, advised me to take this PhD opportunity and supported me whenever I needed your help. I would like to sincerely thank you both for your continuous encouragement and support.

Furthermore, I would like to say thank you to all colleagues who contributed to this work directly or indirectly. In particular, Professor Valerie Speirs, Dr Aruna Chakrabarty, Mike Shires, Ruth Morton, Anke Bruning-Richardson, Filomena Esteves, Gary Shaw and all current and past members of Dr Mavria's and Prof Short's group whose input and support have been invaluable. Finally, it is my pleasure to acknowledge the Frank Stell scheme for offering me this scholarship and the opportunity to carry out a PhD.

Abstract

Blood vessels play a vital role in cancer development and progression as tumours cannot grow beyond a small diameter in their absence. Blood vessels are abundant and intrinsically abnormal in glioblastoma multiforme (GBM), while current antiangiogenic therapies are disappointing as these tumours are either unresponsive or gradually develop resistance. Hence, characterisation of aberrant blood vessels in primary and recurrent GBM, and following radiotherapy could open new therapeutic avenues for GBM in the future. This study identified different blood vessel morphologies in patient-derived glioblastoma samples. Patients presented with varying degrees of blood vessel abnormality which increased in recurrent tumours following surgery, radiotherapy and chemotherapy. High nestin positivity and large lumen size were key characteristics, particularly in recurrent tumours. Nestin positive cells were closely associated with the blood vessel endothelial lining but distinct to CD31 positive endothelial cells. Nestin positive cells were negative for the glioblastoma stem-like cell (GSC) markers OLIG2 and SOX2, and astrocyte or immune cell markers, but positive for the pericyte marker PDGFRβ and smooth muscle cell (SMC) marker alpha smooth muscle actin (α-SMA), suggesting they are distinct from GSCs. Nestin and SMA positive blood vessels were found in close proximity to tumour necrotic regions, but were associated with low hypoxia levels suggesting functionality.

The effects of radiotherapy on blood vessel abundance, morphology and function are poorly characterised, as are the molecular mechanisms of glioblastoma blood vessel formation. DOCK4 is a guanine nucleotide exchange factor (GEF) for the small GTPase Rac1, which is highly expressed in neuronal and endothelial cells, and regulates cellular protrusions, cell migration and blood vessel lumen size. Irradiation experiments were performed using the CT2A model of glioblastoma grown intracranially in syngeneic mice. While a decrease in vascularisation and lumen size were observed early after irradiation, the abundance and size of lumenised blood vessels increased at later stages. Using Dock4 heterozygous knockout mice to overcome early embryonic lethality of homozygous Dock4 deletion, it was shown that reduction of DOCK4 levels reverses the increase in blood vessel size in response to irradiation, however without observed concurrent changes in tumour growth, or survival.

Invasion of cells into the normal brain parenchyma limits the efficacy of surgery and radiotherapy thus contributing to recurrence and poor prognosis of glioblastoma. Glioblastoma invasion is known to take place along white matter tracts and alongside blood vessels. The role of DOCK4 in glioblastoma invasion was investigated in spheroid assays in collagen, using both established glioblastoma cell lines and patient-derived glioblastoma stem-like cells (GSCs). Lentiviral shRNA-mediated knockdown of

DOCK4 reduced invasion into the surrounding matrix in spheroid assays. However, DOCK4 knockdown did not alter invasive capacity when glioblastoma cells were co-cultured with endothelial cells. On the other hand, co-culture with endothelial cells increased the sensitivity of some glioblastoma cell lines to irradiation.

In summary, this study shows that aberrant pericyte/SMC blood vessel coverage and larger blood vessel size are prevalent in GBM and increase with recurrence. These aberrant blood vessels appear functional and may play an important role in glioblastoma resistance to chemo- and radioradiotherapy, and facilitate tumour recurrence. Radiotherapy promotes aberrant blood vessel morphology and size in experimental tumours. DOCK4 inhibition may normalise the glioblastoma vasculature, and concomitantly inhibit invasion of a subpopulation of glioblastoma cancer stem cells.

Table of contents

List of Figures

List of Abbreviations

ANG-1	Angiopoietin -1
BBB	Blood brain barrier
bFGF	Basic fibroblast growth factor
BM	Basement membrane
CD31	Cluster of differentiation 31 (PECAM-1)
CD45	Cluster of differentiation 45
CD68	Cluster of differentiation 68
CNS	Central Nervous System
CSCs	Cancer stem cells
Cx43	Connexin 43
CXCR4	C-X-C Motif Chemokine Receptor 4
DMEM	Dulbecco's Modified Eagle's Medium
DNA	Deoxyribonucleic acid
DOCK4	Dedicator of cytokinesis 4 (Protein)
EC	Endothelial cell
ECM	Extracellular matrix
EGF	Epidermal growth factor
EGFR	Epidermal growth factor receptor
EMT	Epithelial-Mesenchymal Transition
EPC	Endothelial progenitor cells
FFPE	Formalin fixed, paraffin embedded
GBM	Glioblastoma multiforme
GDP	Guanosine diphosphate
GEF	Guanine nucleotide exchange factor
GAP	GTPase activating protein
GFAP	Glial fibrillary acidic protein
GFP	Green fluorescent protein
G-CSF	Granulocyte-colony stimulating factor
GSCs	Glioma stem cells
GSK3β	Glycogen synthase kinase 3β
GTP	Guanosine triphosphate
HCMECs	Human Cerebral Microvascular Endothelial Cells
HEK 293T	Human Embryonic Kidney

HIF	Hypoxia-inducible factor
HLVEC	Human Large Vessel Endothelial Cell
HPA	Human Protein Atlas
HUVEC	Human Umbilical Vein Endothelial Cells
IDH-1	Isocitrate dehydrogenase 1
IHC	Immunohistochemistry
IF	Immunofluorescence
IL-6	Interleukin 6
MGMT	O-6-methylguanine-DNA methyltransferase
MMPs	Matrix metalloproteinases
MRI	Magnetic Resonance Imaging
MVPs	Microvascular patterns
MVD	Microvascular density
NF1	Neurofibromin 1
NO	Nitric oxide
NPC	Neuronal progenitor cell
NSC	Neuronal stem cell
OLIG2	Oligodendrocyte transcription factor 2
OS	Overall survival
PBS	Phosphate-buffered saline
PDGF	Platelet-derived growth factor
PDGFRβ	Platelet-derived growth factor receptor-β
PECAM-1	Platelet Endothelial Cell Adhesion Molecule-1 (CD31)
PFA	Paraformaldehyde
PVN	Perivascular niche
Rac1	Ras-related C3 botulinum toxin substrate 1
RFP	Red Fluorescent Protein
RNA	Ribonucleic acid
RT	Radiotherapy
RTK	Receptor Tyrosine Kinase
SARRP	Small Animal Radiation Research Platform
SDF-1	Stromal Cell-Derived Factor-1
SDS-PAGE	Sodium Dodecyl Sulphate Polyacrylamide Gel Electrophoresis
SHH	Sonic Hedgehog

SMA	Smooth muscle actin
SMC	Smooth muscle cell
shRNA	Short Hairpin Ribonucleic Acid
Sox2	SRY (sex determining region Y)-box 2
SVZ	Subventricular zone
TAMs	Tumour-Associated Macrophages
TGF- β	Transforming growth factor-β
uPA	Urokinase-type plasminogen activator
VE-Cadherin	Vascular endothelial cadherin
VEGF	Vascular endothelial growth factor
VEGFR	Vascular endothelial growth factor receptor
VM	Vascular Mimicry
WB	Western Blot
WHO	World Health Organisation
WT	Wild Type

Chapter 1

Introduction

1.1 Glioblastoma multiforme (GBM)

Glioblastoma multiforme (GBM) is the most prevalent malignant primary brain tumour. Over 12,000 people are diagnosed with brain tumours in the UK each year (CRUK tumour incidence statistics) which accounts for approximately 3% of total cancer cases. Gliomas arise from the uncontrollable growth of glial cells, the cells forming connective tissue that surrounds and protects neuronal cells in the brain and the spinal cord. Glial cells include astrocytes, oligodendrocytes, ependymal cells and microglia. While low-grade gliomas, typically Grade I pilocytic astrocytoma and Grade II oligodendroglioma and oligoastrocytoma may be treated successfully or managed over several years, high-grade gliomas (Grades III and IV) are the malignant forms that are more refractory to treatment and account for most patient deaths. The 2007 World Health Organisation (WHO) classification of CNS tumours classifies GBM histologically as a Grade IV diffuse infiltrative astrocytoma with cytoplasmic and nuclear atypia, mitotic activity, and endothelial proliferation with or without necrosis (Louis et al. 2007). The 2016 WHO classification considered both histological and molecular parameters to better define the CNS tumours, particularly astrocytoma and oligodendroglioma, and also specifically referred to tumours not described in the 2007 classification, namely epithelioid glioblastoma, giant cell glioblastoma and gliosarcoma (Louis et al. 2016). For instance, giant cell epithelioid glioblastoma is classified under IDH wild-type GBM with large eccentric nuclei, eosinophilic cytoplasm and rhabdoid cell type. While it is characterised by its demarcated superficial cerebral location on MRI with 50% of them possessing BRAF V600E mutation, epithelioid glioblastoma lacks EGFR amplification unlike the IDH wild-type group.

1.1.1 GBM molecular subtypes

GBM is highly heterogenous, and different molecular subtypes appear to respond differently to therapy (Verhaak et al. 2010). According to the 2016 WHO classification, GBM is categorised into two major groups: Isocitrate dehydrogenase 1 (IDH1) wild-type and IDH mutant. *IDH1* is a gene which encodes an enzyme isocitrate dehydrogenase and mutation of this gene leads to abnormal function of cellular metabolism and tumorigenesis (Yang et al. 2012). IDH-wild-type GBM is the most common type accounting for 90% of all GBM cases, is of *de novo* origin (primary tumours) and affects elderly patients. IDH-mutant GBM is less common accounting for 10% of all GBM cases, and are secondary tumours (progressing from WHO low grade tumours) which are usually diagnosed in younger individuals (Louis et al. 2016). The abnormal cell metabolism and production of 2-hydroxyglutarate (2-HG) makes IDH mutant patients sensitive to chemotherapy such as temozolomide (TMZ), and as a result patients with IDH mutation have better survival when treated with TMZ (Lu et al. 2017). In addition to their IDH status, GBM tumours are also classified based on their O-6-methylguanine-DNA

methyltransferase (MGMT) status: *MGMT* methylated and *MGMT* unmethylated (Verhaak et al. 2010). The *MGMT* gene encodes for a DNA repair enzyme which protects cells, including cancer cells, from apoptosis by removing alkyl adducts from 0^6 guanine position. However, when *MGMT* promoter is methylated, DNA repair is impaired and alkylating agents like TMZ induces cell death (Thon, Kreth, and Kreth 2013). Hence, a positive link has been identified between *MGMT* methylation and patient response to chemotherapy. Hegi and co-workers found that GBM patients with methylated *MGMT* promoter tumour status have a two-fold survival benefit over patients with non-methylated tumours (Hegi et al. 2005). However, patient survival depends on multiple factors including tumour grade, location, proliferation indices, genetic alterations, patient age and neurological performance status (Louis et al. 2007).

GBM has been categorised relatively recently according to the prevalence of mutations of known oncogenes, and activation of downstream signaling pathways as classical, mesenchymal, neural and proneural (Verhaak et al. 2010). Classical subtypes are characterized by abnormally high levels of epidermal growth factor receptor (EGFR) signaling. Furthermore, EGFR gene amplification or deletion mutation (EGFRvIII) driving high tumour proliferation rates; paired chromosome 7 amplification and chromosome 10 loss; aberration of the retinoblastoma (RB) pathway following CDKN2A deletion; high expression of Nestin; activation of Notch and SHH pathways are very common. EGFR abnormalities are found at a much lower rate in the mesenchymal, neural and proneural subtypes (Verhaak et al. 2010). The classical group shows the best patient outcome in response to aggressive radio-chemotherapy. The tumour suppressor gene *TP53* is the most frequently altered gene in GBM through mutation or loss of heterozygosity (LOH). This gene is not mutated in the classical subtype, however, *TP53* genetic alterations are prevalent (>50%) in proneural tumours. Proneural tumours also have the highest prevalence of mutant-*IDH*; PDGFRA amplification which activates the PI3K/AKT and RAS signaling pathways; high expression of OLIG2 and SOX genes. Patients with proneural tumours are generally of younger age and show better survival, which is not dependent on aggressive treatment. The mesenchymal subtype is characterised by mutations of the *NF1* tumour suppressor gene which activates the MAPK pathway, and mutations of the *PTEN* gene which activates the RAS pathway, as well as high expression levels of CHI3L1, VEGF, CD44 and c-MET. The neural subtype tumours express normal neuronal markers such as NEFL and GABRA1 and have worse patient outcome compared to classical GBM (Verhaak et al. 2010).

Both WHO High Grade III and Grade IV gliomas can be classified within the proneural subtype, while mesenchymal and classical subtypes are mostly limited to WHO Grade IV gliomas. While

mesenchymal and classical subtypes are predominantly characterised by presence of necrosis, the proneural subtype may or may not present with extended necrosis (Phillips et al. 2006). There is a considerable age difference between patients with mesenchymal and proneural tumours as they are common in old and young patient age groups, respectively. While classical subtypes are the most proliferative tumours, mesenchymal subtypes are the most angiogenic and express significantly higher levels of CD31 and VEGFR2 compared to other subtypes (reviewed in Campos et al. 2016). Analysis of 88 primary and 22 recurrent GBM tumours, Li and colleagues found that the mesenchymal subtype as the most common GBM subtype, accounting for 41% and 45% of primary and recurrent tumours respectively (Li et al. 2015). On the other hand, the classical subtype was found to be somewhat more prevalent in primary (36%) compared to recurrent tumours (22%), whereas the proneural subtype was detected less in primary (15%) compared to recurrent GBM (23%). These observations are likely to reflect the wide range of mutational spectra characterising GBM tumours, as well as rapid mutation rate which may manifest itself in recurrences.

1.1.2 Current therapies in GBM

The current standard of therapy for glioblastoma involves de-bulking surgery followed by radiotherapy, and an adjuvant carmustine and alkylating drug TMZ in MGMT methylated tumours (Hegi et al. 2005). In the Zurich annual meeting of the European Association of Neuro-Oncology/ World Federation of Neuro-Oncology Societies (EANO/WFNOS) 2017 several clinical trials were presented including the antiangiogenic agent Bevacizumab, anti-EGFR agent ABT-414, immunotherapy drugs Nivolumab and Ipilimumab, and vaccination against EGFRvIII using Rindopepimut. However, the results of single or combination therapies were invariably disappointing and clearly showed that we are far from a breakthrough for GBM. For instance, although GBM is highly angiogenic the use of antiangiogenic drugs like Bevacizumab eventually failed to stop tumour growth following development of resistance and/or tumour recurrence (Kumar and Arbab 2013). As a result, still to date there is no significant increase in patient overall survival in response to any of these new agents. Patient survival remains dismal at approximately 15 months after surgery followed by radiotherapy and temozolomide chemotherapy.

1.1.3 GBM invasion and recurrence

Recurrence is very common in GBM (Loeffler et al. 1990) and is mainly attributed to the infiltrative nature of cancer cells (Gerstner et al. 2010 and Hanahan and Weinberg 2011). Following primary tumour resection and irradiation, tumour cells infiltrate the brain parenchyma and frequently populate microvessels in the normal brain. This typically results in partial removal of the tumour mass,

and evasion of the infiltrating tumour cells from subsequent radiotherapy and chemotherapy resulting in tumour recurrence. Gritsenko and colleagues have described how cancer cells migrate and invade either as single-cells or as collective strands and multicellular networks (Gritsenko, Leenders, and Friedl 2017). Invasion is known to take place along white matter tracks and alongside blood vessels frequently in response to chemotactic factors such as CXCL12 (Brooks et al. 2013). RNA-sequencing analysis of 75 glioma biopsy samples obtained from core (contrast-enhancing), or infiltrative (non-enhancing) margins of GBM tumours using radiography guided techniques, showed higher proneural, classical and mesenchymal subtype molecular signatures in the core region of the tumours, compared to neural subtype signature in the tumour margins (Gill et al. 2014). Further, the infiltrative margins of proneural subtypes showed higher expression of oligodendrocyte-related genes, while the margins of mesenchymal tumours showed a more of astrocytic and microglial related gene signatures, indicating differences amongst different subtypes as to the composition of cells contributing to tumour infiltration (Gill et al. 2014).

A key feature of GBM tumours is that they frequently undergo subtype evolutionary changes (Wang, Cazzato, et al. 2016). For instance, using comprehensive genomic profiling of 10 primary and recurrent GBM tumour pairs, Neilsen and co-workers observed both common and distinct genetic alterations in the primary and recurrent tumours (Neilsen et al. 2018). The most common genetic alterations observed were CDKN2A and CDKN2B deletion, EGFR mutation, EGFR amplification and telomerase reverse transcriptase (TERT) mutation in 86% versus 53%, 52% versus 10%, 81% versus 45% and 95% versus 51%, respectively for each gene, in primary and recurrent GBMs (Neilsen et al. 2018). However, when primary and recurrent tumours were compared by Andor et al, more mutations were found in patients with recurrent tumours following radio-chemotherapy, as well as MutL Homologue1 encoded by the *MLH1* gene conferring TMZ resistance in recurrent compared to primary tumours (Andor et al. 2014). Further, molecular analysis of 26 paired astrocytomas showed that while 18 tumours maintained their molecular subtype, 7 shifted from proneural to mesenchymal upon recurrence, and additionally showed upregulation of STAT3, YKL40 and CD44, and loss of OLIG2 expression (Phillips et al. 2006). Similarly, transcriptome analysis of radioresistant GSCs showed significant transition from proneural to mesenchymal signatures with activation of proinflammatory pathways, and STAT3 by IL-6, being major mediators of this transition (Stanzani et al. 2017).

1.2 The brain tumour perivascular niche

The perivascular niche (PVN) is known as the distinct area around blood vessels, known to provide signaling cues that maintain the self-renewal and pluripotency of postnatal stem cells in different

tissues (reviewed in Oh and Nor 2015). Endothelial cell secreted factors promote the survival of haematopoietic stem cells in the bone marrow. While several studies support the existence of perivascular progenitor cells in different tissues giving rise to cell lineages typically originating from mesenchymal stem cells such as osteoblasts, myocytes or adipocytes, other studies suggest that pericytes are pluripotent and may give rise to such mesenchymal derived lineages (reviewed in Oh and Nor 2015). In the brain, studies support the existence of mesenchymal stem cells with an expression profile similar to pericytes, which together with endothelial cells, astrocytes and neurons form an important brain structure termed the neurovascular unit. The neurovascular unit plays important roles in angiogenesis, the development and maintenance of a functional blood brain barrier (BBB), the homing and survival of neural stem cells and repair mechanisms in the brain (reviewed in Appaix et al. 2014). In brain tumours, the PVN provides a conducive environment for glioma stem cells (GSCs), the self-renewing and tumorigenic cancer cells (reviewed in Ho and Shim 2017). The perivascular niche supports the maintenance of stemness through EC-secreted nitric oxide and Dll4 ligand activation of Notch signaling in GSCs (reviewed in Sharma and Shiras 2016), invasion by modifying the ECM through secretion of MMPs (reviewed in Manini et al. 2018), resistance through activation of PI3K/AKT signaling (Hambardzumyan et al. 2008), and protection from host immunity through exploitation of immune checkpoints PD-1 and CTLA-4 (Beatty and Gladney 2015) through maintaining a well-orchestrated signal communication mechanisms involving various cell types (Schiffer et al. 2015; Yan et al. 2014 and Louis et al. 2007). As a result GSCs are well protected from therapy and are markers of a poor prognostic patient outcome (Gilbertson and Rich 2007).

The brain tumour PVN comprises of glioma stem cells, cancer cells, endothelial cells, astrocytes, pericytes/smooth muscle cells (SMCs) and immune cells (Schiffer et al. 2015 ans Goldman and Chen 2011). The development of efficacious therapies for glioblastoma will require understanding of the precise nature of these cellular interactions and the molecular mechanisms that maintain them (Charles and Holland 2010). Within the PVN there is a direct relationship between tumour associated macrophages (TAMs) and GSCs (Figure 1.1) as they share common locations including around blood vessels and hypoxic regions (reviewed in Codrici et al. 2016). Most GSCs are located around capillary blood vessel endothelial cells (ECs) located in the hippocampus and SVZ (Jain et al. 2007). Interestingly, while GSCs associated with PVN show high activation of Notch signaling, GSCs around hypoxic niches do not, but unlike GSCs associated with the PVN they show high expression of the stem cell marker CD133, thus exemplifying the high level of heterogeneity of GSCs and/ or the influence of different microenvironmental niches (Bayin et al. 2017).

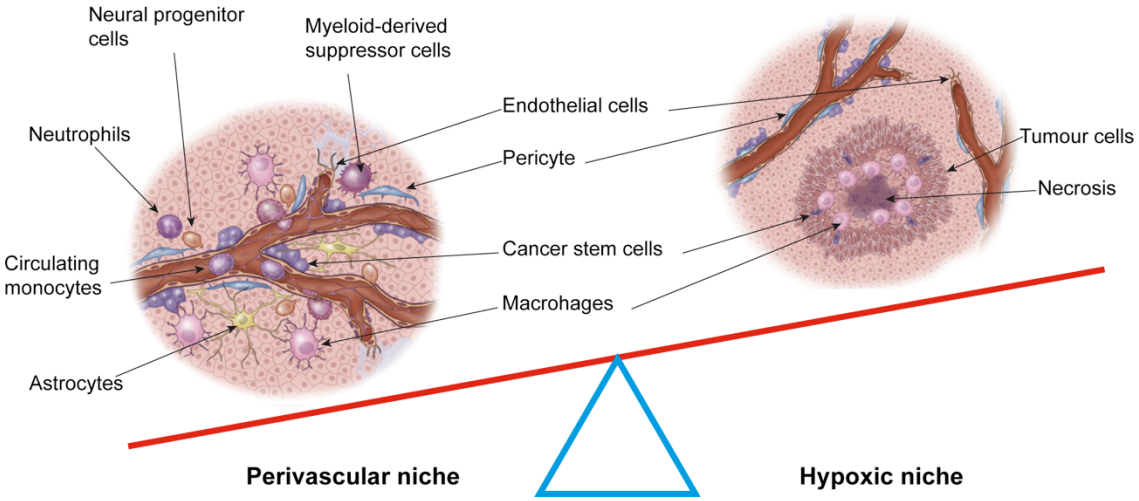

Figure 1.1 The brain perivascular and hypoxic niche

There are two characteristic and well-defined niches in the brain: perivascular and the hypoxic niche. The two niches are different in terms of cell types involved. The perivascular niche is highly populated by GSCs, immune cells, pericytes and astrocytes while the hypoxic niche is more commonly populated by immune cells. Overtime, the perivascular niche may become a hypoxic niche as tumour growth outweighs the blood supply. Adapted from Hambardzumyan and Bergers, 2015 (Hambardzumyan and Bergers 2015).

1.2.1 Endothelial cells

The PVN primarily consists of the tumour vasculature and associated cell types on the type of blood vessel (Armulik et al. 2011 and Nagy et al. 2009). The vasculature is lined by endothelial cells (ECs) connected to form the Blood Brain Barrier. Under normal conditions the brain is well protected by the Blood Brain Barrier (BBB) which separates the blood from the cerebrospinal fluid and presents a barrier to the passages of cells, particles, large molecules and pathogens. The BBB is comprised of pericytes, astrocytic end-feet and SMC/pericytes (Cabezas et al. 2014), and it is mainly made of tightly interconnected ECs with continuous intercellular junctions and restricted transcellular transport (Obermeier, Daneman, and Ransohoff 2013). In addition to providing cells with nutrients and oxygen, both *in vitro* and *in vivo* experiments show that ECs secret different factors which promote tumour growth (Gilbertson and Rich 2007) and stem cell self-renewal (Charles and Holland 2010 and Yan et al. 2014). For instance, ECs secrete SHH, nitrous oxide (NO) and Notch ligands to promote GSCs stemness by activating Sonic Hedgehog (SHH) and Notch signaling pathways in cancer cells (Yan et al. 2014). SHH (Clement et al. 2007) and Notch signaling (Hovinga et al. 2010) promotes GSC stemness, proliferation and self-renewal, growth and survival, and chemo-radioresistance. Further, in addition to increasing GBM cell proliferation, tumour ECs also protect GBM cancer cells from chemotherapy and radiotherapy potentially through regulation of *MGMT* gene (Borovski et al. 2013). GBM associated ECs have characteristic features of large and flat cell morphology, slow proliferation rate and resistance to cytotoxic therapies, increased production of growth factors such as IL-8 and VEGF (Charalambous, Chen, and Hofman 2006). Wang and colleagues showed that macrophages are positioned closely to ECs in the tumour microenvironment and that their recruitment follows release of IL-6 from ECs which promotes cell invasion (Wang et al. 2018)

1.2.2 Glioma stem cells

Glioma stem cells (GSCs) are stem cell-like cells which are a subpopulation of cancer cells with stem cell property and self-renewal capacity and are responsible for both *in vitro* and *in vivo* tumour growth (Singh et al. 2004). Although there is no universal marker for GSCs, they can be identified using various markers including Nestin, CD133, SOX2, OLIG2, NANOG, Musashi, OCT4 and CD44 (Codrici et al. 2016). GSCs locate preferentially in the PVN (Chen et al. 2015) along blood vessels in order to proliferate and self-renew in manner analogous to their neural stem cell (NSC) counterparts - the self-renewing, multipotent cells that generate the cells of the central nervous system during development (Gilbertson and Rich 2007), located in the subventricular zone (SVZ). Yan et al. observed $CD133^{+}$ GSCs in close proximity with SHH^{+} ECs in glioblastoma multiforme tissue, and when they co-cultured ECs with GSCs they observed increased GSC tumorigenicity, and that expression of stemness markers such

as OLG2, SOX2, OCT4, NANOG, c-Myc, Bmi1 and CD133 increased (Yan et al. 2014). These proteins are expressed in GSCs and play important roles in tumorigenesis and stem cell behavior. For example, CD133 promotes proliferation (Brown et al. 2017), SOX2/NANOG self-renewal and stemness (Zbinden et al. 2010 and Berezovsky et al. 2014), and CD44 promotes survival and differentiation (Mooney et al. 2016). Unlike NSCs which assume a quiescent state following therapy, GSCs residing in the perivascular niche activate survival pathways, antagonize apoptosis and promote drug resistance (Kalkan 2015). GSCs modulate tumour ECs through the release of vascular endothelial growth factor (VEGF) which is a key angiogenic growth factor (Charles and Holland 2010). VEGF signaling results in the activation of proliferative and survival pathways in ECs, including MAPK/ERK and PI3K signaling (Chung and Ferrara 2011). On the other hand, GSCs are attracted to ECs through activation of the CXCL12/CXCR4 signaling axis, with ECs secreting stromal derived factor (SDF-1), aka CXCL12, which interacts with CXCR4 expressed by GSCs (Cheng et al. 2013). GSCs are regulated in the PVN by different signaling pathways which include TGF-ß, Notch, Wnt/ß-catenin, OCT4 and c-Myc (Schiffer et al. 2015). For instance, while Wnt/ß-catenin signaling plays an important role in tumour growth and invasion by promoting GSC stemness (Lee et al. 2016), TGF-ß regulates stemness, angiogenesis, invasion and resistance, and also plays an immunosuppressive role (Joseph et al. 2013).

1.2.2.1 Nestin

Nestin, a type VI intermediate filament protein, is a marker of neuronal stem cells (Yan et al. 2016) and immature, poorly differentiated and proliferating endothelial cells (Liang et al. 2015). A study conducted in embryonic mouse brain and heart showed the importance of Nestin in organ development through regulating cell proliferation, and activation of the PI3K/AKT pathway (Liu et al. 2015). Another study demonstrated that when Nestin is down-regulated there is a severe reduction in the number of neurons in the brain, as a consequence of reduced PI3K signaling and survival, highlighting the importance of Nestin in neuronal progenitor cell (NPC) development (Xue and Yuan 2010).

In addition to undifferentiated stem cells, Nestin is a marker of neurogenic tumours such as glioblastoma (reviewed in Neradil and Veselska 2015). Immunohistochemical analysis of low and high grade glioma patient samples showed positive correlation between Nestin, CD133 expression and tumour grade (r_s=0.89). Moreover, the higher the expression of Nestin, the poorer the patient prognosis (Zhang et al. 2008). Suzuki et al demonstrated that Nestin was expressed by endothelial progenitor cells of mouse brain tissue following injury, and this expression declined as these cells become differentiated in culture, or not detected in non-injured brain tissue (Suzuki et al. 2010). Furthermore, the same study reported that in addition to the endothelial cell marker CD31 and nestin,

newly formed blood vessels were positive for the proliferation marker Ki67, while mature blood vessels expressed high levels of von Willebrand factor (vWF) and were negative for Nestin (Suzuki et al. 2010). *In vitro* experiment by Liang and colleagues demonstrated how VEGF regulates neo-angiogenesis through stimulation of Nestin expression, and that deletion of Nestin reduces EC migration by affecting filopodia extension, potentially through the MAPK-ERK pathway (Liang et al. 2015). A characterisation study of the vasculature in human colorectal liver metastases showed Nestin positivity of newly formed vessels, although immunofluorescence staining did not confirm this potentially due to low levels of Nestin expression in ECs (Klein et al. 2014). Klein et al. also showed through bone marrow transplantation experiments utilising Nestin-GFP transgenic mice, that these Nestin positive ECs are likely to be resident cells, rather than derived from the bone marrow (Klein et al. 2014).

1.2.2.2 CD133

CD133, also known as Prominin-1, is a transmembrane protein (Shmelkov et al. 2005) expressed by stem cells and stem-like cells including GSCs (Shmelkov et al. 2008). $CD133^+$ cancer cells have the capacity to proliferate, renew themselves, and form tumour growth both in *in vivo* and *in vitro* (Singh et al. 2004). There is a strong correlation (rs=0.89) between CD133 and Nestin expression in glioma, and their combined increased expression is associated with poor patient survival (Zhang et al. 2008). On the other hand, Dahlrot et al reported that while there was no association between level of CD133 expression and WHO grade of glioma and OS, high level of Nestin expression was found a marker of poor progression free survival (PFS) in WHO grade II tumours (Dahlrot et al. 2014). Further, $CD133^+$ glioma cells are thought to be the GSCs responsible for radioresistant and tumour recurrence (Bao et al. 2006).

1.2.2.3 SOX2

SRY-box2 (SOX2) is a transcription factor that plays important roles in the formation of many tissues and organs during embryonic development. SOX2 is essential for maintaining self-renewal and pluripotency of embryonic stem cells, and plays key roles in maintenance of neural stem cells (Berezovsky et al. 2014). SOX2 knockdown in GSCs isolated from patient GBM tumours resulted in down-regulation of YAP, a component of the Hippo pathway which controls stemness and tumorigenicity, and inhibition of the capacity of GSCs to form spheres in culture. On the other hand, SOX2 knockdown increased expression of the tumour suppressor NF2, which is important regulator of growth of the nervous system (Basu-Roy et al. 2015). Hence SOX2 is important in maintaining cell stemness and function of the nervous system (Basu-Roy et al. 2015). On the other hand, Phi et al. had

suggested that SOX2 is a marker of glial cells rather than stem cells (Phi et al. 2008). This was mainly because the majority of SOX2 positive cells are also positive for GFAP and Nestin in GBM, while SOX2 was also expressed in different grade tumours including Grade III gliomas (Phi et al. 2008). However, Leiss and colleagues showed that SOX2 is not expressed in glial cells in healthy brain but is upregulated in patient GBM (Leiss et al. 2017). The levels of SOX2 expression in GBM appear to depend on the molecular subtype, and whether the tumour is primary or recurrent. Classical, mesenchymal and proneural subtypes do significantly express CD133, Nestin and OLIG2 respectively. While nestin is expressed by all subtypes, the expression of SOX2 appears highly variable (Phillips et al. 2006).

1.2.2.4 OLIG2

Oligodendrocyte transcription factor 2 (OLIG2) is a transcription factor which is only expressed in CNS and promotes proliferation and brain cancer development (Tsigelny et al. 2016). Although OLIG2 is expressed in both NSCs and GSCs, it appears to be more abundant in GSCs (Gilbertson and Rich 2007). OLIG2, like SOX2, is essential for GBM propagation (Ceccarelli et al. 2016). Using organoid spheres, Hubert et al. (2016) showed that in a proliferative outer rim of tumour spheres, GSCs co-express SOX2 and OLG2 (Hubert et al. 2016). Interestingly, in the central hypoxic zone of the sphere, where more of nascent GSCs are found, cells positive for a single marker can also be identified (Hubert et al. 2016). In terms of subtype specific expression, immunofluorescent staining of various cultured cells from the different molecular subtypes showed uniform expression of SOX2 and Nestin, while the expression of OLIG2 and GFAP varied amongst different subtypes (Xie et al. 2015). Strong OLIG2 positivity is a marker of poor outcome in pediatric GBM (Cloughesy, Cavenee, and Mischel 2014). Verhaak and co-workers reported that OLIG2 is highly expressed in proneural tumours where it promotes tumour proliferation by down-regulating the tumour suppressor CDKN1A (Verhaak et al. 2010).

1.2.2.5 NANOG, OCT4, Musashi, and CD44

Other GSC markers include transcriptional factors NANOG and Octamer transcription factor 4 (OCT4); RNA binding protein Musashi1 and cell surface receptor protein CD44 (Bradshaw et al. 2016). Both NANOG and OCT4 are transcription factors (Rodda et al. 2005), while Musashi is an RNA-binding protein (Muto et al. 2012). NANOG is associated with formation of GSC spheres, proliferation and tumorigenicity (Zbinden et al. 2010); OCT4 regulates pluripotency and self-renewal (Rooj, Bronisz, and Godlewski 2016); Musashi1 promotes tumour growth and survival (Chen et al. 2017); CD44, a transmembrane protein, regulates tumour progression (Xu, Stamenkovic, and Yu 2010). While there is a strong correlation between CD44 and CD133 in GBM (Brown et al. 2017), NANOG, OCT4 and SOX2 expression have a positive correlation (Yi et al. 2016).

1.2.3 Pericytes and Vascular smooth muscle cells

Pericytes are mural cells embedded within the basement membrane (BM) of capillary blood vessel wall that regulate vascular morphogenesis during development as well as under pathological conditions (Armulik, Genove, and Betsholtz 2011). Vascular smooth muscle cells (SMCs) normally compose the wall of larger calibre blood vessels and have a contractile phenotype maintaining vascular tone. The definition of pericyte is often controversial and a combination of morphology, location and gene or protein expression are often used to define pericytes. Although pericytes, just like SMCs take a periendothelial location, unlike SMCs they have a continuous cytoplasmic process over the abluminal surface of ECs of the blood vessels often covering several ECs (Armulik, Genove, and Betsholtz 2011). Further, the lack of SMCs in capillaries, and the unique anatomical morphology of SMCs of circumferential orientation around arteries, arterioles and precapillaries differentiate these larger blood vessels from capillaries (Hill et al. 2015). Berthiaume and co-workers demonstrated that ablating pericytes leave capillaries uncovered and dilated although they quickly make an extension to cover it afterwards (Berthiaume et al. 2018). Pericytes are dynamic and their expression of molecular markers depends on the developmental and pathological states of blood vessels. Hence, there is no single pericyte specific marker identified to date, but different markers have been described and validated including PDGFRβ, α-SMA, NG2 and Desmin (reviewed in Armulik, Genove, and Betsholtz 2011).

The origin of pericytes is not unique, studies show that they originate from local normal tissue, but also from bone marrow stem cells (Hanahan and Weinberg 2011). The neural crest has been indicated as the most common origin of brain pericytes, which involves their recruitment through different signaling axis including PDGFB/PDGFRβ, TGF-β/TGF-βR, ANG-1/TIE2 and CXCL12/CXCR4 (Armulik, Genove, and Betsholtz 2011). Pericytes communicate with ECs through both direct cell-cell contact and through paracrine signaling (Charles and Holland 2010 and Bergers et al. 2003). For example, TGF-ß plays an important role in the maintenance of the attachment of pericytes and ECs by up-regulating N-cadherin, mediating physical contact between ECs and pericytes (Armulik, Genove, and Betsholtz 2011). The activation of PDGFRß on pericytes by EC secretion of PDGFB leads to proliferation and migration of pericytes, while Ang-1/Tie 2 signaling leads to maturation and stability of blood vessels through close alignment of pericytes with blood vessels (Hill et al. 2015).

Under physiological conditions, pericytes exist in close association with ECs (Charles and Holland 2010) and cover 22-99% of the abluminal surface of the vasculature (Hill et al. 2015). Pericytes play an essential role in maintaining the integrity of BBB (Hill et al. 2015 and Daneman et al. 2010) and in

guidance of sprouting angiogenesis (Charles and Holland 2010 and Bergers and Benjamin 2003). Using *pdgfb* deficient mice Armulik et al. showed how pericytes are crucial for BBB permeability (Armulik et al. 2010). The mice deficient in *pdgfb* showed decreased pericyte blood vessel coverage, increased blood vessel diameter and increased permeability of the BBB to water and tracers of different molecular weights (Armulik et al. 2010). Another study showed that as well as inhibiting pericyte recruitment, endothelial *pdgfb* deletion led to formation of hyperplastic endothelial cells (Bjarnegard et al. 2004). Pericytes are found in tumour blood vessels, however they are fewer in number and their attachment to endothelial cells is looser, which contributes to increased tumour blood vessel permeability (Armulik et al. 2010), increased metastasis (Chung and Ferrara 2011), as well as higher vulnerability of tumour ECs to radio-chemotherapy (Cheng et al. 2013). In GBM, there is increased presence of pericytes compared to low grade glioma, while more pericytes have been detected in the core region compared to the boundary of tumours (Takeuchi et al. 2010). It has been postulated that increased pericyte coverage protects tumour blood vessels from antiangiogenic therapy, while targeting both pericytes and endothelial cells reduces tumour growth more effectively than targeting endothelial cells lining the blood vessels alone (Takeuchi et al. 2010).

1.2.4 Astrocytes

Astrocytes are glial cells which are tightly attached to the basement membrane of the ECs through integrin, agrin and dystroglycan, and maintain the integrity of BBB both through physical contact and release of soluble factors (Watkins et al. 2014). However, expanding or invading cancer cells can displace these astrocytic end-feet, and the BBB becomes more permeable resulting in molecules such as albumin and cadaverine leaking into parenchyma (Watkins et al. 2014). GFAP, a marker for astrocytes as well as stem cells, is expressed more in mesenchymal and proneural subtypes than in the classical subtype. Deletion of GFAP and vimentin from reactive astrocytes in mice caused lack of intermediate filaments (Hol and Pekny 2015). In addition to GFAP, reactive astrocytes also co-express Musashi1 and Nestin (Oki et al. 2010).

Astrocytes are activated and undergo morphological and functional changes in response to CNS injury to become reactive astrocytes (Pekny and Nilsson 2005). Reactive astrocytes are one of the components of PVN in tumours and play an important role in cancer cell survival by secreting interleukin-6 which enables them to resist apoptosis (Sin et al. 2016). Reactive astrocytes contribute to tumour growth through secretion of metalloproteinases and connective tissue factors (Deb, Wenjun Zhang, and Gottschall 2003). The gap junction protein Connexin (Cx) 43, which is also expressed in reactive astrocytes, contributes to intercellular communication *via* calcium signaling (Sin

et al. 2016). Assessment of eight normal brain tissue samples and 44 astrocytic tumours by immunohistochemistry (IHC) and Northern blot analysis showed high expression of Cx43 in normal brain and lower grade gliomas, while the expression was very low in GBM (Pu et al. 2004). Aberrant Cx43 expression has been associated with poor patient outcome (Bonacquisti and Nguyen 2019). In melanoma reactive astrocytes protect tumour cells from chemotherapy (Lin et al. 2010), and similarly in glioma astrocytes protect cancer cells from therapy through direct physical contact *via* gap junctions (Lin et al. 2016).

1.2.5 Microglia and Macrophages

Brain resident microglia and infiltrating macrophages are tumour associated macrophages (TAMs) which are abundant in brain tumours (Roggendorf, Strupp, and Paulus 1996) and may account for 8-78% of the total GBM tumour microenvironment cell population (Lorger 2012 and Morantz et al. 1979). Further, another study showed that TAMs represent about 20-50% of all cells within the tumour microenvironment (Lapa et al. 2015). While activated microglia in healthy brain play antigen presenting and phagocytic roles (Lorger 2012), in tumours they either suppress or promote tumour growth depending on whether they are naive or activated (Charles and Holland 2010; Hambardzumyan, Gutmann, and Kettenmann 2016 and Schiffer et al. 2015). Macrophages are the main immune cells in brain tumours including GBM, and they are attracted to tumour sites through HIF-1α which activates the CXCL12/CXCR4 signaling pathway (Hambardzumyan, Gutmann, and Kettenmann 2016), and tumour cell derived chemoattractants (Charles and Holland 2010). For instance, macrophages are attracted to glioma secreted granulocyte colony stimulating factor (G-SCF), and following infiltration they start secreting growth factors that promote angiogenesis (Du et al. 2008) and invasiveness (Markovic et al. 2005), such as MMPs, VEGF and MT1-MMP (Hambardzumyan, Gutmann, and Kettenmann 2016). Macrophages and microglia are more abundant around necrotic areas and perivascular regions (Schiffer et al. 2015).

Unfortunately, it can be challenging to differentiate macrophage and microglia. While infiltrating macrophages are usually characterised by strong CD45 positivity and round shaped morphology, resident microglia show weaker CD45 staining positivity (Lapa et al. 2015). Further, macrophage/ microglia are typically divided into the anti-tumorigenic, M1, and pro-tumorigenic, M2, phenotypes. The use of M1 specific marker, CD86, and M2 macrophage specific, CD204, showed that the type of macrophage abundant in GBM is the M2 type (Nijaguna et al. 2015). From the analysis of 80 brain tumour biopsy samples Roggendrof and Paulus identified 3 subgroups of microglia/ macrophages in the brain: ramified, ameboid and perivascular (Roggendorf, Strupp, and Paulus 1996). While they

detected low microglia/ macrophage abundance in low grade glioma, a high number of microglia/ macrophages were observed in anaplastic gliomas and GBM. More recent studies also showed that the higher the abundance of microglia/ macrophages in the intratumoural space, the denser the tumour and the poorer the patient prognosis is (Chung and Ferrara 2011). *In vivo* studies also show that there is a high infiltration of F4/80^{+} macrophages in tumour tissue following irradiation (Morganti et al. 2014).

1.3 GBM vasculature

1.3.1 Normal brain blood vessels

Just like in other organs, blood vessels in the brain initially develop from a vascular plexus (Wacker and Gerhardt 2011), which later develops further to supply oxygen and nutrients and remove waste substances from the body. The process of formation of the vascular plexus is termed vasculogenesis, while the growth of new blood vessels from pre-existing ones is termed angiogenesis (Adams and Alitalo 2007) (Herbert and Stainier 2011) (Chung and Ferrara 2011). In order for blood vessels to form a functional vasculature following vasculogenesis and angiogenesis, they have to undergo extensive remodelling and maturation. For example, many blood vessels that start sprouting but are not incorporated in the developing plexus or the expanding vasculature, are pruned leaving behind 'empty sleeves' characteristic of the remodelling process (Simons et al. 2015). Formation of the lumen which allows the flow of blood is a critical stage in the process of new vessel formation (Eilken and Adams 2010). The recruitment of pericytes/SMCs through signaling pathways regulated by PDGFB, TGF-β and angiopoietins (Chung and Ferrara 2011) is critical for the stabilisation of the newly formed blood vessels (Kuhnert et al. 2008).

In the adult, under physiological conditions except during wound healing and the female reproductive cycle, endothelial cells in blood vessels remain quiescent, due to a balance between angiogenesis inducers such as VEGF-A, and inhibitors of angiogenesis such as trombospondin-1. However, this balance is tipped in tumours where angiogenesis promoters prevail, leading to activation of the angiogenic switch (reviewed in Hanahan and Weinberg 2011). During this process, the surge of VEGF-A makes the blood vessels to start sprouting from a leading cell called the tip cell (Friedl and Gilmour 2009 and Carmeliet and Jain 2011)). In addition to the VEGF receptor VEGFR2, which makes them responsive to VEGF, tip cells also express DLL4, which binds to Notch receptors on the trailing endothelial cells called stalk cells. This downregulates the expression of VEGFR-2 to allow the blood vessel to extend from the tip cell, and prevents surplus angiogenesis. This mechanism is controlled by a VEGF-A gradient which leads to proliferation and migration of the tip cells while the stalk cells are unresponsive to VEGF (Carmeliet and Jain 2011). In abnormal circumstances like in cancer, excessive

expression of VEGF-A results in development of aberrant blood vessels through uncontrolled sprouting angiogenesis which involves high rate of proliferation and collective migration of ECs (Jakobsson et al. 2010; Chung and Ferrara 2011 and Neufeld, Planas-Paz, and Lammert 2014). Overall, the abnormally expressed proangiogenic growth factors in tumours lead to formation of highly branched, convoluted, enlarged and leaky blood vessels with poor blood flow, as endothelial cells remain in a proliferative and sprouting phenotype (Hanahan and Weinberg 2011).

1.3.2 Mechanisms of blood vessel development in GBM

Although it was known for over a century that tumours have their own blood supply, the mechanism by which they do this only came to recognition since 1970s (Nagy et al. 2009). Today, several molecular mechanisms (Figure 1.2) have been identified by which tumor cells form their own blood vessels. These mechanisms include sprouting angiogenesis, vessel co-option, vasculogenesis, vasculogenic mimicry, and transdifferentiation (reviewed in Hardee and Zagzag 2012 and Viallard and Larrivee 2017).

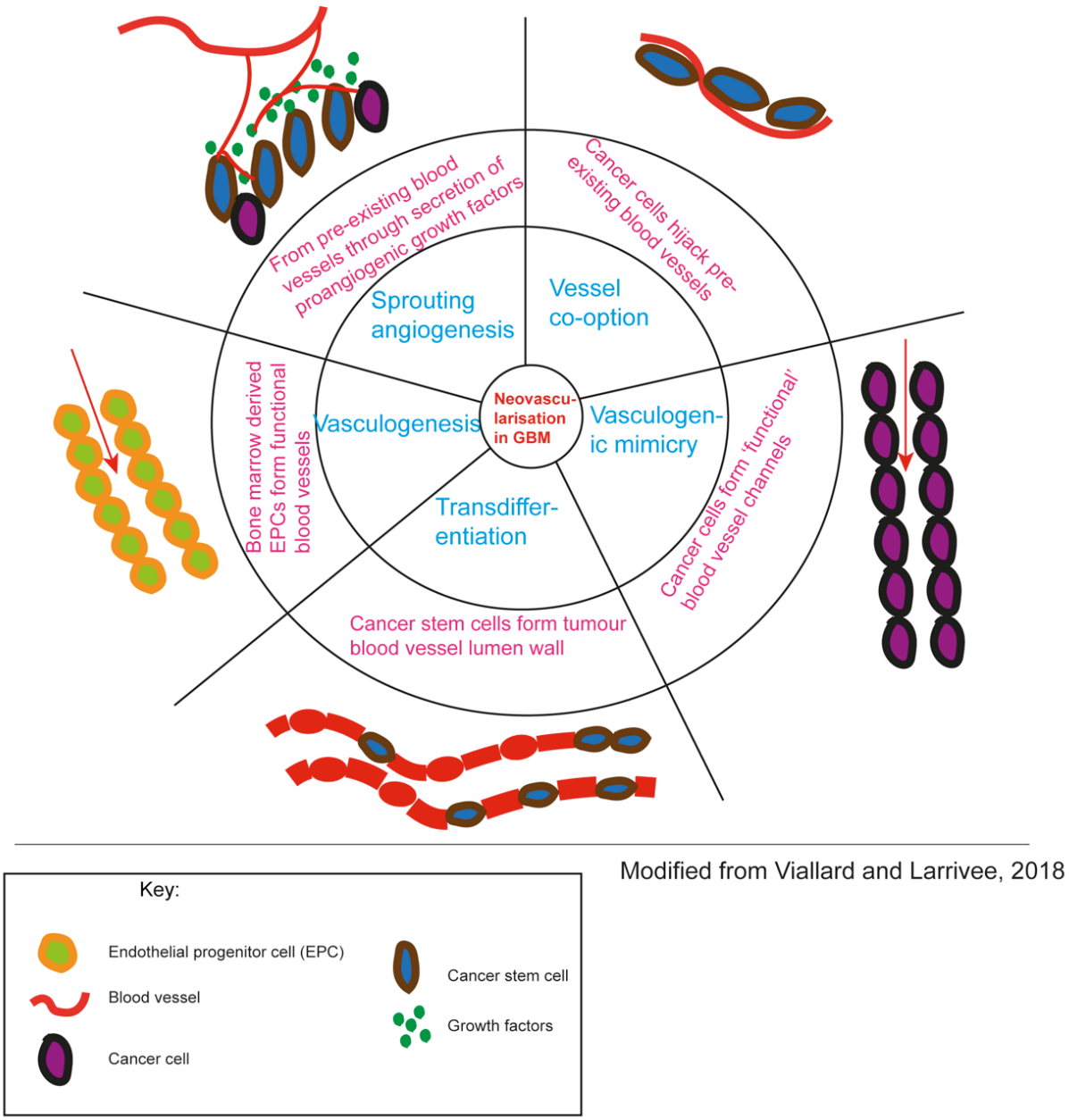

Figure 1.2 Neovascularisation in GBM

Diagram depicting proposed mechanisms by which GBM forms its own blood vessels with theories ranging from classic angiogenesis and co-option where normal ECs line the lumen of blood vessels, to vasculogneic mimicry and transdifferentiation where cancer cells line the blood vessels lumen unmodified or having transdifferentiated to ECs.

1.3.2.1 Sprouting angiogenesis

The proangiogenic factors and signaling pathways implicated in brain tumour angiogenesis are: VEGFA/VEGFR1/2, bFGF/FGFR1, placental growth factor, Angiopoietin 2 and IL-8/CXCR1/2 which interestingly often appear to be activated in cancer cells (reviewed in Anderson, McFarland, and Gladson 2008 and Cea, Sala, and Verpelli 2012). The proliferation of ECs and development of blood vessel in GBM is thought to be a direct consequence of increased and uncontrolled VEGF secretion (Soda et al. 2013 and Schiffer et al. 2015). It is thought that tumour cells at early stages of tumour growth rely on pre-existing blood vessels (He, Niu, and Li 2012). However, once the tumours exceed 1-2mm they start to become hypoxic (Kienast et al. 2010). Hypoxia induces production of proangiogenic growth factors and cytokines through upregulation of the transcription factors HIF-1α and HIF-2α with consequent upregulation of VEGF expression (Ellis and Hicklin 2008; Chung and Ferrara 2011 and Schiffer et al. 2015). Normally, under normoxia, prolyl hydroxylase domain (PHD) enzymes hydroxylate the α-subunits of HIF in the cell, however under hypoxia PHD remains inactive and HIF-1α enters the nucleus and transcription of genes takes place which leads to cancer cell proliferation, survival, angiogenesis and metastasis (reviewed in Sormendi and Wielockx 2018).

VEGF driven angiogenesis is the most common mechanism of blood vessel formation in glioblastoma and other tumours, however anti-angiogenic drugs like Bevacizumab (Avastin) failed to increase the overall survival of GBM patients. Although VEGFA/VEGFR2 signaling is the main signaling pathway for endothelial cell proliferation and blood vessel sprouting, it has been noted that established and mature blood vessels are also abundant in GBM tumours (Bergers and Song 2005). Pericytes appear to be involved in several stages of new vessel formation (Eilken et al. 2017). As the deposition of basement membrane and pericytes are important for the stabilisation of newly formed blood vessels, the basement membrane of the pre-existing vessels must be destroyed and the pericytes must first dissociate for ECs to migrate (Patel-Hett and D'Amore 2011). Metalloproteases are key enzymes involved in this process, as well as in the degradation of extracellular matrix during the migration of endothelial cells within or towards the tumour. For example, MMP9 is actively involved in this process in brain tumours (Anderson, McFarland, and Gladson 2008). Following blood vessel sprouting and expansion, coverage of the blood vessels by pericytes results in mature and stable blood vessels, a step thought to be overridden in most cancers.

1.3.2.2 Co-option

Co-option is a mechanism by which tumour cells migrate towards, and colonise existing blood vessels (Holash et al. 1999 and Winkler et al. 2009). In addition to early development a number of tumours

also use this mechanism for invasion and expansion (Qian 2013). Hence, the proliferating and migratory tumour cells hijack the nearest capillaries for their nutrient and oxygen needs (Dome, Timar, and Paku 2003 and Dome, Timar, and Paku 2003)). It has been reported that co-option is common in blood vessel dense tissues like GBM (Coelho et al. 2017). For instance, Dome et al. demonstrated how glomeruloid bodies are formed from proliferating endothelial cells through co-option (Dome, Timar, and Paku 2003). They showed, using intracarotid artery injection of the melanoma cancer cell line A2058, that tumour blood vessels progressed from simple coiled structures at approximately 14 days post injection, to tortuous and chaotic glomeruloid vascular aggregates around 28 days post injection. Similarly, Kuczynski and co-workers observed in hepatocellular carcinoma formation of new blood vessels through co-option of normal blood vessels in the liver, which later became resistant to sorafenib treatment (Kuczynski et al. 2016). Co-option therefore uses pre-existing blood vessels, however this may take place alongside classic angiogenesis, while tumours may switch between these two modes following therapy. Further, these cellular mechanisms are tumour and organ specific, while their interchange may provide an escape mechanism from anti-angiogenic therapy (reviewed in Donnem et al. 2018).

1.3.2.3 Vasculogenesis

Vasculogenesis refers to the de novo formation of blood vessels (Chung and Ferrara 2011). Under this paradigm, endothelial progenitor cells (EPCs) mobilised from the bone marrow are the source of tumour blood vessel endothelial cells (Schiffer et al. 2015). CXCL12 and VEGF signalings have been implicated as a mechanism by which cancer cells recruit VEGFR2 expressing EPCs from the bone marrow (Soda et al. 2013). Although some studies reported the formation of tumour blood vessels from bone marrow derived EPCs as high as 18% in U87 glioma xenograft, other studies do not support the existence of vasculogenesis in GBM tumours (reviewed in Hardee and Zagzag 2012).

1.3.2.4 Vasculogenic mimicry (VM)

The term vasculogenic mimicry was first described in melanoma, when blood conducting channels were observed lined by melanoma cancer cells (Maniotis et al. 1999). Laser capture microdissection and gene profiling of blood vessels formed by VM and sprouting angiogenesis in melanoma showed the upregulation of angiogenesis and cancer cell related genes (Demou and Hendrix 2008). Common angiogenic molecules and signaling components identified in melanoma VM include VE-cadherin, EphA2, PI3K, FAK, MMPs and hypoxia related signaling pathways (Hendrix et al. 2016). Evidence for VM in GBM has been provided by Scully and colleagues who described blood vessels in patient tumours that are lined by cells expressing SMA, PDGFRβ and VEGFR2, but not CD31 or VE-Cadherin

(Scully et al. 2012). Expression of EGFR by these cells supported the idea that they originate from cancer cells (Scully et al. 2012).

1.3.2.5 Transdifferentiation

Ricci-Vitiani and co-workers showed that a large proportion of endothelial cells in GBM show similar genomic alterations to GSCs suggesting that endothelial cells in GBM have a neoplastic origin (Ricci-Vitiani et al. 2010). Using both *in vitro* and *in vivo* experiments the authors showed that endothelial-like cells were generated from GSCs (Ricci-Vitiani et al. 2010). While culturing GSCs produced endothelial-like cells, culturing of the non-stem cancer cells failed to do so. Using a mouse model GBM tumorigenesis, Soda and colleagues also showed that cancer cells may transdifferentiate to endothelial cells and form functional blood vessels (Soda et al. 2011). This was particularly observed in the deep hypoxic regions of the experimental tumours compared to their periphery, while hypoxia was shown to be the key driver of transdifferentiation of GSCs to ECs, a process refractile to VEGF inhibition which could explain the resistance of GBM to Avastin (Soda et al. 2011). In support, Wang and co-workers had demonstrated that it was only when Notch 1 or γ-secretase were inhibited, but not when VEGF or VEGFR2 were blocked that transdifferentiation of cancer cells to endothelial cells stopped (Wang et al. 2010).

1.3.3 Characteristic features of GBM blood vessels

Tumour blood vessels have been generally described as the most irregularly branched, haphazardly interconnected, chaotic, mostly immature, highly heterogenous ranging from leaky and thin walled, enlarged capillaries, to a network of glomeruloid blood vessels (Carmeliet and Jain 2011). Hence, tumour blood vessels are both structurally and functionally abnormal. Abnormally regulated proangiogenic growth factors are usually responsible for the formation of such highly branched, convoluted, enlarged and leaky blood vessels with poor blood flow (Hanahan and Weinberg 2011). Studies show the presence of both angiogenic and established vessels in GBM (Bergers and Song 2005). In much earlier experiments, Benjamin and colleagues had performed *in vivo* experiments whereby VEGF was conditionally expressed in the rat C6 glioma model. In the absence of VEGF all immature blood vessels regressed while the mature blood vessels which had already recruited pericytes persisted (Benjamin et al. 1999). They found that the proportion of immature blood vessels, which yet not recruited peri-endothelial cells, was proportionally higher in pre-clinical models but also in patient primary tumour samples.

Despite the lack of overall agreement on the characterisation of blood vessels in GBM (Preusser et al. 2006), the presence of certain morphologies has been associated with poorer patient prognosis. Rojiani and Dorovini-Zis identified aggregates of microvascular structures termed glomeruloids in 50% of the 24 GBM specimens analysed (Rojiani and Dorovini-Zis 1996). Further, characterisation of 78 GBM samples by Chen and colleagues using CD34/Periodic Acid-Schiff (PAS) dual staining identified 5 different clusters of microvascular patterns (MVPs) which were later classified into type I MVPs (microvascular sprouting and vascular cluster) and II MVPs (vascular garland, glomeruloid vascular proliferation and vasculogenic mimicry) (Chen et al. 2015). Accordingly, patients with more of type II MVPs had poorer PFS and OS compared to patients with type I MVPs (Chen et al. 2015). Similarly, Birner et al. using CD34 staining of 114 primary GBM patient samples found poor survival in patients with a higher proportion of abnormal vascular patterns (glomeruloid, garland and clusters), compared to patients with classical angiogenic blood vessel patterns (Birner et al. 2003).

1.4 Radiotherapy in GBM

1.4.1 Effects of radiation on GBM tumour growth

Ionising radiation kills tumour cells by damaging DNA and is an effective therapy in cancer (Baskar et al. 2014). Various doses of ionising radiation have been used in orthotopic mouse models of glioblastoma and shown significant reduction in tumour growth (Table 1.1). In patients, radiotherapy is the most important treatment modality, following gross resection, increasing patient survival by approximately 1 year (Zinn et al. 2013). However, development of radio-resistance and tumour recurrence, typically within a 2cm margin of the post-operative cavity, is an ongoing challenge (Li et al. 2018). GSCs are thought to be primarily responsible for radio-resistance and tumour recurrence, and interestingly they appear to localise in the SVZ between the striatum and the lateral ventricles from where they are thought to repopulate the excised tumour following irradiation (reviewed in Smith, Mehta, and Wernicke 2016). *In vivo* studies by Goffart and co-workers showed that SVZ located GSCs display a mesenchymal phenotype (Goffart et al. 2017). The molecular mechanism behind their radio-resistance was found to be upregulation of CXCL-12, and consequently, targeting the CXCL12/CXCR4 pathway improved the radio-sensitivity of GSCs. Further, using both *in vitro* and *in vivo* models Bao et al. demonstrated that $CD133^+$ enriched cancer stem cells were responsible for radio-resistance (Bao et al. 2006). When $CD133^+$ cancer cells were irradiated their $CD133^+$ expression increased by four-fold compared to untreated controls, while this was not observed in $CD133^-$ cells. Radiotherapy also increased the overall incidence of $CD133^+$ cells over 3-fold *in vivo* (Bao et al. 2006).

One interesting finding in the studies by Bao and co-workers was the presence of increasingly more activated checkpoint proteins such as ATM, Rad17, Chk1 and Chk2 in $CD133^+$ cancer cells compared to $CD133^-$ cancer cells following DNA damage. This eventually led to the downstream effect of cell cycle arrest and DNA repair, which was then reversed by checkpoint inhibition (Bao et al. 2006), demonstrating that radio-resistance may be overcome by inhibition of certain signaling pathways that are deregulated by ionising radiation. Analysis of samples taken from GBM patients before and after irradiation using micro-dialysis showed increased expression of IL-8, IL-6 and MCP-1 at various stages following therapy (Tabatabaei et al. 2017), suggesting that these molecules may also be involved in radio-resistance and may constitute potential therapeutic targets. In addition to upregulation of signaling pathways which promote survival, it has also been postulated that some cancer cells are intrinsically resistant to irradiation but the molecular basis of this resistance is not understood (Sambade et al. 2011). Interestingly, Huang et al demonstrated upregulation of activated caspase-3, an apoptotic marker, following irradiation *in vivo* which led to repopulation of tumour cells (Huang et al. 2011). Counterintuitively, this high caspase-3 expression was associated with high recurrence rate and poor prognosis. These observations were backed by *in vivo* experiments using both caspase-3 knockout mice and caspase-3 deficient tumours which showed increased radio-sensitivity in the absence of caspase-3 (Huang et al. 2011). Interestingly, high caspase-3 expression has also been associated with poor survival in breast cancer patients (Pu et al. 2017).

1.4.2 Effect of irradiation on the tumour vasculature

Ionising radiation targets dividing cells. Like cancer cells being highly proliferative, tumour ECs also proliferate at a 20-2000 times faster rate than ECs in normal tissue. This effectiveness of radiation against cancer cells and the microenvironment has established radiotherapy one of the most commonly applied therapeutic tools in cancer patients (Hobson and Denekamp 1984). However, although irradiation does target ECs, its effects on other components of the tumour microenvironment are highly complex and mainly involve inflammation and immunomodulation, hypoxia, revascularisation and ECM remodelling which may support, rather than compromise tumour growth (Barker et al. 2015). For instance, hypoxia not only hinders the effects of radiotherapy and immunotherapy (Barker et al. 2015), but also plays an important role in promoting tumour cells to migrate from perinecrotic region to blood vessel rich regions as a result of up-regulation of HIF-1 (Harada et al. 2012).

Following irradiation, unlike ECs in normal blood vessels, tumour ECs undergo G2 arrest (senescence), both *in vitro* and *in vivo* (Borovski et al. 2013). *In vitro*, irradiation with as small a dose as 2Gy results

in reduced survival of HUVEC (Helm et al. 2016). Various doses of ionising radiation have been used in orthotopic mouse models of glioblastoma as shown in Table 1.1 with varying responses to which endothelial damage appeared to contribute. Although there are some contradicting reports regarding the effect of radiation on brain tumour blood vessels, overall an optimal radiation dose of 5-10Gy/fraction appears to have a measurable but limited effect on the morphology and function of the tumour vasculatures at early stages of growth, while this effect diminishes as the tumour advances. However, higher doses of irradiation (>10Gy/fraction) can damage blood vessels and contribute to tumour regression (reviewed in Park et al. 2012). Interestingly, larger blood vessels appear more radioresistant, as in a human melanoma xenograft irradiation experiment *in vivo* 5-15 μm blood vessels were significantly damaged by 16Gy irradiation doses, while larger, 25-35 μm diameter blood vessels required a higher dose of 20Gy to regress (Park et al. 2012).

Studies show that radiation induces detachment of ECs from the basement membrane, increased endothelial cell permeability, recruitment of immune cells, increased acid sphingomyelinase which is linked with vascular damage and development of hypoxia (reviewed in Barker et al. 2015). Hence, one characteristic feature of the irradiated tumour is the reduction of tumour microvascular density (MVD), which subsequently leads to decreased vascular perfusion and increased tumour hypoxia (Tsai et al. 2005). Furthermore, some of the structural changes of tumour blood vessels following irradiation include thickening of the intima and consequently atherosclerosis, thrombosis, fibrosis and necrosis (Barker et al. 2015). However, the effect of radiotherapy on tumour vasculature also depends on several factors including the location, size, stage of tumour and dose of radiation used, the characteristic nature of high endothelial cell proliferation rate, presence of basement membrane and pericyte coverage of blood vessels in the tumour compared to the surrounding parenchyma (Barker et al. 2015). For example, Potiron et al. observed increased susceptibility of tumour blood vessels to irradiation when pericyte coverage was less (Potiron et al. 2013). However, Tsai and co-workers had provided earlier evidence that pericytes do not protect ECs from irradiation (Tsai et al. 2005).

Different signaling mechanisms have been identified in tumour regrowth following irradiation which may involve effects on the vasculature. For instance, radiation induces the expression of CXCL12, which in turn promotes vasculogenesis by recruiting $CD11b^+$ monocytes (Walters et al. 2014). In an *in vivo* experiment, when Liu et al. blocked the chemokine CXCL12 following irradiation, this inhibited recurrence of a rat brain tumour (Liu et al. 2014). In another *in vivo* experiment using a combination of CXCR7 blockade and irradiation, significantly reduced tumour growth and recurrence in mice were observed (Walters et al. 2014). Irradiation also activates inflammatory signals (TNF-α and IL-1) and

increases recruitment of local immunosuppressive and relatively radioresistant tumour associated macrophages (TAMs), myeloid-derived suppressor cells (MDSCs) and regulatory T cells (Tregs) (Barker et al. 2015). Hence, despite its effectiveness in targeting cancer cells and blood vessels, radiation also modulates the tumour microenvironment in a way conducive to tumour progression. Normalisation of these microenvironmental responses should increase the effectiveness of radiotherapy in the treatment of brain tumours.

1.4.3 Effects of radiation on tumour invasion

Despite its popular usage in cancer treatment, ionising radiation increases the invasive potential of several cancer cells including breast, brain and lung (Artacho-Cordon et al. 2012). One of the mechanisms of this increased invasiveness is the upregulation of MMPs (Artacho-Cordon et al. 2012). Hence, both *in vivo* and *in vitro* experiments have implicated several genes in the induction of tumour invasion in response to irradiation. One of the characteristics of this increased invasiveness following irradiation is the change of cell morphology. For instance, in endometrial carcinoma, ionising radiation increased cell invasion of HEC1A cells through epithelial-mesenchymal transition (EMT) and upregulation of Twist, inhibition of which reduced invasion (Tsukamoto et al. 2007). Fujita et al. demonstrated increased invasiveness of the normally amoeboid pancreatic cancer cell line MIA PaCa-2 following ionising irradiation through increased expression of MMP-2, while inhibition of MMP2 induced the reverse of EMT mesenchymal-amoeboid transition (Fujita et al. 2011). In *in vivo* experiments using the C6 cell line Park et al. demonstrated increased metastasis of cancer cells following radiotherapy through activation of markers associated with EMT markers including MMPs (Park et al. 2012). In human melanoma irradiation increased IL-8 mRNA production and tumour metastasis *in vivo* in immunocompromised mice.

In U251 cells, ionising radiation highly upregulates expression of the MET oncogene through activation of the ATM-NF-*k*B pathway, which consequently leads to tumour invasion and radioresistance (De Bacco et al. 2011). Using a spheroid assay Gogineni et al. reported a reduced invasion and consequent apoptosis of malignant meningioma cells in siRNA mediated knockdown of MMP-9 and this was through activation of MAPK-ERK & AKT signaling pathways (Gogineni et al. 2009). Similarly, in both U87 and U251 glioma cell lines, inhibition of MMP-2 using siRNA and radiotherapy significantly reduced cancer cell growth, invasion and angiogenesis in spheroid assays (Badiga et al. 2011). Further, using matrigel assay, Dong et al. demonstrated increased invasion of U87 cells in response to irradiation through nuclear translocation of ß-cantenin (Dong et al. 2015). The translocation of ß-cantenin into the nucleus increased transcription and upregulation of downstream target genes

including MMP2/9, AXIN2, CD44 and VEGF (Dong et al. 2015). It has also been demonstrated that irradiation increase IL-8 secretion from melanoma cells and in *in vitro* experiments using matrigel, IL-8 transfected melanoma cells up-regulated MMP-2 and increased invasion (Luca et al. 1997). Ionising radiation also increased migration and invasion of neuroblastoma cells in spheroid and matrigel assays by increasing expression of MMP-9, VEGF and uPA. Altogether, these studies support the presence of a common mechanism by which ionising radiation increases nuclear translocation of ß-cantenin in cancer cells with subsequent increase in invasion through upregulation of MMPs and other matrix modifying enzymes, and concomitant increase in angiogenic factors (Gialeli, Theocharis, and Karamanos 2011). In support, conditioned media from irradiated neuroblastoma cells increased angiogenesis in human microvascular endothelial cells (HMECs) (Jadhav and Mohanam 2006).

There is evidence that Rho GTPase signaling play a role in the stimulation of invasion in response to irradiation. ROCK and Rac1 have an opposing effect on glioma invasiveness. While activation of Rac1 increases cell invasion, this invasion was supressed when ROCK was activated (Hara et al. 2016). Further, the role of Rac in cell migration and invasion has been somewhat controversial and reported to depend on cell type. For instance, in the rat glioma cell line C6 suppression of Rac by dominant-negative Rac (RacN17) increased cell migration and this migration was further stimulated by irradiation (Hwang et al. 2006). However, it must be noted that the use of dominant negative counterparts of Rho GTPases is unreliable, as their overexpression may act to mop up guanine nucleotide exchange factors (GEFs) and GTPase activating proteins (GAPs) which act on multiple Rho proteins. Nevertheless, those studies eluded to a mechanism of increased migration through activation of JNK and reduction of adhesion molecules such as paxillin and FAK (Hwang et al. 2006). Interestingly, Rac1 knockdown reduces random cell motility but increases directional migration in U87 cells (Pankov et al. 2005), suggesting that the levels of Rac1 activation must be accurately controlled during the process of invasion.

Table 1.1 Review of published *in vivo* brain tumour experiments to determine the effects of RT

Sr. No.	Tumour model	Strain, Sex, age	Dose	Irradiation post implantation	Effects of radiotherapy	Reference
1	GL261	C57BL/6J mice Female 10-12 weeks old	8Gy WBRT 4Gy/day 24hr interval	Day 15 & Day 17	Improved survival (6 days). Combination with immunotherapy (83 days).	(Newcomb et al. 2010)
2	GL261	C57BL/6J mice Female 6-8 weeks old	20Gy WBRT 2Gy/ day	Day 10	Improved survival (21 days). Reduced invasiveness in combination with CXCR4 targeting (37 days).	(Yadav et al. 2016)
3	SMA-560 (murine glioblastoma)	Syngenic VM/Dk mice	6Gy	Day 4	Improved survival (14 days) in combination with blocking CD95L (Fas ligand).	(Blaes et al. 2018)
4	U87-MG	Nude mice Female 5-6	30Gy Subcut 5Gy/ day	Day 5	Improved survival (6 days).	(Bradley et al. 1999)
5	U87-MG	Balb/c_Nude mice Female 8-week old	10Gy Focal RT 2Gy/ day	Day 15	Improved survival in combination with targeting of TIGAR expressed in glioma cells.	(Zhang et al. 2017)
6	C6 glioma	Wistar rats Male 6-8 weeks old	40Gy WBRT 8Gy/ day	Day 5	Improved survival (~10 days). Increased tissue permeability.	(Zawaski et al. 2012)
7	Patient-derived GBM (U1242)	Nude mice Female	10Gy WBRT 2.5Gy/ day	Day 11	Improved survival (21 days). Combination with inhibitor of gene MDA-9/Syntenin (37 days).	(Kegelman et al. 2017).
8	Patient-derived GBM (GB130)	Nude mice	30Gy 6Gy/ day	Day 75 AMD treatment D70	Inhibition of CXCL12 with AMD improved sensitivity.	(Goffart et al. 2017)

Table shows different tumour models used in pre-clinical studies *in vivo* ranging from GBM syngeneic models to established cell lines and patient-derived GBM cancer cells orthotopically implanted in mice followed by delivery of whole brain irradiation (WBRT) or focal irradiation. The time and dose of irradiation varies and in most cases the total dose was delivered over days in a fractionated form. In general, there was significantly higher overall survival in response to irradiation which improved further in some combination therapies.

1.5 Dedicator of cytokinesis 4 (DOCK4)

Mammalian Rho GTPases comprise 20 small intracellular signaling molecules which regulate normal cell migration and tumour metastasis, through control of the actin cytoskeleton amongst other mechanisms of action (Hiramoto, Negishi, and Katoh 2006). The prototypical members of Rac1, RhoA and Cdc42 have been studied extensively (Etienne-Manneville and Hall 2002; Kobayashi et al. 2014 and Gadea and Blangy 2014). The majority of Rho proteins cycle between a GTP-bound active and a GDP-bound inactive form (Figure 1.3). This cycling is regulated by positive regulators, guanine exchange factors (GEFs) which catalyse the exchange of GDP for GTP and negative regulators, GTPase-activating proteins (GAPs) which accelerate the intrinsic GTPase activity for the hydrolysis of GTP to GDP. Guanine nucleotide-dissociation inhibitors (GDIs) retain GDP-bound Rho proteins in the cytoplasm precluding their activation by GEFs in the plasma membrane (Ridley 2012; Bustelo, Sauzeau, and Berenjeno 2007 and Nobes and Hall 1995). There are 11 mammalian subfamilies of the Dock180 superfamily which serves as a GEF for the Rho family GTPases (Hiramoto, Negishi, and Katoh 2006). Dock4, dedicator of cytokinesis 4, located on chromosome 7q31 in human (Yajnik et al. 2003), is a member of the evolutionarily conserved superfamily of Dock180 proteins which regulates several biological activities within a cell by activating Rho GTPase signaling (Cote and Vuori 2002).

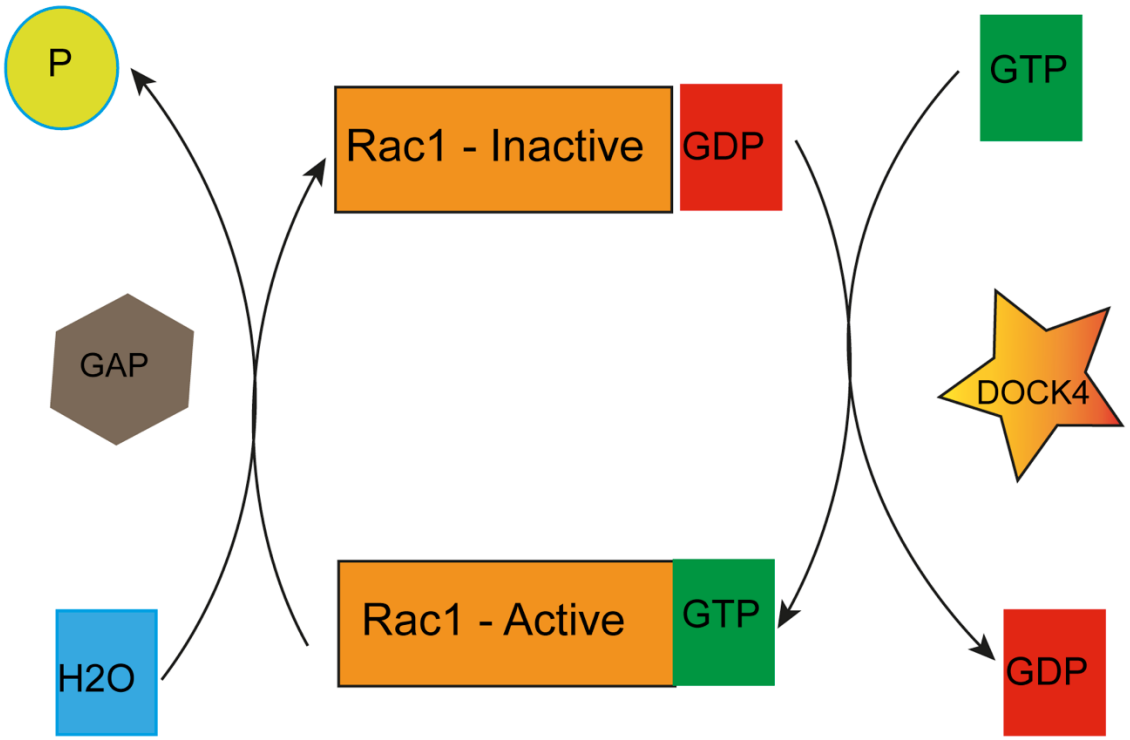

Figure 1.3 The role of DOCK4 in Rac1 cycle

DOCK4 activates a GDP bound inactive Rac1 through addition of phosphate group, GTP, and cycle continues by GAP which removes a phosphate group from GTP bound active Rac1 back to inactive and GDP bound Rac1.

Adherens junctions are transmembrane molecules which has an important role in vasculogenesis and angiogenesis through cell-cell adhesion, cell morphogenesis and intracellular signaling mechanisms (Petzelbauer, Halama, and Groger 2000). DOCK4 activates Rap GTPases which results in increase of adherens junctions and tighter cell-cell contacts (Yajnik et al. 2003). In HEK293T cells Hiramoto et al showed that DOCK4 is a GEF for Rac1 and that consistently, DOCK4 interacts with Rac1 but not with Cdc42 or RhoA (Hiramoto, Negishi, and Katoh 2006). The DHR-1 (CZH-1) and DHR-2 (CZH-2) domains of DOCK4 (Figure 1.4) are conserved throughout all the DOCK180 family, while in addition DOCK4 possess an SH3 (Src-homology 3) domain at its N-terminus and proline-rich region on its C-terminus (Hiramoto, Negishi, and Katoh 2006). The DHR-2 domain mediates the exchange of GDP for GTP and thus a DOCK4 mutant which lacks the DHR-2 region does not activate Rac1 (Hiramoto, Negishi, and Katoh 2006). Being a large multimeric protein DOCK4 is able to interact with other proteins, namely ELMO (Xiao et al. 2013 and Hiramoto, Negishi, and Katoh 2006)) and DOCK9 (Abraham et al. 2015) through its SH3 domain (Abraham et al. 2015), and with cortactin (Ueda et al. 2013).

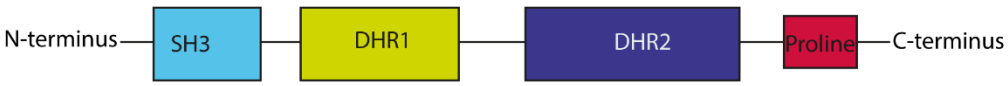

Figure 1.4 The structure of DOCK4

DOCK4 has DHR1 and DHR2 domains, which are ubiquitously conserved in all DOCK families, and SH3 domain on its N-terminus while proline-rich domain is located on the C-terminus.

1.5.1 The role of DOCK4 in angiogenesis

The Rac subfamily of Rho GTPases, Rac1, Rac2, Rac3 and RhoG proteins share sequence similarity and stimulate lamellipodia formation and extension of cell membrane during phagocytosis by activation of Rac GEF DOCK180 proteins (Heasman and Ridley 2008). For instance, attachment VEGF ligand to its cell surface receptor VEGFR2 activates an intracellular Rho GTPase signaling cascade that leads to the induction of angiogenesis (Holmes et al. 2007; Eilken and Adams 2010 and Abraham et al. 2015). Tan et al demonstrated how Rac1 is involved in EC migration, lumen formation, and adhesion in response to VEGF and sphingosine-1-phosphate (S1P) (Tan et al. 2008). Once Rho proteins are activated they interact with the proteins known as effectors to initiate cellular responses including migration, adhesion, morphogenesis, and neuronal development (Heasman and Ridley 2008).

Abraham et al showed the role of the DOCK4-Rac1 signaling axis in sprouting angiogenesis (Figure 1.5) through the control of filopodia formation downstream of RhoG activation (Abraham et al. 2015). ELMO is a downstream effector of the DOCK4-Rac1 axis, while Rac1 activation by DOCK4 activates Cdc42 through the GEF DOCK9 (Figure 1.5). The study further demonstrated that DOCK4 controls blood vessel lumen formation in a tissue culture organotypic angiogenesis assay through early remodelling of the actin cytoskeleton and lateral cell-cell adhesion; and blood vessel lumen size in the normal brain, and in a model of breast cancer brain metastases (Abraham et al. 2015). DOCK4 controls lateral filopodial protrusions in endothelial cells however, proximal tip filopodia can exist in the absence of Dock4 (Abraham et al. 2015). The work of Abraham et al concluded that the signaling cascade of RhoG-Dock4-Rac1-Dock9 and Cdc42 (Figure 1.6) leads to the formation of lateral filopodia, which is important in sprouting angiogenesis (Abraham et al. 2015).

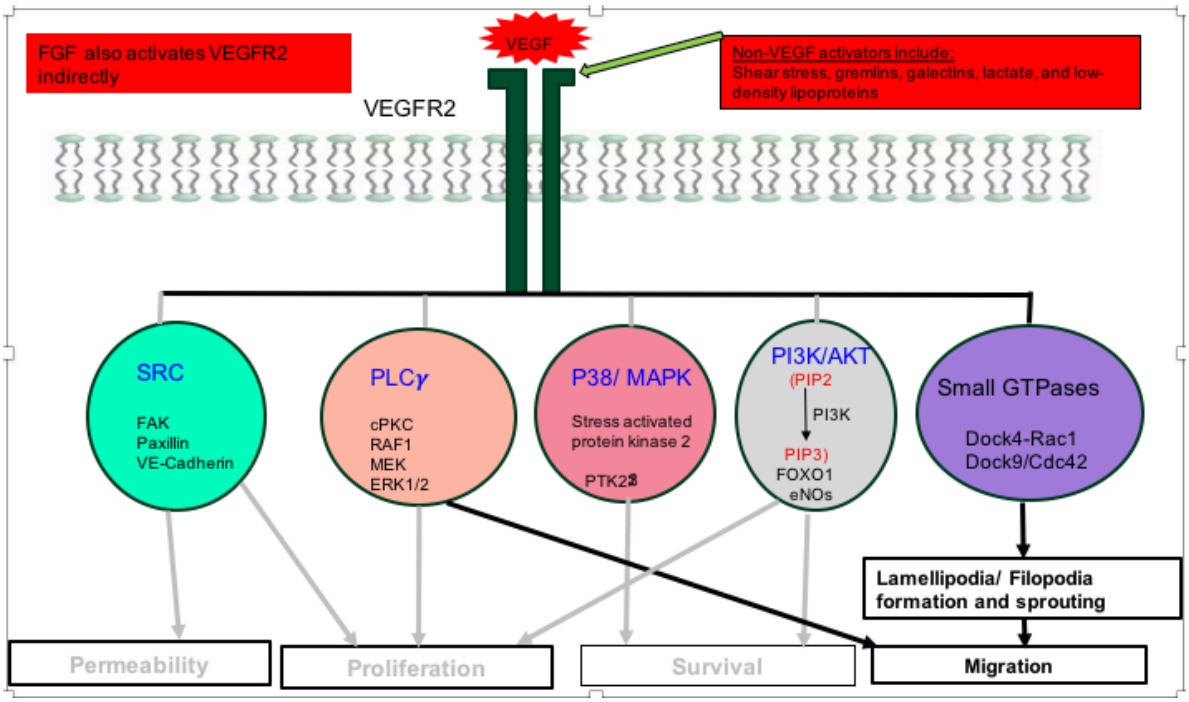

Figure 1.5 VEGF downstream signaling pathway in endothelial cells (ECs)

The DOCK4 signaling pathway controls filopodia formation and lumen size by switching the GDP-bound inactive form of Rac1 into GTP-bound active state of Rac1, and regulating filopodia formation and sprouting at the downstream of VEGF. Modified from Lena Claesson-Welsh [(Simons, Gordon, and Claesson-Welsh 2016). Nat Rev Mol Cell Biol 2016].

1.5.2 The role of Dock4 in neuronal cells and cancer cells

DOCK4 and Rac1 are essential for normal development as their global deletion is embryonic lethal (Heasman and Ridley 2008 and Abraham et al. 2015). Furthermore, both Rac1 and DOCK4 are highly expressed in the brain with DOCK4 expression being more restricted to neuronal cells and endothelial cells (Ueda et al. 2008 and Abraham et al. 2015). DOCK4 is temporally regulated during rat brain development with expression detected from E18 through to the adult stage reaching the highest levels on postnatal day 20 in hippocampal neurons (Ueda et al. 2008). When different regions of the brain were compared the highest DOCK4 expression was found in the hippocampus, cortex and cerebellum, in a decreasing order. DOCK4 is particularly localised in dendritic spines and plays an important role in spine formation by interacting with cortactin, while dysfunction of DOCK4 in dendrites resulting from germline mutations is associated with psychiatric problems such as schizophrenia, autism and dyslexia (Gadea and Blangy 2014). In an *in vitro* cultured hippocampal neurons experiment, knockdown of DOCK4 resulted in impairment of dendritic growth and branching which was reversed by overexpression of DOCK4 and its binding partner ELMO (Ueda et al. 2008).

The fact that DOCK4 controls both cell-cell adhesion and migration makes it both a tumour suppressor and tumour promoter (Gadea and Blangy 2014). Studies reported Dock4 mutations in ovarian cancer, human prostate, gliomas, breast and mouse osteosarcoma cells (Kuo et al. 2009 and Yajnik et al. 2003). Kuo et al detected homozygous Dock4 deletion in high grade serous carcinoma using SNP arrays and analyses of DNA copy number changes in 37 ovarian serous neoplasms (Kuo et al. 2009). Quantitative real-time PCR analysis detected downregulation of several genes including Dock4 in $CD133^{+}/CD34^{+}$ cancer cells from chronic myeloid leukemia patients (Okamoto et al. 2007). Sundaravel et al found a low expression of DOCK4 in myelodysplastic syndromes (MDS) (Sundaravel et al. 2015). Recently, Debruyne and colleagues found reduced expression of DOCK4 in mitotic, proliferative and SOX2 & OLIG2 positive GBM cells (Debruyne et al. 2018). However, in breast cancer cells DOCK4 controls migration suggesting it may be involved in the process of metastasis. DOCK4-dependent activation of Rac1 downstream of EGFR and EphA2 (Figure 1.6) is regulated by the small GTPase RhoG and requires the downstream effector ELMO (Hiramoto, Negishi, and Katoh 2006). It has been observed that EphA2, DOCK4 and the actin regulator cortactin co-localise at the tip of migrating breast cancer cells and in such cells activated RhoG binds to ELMO and then recruits DOCK4 to form a complex which translocate to the plasma membrane where it activates Rac1 (Hiramoto, Negishi, and Katoh 2006). In support of its putative role in breast cancer metastasis DOCK4 was found to be a potential biomarker of the risk of breast cancer metastasis to the bone (Westbrook et al. 2018). In lung adenocarcinoma (ADC) high DOCK4 expression has been directly associated with increased Smad activation and poor

patient survival, implying essential role of DOCK4 in the TGF-β/Smad pathway to enhance the extravasation and metastasis of lung cancer cells to the liver (Yu et al. 2015). The mechanism for this involvement of DOCK4 in the Wnt pathway had been demonstrated earlier by Upadhyay and colleagues (Upadhyay et al. 2008).

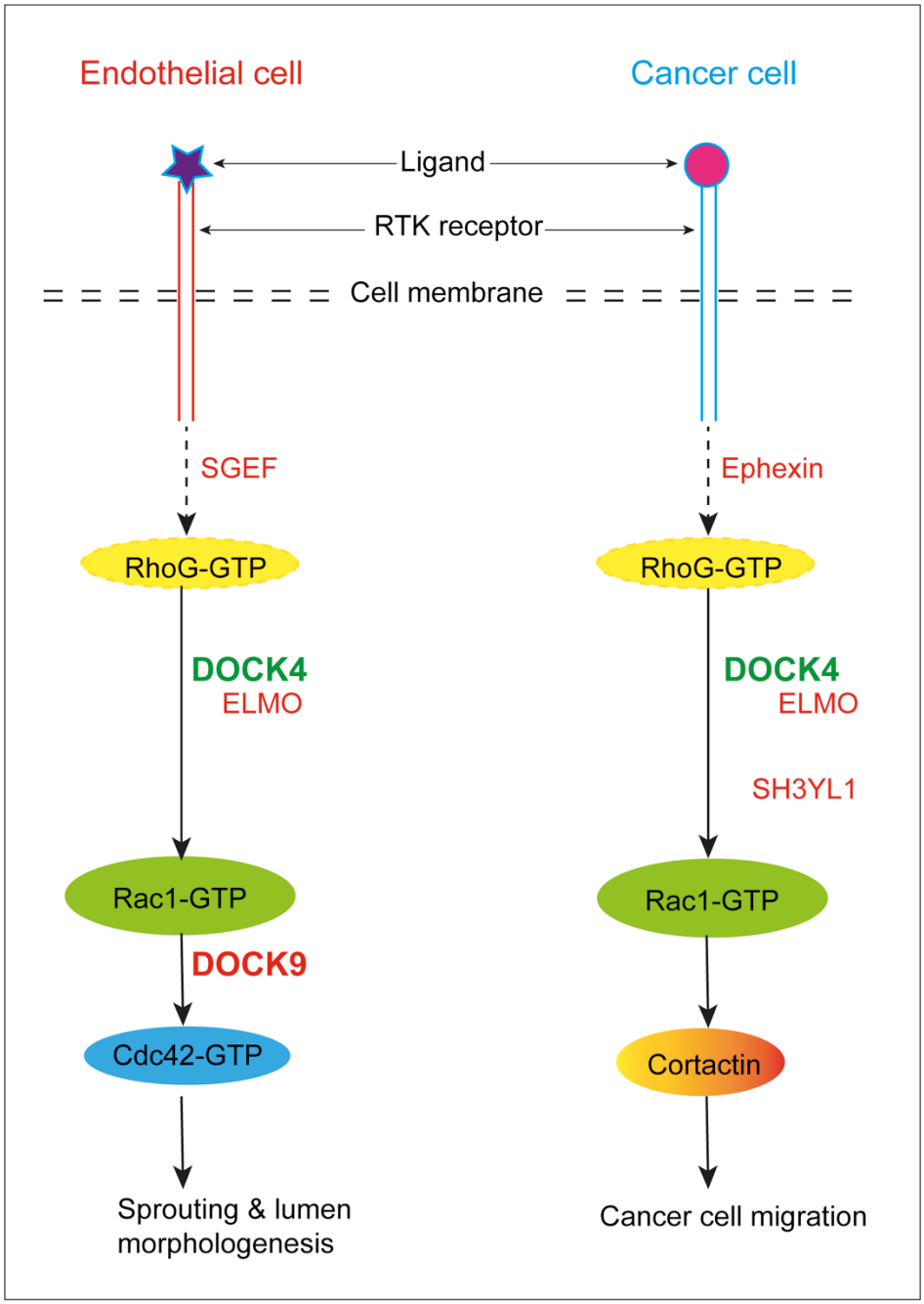

Figure 1.6 DOCK4 signaling pathway in endothelial cells and cancer cells

DOCK4 functions downstream of the tyrosine kinase receptor (RTK) VEGFR2 in endothelial cells, and EGFR in cancer cells to regulate actin cytoskeleton, sprouting angiogenesis and cancer cell migration.

Normally, β-catenin interacts with protein complex which includes adenomatosis polyposis coli (APC), the signaling scaffold protein Axin, and serine-threonine kinase glycogen synthase kinase 3β (GSK3β) which phosphorylates β-catenin. This allows its ubiquitination and degradation by the proteasome (Choi et al. 2004). When Wnt3A binds to its surface receptor DOCK4 interacts with the degradation complex and displaces β-catenin leading to its stabilisation and subsequent translocation to the nucleus where it serves as transcription factor (Figure 1.7) leading to increased cell growth and neoplasia (Upadhyay et al. 2008). Differentiated GBM cancer cells respond differently to β-catenin translocation to the nucleus with growth arrest, explaining the tumour suppressing effects of DOCK4 overexpression in GBM cancer cells (Debruyne et al. 2018). Consistently, Debruyne et al found low levels of DOCK4 in GBM cancer stem cells (Debruyne et al. 2018), but the effects of DOCK4 knockdown were not investigated. Altogether, these published studies show that DOCK4 plays different roles in different cancers and at different stages of tumour development and progression.

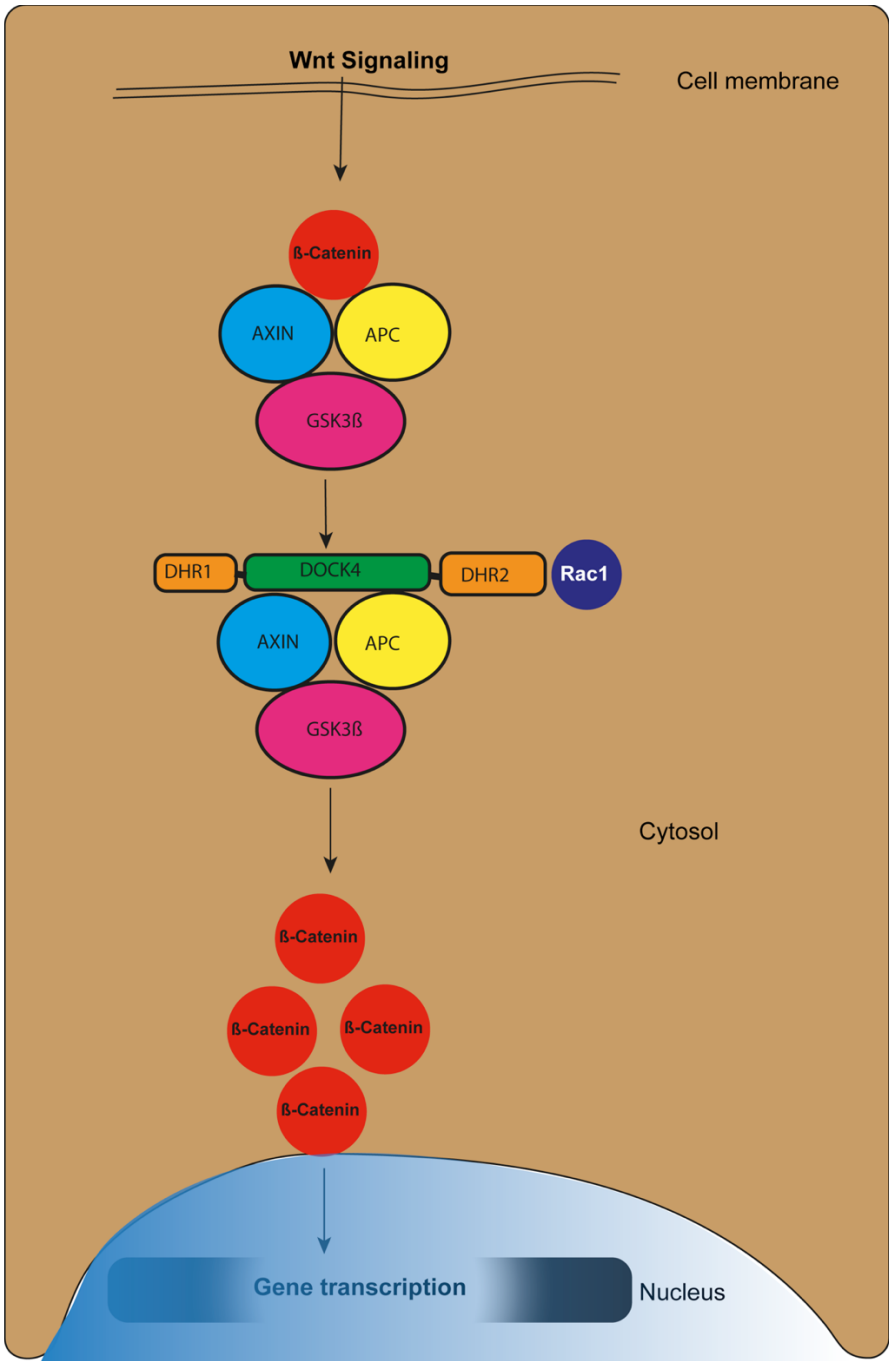

Adopted from Upadhyay et al., 2008

Figure 1.7 DOCK4 forms complex with GSK3β, AXIN and APC downstream of Wnt signaling

Figure depicts the involvement of DOCK4 in Wnt signaling. In absence of DOCK4 GSK3β phosphorylates β-catenin allowing its degradation by the proteasome (not shown). However, when DOCK4 binds AXIN and APC, β-Catenin is released from the degradation complex resulting in its translocation into the nucleus where it activates gene transcription.

Chapter 2

Materials and Methods

2.1 Cell culture techniques

2.1.1 Cell lines

Patient-derived GBM cells, GBM1 and GBM20, originally isolated by Wurdak et al, were kindly obtained from Prof Susan Short's lab, Leeds Institute of Medical Research at St James's (LIMR, University of Leeds). The established cell line U251 (Sigma Aldrich) was also obtained from Prof Susan Short's lab. CT2A cell line which was originally from David Stojdl and Charles Lefebvre of the Children's Hospital of Eastern Ontario (CHEO) Research Institute in Ottawa, Canada was kindly donated by Dr Wurdak's Group (LIMR, University of Leeds). GL261 murine cancer cells were from Dr G Mavria's lab (LIMR, University of Leeds). While Human Umbilical Vein Endothelial Cells (HUVEC) and Human Embryonic Kidney (HEK 293T) cell line (originally from Clontech Laboratories) were from Mavria's lab, the Human Cerebral Microvascular Endothelial Cells (HCMEC) were kindly donated by Prof Cook's group (LIMR, University of Leeds).

2.1.2 Coating cell culture flasks

Unlike U251, GL261 and CT2A, the patient-derived primary samples do not grow in non-coated normal flasks. Hence, any flasks used to grow these patient-derived GBM cells were coated firstly with poly-L-ornithine (Sigma P3655 (100μg/10ml/T75 flask in TC grade water)) and kept at room temperature for 1 hr before washing it off with TC grade water. Then, each flask was coated again with laminin (Invitrogen 10267092 (20ug/ 10ml/T75 flask in TC grade PBS)). These flasks were sealed and left overnight at room temperature and then stored in a freezer until needed or used straightaway. HEK 293T cells and HCMECs flasks were coated using either Poly-L-lysine (Cat.No. P8920, Sigma-Aldrich) in a 1:40 dilution in PBS or 0.2% gelatin freshly prepared in the lab.

2.1.3 Culturing mammalian cells

GBM1 and GBM20 cells were cultured in neurobasal medium (Invitrogen #21103049) with supplements including 0.5 x B27 Serum-Free Supplement (Invitrogen #17504044) and 0.5 x N2 Supplement (Invitrogen #17502048), and growth factors 40 ng/ml recombinant human EGF (R&D Systems #236-EG-200) and 40 ng/ml recombinant human basic fibroblast growth factor (bFGF) (R&D Systems #233-FB-025/CF) in laminin-coated flasks. The cells were trypsinised when they reached about 80% confluence and centrifuged at 1200 rpm for 3 minutes in order to get rid of trypsin before passaging or using for the next experiment. Both CT2A and GL261 cancer cell lines were cultured in Dulbecco's Modified Eagle's Medium (DMEM) (Sigma Life Science) supplemented with 10% foetal calf serum (Gibco), 1% L-Glutamine (Gibco) and 1% penicillin and streptomycin (Gibco). U251 cells were

cultured in a similar medium as CT2A and GL261 cell lines except the absence of L-Glutamine. All cells were cultured in appropriate flasks and kept in a humidified incubator at 37°C with 5% CO2.

Both HUVEC and HCMEC cells were cultured on Poly-L-lysine coated flasks using Human Large Vessel Endothelial Cell (HLVEC) basal medium (Cat. No. KC1015) supplemented with growth factors (KC1014) and antibiotic, Amphotericin B/Gentamycin, 1000X (KC1019). HEK 293T cells were cultured on poly-lysine coated flasks using DMEM basal medium supplemented with 10% FBS (Biosera Ltd), 1% L-Glutamine, and 1% P/S (Sigma Aldrich). All cultured cells were allowed to grow in a 37^0C incubator with 5% CO_2 and cells were trypsinised and passaged when they reached ~ 80% confluence. Cells were frozen down using 90% foetal calf serum (FCS) and 10% dimethyl sulfoxide (DMSO) and were temporarily kept in -80^0c freezer until they were moved into liquid nitrogen for a long-term storage.

2.1.4 Standard solutions

The lists of different solutions used throughout this thesis for purposes like cell culture, western blot (WB), polymerase chain reaction (PCR), spheroid assay and IHC/IF are shown in Table 2.1. These solutions were either purchased or prepared in the lab.

Table 2.1 Commonly used standard solutions in this study

Sr.No.	Solution	Recipes or Cat. No
1	PBS	500 ml distilled water (disH_20) + 2 PBS tablets (Cat.No. P4117, Sigma) + 1 PBS tablet (Ca.No. BR0014G, OXOID)
2	Lysis Buffer (PCR)	100 mM Tris (PH 8.5), 5 mM EDTA, 0.2% SDS, 200 mM NaCl
3	Lysis buffer (WB)	50 mM TRIS PH 7.4, 10% Glycerol, 1% NP40, 5 mM MgCl2, 100 mM NaCl
4	Rac Lysis buffer	50 mM TRIS PH 7.4, 10% Glycerol, 1% NP40, 5mM MgCl2, 100 mM NaCl, 25x Complete Inhibitor (no EDTA) and 1mM DTT
5	10xTBS	100 ml 1M Tris-Base PH 7.5 + 200 ml 5M NaCl (900 ml disH_20 + 24 gm Tris Base + 88 mg NaCl)
6	1xTBS	900 ml disH_20 + 100ml 10xTBS
7	TBST	1xTBS + 0.1% Tween-20 (900 ml disH_20 + 200 ml 10TBS + 1 ml Tween-20)
8	Running Buffer	50 ml 20xT.A + 950 ml disH_20
9	Transfer Buffer	70% disH_20, 20% methanol and 10% 10XTBS
10	4% PFA	500 ml PBS + 20 gm PFA powder (PH adjusted using 1M NaOH)
11	5X DMEM	100 ml disH220 + 6.74 gm DMEM + 40 gm or 1.85 gm or 0.37gm NaHC03
12	Laura Broth (LB) medium	20 gram LB powder in 1 litre distilled water and then autoclaved
13	LB agar	15 gram agarose powder in 1 litre LB medium
14	Tris-EDTA (TE) buffer (PCR)	5ml 1M Tris (PH8), 1ml 0.5M Na_2EDTA
15	Access Revelation (10x)	Antigen Retrieval (Cat.No. MP-607-X500, MenaPath)
16	TBS Automation Wash Buffer (20x)	Washing buffer (Cat. No. MP-945-X500, MenaPath)
17	5xDMEM	674 mg of DMEM powder + 37 mg of NaHCO3 in 10ml distilled water

2.1.5 Culturing bacteria

A total of 6 plasmids including Dock4sh1, Dock4sh2, empty vector and non-targeting, envelope (pMD2G) and packaging (psPAX2) were amplified from scrapes of stock plasmid glycerol with ampicillin (100 μg/ml) in a liquid broth (LB). The mix was incubated overnight at 37^0C in a shaking incubator (220/min) and next day the mix was centrifuged at full speed for 30-45 minutes once aliquoted into 50 ml falcon tubes. This was followed by either maxiprep (Life Technologies) or Miniprep (QIAGEN) for purification of plasmid DNA. As the total DNA production from the maxiprep and miniprep was too small, particularly for the packaging and envelope plasmids, I transformed more plasmids from StbI3 E.Coli which was stored in our lab at -80°c. Briefly, 20-30ul of StbI3 was aliquoted into 3 different eppendorf tubes and 1μl each from pGIPZ1, pPAX and pMD2 plasmids were added to respective tubes and placed on ice for 30 minutes without mixing by pipetting. The bugs were heat-shocked by incubating on 42^0c for 45 seconds and placed back on ice and kept for 2 minutes. After this, 250 μl LB medium was added to each tube and incubated for 1 hr in a shaking incubator at 225 rpm in a 37^0c incubator. After 1hr, 200 μl was taken from each eppendorf tubes and plated on pre-warmed agar plate with ampicillin and incubated overnight at 37^0c. Next day, 2-3 colonies from the plates were seeded in a 15 ml falcon tubes containing LB in the presence of ampicillin and run overnight in an incubator at 225 rpm at 37^0c and continued with miniprep then after.

2.1.6 Lentivirus production

Following purification of enough DNA plasmids the Trono lab protocol was followed to generate the respective lentiviruses. Briefly, HEK 293T cells were seeded on Poly-Lysine (Sigma) coated 10 cm dishes at a density of $4x10^6$ cells and the next day, cells were transfected with lentiviral plasmids in Opti-MEM (Gibco) using Lipofectamine 2000 (Invitrogen) when they reached 70-80% confluence they. Medium was removed on second day following lentiviral transfection and fresh medium was added. The supernatant was harvested on third day and filtered through 0.45 μm Millex HV filter and stored as first harvest and then repeated on day 4 and stored as second harvest. Both harvests were kept in -80^0c until required for transduction.

2.1.7 Lentiviral transduction

Dock4 shRNA

In order to knockdown DOCK4 protein from cancer cells, DOCK4 shRNA plasmids, which were originally from Dharmachon GE Life Science, were transduced into cancer cells. Two types of DOCK4 shRNA were used:

DOCK4 shRNA1 mature antisense – CTCAGTATTTGCAGATATA and

DOCK4 shRNA2 mature antisense - CGCAAGGTCTCTCAGTTAT

Cells to be transfected (U251 and patient-derived GBM1) were cultured and brought to confluence, 50-80%, before transducing them with lentivirus (virus to media ratio was 1:5 for Dock4 and 1:10 for empty vector). Lentiviral vectors play an important role in transducing Dock4 shRNA into the cell nucleus and consequently knockdown a gene of interest. The cell cultures were incubated at 37°C in a humidified incubator with 5% CO_2 overnight with the lentivirus and polybrene at 1µl/1ml of the transfection solution. The media was replaced the next morning with a fresh media. The transfection efficiency was monitored using vector incorporated reporter genes such as enhanced green fluorescent protein (eGFP), which gives green fluorescent light when observed under EVOS® microscope after 24 hrs.

2.1.8 Cell sorting

Transduced cells were trypsinised, mostly after 72 hrs, neutralised with cell culture medium, centrifuged, filtered and collected in polystyrene capped 5ml FACS tubes at a maximum concentration of $5x10^6$ cells/ml. Cells were sorted using the LIMM cell sorting facility for the brightest cells. GFP positive cells were cultured for experimental use and in order to confirm efficiency of DOCK4 gene knockdown cell lysates were prepared and used to run western blot (WB).

2.1.9 Cell lysate and Western blot

For WB assay cells were cultured on 10 cm plate and allowed to grow to a confluence of ~80% and lysed using lysis buffer (Table 2.1). A typical 1ml Rac lysis buffer was composed of 50µl of 1M TRIS (PH 7.4), 250µl of 40% Glycerol, 100µl of 10% NP40, 5µl of 1M $MgCl_2$, 20µl of 5M NaCl, 40µl of 25X Complete Protease Inhibitor (Roche Applied Science), 1µl of 1M Dithiothreitol made to 1ml with distilled water (dis H_2O). Before lysis the supernatant medium was removed and cells were washed 3X using 10ml PBS. Then the 10cm plate was immediately placed on ice and 200µl of the lysis buffer was added. The plate was scraped using a scraper in order to release cells adhered to the plate. The cells were repeatedly pipetted up and down in order to lyse the cells and the cell lysate was transferred to an eppendorf tube. Another 200µl buffer solution was added and the above steps were repeated. Finally, the lysate was centrifuged at 13000 rpm for 5 minutes in a 4^0C centrifuge and the supernatant was kept at -80^0C until needed for WB.

The protein concentrations of cell lysate samples were quantified using both spectrophotometer cuvette tubes using BSA standard curve or the 96 well plate Pierce BCA Protein Assay kit (Thermo

Fisher Scientific) methods. Once protein quantification was completed and calculated for WB, the samples were placed on a heater at 100^0C for 10 minutes to breakdown the DNA. Following this, the samples were loaded on to gel (SDS-PAGE - sodium dodecyl sulphate polyacrylamide gel electrophoresis) while in a 1L running buffer holding Electrophoresis apparatus (both from Invitrogen) along with 5μl DNA ladder. Next, 435μl NuPAGE® Antioxidant (Invitrogen) was added onto the buffer and the gel was run at 150 volts for 1-2 hrs. This was later transferred onto a membrane (Immobilon™-FL PVDF Transfer Membrane (Sigma-Aldrich)) using TE42 Standard Transfer Tank (Hoefer) and transfer buffer, and run at 0.1A in a cold room overnight. Finally, the membrane was blocked, fixed with primary and secondary antibodies and the result of the knockdown was demonstrated using ECL detection system (GE-Healthcare-Amersham). After the first ECL was stripped of using 50 ml disH_20 and 50 ml 0.1M NaOH for 10 minutes each, the membrane was fixed with GAPDH in order to check whether equal amounts of proteins were loaded.

2.1.10 Spheroid assays

In order to study cancer cell invasion in *in vitro* model different cancer cell types with or without endothelial cells were cultured using a spheroid assay as previously described (Cheng et al. 2015). Briefly, cells were cultured in appropriate flasks and were trypsinised at confluence, counted and diluted to $5x10^3$ cells/ml in their respective culture medium. Next, $1\text{-}2x10^3$ cells were seeded in a low adherent and round bottom 96-well plates (Sigma cat No. 7007) in 200 μl 5xDMEM, neurobasal, 5xDMEM and HLVEC or neurobasal with HLVEC medium for U251, GBM and or when these cells were seeded with ECs, respectively. After 3-5 days when a sphere was formed, supernatants were removed and 100μl collagen was added per well at 6.8 : 1 ratio of Collagen to respective medium and neutralised by 0.7% 1M NaOH. Finally, 100μl of the respective medium was added to each well and the plate was incubated at 37^o and 5% CO_2. Cancer cell invasion was measured at Days 0, 3, 7, and 11 following the addition of collagen using EVOS at 4x magnification. ImageJ 32 software was used to measure and calculate cancer cell invasion. Briefly, a polygon shape was used to draw a line along the edge of the sphere starting from the day collagen was added and this was repeated 2-3 days apart until the spheres appeared to reach their maximum growth and invasion. Other than the first day, where a proper circle was drawn around the sphere, the drawing covered at least 75% of the outgrowth of the invading tumours from which total area was calculated by the software. Finally, Migration Index (MI) was calculated by subtracting the core area from the respective outgrowth area and then divided by the outgrowth area.

2.2 Patient sample processing and characterisation

2.2.1 Patient-derived samples

GBM tissue samples were collected from patients who attended Leeds Teaching Hospital (LTH) following their consent and ethical approval from the University of Leeds Research Ethics Committee. Out of a total of 52 FFPE blocks available for IHC analysis only 21 blocks were chosen following exclusion of blocks with either small or inadequate sample size or those samples with predominantly necrotic regions (Appendix 1). Furthermore, 10 pairs of primary and recurrent patient-derived GBM samples were obtained from Imperial College through Brain UK (Appendix 2). Altogether, I characterised a total of 26 primary GBM patient samples and 15 pairs of primary and recurrent WHO Grade IV GBM samples. One normal brain tissue sample dissected from a corpse was also included as a control.

2.2.2 Immunohistochemistry (IHC)

Both patient and mouse brain tumour tissue samples which were embedded in paraffin were sectioned at 4 µm thickness and mounted on a Superfrost Plus microscope slides (Thermo Fisher Scientific). For IHC staining slides were placed on a heater (70^0C) to melt the wax followed by antigen retrieval process using Mena Path Access Revelation solution (Cat. No. MP-607-X500) in a pressure cooker for about 40 minutes. At the end of the antigen retrieval the slides were immediately rinsed in preheated Mena Path TBS Automation washing Buffer (Cat. No. MP-945-X500) or TBST (1xTBS and 0.2% Tween 20) followed by washing under a running tap water. A hydrophobic pen (Vector Lab) was used to encircle around the tumour tissue samples on each slide and washed in washing buffer, and all endogenous antibodies were blocked using BloxAll (SP-6000) for 15 minutes in a wet chamber. Then, slides were washed in a wash buffer and incubated for another 15 minutes in a Normal Horse Serum (Vector lab) to avoid non-specific binding. Then, slides were washed in a washing buffer and incubated with the right antibody at the right dilution depending on the type of staining - single or double staining (Table 2.2).

All primary antibodies were diluted in Antibody Diluent Solution (Invitrogen; 00-3218) and 100-200 µl volume was added depending on the size of the tissue on the slide. Then, slides were washed in washing buffer, 3x 3 minutes each, before incubating with the appropriate secondary antibody for 30 minutes. ImmPRESS HRP anti-rabbit IgG (Cat. No. MP-7401) and ImmPRESS HRP anti-mouse IgG (Cat. No. MP-7400) both raised in horse and pre-prepared Vector secondary antibodies were used. This was followed by 3x 3 minute washes and the slides were incubated for 5 minutes with ImmPACT DAB peroxidase substrate Vector SK-4105 (Vector lab) mixing one drop DAB CHROMOGEN and 1ml DAB

Diluent to produce a brown staining which is insoluble in alcohol and xylene. While all the single antibody staining directly go through a quick H&E counterstaining procedure, except Eosin, slides with double primary antibodies were stained for Fast Red Cocktail (ImmPACT Vector Red – Alkaline phosphatase; SK-5105) for 15 minutes before finishing off with Haematoxylin counterstaining for nuclei. All patient-derived GBM tumour tissue samples were stained for rabbit polyclonal anti-CD31 and mouse monoclonal anti-nestin antibody using the double immunostaining techniques. In addition, selected patient GBM tumour samples and mouse tumour samples were stained for IHC using different antibodies (Table 2.2).

Table 2.2 List of primary and secondary antibodies used in immunohistochemistry

Sr.No.	Primary Antibody	Dilution	Reactivity	Cat No./ Source
1	Rabbit polyclonal Anti-CD31 antibody	1:30	Mouse, Human, Pig	Ab28364/ABCAM
2	Mouse Monoclonal anti-CD31 antibody	1:20	Human	M0823/DAKO
3	Mouse monoclonal Anti-human Nestin antibody	1:10,000	Human	MAB1259/ R&D Systems
4	Mouse/Rat monoclonal anti-mouse Nestin antibody	1:10,000	Mouse, Rat	MAB2736/ R&D Systems
5	Rabbit polyclonal anti-DOCK4 antibody	1:100	Human, Mouse	A302-263A/ Bethyl Laboratories
6	Rabbit polyclonal anti-alpha smooth muscle Actin antibody	1:100	Mouse, Human and others	Ab5694/ ABCAM
7	Rabbit polyclonal anti-alpha SMA antibody	1:100	Human, Mouse, Rat	55135-1-AP/ Proteintech
8	Mouse monoclonal anti-SMA	1:400	Human	M0851/DAKO
9	Rabbit polyclonal anti-Carbonic Anhydrase IX antibody	1:1000	Human	ab15086/ ABCAM
10	Rabbit polyclonal anti-OLIG2 antibody	1:1000	Human	HPA003254-1/ SIGMA
11	Rabbit polyclonal anti-GFAP antibody	1:2000	Human, Mouse and more	Z0334/ DAKO
12	Rat monoclonal F4/80	1:200	Human, Mouse	ab16911/Abcam
13	Rabbit polyclonal anti-Cleaved caspase-3	1:100	Human, Mouse	Asp175/ Cell Signaling Technology
14	Rabbit monoclonal anti-PDGFRβ Ab	1:100	Mouse, Rat, Human	ab32570/ ABCAM
15	Rabbit monoclonal anti-γH2AX Ab	1:400	Human, Mouse, Rat, Monkey	9718S/ Cell Signaling Technology
16	Rabbit polyclonal anti-CD45 Ab	1:100	Mouse/Rat/Human/Pig	ab10558/ABCAM
17	Mouse monoclonal anti-hCD68	1:100	Human	M0876/DAKO
18	Mouse monoclonal anti-SOX2 Ab	1:25	Human/Mouse/Rat	MAB2018/ R&D Systems
19	Rabbit polyclonal anti-Ki67	1:1000	Mouse/Human/others	ab15580/ABCAM
20	Mouse monoclonal anti-RFP Ab	1:1000	Mouse	GTX82561/ GeneTex
Secondary Antibodies				
1	Horse anti-Rabbit HRP	RTU	Rabbit	MP-7401/ Vector lab
2	Horse anti-mouse HRP	RTU	Mouse	MP-7402/ Vector lab

2.2.3 Immunofluorescence (IF)

For immunofluorescence staining patient-derived GBM tumour tissue samples were sectioned from FFPE blocks, mounted on Superfrost Plus slides and heated at 90 degree for at least 30 minutes. The slides were deparaffinised in xylene, 2x 10 minutes and rehydrated in graded ethanol for 5 minutes while being agitated every 30 seconds. For antigen retrieval water bath was set at 95^{o}C and slides were kept in Menarin antigen retrieval solution in the water bath for 20 minutes. After cooling down and washing under running water for 5 minutes, the slides were blocked using a blocking solution containing 1% BSA and 2% FCS in PBS for 1hr on a rocking platform. Primary antibodies diluted in a blocking solution were added to the slides and incubated overnight in a cold room. GBM tumour tissue samples were stained using different primary antibodies as shown in Table 2.3. Next day, fluorophore-conjugated secondary antibodies were added following 3x 5 minute washes in TBST. The slides were then incubated in 1µg/ml DAPI in PBS for 10 minutes to stain nuclei at room temperature. Finally, 150-200 µl Vector True View (Cat. No: SP-8400) was used to quench autofluorescence for 5 minutes and 20 µl Vectashield Hardset mounting medium (Cat. No: H-1400) was applied on each tissue sample before adding coverslip. Images were acquired using Nikon A1 confocal microscope or AxioImage Z1 fluorescence microscope (Zeiss).

Table 2.3 List of primary and secondary antibodies used in immunofluorescence

No.	Primary Antibody	Dilution	Cat No./ Source
1	Mouse monoclonal anti-hNestin Ab	1:5000	MAB1259/ R&D Systems
2	Rabbit polyclonal anti-CD31 Ab	1:30	Ab28364/ ABCAM
3	Mouse monoclonal anti-hCD31 Ab	1:20	M0823/DAKO
4	Rabbit monoclonal anti-PDGFRβ Ab	1:100	Ab32570/ ABCAM
5	Mouse monoclonal anti-hSMA Ab	1:200	M0851/ DAKO
6	Rabbit polyclonal anti-SMA Ab	1:100	55135-1-AP/ Proteintech
7	Mouse monoclonal ant-SOX2 Ab	1:25	MAB2018/ R&D Systems
8	Rabbit polyclonal anti-GFAP antibody	1:1000	Z0334/ DAKO
9	Mouse monoclonal anti-hCD68	1:50	M0876/DAKO
Secondary IF Antibodies			
1	Alexa Fluor 488 Goat-anti Rabbit IgG	1:200	A11034/ Invitrogen
2	Alexa Fluor 594 Goat-anti Mouse IgG	1:200	A11032/ Life-Technologies
3	DAPI for nuclear counterstaining with excitation wavelength of 340	1ug/ml	Sigma-Aldrich

2.2.4 Characterisation and quantification of patient GBM tumour vasculatures

Each tumour tissue sample was characterised and quantified for different blood vessel morphologies and expression level of different proteins. Briefly, the stained slides were scanned using Apeiro AT Virtual Slide scanner and characterised using Apeiro ImageScope software. An area of $1mm^2$ boxes were placed on the viable non-necrotic part of the tumour tissue at low magnification (Figure 3.2). At least 75 % of the viable, non-necrotic tissue regions from each sample was covered by boxes in order to represent different regions of the tumour tissue sample. All boxes were given an identification number and as a guideline a minimum of 9 and a maximum of 16 representative boxes were randomly selected based on the size of the tissue specimen for GBM vasculature characterisation study. Where the maximum available total number of boxes on a given tumour specimen was less than 9, all of them were characterised. Once the boxes were identified, each blood vessel was characterised using ImageScope software at 20x magnification. All blood vessels with length $\leq$ 20 μm were excluded if they were found with a minimum lumen diameter less than 10 μm, at 20x magnification as it was found practically difficult to characterise such small blood vessels.

Overall, a total of 5,829 blood vessels (3,819 from LTH and 2,010 from Imperial College) were characterised based on predefined and optimized morphologies. The characterisation of vascular morphologies was based on 5 different glioblastoma vascular morphologies (Fig. 3.3 & 3.4). In this study, while 'Normal' vessel morphology refers to that of normal brain blood vessels, 4 more distinct morphologies were identified in glioblastoma patient samples: Normal-like, Nestin +ve, Glomeruloid nestin -ve and Glomeruloid nestin +ve. The extent of nestin expression by ECs and that of their surrounding stroma was mainly used in GBM blood vessel morphology classification and characterisation. In parallel, the diameter of each blood vessel was also measured using ImageScope software.

2.3 *In vivo* mouse models

All *in vivo* experiments were conducted in accordance with the Animal (Scientific Procedures) Act 1986 and NCRI Guidelines and approved by Home Office Project Licence governing body and locally by University of Leeds Animal Welfare and Ethical Review Committee. In order to further my understanding of how glioblastoma tumours form their vasculature I mostly used Dock4 heterozygous mice and their litter mates in this thesis. This was mainly because homozygous Dock4 deletion is embryonically lethal (Abraham et al. 2015). However, I also used some Dock4 conditional knockout mice in a pilot study to see the effect of endothelial cell specific Dock4 gene deletion on tumour growth.

2.3.1 Mouse lines and breeding

Heterozygous Dock4 mice with C57BL/6J background were crossed with BL6 mice and pups were ear biopsied for genotyping at 3 weeks old. All genotyping was processed by Transnetyx (TN, USA). Conditional Dock4 knockout mice were bred using Dock4f/f which were generated and imported from Ozgene, Australia and VEC-Cre;Rosa26Td mice from Beatson Institute, Glasgow. In order to confirm endothelial specific deletion of Dock4 and to test how well VEC-Cre deleted the stop codon 2mg tamoxifen/mouse was injected intraperitoneally for 5 consecutive days. Tumour tissue samples from mice carrying Dock4f/f gene with either Cre+ or Cre-;Rosa26TdTomato gene were stained using red fluorescent antibody (RFP) to confirm Dock4 deletion which allows TdTomato to be expressed in the presence of Cre. All mice were bred and kept in St James's Biological Services (SBS) animal facility, University of Leeds.

Table 2.4 *In vivo* experiments conducted in this study

Exp. No.	Cell type and dose	Number of mice, sex strain and age	Overall Survival (average days)	Comments
1	5x10^5 CT2A 4x10^4 GL261	2F BL6@ 9wks 2F BL6 @10wks	21 20.5	Mice developed neurological symptoms
2	1x10^5 CT2A	8F Dock4 het @18-22 wks 5F BL6 @ 18-22 wks	Mice were taken down following observation of symptoms in one mouse (Day 28)	Targeted radiotherapy (RT) 5x2Gy and 3x5Gy using SARRP
3	1x10^5 CT2A-luc	4F Dock4 het @8 wks 4M DOCK4 het @ 8 wks 9M BL6 @ 8 wks	Mice were taken down following observation of symptoms in one mouse (Day 21)	Whole brain irradiation (WBRT) using X-ray irradiator (IVIS + MRI)
4	1x10^5 CT2A-luc	26F Dock4 het @8-10 wks 26F BL6 @ 8-10 wks	WT ctrl – 21.2 Het ctrl – 20.1 WT RT – 33.7 Het RT - 32	WBRT using SARRP (IVIS + MRI), 3 mice/Group taken down early
5	1x10^5 CT2A	5F&7M VE-cad-iCreERT^{-Cre} Dock4f/f @ 9wks 4F&3M VE-cad-iCreERT^{+Cre} Dock4f/f @ 9wks	18.5 (of 4 mice) 19 (2F&1M)	12 mice taken down 11 days post injection and 7 mice upon development of symptoms

2.3.2 Genotyping

Ear biopsy samples were collected from 3 weeks old mice and placed in a pre-designated 96 well plates. The samples were either sent to Transnetyx straightaway or kept at -20 degree freezer until collected. For shipping purpose each plate was sealed in FedEx envelope at room temperature and sent to Transnetyx the same day which usually took 2-3 days to reach them. The samples were processed according to Transnetyx protocol (https://www.transnetyx.com/home?gclid=EAIaIQobChMIoaPi6MaX3wIVCYjVCh1KNgX_EAAYASAAEgKy-_D_BwE) and the results were obtained within 72 hours.

2.3.3 Intracranial injection

For all *in vivo* experiments the murine brain tumour model CT2A was used, except the initial comparison made against GL261 cell line. A total of $1x10^5$ CT2A cancer cells in 2μl DMEM were injected intracranially into the right hemisphere of the brain of 8-10 week-old mice (Table 2.4). Stereotactic machine was used to inject mice as described previously (Lorger et al. 2009). Briefly, mice were anaesthetised using isoflurane and the head regions were shaved using hair clipper a day before surgery. Two mice were restrained at the same time on a stereotactic machine, which was connected to a source of isoflurane and oxygen generator through one tube and a scavenger unit to extract the isoflurane waste through another tube, and ear bars were applied to fix the heads firmly for intracranial injection. Mice were injected 5mg/ml Metacam (Boehringer Ingelheim, UK) and 2.5% Baytril (BAYER) before making a small incision over the injection site. A small dent or hole was drilled 1mm to the right and 1mm anterior to bregma using a driller in order to ease the advancement of Hamilton syringe. A Hamilton syringe with 5 μl needle was loaded with cancer cells and injected 4mm deep into the striatum using a ruler on a stereotactic machine as a guide. The 2 μl tumour cells were injected at 3mm depth, 1 μl at a time at 1 minute interval and then gradually withdrawn 1 mm at a time after every 30 seconds. Finally, after withdrawal of the needle wax was applied to seal the hole and skin incision was stitched back together using glue. Mice were allowed to recover in a recovery chamber (37^oC) before putting them back in their cages. They were routinely monitored and checked for development of neurological symptoms.

2.3.4 Irradiation

Mice in the ionising radiation treatment group received either a total of 10Gy or 15Gy ionising radiation post tumour implantation using either Small Animal Radiation Research Platform/SARRP (Xstrahl Life Sciences) or RAD X-ray irradiator (RS2000 X-ray Irradiator – Rad Source). Most brain tumour irradiation experiments in this study were conducted using SARRP and both whole brain and

targeted irradiation were used. While whole brain ionising irradiation was carried out using 9 mm x 9 mm collimator, targeted therapy was delivered using 3mm x 9mm collimator. In both cases an Arch beam from 60^{o} to -60^{o} was used in order to avoid damage to sensitive body parts like the throat region. Mice were first imaged using cone beam computed tomography (CBCT), SARRP, and the images were uploaded onto Muriplan software in order to locate the area of irradiation. The total radiation dose was delivered to the tumour with a maximum dose at the centre and gradually decreasing towards the edge of the tumour using isocentre as a centre of reference to the tumour.

For the irradiation experiment conducted using X-ray irradiator as a source of ionising radiation mouse was anaesthetised and placed on aluminium shelf plate at level 5 in the RAD Source (RS 2000) X-ray irradiator machine. A total irradiation dose was calculated at 160 kV and 25 mA and delivered at a rate of 4.5 Gy/min to the brain region guided by a collimator with a red light laser. The ionising radiation dose was calculated based on the level the shelf holding the mouse in the RS 2000 irradiator.

2.3.5 IVIS imaging

Tumour growth was monitored in CT2A-luc implanted mice using non-invasive bioluminescence IVIS spectrum imaging (PerkinElmer) 2x/week, with a maximum of 5-6 IVIS imaging/mouse. Each mouse was injected with luciferase subcutaneously and imaged after 20 minutes. The images were processed using IVIS spectrum software and tumour growth rate was determined for different groups.

2.3.6 Magnetic resonance Imaging (MRI)

Selected mice from different treatment groups were scanned in axial or coronal slices using M7 Compact Magnetic Resonance Imaging (MRI). Briefly, isoflurane was used to anaesthetise mouse in an anaesthetic chamber and moved over to the LSD23 Head Coil bed and restrained. The restrained and stably breathing mouse was transferred into the MRI machine gently and continuously monitored while in MRI for respiration and pulse using physiological monitoring software. Using Aspect imaging software orientation (feet first), scout (Mouse Head), axial or coronal section and slice thickness were selected and scanned to capture a T2-Weighted MR image.

2.3.7 Terminal perfusion

Mice were taken down by terminal perfusion either at the same timepoint when one single mouse developed neurological symptoms or individually when each mouse started to show neurological symptoms. Once mice were perfused using PBS and 4% PFA, brain tissue samples were collected and

the samples were fixed in 4% PFA overnight in a fridge. The next day the samples were transferred into 70% ethanol and kept in a fridge until embedded in paraffin.

2.3.8 Processing of mouse tumour samples

Mouse tissue samples from *in vivo* experiments which were fixed in 4% PFA overnight and then transferred into 70% ethanol were paraffin embedded. Briefly, fixed tumour tissue samples were placed in different size cassettes and labelled. Then the cassettes went through a series of dehydration (70% -100% graded ethanol), clearing (3x xylene) and infiltration (3x paraffin wax) at 65^{o}c using automatic tissue processor overnight. The next day the cassettes were taken out form the tissue processor and placed in a paraffin dispenser machine. The tissue samples were removed from their cassettes and placed in a metal box in order to embed using pure paraffin in a desired orientation for sectioning. Finally, the original cassette was placed back on the metal box and more paraffin was added to complete the embedding process. The block was placed on a cold place and then stored at room temperature until sectioned.

The embedded mouse tumour tissue samples were sectioned almost exactly the same way as the patient GBM tissue samples as described under Section 2.2.2 above. Briefly, mouse brain tumour tissue samples were cut at 4 μm thickness using a coronal section from anterior to posterior starting from olfactory region. The 4 μm tissue samples were mounted on Superfrost Plus slides, left overnight to dry in 37^{o}C incubator and stained for different antibodies (Table 2.2). Stained slides were scanned as above (2.2.2). An area of 0.5mm x0.5mm (0.25mm^{2}) boxes were placed on the tumour tissue samples at low magnification and blood vessels were characterised at 20x magnification. All boxes were given an identification number and a minimum of 2 and a maximum of 6 boxes were analysed per tumour tissue sample. Blood vessels with length ≤20 μm and/or lumen <10 μm were excluded from this study. ImageScope software at 20x magnification was used to measure blood vessel lumen diameter. Percentage lumenised vessels was defined as total number of vessels with lumen ≥ 10 μm divided by total vessel count with length >20 μm and/or lumen > 10 μm.

2.4. Statistical Analysis

All data were analysed using GraphPad Prism and a P value of <0.05 was considered as statistically significant.

Chapter 3

Characterisation of the patient glioblastoma vasculature

3.1 Introduction

Microvascular proliferation is a hallmark of glioblastoma. However, there are contradictory reports as to the role of GBM vasculature in relation to patient outcome. Most previous studies described aberrant GBM blood vessels in terms of microvascular density (MVD), and only a handful of studies considered vascular structures to assess the prognostic values of these blood vessels in GBM ((Preusser et al. 2006) and (Birner et al. 2003)). Further, the majority of these reports are descriptive and lack fundamental components of molecular cell biology and mechanisms as to the formation of such abnormalities. Various mechanisms including sprouting angiogenesis, co-option, vasculogenesis, vascular mimicry and transdifferentiation have been described as potential mechanisms of GBM blood vessel development. However, there is considerable disagreement as to how and to what extent each mechanism contributes to the abnormality of glioblastoma blood vessels. For instance, while some studies supported transdifferentiation of GSCs to GBM blood vessels ((Ricci-Vitiani et al. 2010); (Soda et al. 2011)), others reported that GSCs transdifferentiation only gives rise to pericytes (Cheng et al. 2013). In a consequent experiment, the same group demonstrated improved efficacy of chemotherapy by targeting pericytes (Zhou et al. 2017). However, other studies in this area did not support the existence of such mechanisms (El Hallani et al. 2014). Hence, to this date the precise identity, prevalence, and prognostic value of GBM blood vessel morphologies are not well defined.

In this study, I set out to characterise the vasculature in GBM patient samples and define the prevalence of different blood vessel morphologies using immunohistochemical techniques to identify ECs and other cell types within the brain perivascular niche. Five different blood vessel morphologies were previously identified in the laboratory which I first confirmed and then quantified using the EC marker CD31 and stem cell marker nestin, in order to interrogate the presence of GSC-derived ECs. Blood vessel morphologies were scored in randomly selected areas within viable tumour tissue regions from a patient cohort treated in Leeds which was used as a training cohort. More samples were obtained from Imperial College to validate the findings. Within these patient cohorts paired primary and recurrent tumour samples, where available, were analysed in order to understand the effects of therapy on blood vessel characteristics. Further, blood vessel morphologies were associated with patient outcome.

3.2 Patient GBM blood vessels are abnormal

In order to identify the different types of blood vessel structures present in GBM, the endothelial cell marker CD31 and stem cell marker Nestin were used. As some studies suggested that GSCs transdifferentiate to ECs of GBM blood vessels ((Ricci-Vitiani et al. 2010; Soda et al. 2011)) or cancer

cells themselves form blood transporting vessel channels (Wang et al. 2013 and Yao et al. 2015) it was appropriate to expect at least a proportion of GBM blood vessels to stain Nestin positive and CD31 negative. Nestin/CD31 double immunostaining of normal brain tissue identified about 85% as CD31 positive small size capillaries (<10 μm) and larger blood vessels (with >10 μm had average diameter of 23 μm) lined by spindle shaped ECs with relatively low to none nestin positivity (Figure 3.1). In glioblastoma patient samples there were both small calibre capillaries and larger calibre blood vessels, often organised in glomeruloid structures, which appeared lined by rounded cells with strong nestin positivity (Figure 3.1). The term glomeruloid is commonly used to describe blood vessels organised in close proximity within common stroma (Rojiani and Dorovini-Zis 1996; Sundberg et al. 2001 and Brat and Van Meir 2001). The strongly nestin positive blood vessels were similar in appearance to the cancer cells within the tumour cell compartment (Figure 3.1), suggesting that they could represent the transdifferentiated CD31 positive GSCs described by Soda and co-workers (Soda et al. 2011).

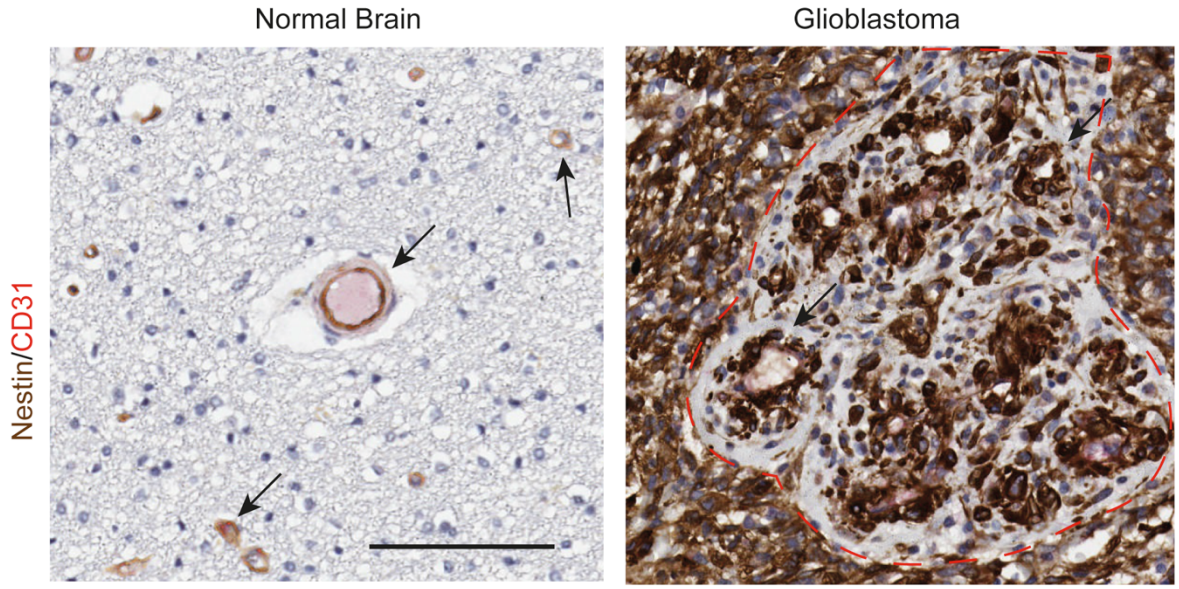

Figure 3.1 Blood vessel morphologies in normal brain and glioblastoma tissue

Normal brain or glioblastoma tissue samples were formalin fixed, paraffin embedded and sectioned. Following antigen retrieval, the samples were immunostained using antibodies against the stem cell marker Nestin and endothelial cell marker CD31. Black arrows point to blood vessels. Note abnormal blood vessels in GBM in a glomeruloid organisation within common stroma (red dotted circle). Scale bar, 100 µm.

In order to characterise in detail and quantify blood vessels in the GBM patient samples, 1mm^2 boxes were placed at 1x magnification on scanned images of stained slides to cover the non-necrotic, viable tumour tissue area (Figure 3.2A). Blood vessels in each box were analysed at 20x magnification of the scanned sample (Figure 3.2B). As the size of available patient tumour samples varied, the total number of boxes characterised ranged between 2 and 16. Blood vessels with a minimum length of 20 μm length and or with minimum diameter of 10 μm were characterised as it was found difficult to practically measure those smaller vessels. For the number of boxes and total number of blood vessels analysed from each tumour see Appendix 3. Overall, GBM blood vessels were morphologically classified as Single perivascular, Multi perivascular, Nestin +ve, Glomeruloid nestin -ve and Glomeruloid nestin +ve. Single-perivascular and Multi-perivascular blood vessels were predominantly characterised by their unique spindle shaped and CD31 positive ECs just like those blood vessels in normal brain. The multi-perivascular blood vessels are different from the single-perivascular in that the former have additional layers of cells around CD31 positive ECs resembling higher calibre blood vessel in the normal brain. Hence, the single- and multi-perivascular blood vessels were considered as 'Normal-like' blood vessels in GBM (Figure 3.3).

One of the most characteristic features of the blood vessels found in GBM was their strong nestin positivity. While blood vessels in the normal brain stained weakly positive for nestin, blood vessels in GBM showed a range of nestin positivity with some blood vessels being predominantly lined by round and strongly nestin positive cells (Figure 3.1). Some nestin positive blood vessels showed a glomeruloid organisation (Figures 3.1 and 3.4). Glomeruloid blood vessels that appeared negative for nestin were also identified as Glomeruloid nestin negative (Figure 3.4). Hence, most nestin positive blood vessels appeared to show a total replacement of spindle-shaped CD31 positive ECs (Figure 3.4).

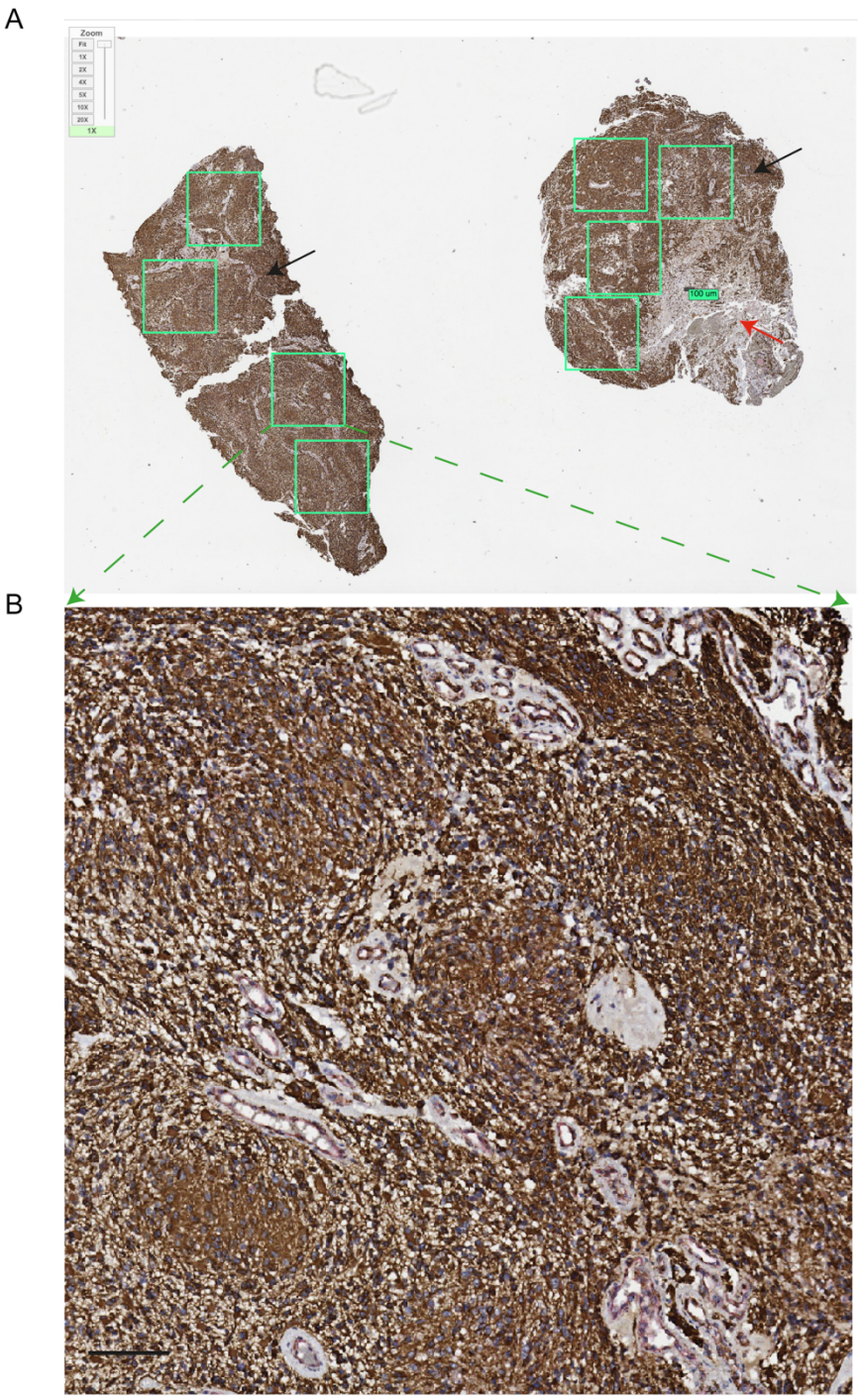

Figure 3.2 Areas of characterisation in patient tumour samples

(A) Image depicts a scanned slide following staining for Nestin (brown) and CD31 (red). Boxes of 1mm^2 size were placed on viable tumour tissue to cover a minimum area of 75% of the sample (black arrows). Red arrow points to a necrotic region excluded from the analysis.

(B) Image showing zoomed area in 'A' using ImageScope. Blood vessels were characterised at 20x magnification. Scale bar, 100 µm.

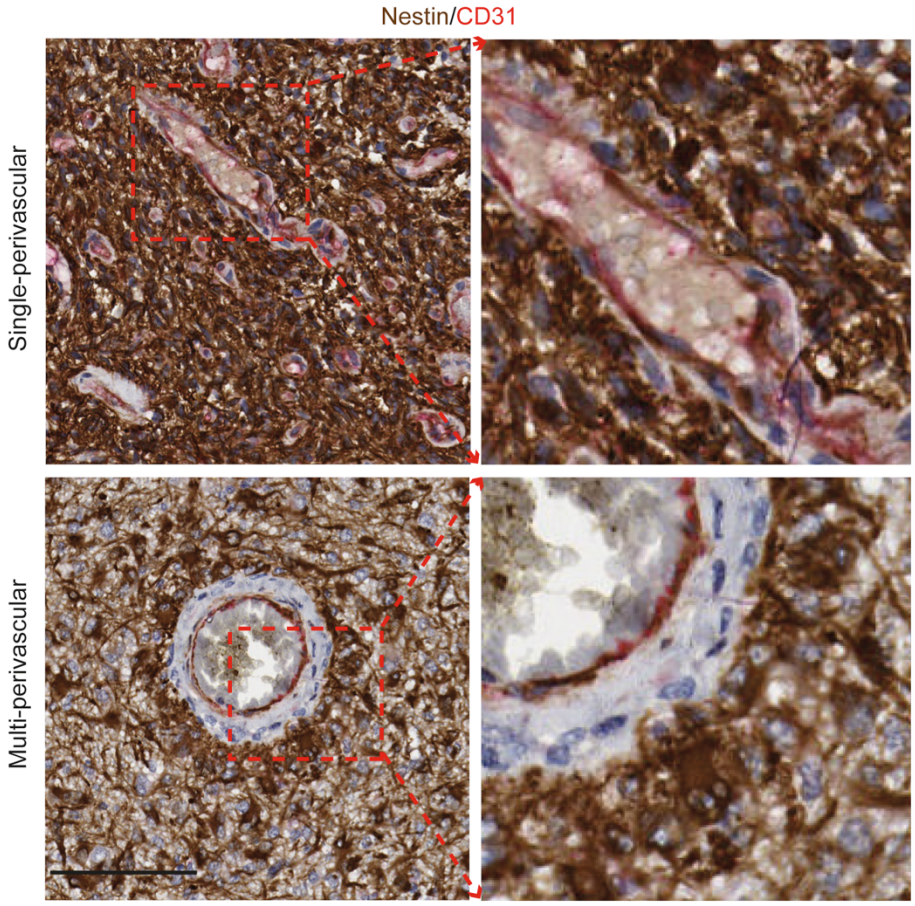

Figure 3.3 Normal-like blood vessel morphologies identified in patient GBM samples

GBM patient samples were stained for Nestin (brown) and CD31 (red). In the Single perivascular morphology blood vessels are lined by spindle-shaped CD31 positive ECs; Multi-perivascular blood vessels are lined by spindle-shaped CD31 positive ECs and layers of non EC perivascular cells. Single-perivascular and multi-perivascular blood vessels have been together classified as 'Normal-like' due to the EC lining being similar to those in the normal brain. Insets on the left-hand panels are shown at higher magnification on the right-hand side. Scale bar, 100 µm.

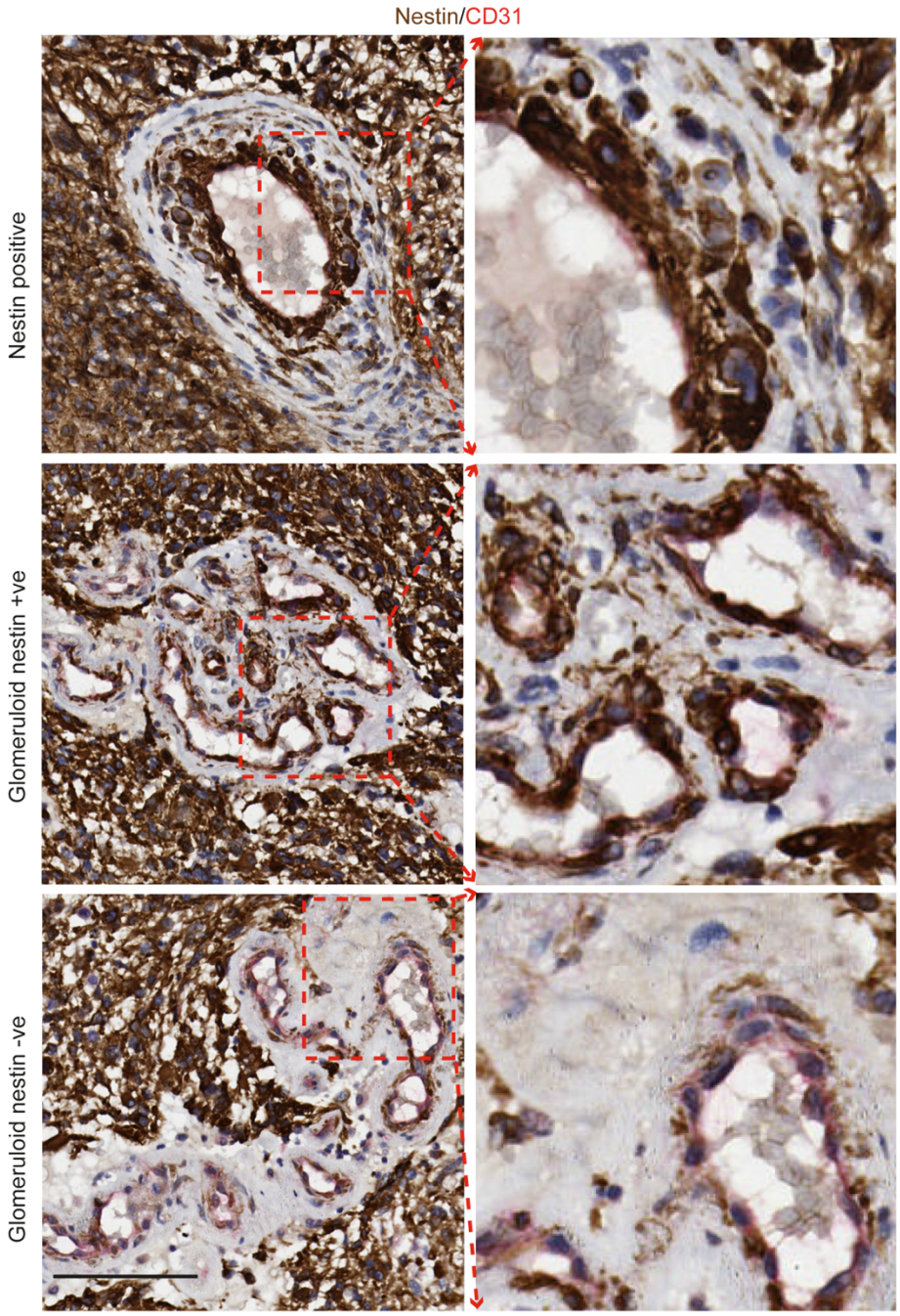

Figure 3.4 Abnormal blood vessel morphologies identified in patient GBM samples

GBM patient samples were stained for Nestin (brown) and CD31 (red). Nestin positive blood vessel morphology is characterised by the presence of nestin positive, rounded cells appearing to replace spindle-shaped ECs lining the blood vessels. Glomeruloid blood vessels are arranged as a network within common stroma lined by either nestin positive or nestin negative cells. Nestin positive and glomeruloid morphologies were only found in tumour samples and were hence classified together as 'Aberrant morphologies'. Insets on the left-hand panels are shown at higher magnification on the right-hand side. Scale bar, 100 µm.

3.3 GBM patients present with different degrees of blood vessel abnormality

Analysis of sixteen samples from Leeds patients (Appendix 1) with primary GBM showed high level of heterogeneity in tumour blood vessel morphologies. All 5 morphologies were identified in almost all tumours (Figure 3.5). In 12/16 (75%) of samples analysed the Normal-like morphology was significantly higher than the abnormal morphologies detected in those primary tumours. One tumour only, GBM37, had a significantly higher proportion of Nestin +ve blood vessels compared to normal-like blood vessels. This analysis showed that GBM patients present with different degrees of abnormality, although abnormal blood vessels appear at lower or similar abundance to normal-like blood vessels in primary tumours. In order to validate these findings in a new patient I analysed 10 more primary GBM patient samples from Imperial College, London (Appendix 2). These analyses confirmed that there are different degrees of blood vessel abnormality in GBM patients (Figure 3.6) in accordance with the findings from the Leeds patient cohort. All primary GBM tumours in the Imperial had a significantly higher proportion of normal-like blood vessel morphologies compared to the aberrant blood vessel morphologies.

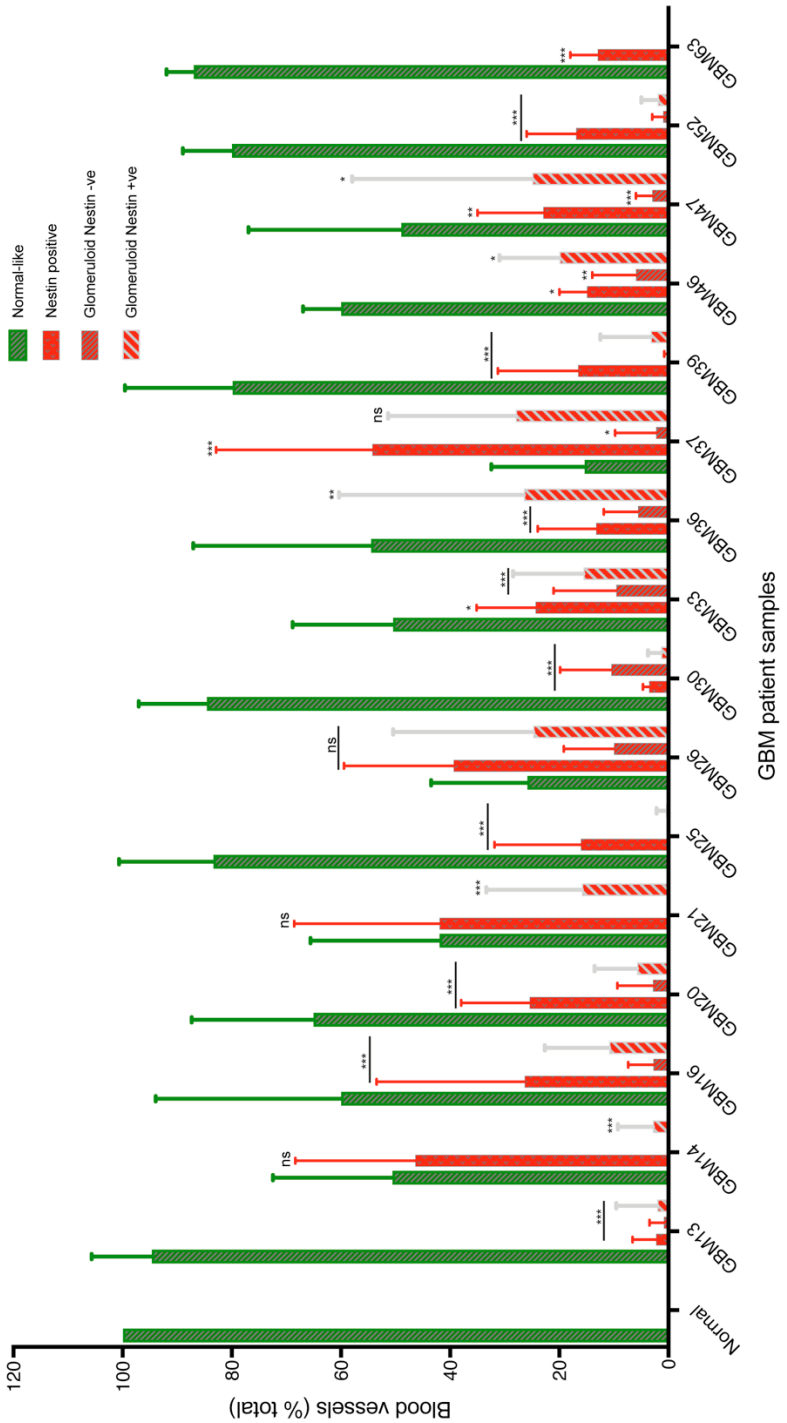

Figure 3.5 Quantification of GBM blood vessel abnormalities in the Leeds patient cohort

Primary GBM patient samples were characterised for the prevalence of different blood vessel morphologies. Histogram shows blood vessels showing a particular morphology as percentage of total blood vessels characterised in a sample ± SD; N = number of 1mm^2 areas analysed (shown in Appendix 3); an average of 176 blood vessels were characterised per patient sample; note that all patient samples showed both normal-like and aberrant blood vessel morphologies. P values *<0.05, **<0.01, *** <0.001 relative to normal-like.

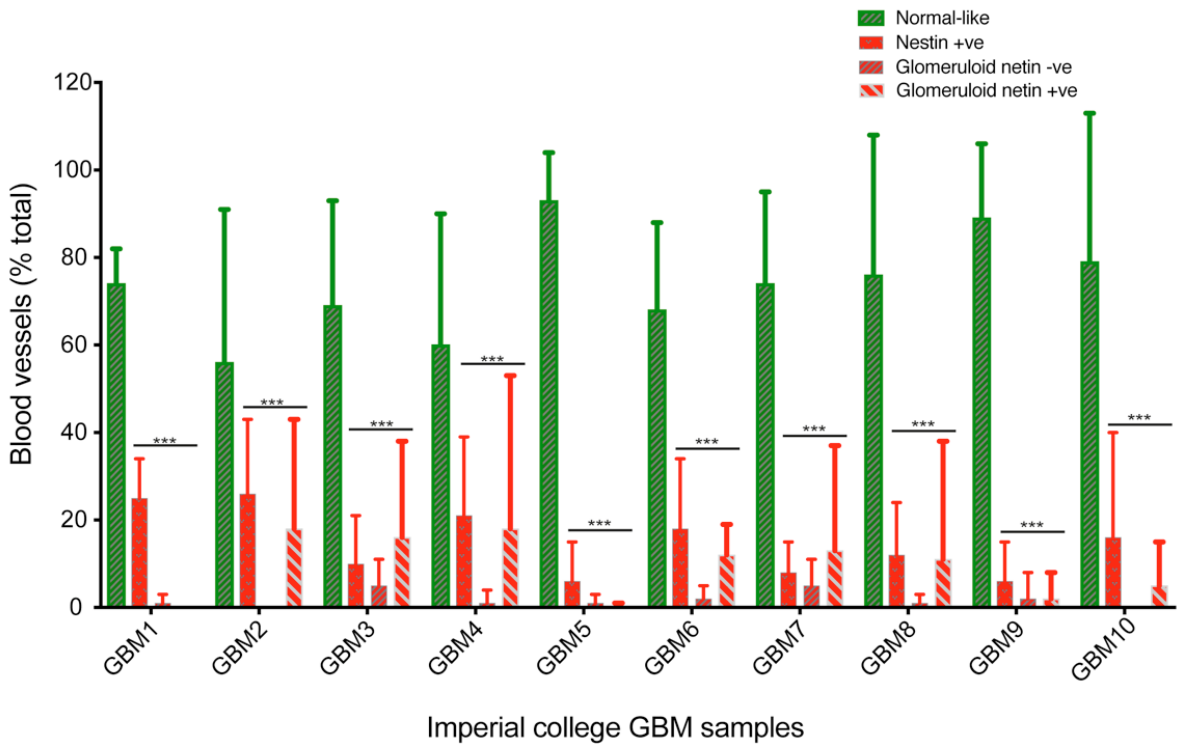

Figure 3.6 Quantification of patient GBM blood vessel abnormalities in the Imperial patient cohort

Primary GBM patient samples were characterised for different blood vessel morphologies. Histogram shows blood vessels as percentage of totals, N = No. of 1mm^2 areas, Mean ± SD (Appendix 3). Multiple 1mm^2 areas were analysed and an average of 261 blood vessels were characterised per patient sample and all patients demonstrated both Normal-like and aberrant morphologies. P values *** <0.001 relative to normal-like.

3.4 Association between nestin positivity and GBM patient survival

Since the presence of rounded cells with strong nestin positivity was a prevalent feature of blood vessels in GBM, I investigated whether nestin positivity was particularly associated with poor patient outcome. Here, this analysis was only possible for the Leeds patient cohort since clinical data were available (Table 3.1), whereas clinical data were not available for the Imperial patient cohort. Li and colleagues used median value as a cut-off point to calculate the association of patient outcome and level of protein expression (Li et al. 2017). The Human Protein Atlas also considers median value as a cut-off value to calculate the association of high and low protein expression against patients' outcome. Here, while the median glomeruloid nestin +ve blood vessels was 11.5 that of overall nestin positivity was 30. Hence, in this study I used 10% and 30% as a cut-off point for glomeruloid nestin +ve and overall nestin positive blood vessels, respectively. A survival curve showed that patients with low nestin positivity or relatively low nestin positive glomeruloids did not have a significantly better overall survival (Figure 3.7). Further, despite the observed trend, there was no statistically significant correlation between blood vessel nestin positivity and GBM patient survival (Figure 3.8).

Table 3.1 Leeds GBM patient data and summary of blood vessel characterisation

	OS	Blood vessels (% total)			Molecular subtype	IDH mutation	MGMT methylation	Gender/ Age	Tumour location	Treatment
		Normal-like	Total nestin positive	Nestin positive glomeruloid						
GBM13	22	95	5	3	Proneural	No	unknown	F/ 79	LF	RT
GBM14	39	53	47	2	Proneural/ mesenchymal	No	Moderate	M/ 58	RC	RT + TMZ
GBM16	3	64	36	13	unknown	No	No	F/63	LP	RT
GBM20	17	66	34	9	Proneural/ mesenchymal	No	No	M/50	RT	RT (Sep-Nov)&TMZ
GBM21	5	44	56	18	unknown	No	Yes	M/72	LT	RT
GBM25	58	85	15	0	unknown	Yes	Yes	F/38	LF	RT + TMZ
GBM 26	5.5	33	67	21	unknown	No	No	M/63	RT	RT + TMZ
GBM 30	26	87	13	10	Classical	No	No	F/50	RF	RT + TMZ, PCV avastin
GBM33	9	46	54	30	unknown	No	No	M/42	R	TMZ
GBM 36	42	68	32	18	unknown	No	No	M/64	LP-O	RT + TMZ + Lamustine
GBM 37	49	15	85	22	unknown	No	No	F/61	RF	RT + TMZ
GBM 39	6	82	18	2	unknown	No	No	M/47	RF	RT+TMZ
GBM46	10	77	23	15	unknown		unknown	M/66	RP	RT
GBM47	21	71	29	19	unknown		unknown	M/52	LF	RT+TMZ
GBM52	9	80	19	2	Classical	No	unknown	M/56	RO	TMZ
GBM63	15	75	25	0	Classical	No	No	M/57	LP	RT+TMZ,AV

Table shows list of Leeds patient clinical data including overall survival (OS), GBM blood vessel morphologies, molecular subtype, mutations tumour location and type of treatment received following surgery. F- Female; M – Male; Tumour location was identified by two letters (the one on the left-hand side indicates whether the tumour was in the right or left hemisphere, and the letter on the right hand side indicates whether the tumour is in temporal, occipital, parietal, frontal or central) e.g. LF – left frontal. Most patients received radiotherapy (RT), and combination of RT and temozolomide (RT + TMZ).

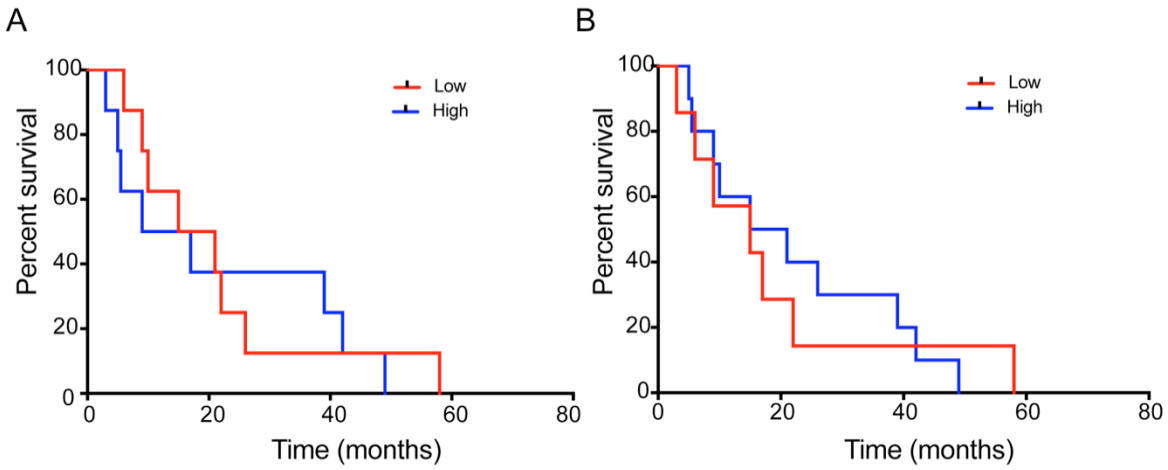

Figure 3.7 Overall patient survival and blood vessel nestin positivity

High nestin positivity defined as over 30% blood vessels showing coverage by round, strongly nestin positive cells and high glomeruloid nestin positivity was defined as over 10%. Overall log-rank test, P-values: 0.75 (nestin positivity) and 0.93 (glomeruloids).

(A) Kaplan-Meier curve of overall survival in GBM patients according to level of blood vessel nestin positivity. N = number of tumours with overall nestin expression on blood vessels morphologies of < 30%, 8 and >30%, 8.

(B) Kaplan-Meier curve of overall survival in GBM patients according to level of blood vessel nestin positive glomeruloids. N = number of tumours with overall nestin expression on glomeruloid blood vessel morphologies with <10%, 8 and >10%, 8.

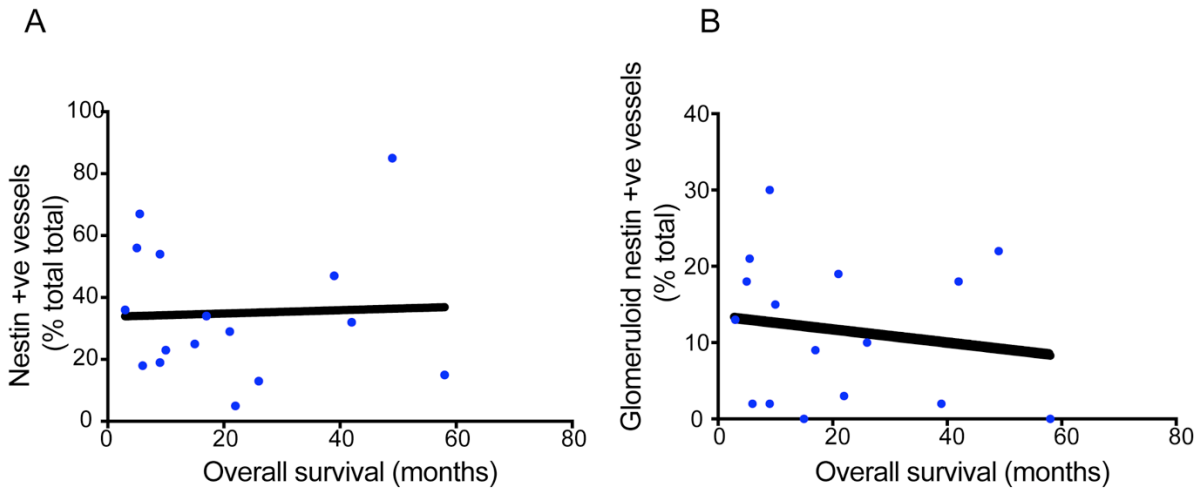

Figure 3.8 Correlation between nestin positivity and patient survival

Linear regression curves show lack of significant correlation between patient OS and nestin positivity or Glomeruloid nestin positive blood vessels.

(A) Lack of correlation between overall nestin +ve blood vessels and patient's OS (R^2 = 0.002, p=0.9).

(B) Glomeruloid nestin +ve blood vessels and OS (R^2=0.03, p=0.6).

3.5 GBM blood vessels are larger in calibre compared to vessels in normal brain

A well-described effect of VEGF action on pre-established blood vessels in animal models is blood vessel dilation due to detachment of pericytes, followed by further increase in vessel calibre by formation of glomeruloid structures and/or coverage by pericytes and smooth muscle cells (Nagy et al. 2009). Given the abundance of abnormal blood vessel morphologies including vessels that appear larger in diameter compared to normal blood vessels in the brain (Figures 3.3 and 3.4) I sought to quantify the blood vessel size in the GBM patient samples. Microvascular capillary size ranges between 8 μm and 20 μm in the normal human brain (Xiong et al. 2017). As stated earlier, the resolution of images from the scanned stained slides allowed me to characterise with confidence blood vessels that were over 10 μm diameter. Firstly, I found a higher proportion of smaller blood vessels in a normal brain tissue sample. Analysis of the Leeds patient cohort showed abnormally high blood vessel diameters in GBM. Figure 3.9 shows that in 11 out of 16 patients (69%) with primary GBM analysed, there was a higher number of blood vessels of larger calibre (20-50 μm and >50 μm) compared to smaller calibre blood vessels (10 - 20 μm). GBM blood vessel size was comparable to normal brain in patients GBM13, GBM25, GBM52 and GBM63. In the Imperial patient cohort, 4 out of 10 patients (40%) had a higher proportion of blood vessels with abnormally high size (Figure 3.10).

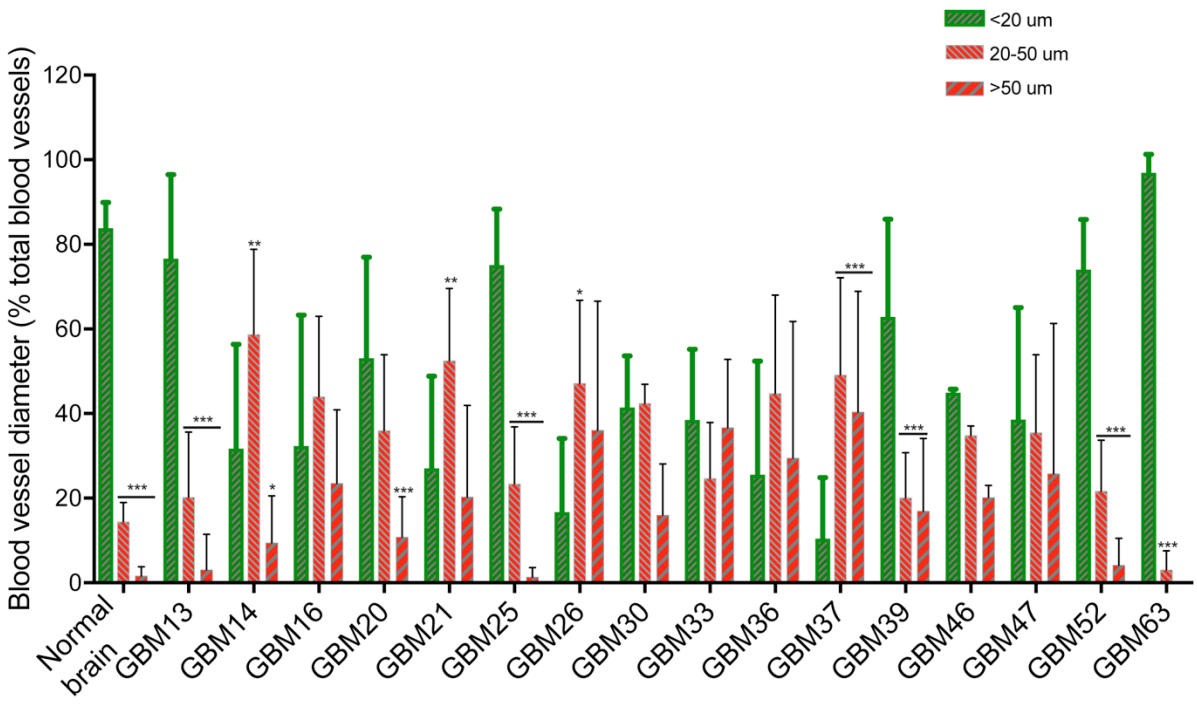

Figure 3.9 Quantification of patient GBM blood vessel lumen size in the Leeds patient cohort

Primary GBM patient samples were characterised for blood vessel lumen size. Note that tumours showed various degrees of relatively small (10-20 μm), medium (20-50 μm) and large (>50 μm) blood vessel diameters. Histogram shows blood vessels as percentage of totals, N = No. of $1mm^2$ areas, Mean ± SD (Appendix 3). *<0.05, **<0.01 and *** <0.001.

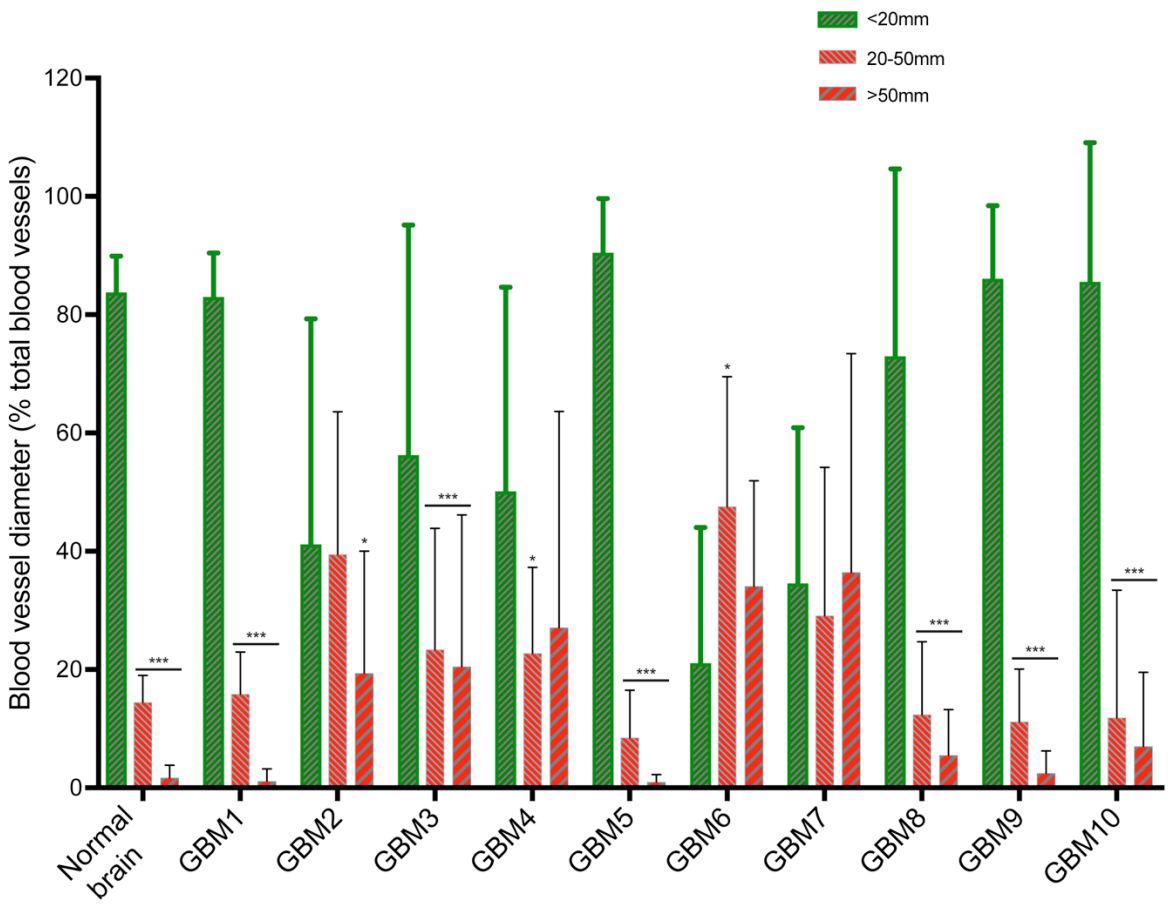

Figure 3.10 Quantification of patient GBM blood vessel diameter in the Imperial patient cohort

Primary GBM patient samples were characterised for blood vessel lumen size.

Note that tumours showed various degrees of relatively small (10-20 μm), medium (20-50 μm) and large (>50 μm) blood vessel diameters. Histogram shows blood vessels as percentage of totals, N = No. of 1mm2 areas, Mean ± SD (Appendix 3). *<0.05, **<0.01 and *** <0.001.

3.6 Tumour blood vessel abnormality increases with tumour recurrence

Following characterisation of blood vessel morphologies in primary GBM tumour samples I investigated whether these morphologies change following recurrence. I compared 5 recurrences available in the Leeds cohort to their corresponding primary tumours. Analysis showed that the same morphologies were present, but their prevalence had changed considerably in the recurrences (Figure 3.11). In 4 out of 5 recurrences the percentage of abnormal morphologies was significantly higher compared to the primary tumours. Consistently, normal-like blood vessels decreased with recurrence. Significant changes were observed in nestin positive morphology and glomeruloid nestin positive morphology for which higher proportions were found in recurrent compared to primary tumours. In order to find out whether those changes held in a larger cohort of paired samples, I analysed the recurrent tumours of the Imperial GBM patients. Consistent with the analyses of the Leeds samples, in 8/10 of the tumour samples analysed, the aberrant morphologies increased significantly upon recurrence (Figure 3.12).

3.7 Blood vessel calibre increases with tumour recurrence

Aberrant blood vessel morphologies appeared associated with increase in blood vessel calibre. To test this, I compared the calibre of blood vessels both in the Leeds and Imperial GBM samples. Analysis of the 5 Leeds pairs showed that the number of smaller calibre vessels (10-20μm) decreased in all recurrent tumours. Blood vessels with large lumen size also sharply increased in recurrent tumours (Figure 3.13). Again, I analysed additional 10 pairs of Imperial College tumour samples and 8/10 recurrent tumours had an increased blood vessel lumen size compared to primary GBM samples (Figure 3.14). However, in two tumour samples, GBM6 & GBM7, the small size blood vessels showed a trend of slight increase upon recurrence. Overall, this analysis showed that it is not only the prevalence of aberrant morphologies that increased with recurrence, but also the abundance of higher calibre blood vessels.

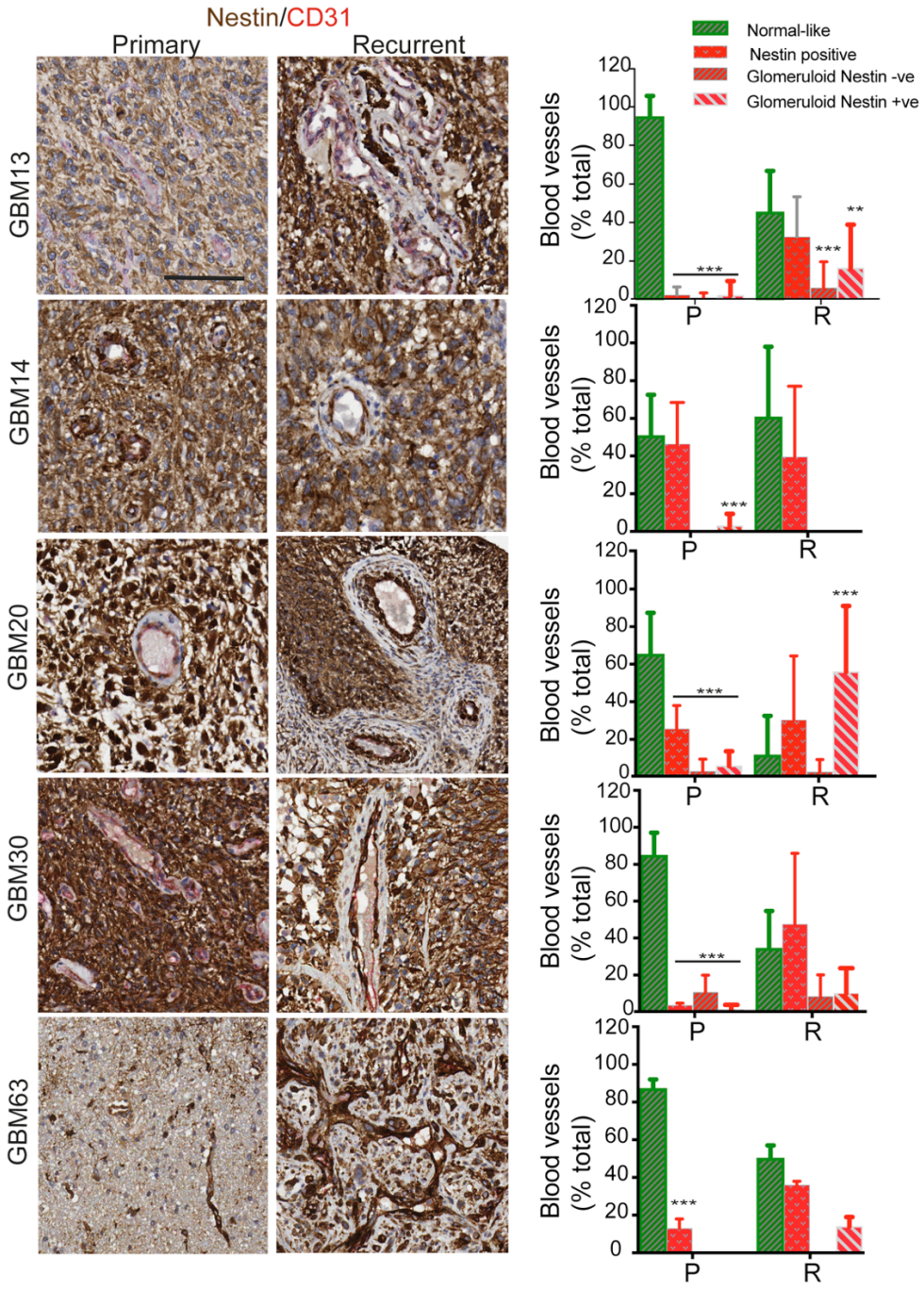

Figure 3.11 Comparison of the abundance of patient GBM blood vessel abnormalities in primary and recurrent tumours in the Leeds patient cohort

Recurrent GBM patient samples were characterised for the prevalence of different blood vessel morphologies and compared to primary GBM tumours. Images depict most prevalent morphologies in samples. Histograms show blood vessel morphologies as percentage of total blood vessels characterised in the primary (P) and recurrent (R) samples ± SD; N = number of 1mm^2 areas analysed as shown in Appendix 3; Scale bar, 100 μm. P values *<0.05, **<0.01, *** <0.001 relative to Normal-like.

Normal Like
Nestin Positive
Glomeruloid Netin -ve
Glomeruloid Netin +ve
Blood vessels (% total)
0
20
40
60
80
100
120
GBM1P
GBM1R
GBM2P
GBM2R
GBM3P
GBM3R
GBM4P
GBM4R
GBM5P
GBM5R
GBM6P
GBM6R
GBM7P
GBM7R
GBM8P
GBM8R
GBM9P
GBM9R
GBM10P
GBM10R
Imperial college GBM samples

Figure 3.12 Comparison of the abundance of patient GBM blood vessel abnormalities in primary and recurrent tumours in the Imperial patient cohort

Recurrent GBM patient samples were characterised for the prevalence of different blood vessel morphologies and compared to GBM tumours. Histograms show blood vessel morphologies as percentage of total blood vessels characterised in the primary (P) and recurrent (R) samples ± SD;
N = number of 1mm^2 areas analysed as shown in Appendix 3; P values *<0.05, **<0.01, *** <0.001 relative to Normal-like.

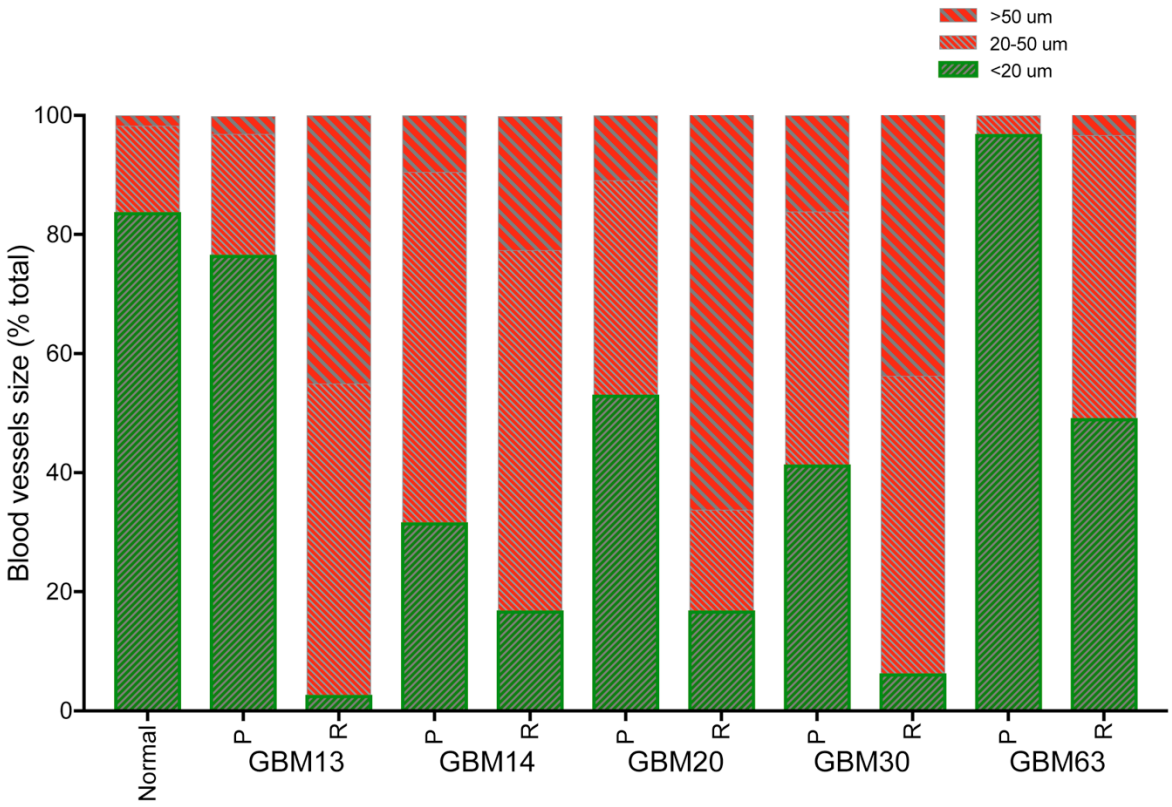

Figure 3.13 Comparison of blood vessel lumen size in primary and recurrent GBM in the Leeds patient cohort.

Blood vessels lumen size from normal brain and 5 pairs of primary and recurrent Leeds GBM tumour samples were measured using ImageScope and classified into 3 groups: small lumen size (<20μm), medium size (20-50μm) and large blood vessels (>50μm). N= % blood vessel sizes per 1mm^2 areas, Mean +/- SD (Primary, 5 and Recurrent, 5 tumours; Number of 1mm^2 per tumour shown in Appendix 3). The average number of blood vessels analysed for primary and recurrent tumours were 221 and 57, respectively. P, Primary and R, recurrent tumours.

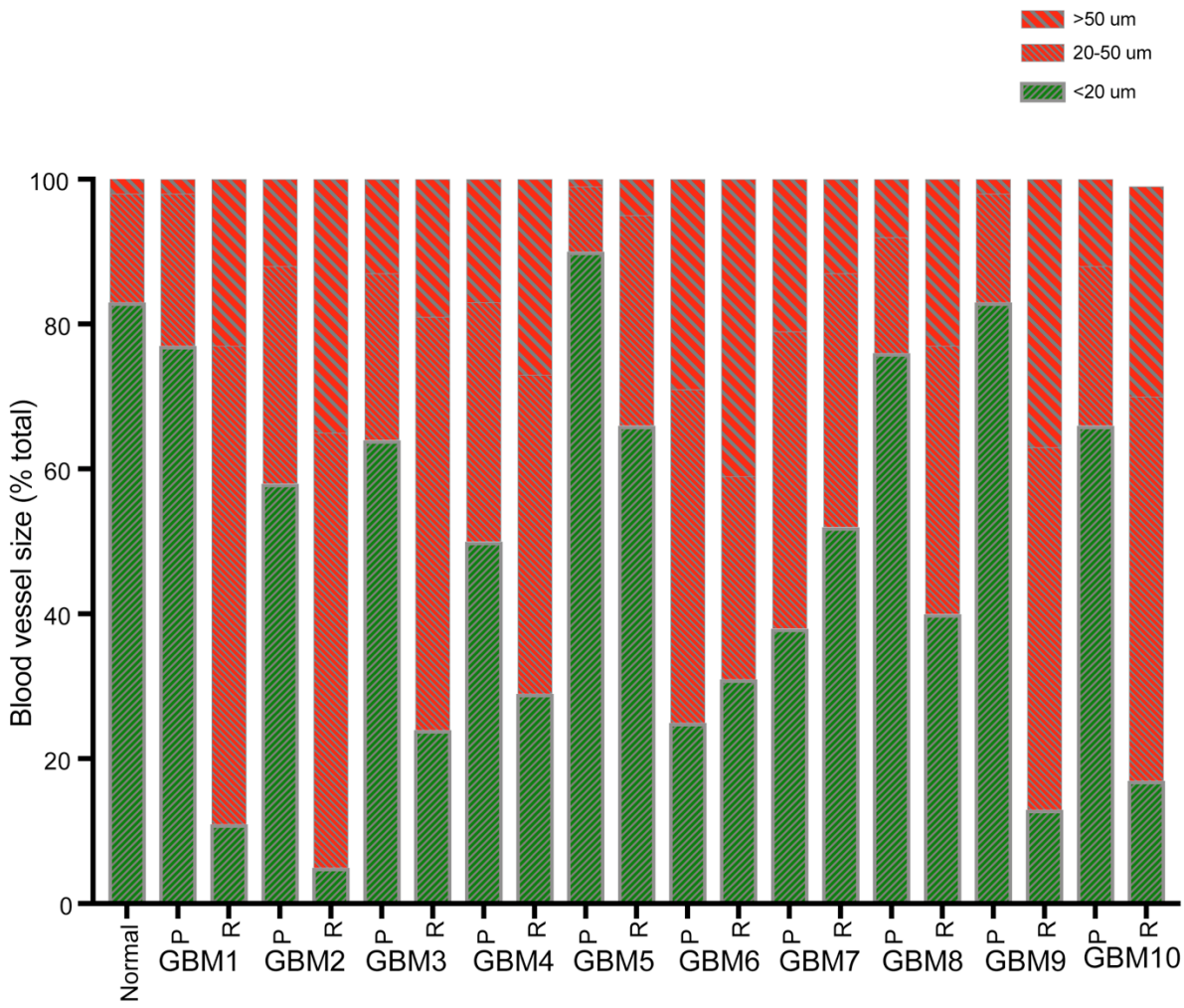

Figure 3.14 Comparison of blood vessel lumen size in primary and recurrent GBM in the Imperial patient cohort

Blood vessels lumen size from normal brain and 10 pairs of primary and recurrent Imperial GBM tumour samples were measured using ImageScope and classified into 3 groups: small lumen size (<20μm), medium size (20-50μm) and large blood vessels (>50μm). N= % blood vessel sizes per 1mm^2 areas, Mean ± SD (Primary, 10 and Recurrent, 10 tumours; the number of 1mm^2 boxes analysed per tumour are shown in Appendix 3). P, Primary and R, Recurrent tumours.

3.8 Recurrent GBM tumours have less MVD than primary GBM tumours

Given the increases in aberrant morphologies and blood vessel calibre I sought to determine whether the overall density of the blood vessels increased in the recurrences. I quantified the number of blood vessels per unit area based on their Nestin/CD31 positivity after excluding smaller size blood vessels < 10µm in diameter as those blood vessels could not be identified and quantified reliably. Figure 3.15 shows the pooled MVD from the Leeds and Imperial patient cohorts. The quantifications showed that there was significantly less microvascular density (MVD) in recurrent tumours compared to primary tumours, a trait found both in samples obtained from Leeds (Figure 3.15A) and Imperial (Figure 3.15B).

Altogether the analysis of primary and recurrent patient GBM showed that there was a shift in blood vessel morphology seen both in the Leeds and Imperial patient samples from higher proportion of normal-like blood vessels in primary tumours, to higher proportion of strongly nestin positive and glomeruloid aberrant type in recurrent tumours (Figure 15C, D). In addition, there was increased blood vessel calibre in recurrent tumours in both patient cohorts (Figure 15E, F). Consistently, the number of blood vessels per unit area decreased in the recurrent tumours when compared to primary tumours (Figure 15 A, B).

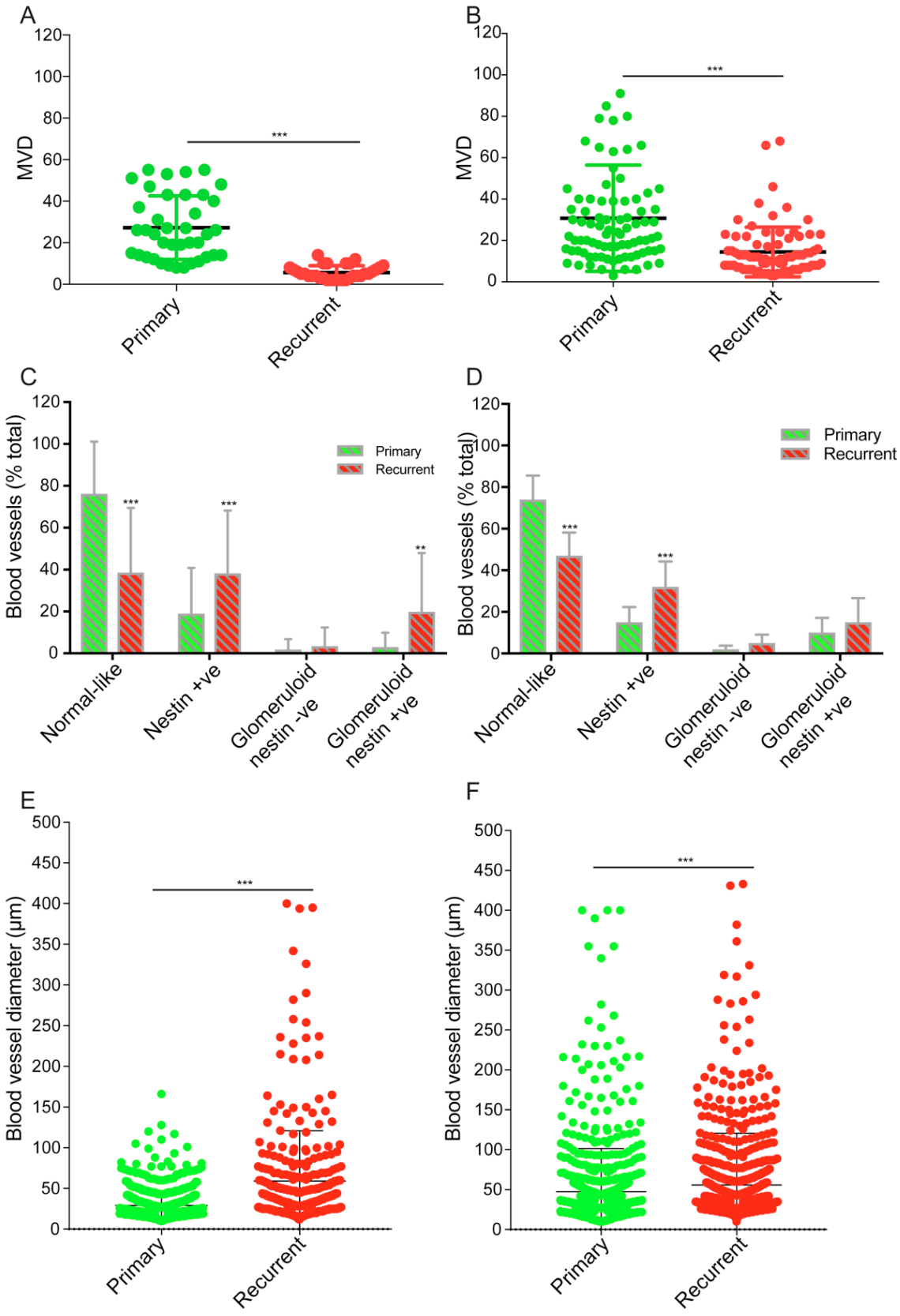
A
MVD
120
100
80
60
40
20
0
***
Primary
Recurrent
B
MVD
120
100
80
60
40
20
0
***
Primary
Recurrent
C
Blood vessels (% total)
120
100
80
60
40
20
0
Primary
Recurrent
***
***
**
Normal-like
Nestin +ve
Glomeruloid nestin -ve
Glomeruloid nestin +ve
D
Blood vessels (% total)
120
100
80
60
40
20
0
Primary
Recurrent
***
***
Normal-like
Nestin +ve
Glomeruloid nestin -ve
Glomeruloid nestin +ve
E
Blood vessel diameter (µm)
500
450
400
350
300
250
200
150
100
50
0
***
Primary
Recurrent
F
Blood vessel diameter (µm)
500
450
400
350
300
250
200
150
100
50
0
***
Primary
Recurrent

Figure 3.15 Quantification of MVD, abundance of blood vessel morphologies and lumen size in primary and recurrent GBM tumours

Primary and recurrent GBM tumours were analysed from the Leeds (5 pairs) and Imperial (10 pairs) patient cohorts.

(A, B) Dot plots show number of blood vessels per 1mm^2 area. Lines are the mean ±SD. (A) Primary GBM (N= 43 1mm^2 areas) against recurrent GBM (N= 32 1mm^2 areas) in the Leeds cohort. (B) Primary GBM (N= 85 1mm^2 areas) against recurrent GBM (N= 83 1mm^2 areas) in the Imperial cohort.

(C, D) Histograms show quantification of blood vessel morphologies as % total blood vessels±SD. (C) Primary GBM (N= 41 1mm^2 areas) against recurrent GBM (N=31 1mm^2 areas) in the Leeds cohort. (D) Primary GBM (N= 92 1mm^2 areas) versus recurrent GBM (89 1mm^2 areas) in the Imperial cohort.

(E, F) Dot blots show vessel diameter with lines representing the mean ±SD. (E) Primary GBM N= 749 blood vessels measured) against recurrent GBM (N=325 blood vessels measured) in the Leeds cohort. (F) Primary GBM (N= 995 blood vessels measured) against recurrent GBM (N= 1018 blood vessels measured) in the Imperial cohort. **p<0.01; ***p<0.001 by two-tailed *t*-test.

3.9 Nestin positive GBM blood vessels are lined by CD31 positive ECs

Following the findings of heterogenous blood vessel morphologies in both primary and recurrent GBM patient samples I characterised further the nestin positive blood vessels seen in abundance in GBM and particularly in recurrent tumours. Previous studies had described how blood vessels in tumours maybe lined directly by cancer cells, a process termed vasculogenic mimicry (Maniotis et al. 1999 and Wang et al. 2013), or by ECs which are transdifferentiated from cancer cells (Ricci-Vitiani et al. 2010 and Soda et al. 2011). Hence, in order to better understand the identity of those nestin positive blood vessels, I stained serial sections of selected GBM tumour samples (primary and recurrent), exhibiting a range of the characterised morphological abnormalities. An interesting finding of this analysis was the presence of intact CD31 positive blood vessels which normally appeared to be lined by nestin positive cells upon nestin and CD31 double staining. Hence, a single staining for CD31 showed that blood vessels were clearly lined by CD31 positive cells, whereas nestin positive cells were situated on the abluminal side of the tumour blood vessels. Surprisingly, the single CD31 staining in this study clearly showed that almost all blood vessels maintained their CD31 positivity both in primary and in recurrent tumours (Figure 3.16).

Following the observation that nestin and CD31 positivity by IHC appeared to overlap, particularly in recurrent tumours, I investigated whether the same cells were expressing both markers and whether these cells were distinct from each other. Therefore, in order to determine the degree of co-expression of CD31 and Nestin, I stained tumour tissue samples from both primary and recurrent GBM samples by immunofluorescence (IF). This staining showed complete lack of co-localisation or co-expression of these two markers (Figure 3.17). While CD31 positive cells lined the blood vessels, nestin positive cells were distinct but at close proximity to the CD31 positive endothelial cells (Figure 3.17). Hence, it can be concluded that GBM blood vessels maintained their CD31 positivity and that CD31 positive cells are distinct to the nestin positive cells.

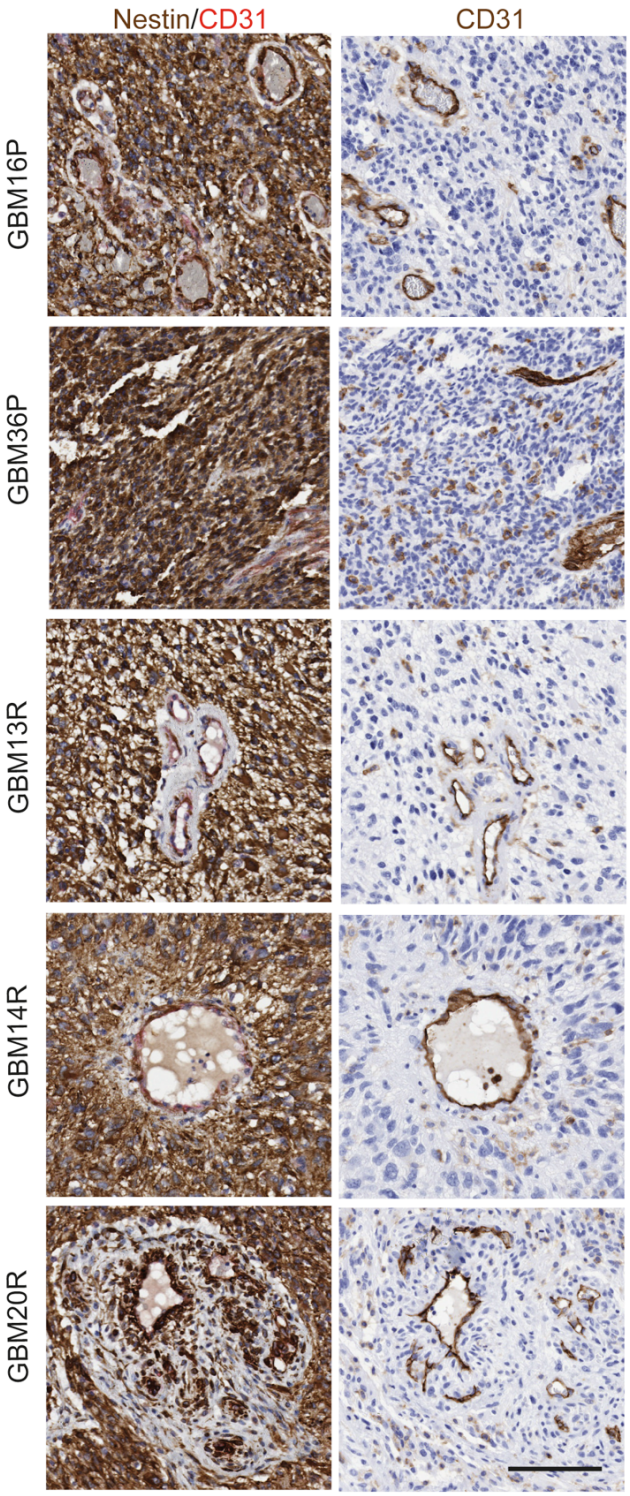

Figure 3.16 Nestin positive blood vessels are lined by an uninterrupted layer of CD31 positive ECs

Serial sections of selected tumour samples (GBM16P, GBM36P, GBM13R, GBM14R and GBM20R) were stained by IHC for Nestin and CD31. Blood vessels were first identified based on their positivity for Nestin/CD31 and then the corresponding slides were checked for the presence of CD31 positivity. P=Primary & R=Recurrent. Scale bar, 100µm.

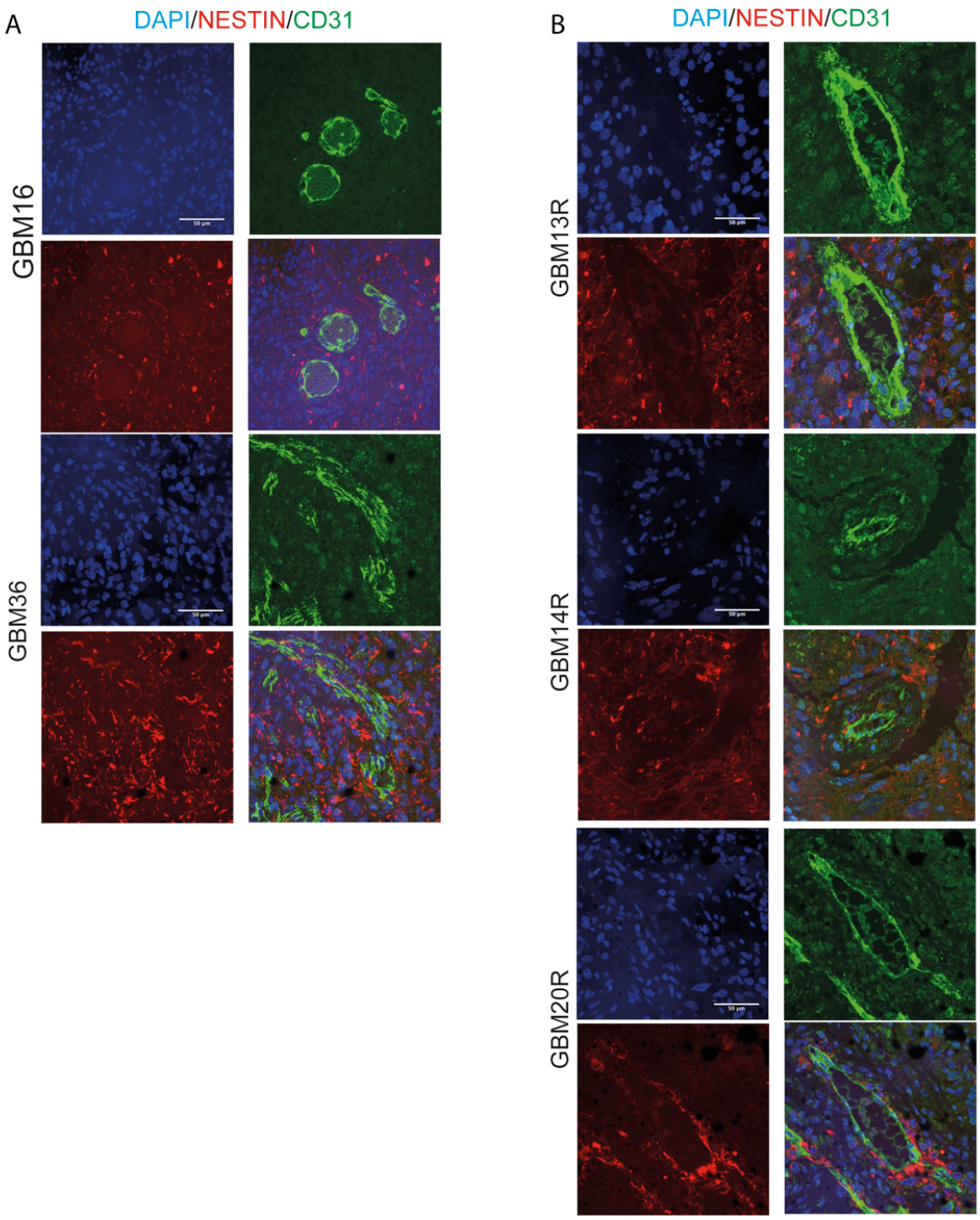

Figure 3.17 Lack of co-expression of Nestin and CD31 in patient GBM blood vessels

Serial sections of selected tumour samples (GBM16P, GBM36P, GBM13R, GBM14R and GBM20R) were stained by IF for Nestin and CD31. Note the presence of nestin positive cells around blood vessels particularly in recurrent GBM samples, but absence of co-expression of nestin and CD31. P=Primary & R=Recurrent. Scale bar, 50 µm.

3.10 Nestin positive GBM blood vessels are negative for stem cell and immune cell markers, but positive for pericyte and smooth muscle cell (SMC) markers

Following the establishment that nestin positive GBM blood vessels are distinct from endothelial cells, I examined whether any of the perivascular cells in the brain tumour microenvironment such as cancer cells, cancer stem cells, immune cells or pericytes could have contributed to the formation of nestin positive blood vessels. I stained serial sections from the selected 5 tumour samples (GBM16P, GBM36P, GBM13R, GBM14R and GBM20R) first for two other stem cell markers expressed by GBM cancer cells, OLIG2 and SOX2. Figure 3.18A shows that blood vessel perivascular cells lacked positivity for these stem cell markers. In addition to the 5 selected samples, analysis of further 4 randomly selected GBM samples (total of 629 tumour blood vessels analysed from 9 GBM samples) showed complete absence of SOX2 positivity in all blood vessels analysed which included normal-like, Nestin +ve and Glomeruloid blood vessels. Interestingly, CD45 and CD68 staining revealed that there were immune and/ or macrophage/ microglia cells in the GBM perivascular niche as previously reported (Yi et al. 2011 and Hambardzumyan, Gutmann, and Kettenmann 2016)), however they were distinct to the nestin positive cells, and more associated with the tumour cell compartment (Figure 3.18B, C). The nestin positive blood vessels were negative for the differentiated cancer cell and astrocyte marker GFAP (Figure 3.18D) but positive for the smooth muscle cell (SMA) and pericyte markers α-SMA and PDGFRß (Figure 3.18C, D). Further, the nestin positive perivascular cells were proliferative as evidenced by positivity for the proliferation marker Ki67 (Figure 3.18B). Analysis of tumour blood vessels from the 5 selected GBM tumours showed different degrees of nestin and α-SMA positivity that has been summarised on Table 3.2. The data show that in 3/5 GBM samples there was a positive correlation between nestin and α-SMA expression in agreement with the IF analysis.

Increase in blood vessel size may result from blood vessel dilation following detachment of pericytes in response to the action of angiogenic growth factors, or blood vessel development and maturation (Nagy et al. 2009). Given GBM blood vessels showed increased coverage by α-SMA cells, particularly in recurrences, I investigated whether this was related to the larger blood vessel calibre observed in GBM and in recurrent tumours (Figures 3.13 and 3.14 showing blood vessel diameters in recurrent Leeds and Imperial samples). Figure 20 shows that there was a positive correlation between blood vessel size and coverage by α-SMA positive cells. Altogether, this larger vessel size and coverage by α-SMA positive cells suggests that the aberrant, strongly nestin positive blood vessels in GBM represent mature and stable blood vessels.

Based on the finding that most nestin positive blood vessels also stained positive for SMA and PDGFRß, I hypothesised that nestin expressing cells are the same as α-SMA and PDGFRß expressing cells in the tumour blood vessels. Accordingly, I took tissue samples from previously selected GBM tumours and stained for combinations of different markers such as Nestin, α-SMA, PDGFRß and CD31 by IF. The stainings showed co-expression of nestin and α-SMA, and also co-expression of nestin and PDGFRß; however, the α-SMA cells were distinct from CD31 cells (Figure 3.19A) as seen in Nestin/CD31 staining (Figure 3.17). In order to quantify α-SMA expression I used a scoring system shown in Figure 3.19B. When I quantified SMA expression in respect with different morphologies, I found that Nestin +ve and Glomeruloid morphologies had significantly higher proportion of SMA positivity compared to normal-like morphologies (Figure 3.19C). This indicated that the nestin positive tumour blood vessels are distinct from cancer stem cells, immune cells, astrocytes or ECs, but represent pericytes and SMCs.

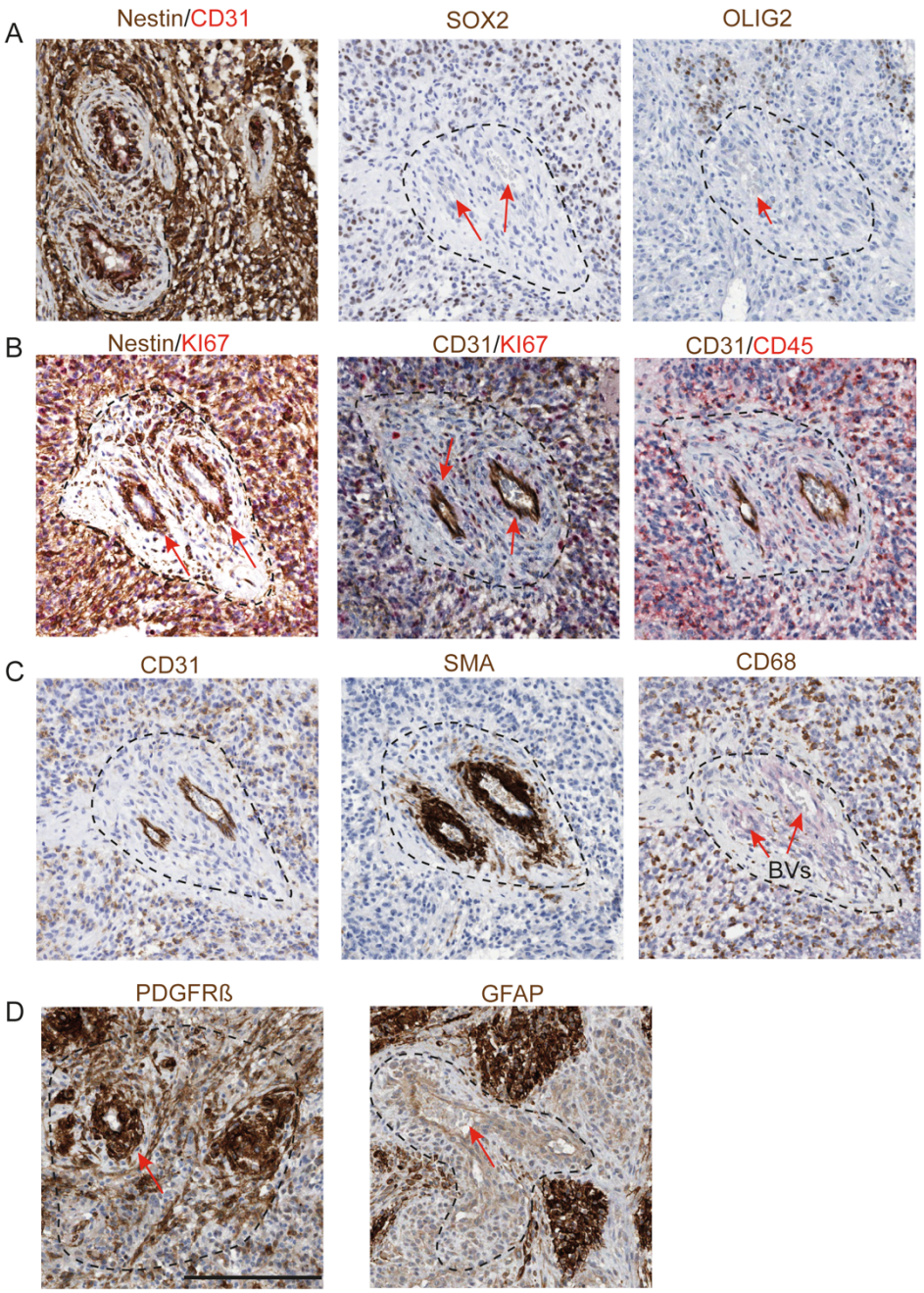

Figure 3.18 Nestin positive GBM blood vessels are negative for the stem cell markers OLIG2 and SOX2 and immune cell markers, but positive for the pericyte and smooth muscle cell (SMC) markers PDGFRβ and α-SMA

Sections from patient GBM (GBM20R) were stained for Nestin, SOX2, OLIG2 and CD31 (A); Nestin, CD31, Ki67 and CD45 (B); CD31, α-SMA and CD68 (C); and PDGFRβ and GFAP (D). Red arrows point to blood vessels with lack of positivity for the markers SOX2, OLIG2, CD68 and GFAP in different antibody markers in panels A, C and D; and Ki67 positivity in B. Scale bar, 100µm.

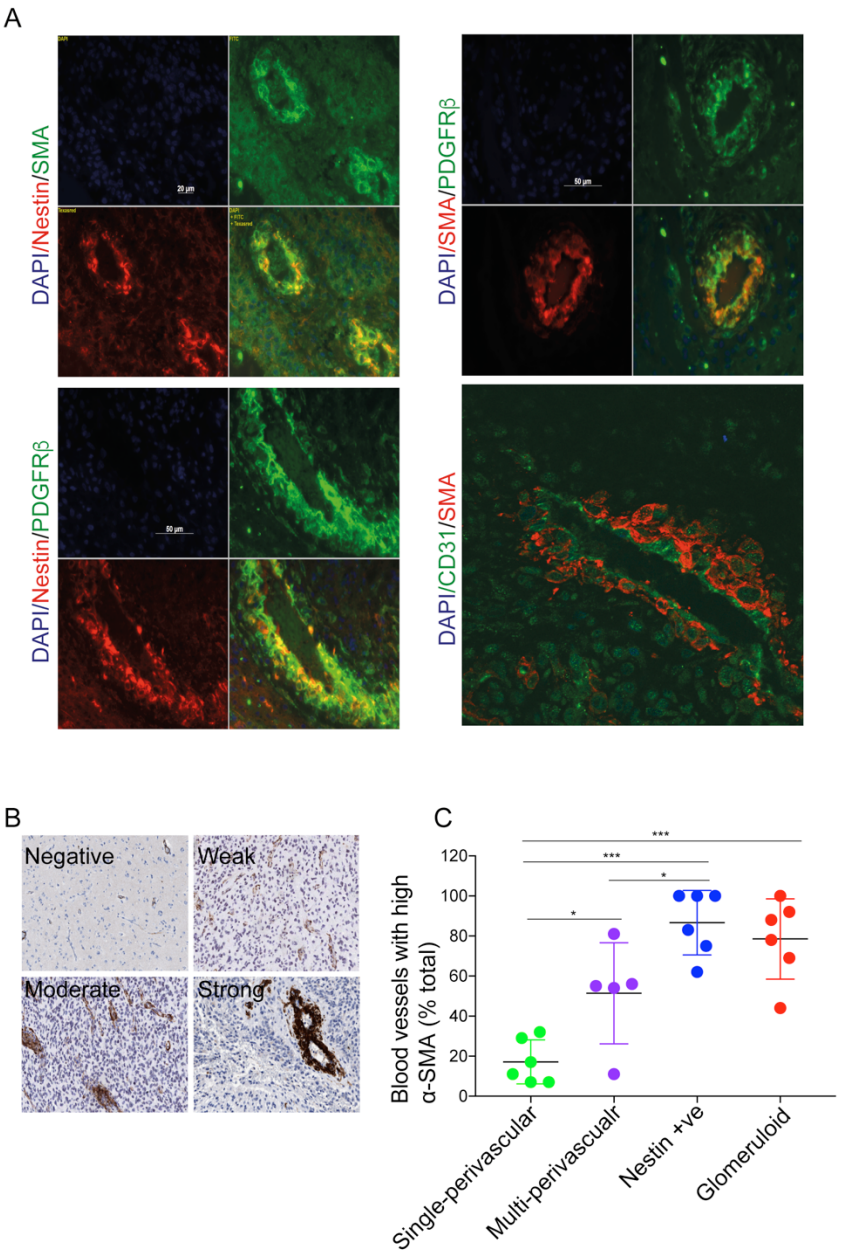

Figure 3.19 Nestin positive perivascular cells express high α-SMA and PDGFRβ

(A) Images show expression of α-SMA and PDGFRβ in Nestin +ve blood vessels by IF (GBM20).

(B) Images depict weak, moderate and strong α-SMA levels by IHC staining. Moderate and strong expression were considered as High SMA in (C).

(C) Expression of α-SMA in blood vessels with different morphologies as defined by their nestin positivity. Blood vessels in GBM samples GBM13, GBM16, GBM36, GBM13R, GBM14R, GBM20R, GBM37, GBM30R and GBM39 were scored based on the intensity of α-SMA expression on parallel sections as shown in (B). Each dot represents the average percentage of blood vessels with high α-SMA expression in a tumour. The number of areas and blood vessels scored are shown in Appendix 3. Samples with ≤3 blood vessels per 1mm^2 for a particular morphology were excluded from the scoring.

Table 3.2 Expression of Nestin, OLIG2 SOX2 and α-SMA in GBM patient samples

	GBM16P	GBM36P	GBM13R	GBM14R	GBM20R
Total blood vessel count	82	123	34	48	23
Number of Nestin +ve vessels count	52	56	21	19	22
% of Nestin +ve blood vessels	63	46	62	40	96
Number of SOX2 +ve vessels count	0	0	0	0	0
% of SOX2 +ve vessels	0	0	0	0	0
Number of OLIG2 +ve vessels count	0	0	0	0	0
% of OLIG2 +ve vessels	0	0	0	0	0
Number of α-SMA +ve vessels count	49	29	25	40	18
% of α-SMA +ve vessels	60	24	74	83	78

Five GBM (GBM16 and GBM36 primary; and GBM13, GBM14 and GBM20 recurrent) patient samples were serially sectioned and stained for their expression of stem cell markers (Nestin, SOX2 and OLIG2), and pericyte/SMCs marker α-SMA. A total of 310 blood vessels were analysed and the expression was scored as indicated in Figure 3.19B. P, Primary and R, recurrent tumours.

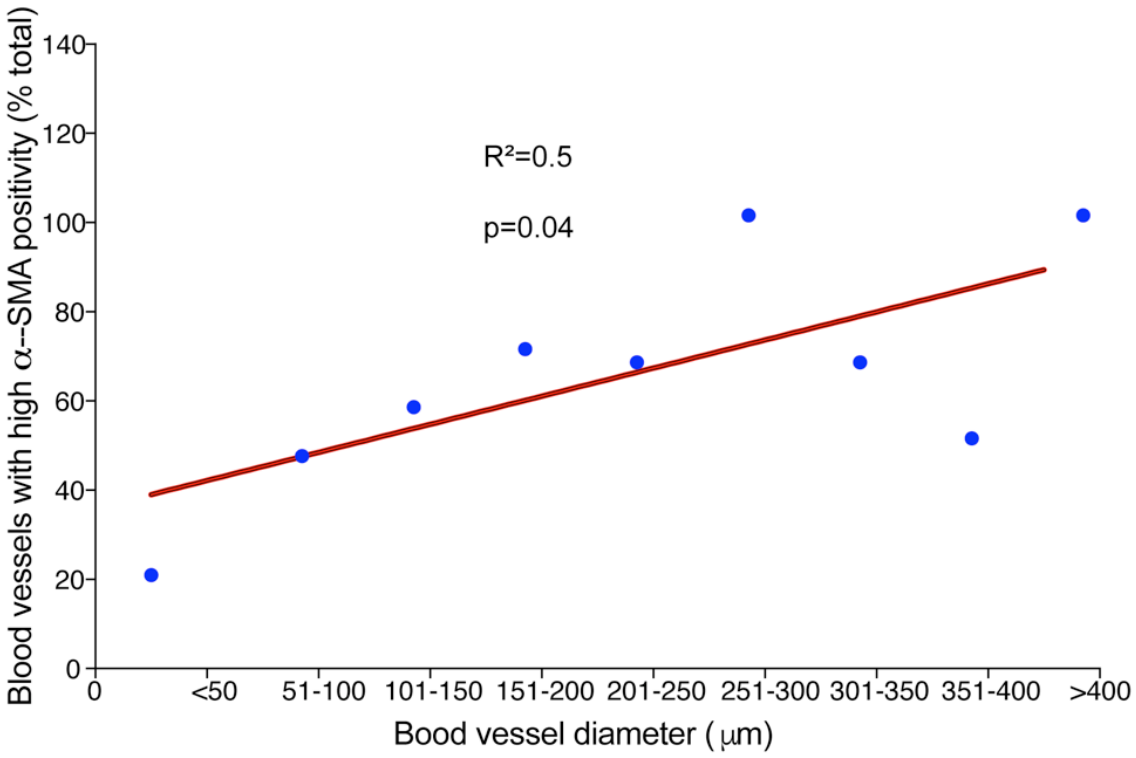

Figure 3.20 Association of blood vessel lumen size with levels of α-SMA expression

The percentage of blood vessels with high α-SMA positivity is shown with corresponding blood vessel diameters <50 μm (N=152), 51-100 μm (N=230), 101-150 μm (N=150), 151-200 μm (N=96), 201-250 μm (N=100), 251-300 μm (N=26), 301-350 μm (N=51), 351-400 μm(N=2), >400 μm (N=4) were counted from a total of 9 GBM patient samples (GBM13P, GBM16P, GBM36P, GBM37P, GBM39P, GBM13R, GBM14R, GBM20R and GBM30R). A total of 6 x 1mm^2 areas per each tumour sample was analysed except in GBM30R where only 5 of such areas were available. The percentage blood vessels with high α-SMA expression was plotted against the blood vessel diameters. Note the significant correlation between blood vessel size and α-SMA positivity. Each dot represents the percentage of blood vessels with high α-SMA expression for the respective blood vessel diameter range. R, Spearman's rank correlation coefficient. P, Primary and R, Recurrent tumour. P value, statistical significance.

3.11 Nestin positive blood vessels and glomeruloids are situated close to areas of necrosis

One way of defining distinct areas within the heterogenous GBM tumours is through reference to the tumour edge and tumour core. Kim and co-workers showed that tumour cells at the edge of tumours are viable and highly invasive through expression of MMPs, while the core is characterised by widespread areas of necrosis (Kim et al. 2011). Scoring of blood vessels within the 5 selected tumours for their proximity to tumour necrosis showed that the single perivascular blood vessels were mainly located away from areas of necrosis (Figure 3.21A, B). Separate analysis of these samples as primary and recurrent showed that in primary tumours normal-like blood vessels are located away from areas of necrosis, whereas abnormal nestin positive vessels are situated close to areas of necrosis (Figure 3.21C). On the other hand, a significantly higher proportion of nestin positive blood vessels were associated with necrotic regions in the recurrent tumours (Figure 3.21D).

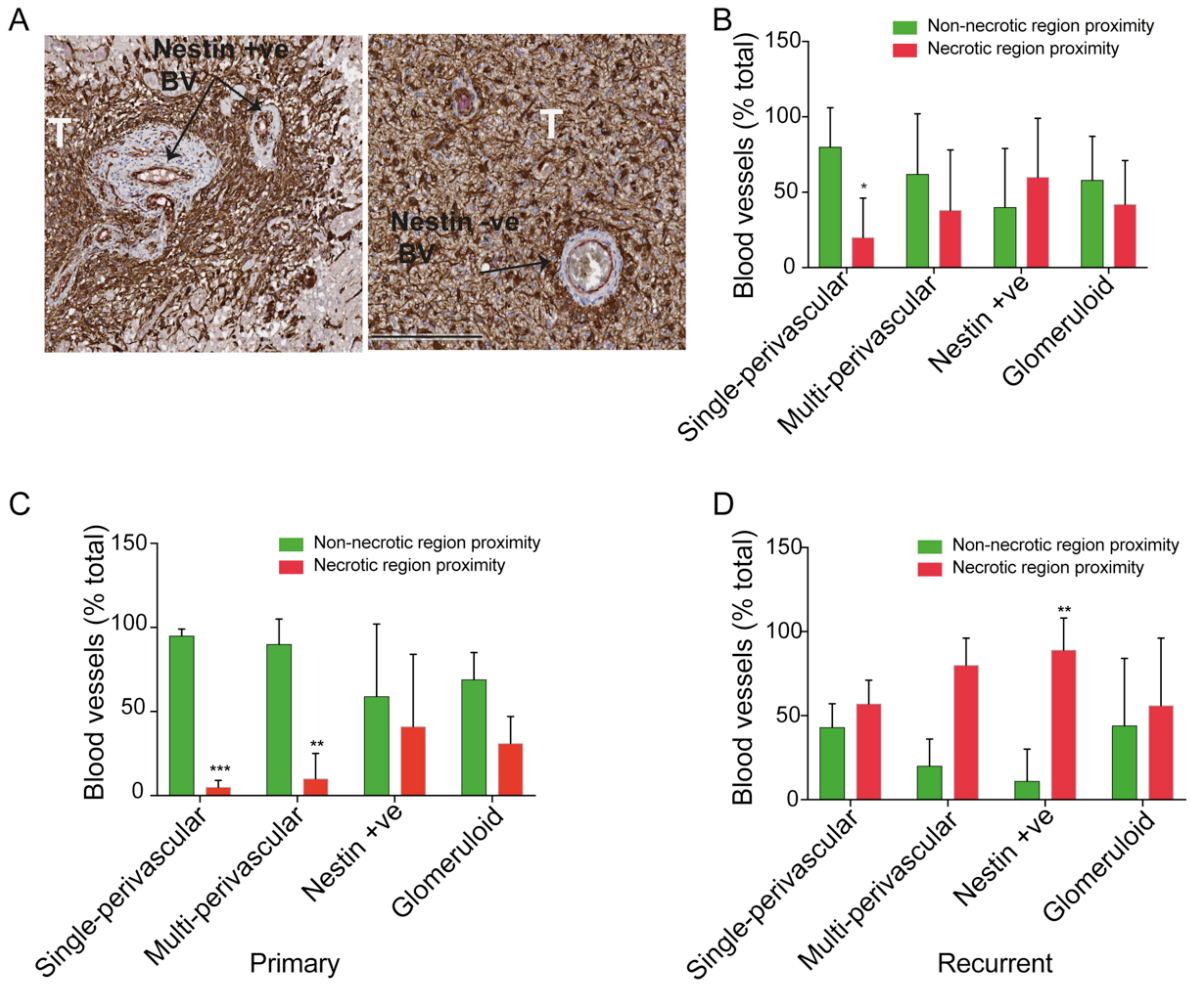

Figure 3.21 Proximity of blood vessels with different morphologies to necrotic regions

Blood vessels with different morphologies were scored based on their proximity (100 μm) to areas of necrosis.

(A) Images depict Nestin +ve and Nestin -ve blood vessels close to necrosis (left-hand panel), and within viable tumour areas (right-hand panel). Scale bar, 100 μm.

(B) Quantification of blood vessel morphologies according to their proximity to areas of necrosis shown as percentage total blood vessels ± SD (N=number of 1mm^2 areas analysed in 5 tumours).

(C) As in (B) for the primary tumours only (2 tumours).

(D) As in (B) for the recurrent tumours only (3 tumours).

3.12 Recurrent tumours are more hypoxic than primary GBM tumours

The observation that nestin positive blood vessels were associated with areas of necrosis raised the question whether they contributed to hypoxia and necrosis, or protected cancer cells from cell death. GBM is characterised by widespread hypoxia (Kaur et al. 2005). In order to investigate whether the presence of hypoxia is associated with particular blood vessel morphologies, I stained the 5 tumour cohort for the hypoxia marker CAIX (Wykoff et al. 2000) and used the scoring shown in Figure 3.22A to assign negative, weak, moderate or strong hypoxia levels to cancer cells around blood vessels. First, quantification showed overall higher hypoxia in recurrent tumours compared to primary tumours (Figure 3.22B). Next, I investigated the potential association of hypoxia with blood vessel type and lumen size in the recurrent tumours. Strikingly, I found low hypoxia levels around blood vessels with SMA positivity suggesting that these vessels are functional (Figure 3.23 and 3.24A), whereas blood vessels with normal-like morphologies were associated with higher levels of hypoxia (Figure 3.24B). To summarise, recurrent tumours appeared more hypoxic than primary tumours. Within recurrent tumours Normal-like blood vessel morphologies which are mostly small in size, are more hypoxic compared to large size Nestin +ve and Glomeruloid blood vessels.

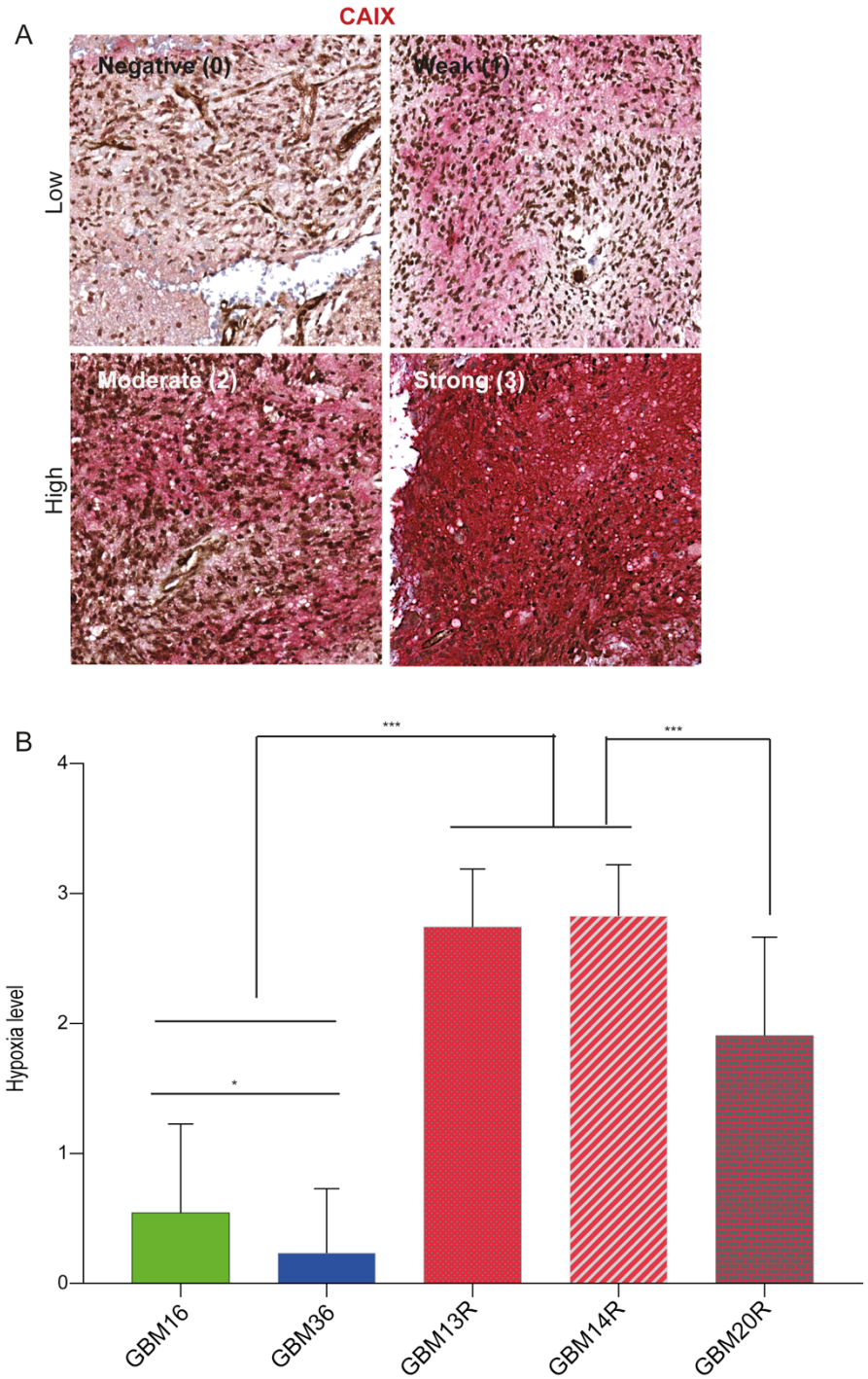

Figure 3.22 Hypoxia levels are higher in recurrent tumours compared to primary tumours

(A) Images depict intensities of CAIX staining

(B) Histogram shows the scoring of hypoxia in cancer cells around immediate proximity of blood vessels. N= number of blood vessels per 1mm^2 area ± SD (GBM16, 40; GBM36, 75; GBM13R, 36; GBM14R, 12 and GBM20R, 34) *<0.05 and ***<0.001.

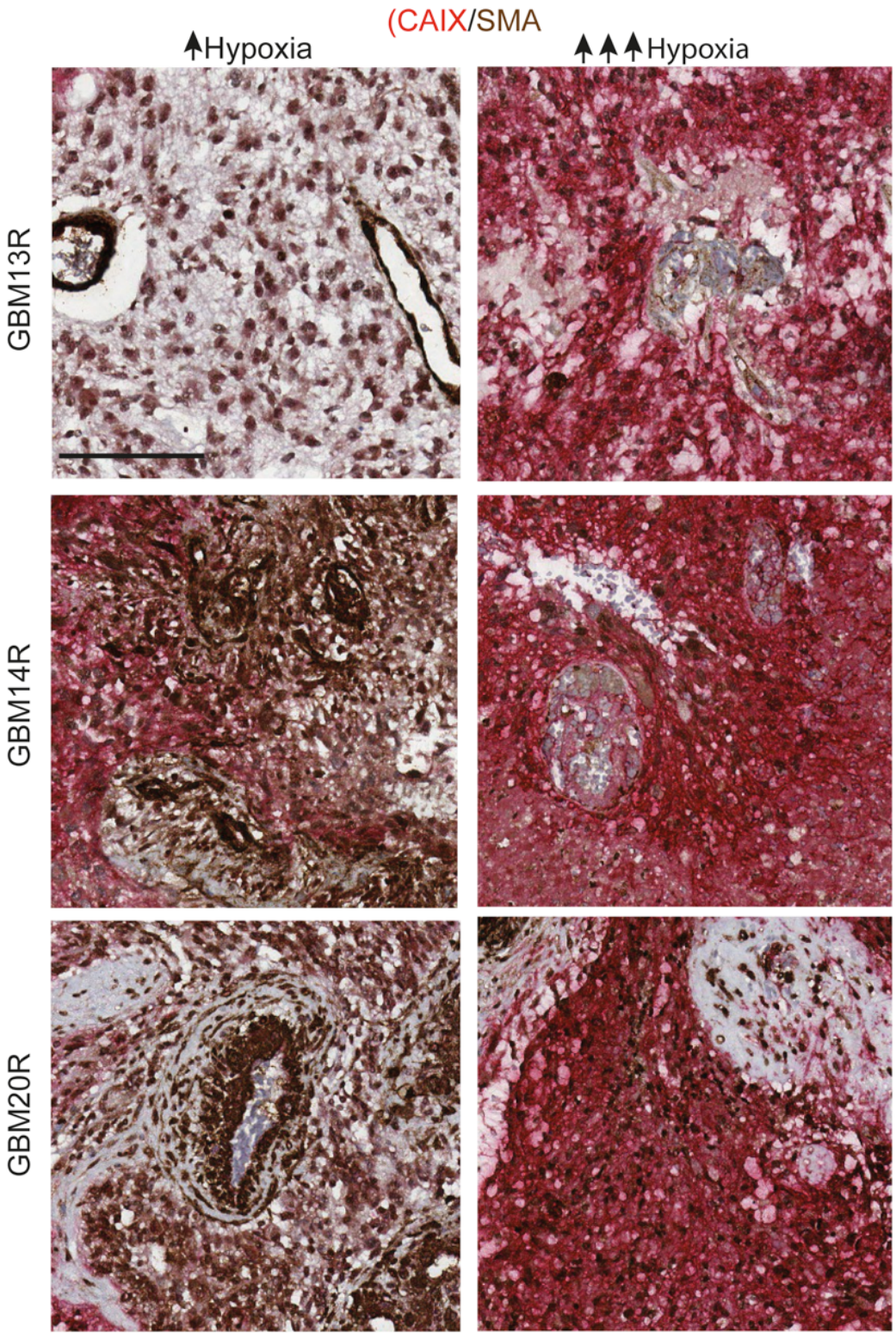

Figure 3.23 Nestin +ve blood vessels are less hypoxic than Normal-like blood vessels in recurrences

CAIX and α-SMA staining of recurrent GBM tumour samples show that α-SMA positive blood vessels have less hypoxia around them (left-hand panels), while occluded or normal-like blood vessels had the highest hypoxia around them (right-hand panels). Scale bar, 100 μm.

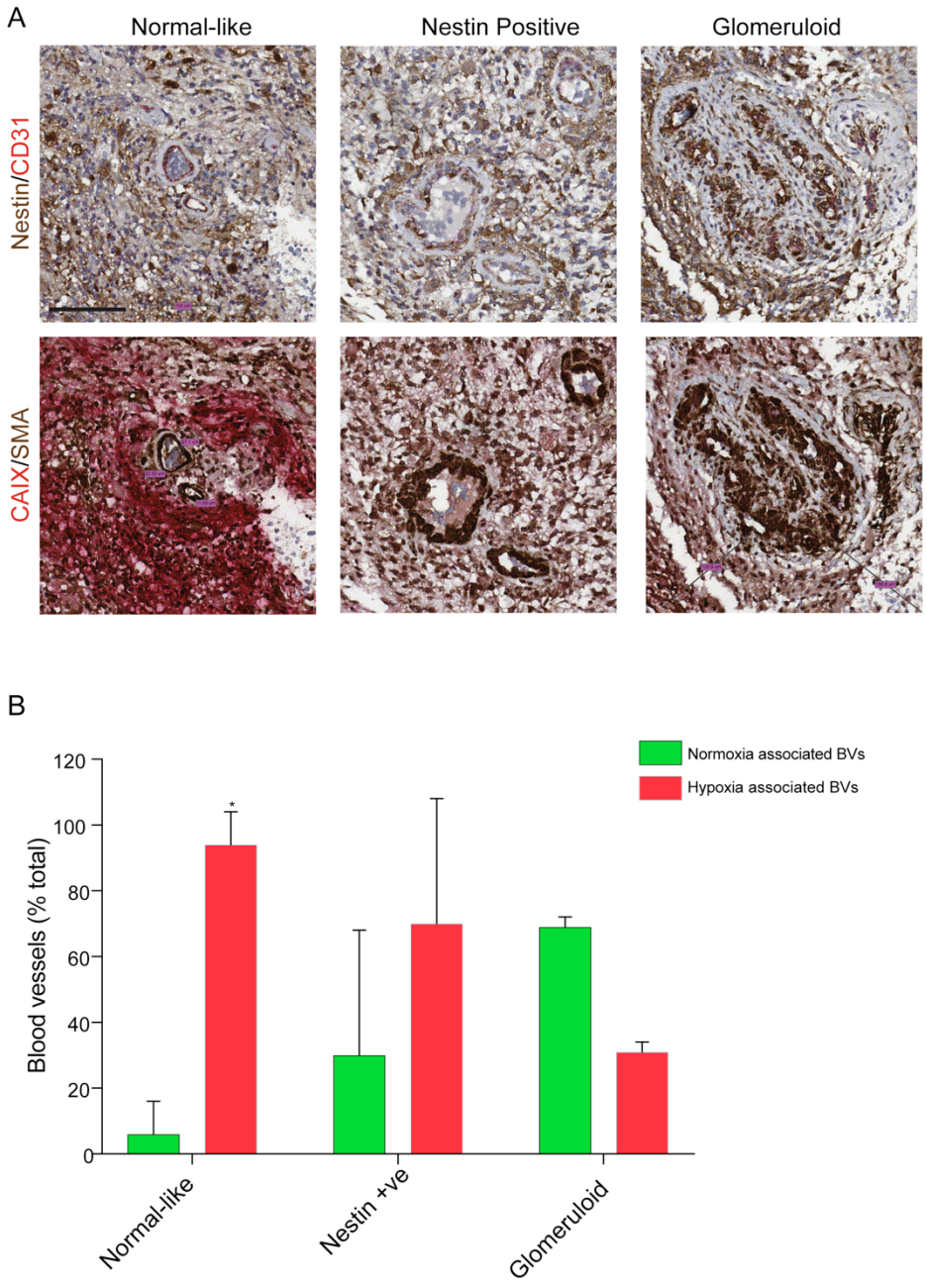

Figure 3.24 Serial sections of GBM samples stained for Nestin/CD31 and CAIX/SMA and quantification of association with normoxia and hypoxia

(A) Double immunostaining of serial sections of recurrent patient GBM tumour tissue samples using Nestin/CD31 and CAIX/SMA. Note low levels of hypoxia around nestin +ve blood vessels and glomeruloids. Scale bar, 100µm.

(B) Histogram shows quantification of blood vessel morphologies in normoxic and hypoxic tumour areas surrounding blood vessels (100 µm) as percentage total blood vessels ±SD in the 3 recurrent GBMs (GBM13, GBM14 and GBM20) of the 5 selected tumour cohort. *<0.05.

3.13 Conclusions

The analysis of blood vessel morphologies in this chapter identified 5 different blood vessel morphological types in patient-derived GBM samples based on expression of the stem cell marker nestin and endothelial cell marker CD31. While the blood vessel types Normal-like, Single-perivascular and Multi-perivascular were also detected in the normal brain, Nestin +ve and Glomeruloid (nestin –ve and nestin +ve) blood vessel morphologies were only found in GBM samples. Notably, the majority of glomeruloid blood vessels were nestin positive, making nestin positivity a hallmark of aberrant GBM blood vessels. The analysis shows that overall, at the point of first surgery which is normally close to the time of diagnosis, blood vessel morphologies are heterogenous and normal-like morphologies prevail. However, when primary and recurrent patient samples were compared, the aberrant morphologies increased significantly and in 11 out of 15 paired samples analysed those were more abundant than the normal-like morphologies. In addition to morphology, the analysis showed that blood size was also heterogeneous in patient samples. Consistent with the increase in the abundance of highly nestin positive and glomeruloid blood vessels in recurrent tumours, abnormal blood vessel size also increased in recurrence. Altogether, the analyses show high nestin positivity is a key feature of GBM. Interestingly, I also found that as tumours recurred the microvascular density (MVD) decreased, pointing to dominance of a fewer number of blood vessels with larger calibre in recurrent tumours.

Previous studies had shown that cancer cells can line the lumen of GBM tumour blood vessels, a phenomenon resembling vasculogenic mimicry in melanoma (Maniotis et al. 1999; Wang et al. 2013 and Francescone et al. 2012), or following transdifferentiation of cancer stem cells to endothelial cells (Ricci-Vitiani et al. 2010 and Soda et al. 2011). CD31 staining of tumours showed uninterrupted coverage of blood vessels showing that unlike melanoma, GBM blood vessels are only lined by CD31 positive endothelial cells. In almost all GBM tissue samples analysed blood vessels consistently maintained their intact CD31 positivity. Further, the strongly nestin positive blood vessels initially observed by means of nestin/CD31 double immunostaining, were also entirely covered by intact CD31 positive cells, while the use of double immunofluorescence showed that CD31 positive ECs were distinct to nestin positive peri-vascular cells, as there was no co-localisation or co-expression of nestin and CD31 by IF. When I further stained the GBM tissues for additional cancer cell markers (SOX2 and OLIG2) that were expressed abundantly in the tumour cell compartment, those were not expressed by the perivascular nestin positive cells, which were also negative for immune cell markers CD45 and CD68. However, the nestin positive cells were positive for pericyte and smooth muscle cell markers α-SMA and PDGFRβ.

Altogether, the pericyte/SMCs coverage together with the larger vessel calibre and changes in MVD identified through the analysis of primary and recurrent tumours indicates that there is a variable proportion of stable and mature blood vessels in primary patient tumours accounting for 28% (0 -82%) of total GBM vessel morphologies that increased with tumour recurrence to 39% (9-86%). Notably, glomeruloids, scored as single entities here, have a much wider area coverage, and therefore represent a significant proportion of the tumour vasculature as seen in Figures 3.1 and 3.4. Scoring for the proximity of nestin positive blood vessels and glomeruloids to areas of necrosis and hypoxia showed they are associated with areas of necrosis. On the other hand, there was a higher proportion of nestin positive and glomeruloid blood vessels associated with normoxia in the tumour cell compartment surrounding the blood vessels compared to normal-like vessels. Strikingly, there was widespread hypoxia associated with normal-like blood vessels in recurrent tumours. There are high levels of VEGF expression in GBM (Wang, Zhang, et al. 2016). Tumour cells at the edge of tumours are viable and highly invasive, and capable of moving to the normal brain parenchyma where they co-opt new blood vessels. Dvorak and co-workers have shown that established blood vessels in experimental models respond to high levels of VEGF first by dilation, which leads to the development of unstable vessel structures termed mother vessels (Nagy et al. 2009). This is followed either by vessel maturation and recruitment of SMCs, or formation of glomeruloid structures which were also reported to be immature and unstable. The inability of normal-like blood vessels in GBM to support normoxia suggests that they represent mother vessels. And that maturation to the Nestin/α-SMA positive aberrant vessels is necessary to support tumour growth.

Overall, this study shows that the nestin positive cells surrounding blood vessels in GBM have smooth muscle cell characteristics, namely α-SMA expression and tight association with larger calibre blood vessels. Particularly, the larger the blood vessels the higher the α-SMA positivity, consistent with a more mature and stable phenotype.

Chapter 4

The role of DOCK4 in blood vessel growth and tumour progression in GBM and in radiation therapy

4.1 Introduction

One characteristic feature of the glioblastoma vasculature observed in the patient-derived GBM samples was their large size and abnormal coverage by nestin positive pericyte/smooth muscle cells. Tumour blood vessel lumen size increased in recurrent patient GBM tumour samples compared to primary samples. The aberrant vasculatures of the tumour support the development of hypoxia (Brown and Giaccia 1998) which is thought to contribute to radiotherapy resistance through stabilisation of HIF-1α (Marampon et al. 2014 and Moeller et al. 2004). It has been proposed that normalisation of tumour blood vessels through inhibition of the molecular regulators of abnormal vascularisation can improve therapy (Goel et al. 2011). A key driver of abnormal blood vessel formation in tumours including glioblastoma and target of HIF-1 is the proangiogenic factor VEGF which controls development of new blood vessels (Aonuma et al. 1999). Previous work in our laboratory has shown that downstream of VEGF signaling by the Rac1 exchange factor DOCK4 is important for blood vessel growth (Abraham et al. 2015). Global heterozygous deletion of Dock4 reduced blood vessel lumen size in EO771 tumours (a model of breast cancer brain metastases) growing intracranially in mice (Abraham et al. 2015). Hence, I hypothesised that *Dock4* deletion could normalise tumour blood vessels and potentially improve radiotherapy in GBM, which I set out to test in the heterozygous *Dock4* knockout model since homozygous deletion is embryonic lethal (Abraham et al. 2015).

Two syngeneic tumour models were compared for these studies, as patient-derived GBM tumours don not grow in immunocompetent mice: GL261 (Szatmari et al. 2006) and CT2A (Martinez-Murillo and Martinez 2007) are the two most commonly used syngeneic tumour models in pre-clinical studies. Tumour cells were expanded in culture, trypsinised and injected into the striatum of the right brain hemisphere, and mice were monitored for tumour growth using IVIS and neurological symptoms. The tumour tissue samples were fixed in 4% PFA, paraffin embedded, sectioned and stained for analysis. Analysis showed that CT2A tumour growth resembled more that of patient GBM compared to GL261 tumours as cancer cells readily co-opted blood vessels in the tumour periphery, and therefore the CT2A tumour model was used in the subsequent *in vivo* experiments. The increase in blood vessel abnormality seen in recurrent tumours was following treatment of patients with radiotherapy and temozolomide chemotherapy. In order to investigate the potential contribution of radiotherapy in the development of aberrant blood vessel morphologies, tumour bearing mice were irradiated using the X-Ray irradiator or the small animal radiation research platform (SARRP) which delivers radiation accurately and specifically to the tumour mass. Blood vessel lumen size was analysed in wild type and *Dock4* heterozygous knockout mice in the presence or absence of irradiation. Further, lumen size

analyses were carried at different stages of tumour growth post irradiation. Finally, a *Dock4* conditional knockout mouse line was bred to homozygosity and endothelial-specific *Dock4* deletion and a pilot experiment was conducted using these mice.

4.2 Establishing an experimental tumour model which recapitulates patient glioblastoma growth *in vivo*

In order to elucidate the role of DOCK4 in the glioblastoma tumour vasculature I started experiments using two commonly employed mouse glioblastoma tumour models; CT2A and GL261. I found that while GL261 tumours have a more of restricted and circumscribed edge, CT2A tumours are more infiltrative with cancer cells co-opting blood vessels in the surrounding normal brain parenchyma, a trait not observed extensively in the GL261 tumour model (Figure 4.1A). In addition, while Haematoxylin and Eosin (H&E) staining of GL261 tumours showed a large number of vacuole-like empty spaces the CT2A tumour tissue appeared dense and largely similar to patient GBM tumour samples. Specifically, when sections of CT2A tumour tissues were stained for endothelial cell marker CD31 blood vessels with smaller lumen size were observed in the Dock4 het mice compared to WT control mice (Figure 4.1B). Vessel co-option mechanism is one of characteristic features of glioblastoma tumours (Holash et al. 1999) and hence I decided to take forward CT2A as chosen tumour model for further *in vivo* experiments.

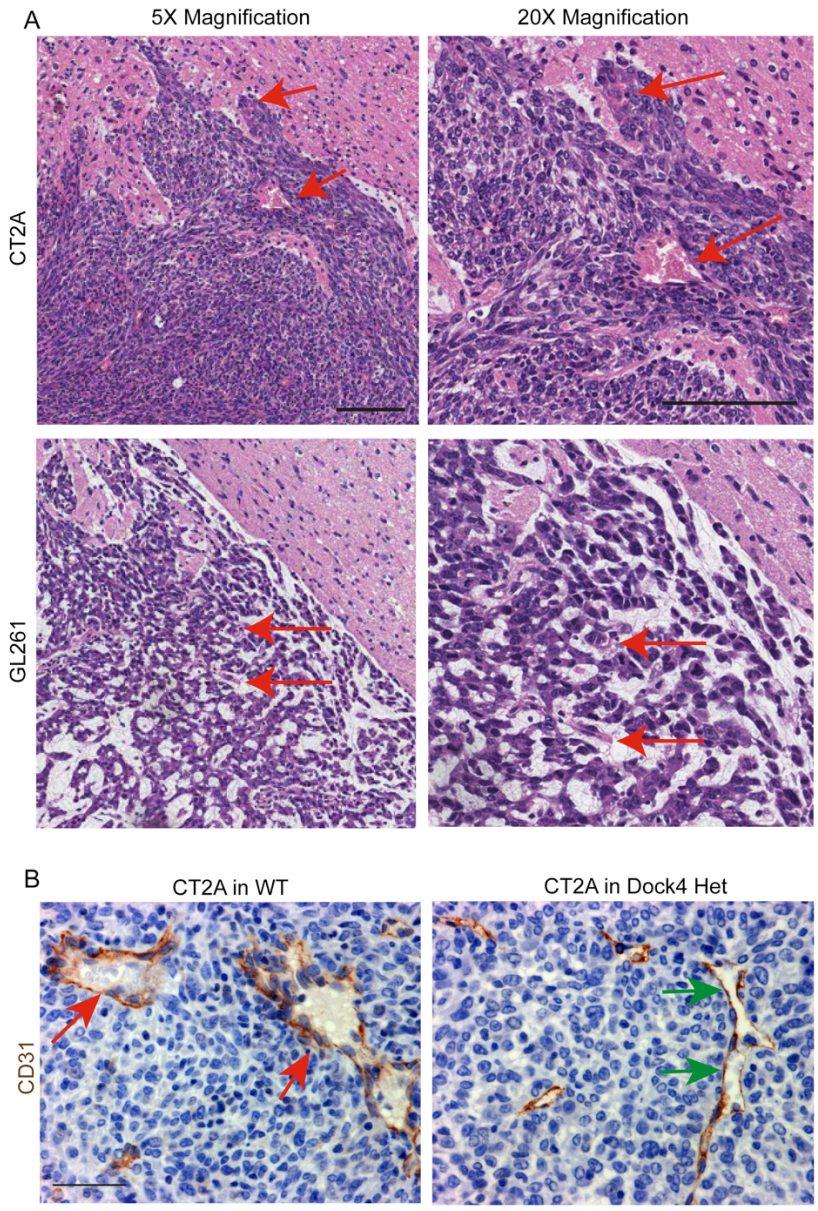

Figure 4.1 The growth patterns of GL261 and CT2A mouse glioma cell lines *in vivo*

GL261 and CT2A tumour cells ($4x10^4$ and $1x10^5$ respectively) were injected intracranially into the striatum of C57BL/6 wild type and *Dock4* heterozygous knockout mice.

(A) H&E staining of CT2A and GL261 tumours. Arrows point to blood vessels. Note the invasive edge of CT2A tumours and co-option of blood vessels (top arrow) compared to circumscribed periphery of GL261 tumours. Scale bar, 100 µm.

(B) CD31 staining of CT2A tumours grown in wild type (WT) or *Dock4* heterozygous (het) mice. Red arrows point to large blood vessels in WT control CT2A tumour sample and green arrows point to smaller diameter blood vessels in *Dock4* heterozygous mice. Scale bar, 50 µm.

4.3 Optimisation of radiotherapy in the CT2A tumour model using SARRP

Previous *in vivo* experiments have used clinically relevant doses of ionising radiation, ranging from 4Gy to 30Gy, to treat different glioblastoma tumour models in mice. For example Newcomb and co-workers (Newcomb et al. 2010) and Yadav and co-workers (Yadav et al. 2016) showed inhibition of glioblastoma tumour growth when delivering total doses of 8Gy over two days (4Gy/day) and 20Gy over 10 days (2Gy/day) respectively. In this study, initially I compared doses of 10Gy and 15Gy delivered at 2Gy/day and 5Gy/day, respectively. CT2A tumour cells were injected intracranially and after one week following implantation, mice were irradiated using a small animal radiation research platform (SARRP) available in our Institute. SARRP enables researchers to image the animal using Cone beam-CT, contour tumour and organs at risk, calculate and deliver the desired dose with an accuracy equivalent to the current clinical radiotherapy used in patients. All the mice were sacrificed following the onset of neurological symptoms in control mice.

H&E staining of tumour samples showed a significant reduction of tumour mass with irradiation (Figure 4.2). None of the mice showed any signs of toxicity following irradiation at either 10Gy or 15Gy. There was a smaller tumour mass remaining with a dose of 15Gy compared to 10Gy, with a dose of 15Gy ablating almost all tumour growth (Figure 4.2). Interestingly, at a higher magnification, I could observe small colonies of cancer cells around blood vessels with visible lumens in irradiated tumours which were more prominent at 15Gy. Following this finding I decided to use a 10Gy irradiation regime in experiments with combination of Dock4 deletion, in order to be able to assess the contribution of Dock4 in residual tumour growth.

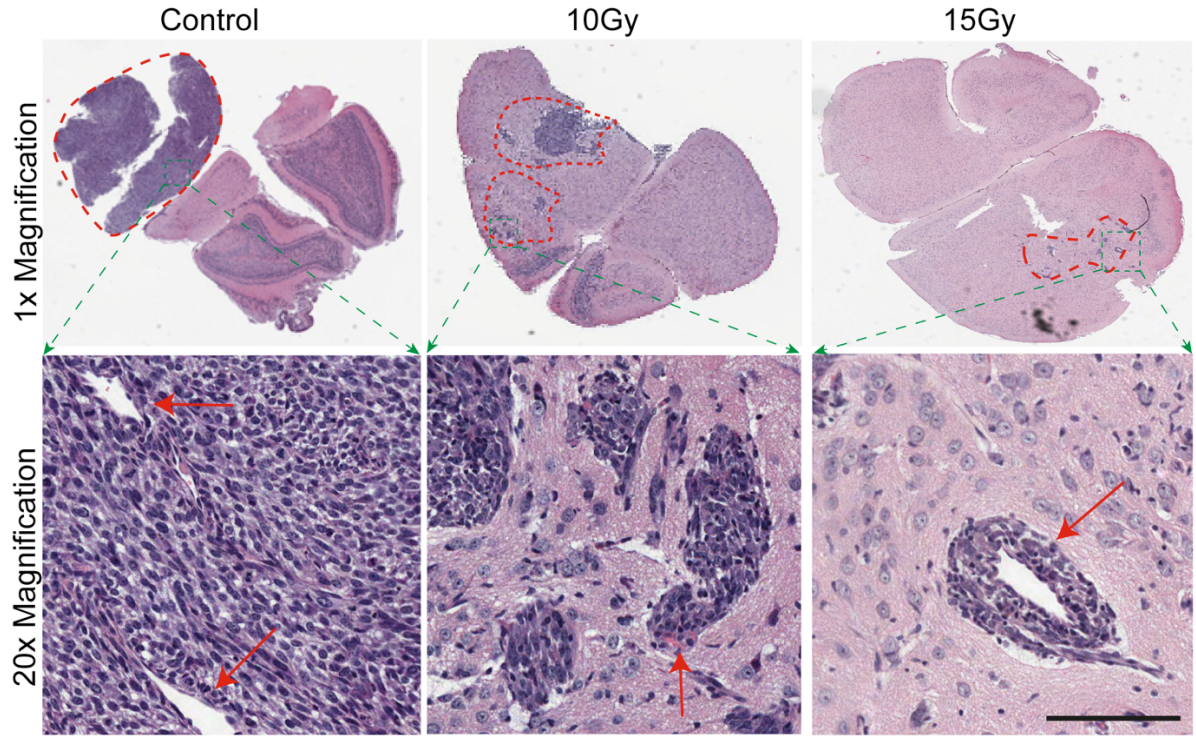

Figure 4.2 Comparison of 10Gy and 15Gy radiation doses in CT2A tumours

CT2A cells ($1x10^5$) were injected intracranially into the striatum of C57BL/6 wild type and two different doses of targeted irradiation were applied using SARRP (3mm x 9mm collimator). 2Gy/day for 5 consecutive days (total 10Gy) or 5Gy/day for 3 consecutive days (total 15Gy). Mice were sacrificed upon development of neurological symptoms in control mice. Tumour tissue samples were embedded in paraffin and sectioned using a microtome. Images show haematoxylin and eosin (H&E) staining of 4 μm tumour sections.

Top panels: Microscopic images at 1x magnification show tumour lesions in different groups (dotted red circles).

Bottom panels: Enlarged images of boxed areas in top images. The images are representative of different tumours for each condition: Control, 5; 10Gy, 4; 15Gy, 4).

4.4 The effect of heterozygous *Dock4* deletion on the efficacy of radiotherapy

Next, I investigated whether *Dock4* heterozygous deletion could contribute to the efficacy of irradiation. CT2A-luc cells stably expressing luciferase were injected intracranially in wild type (WT) and Dock4 heterozygous mice. Mice were randomised based on their IVIS reading just before therapy. As the number of male Dock4 mice available for this experiment were not enough two female mice were added to the Dock4 het control group as this was the only cohort available at that point of breeding (Appendix 4). Further, because SARRP was not available I used a whole brain irradiation using RAD X-Ray irradiator. Tumour growth was regularly monitored up to 21 days post intracranial implantation using IVIS after subcutaneous injection of luciferin in order to image the growth of intracranially injected luciferase labelled CT2A cancer cells using non-invasive IVIS bioluminescence imaging (Figure 4A). Figure 4B shows a significant reduction of tumour growth in irradiated WT mice compared to WT control mice ($p=0.003$).

Similarly, tumour growth was significantly reduced in irradiated Dock4 het compared to Dock4 het control ($p<0.0001$). However, there was no significant difference between WT irradiated and Dock4 irradiated mice ($p=0.98$). Surprisingly, the growth of tumour in wild type control appeared decreased compared to Dock4 het control on day 20 ($p=0.005$). However, this was due to the use of mixed sex in the Dock4 het group, as the female mice had faster tumour growth compared to the male mice (Figure 4.3B) compared to the male mice at days 17 ($p<0.0001$) and 20 ($p=0.0001$) post intracranial injection. Overall, while there was significant difference between the growth of control and irradiated mice, there was no difference between WT and *Dock4* het mice, under control or irradiation conditions in this experiment.

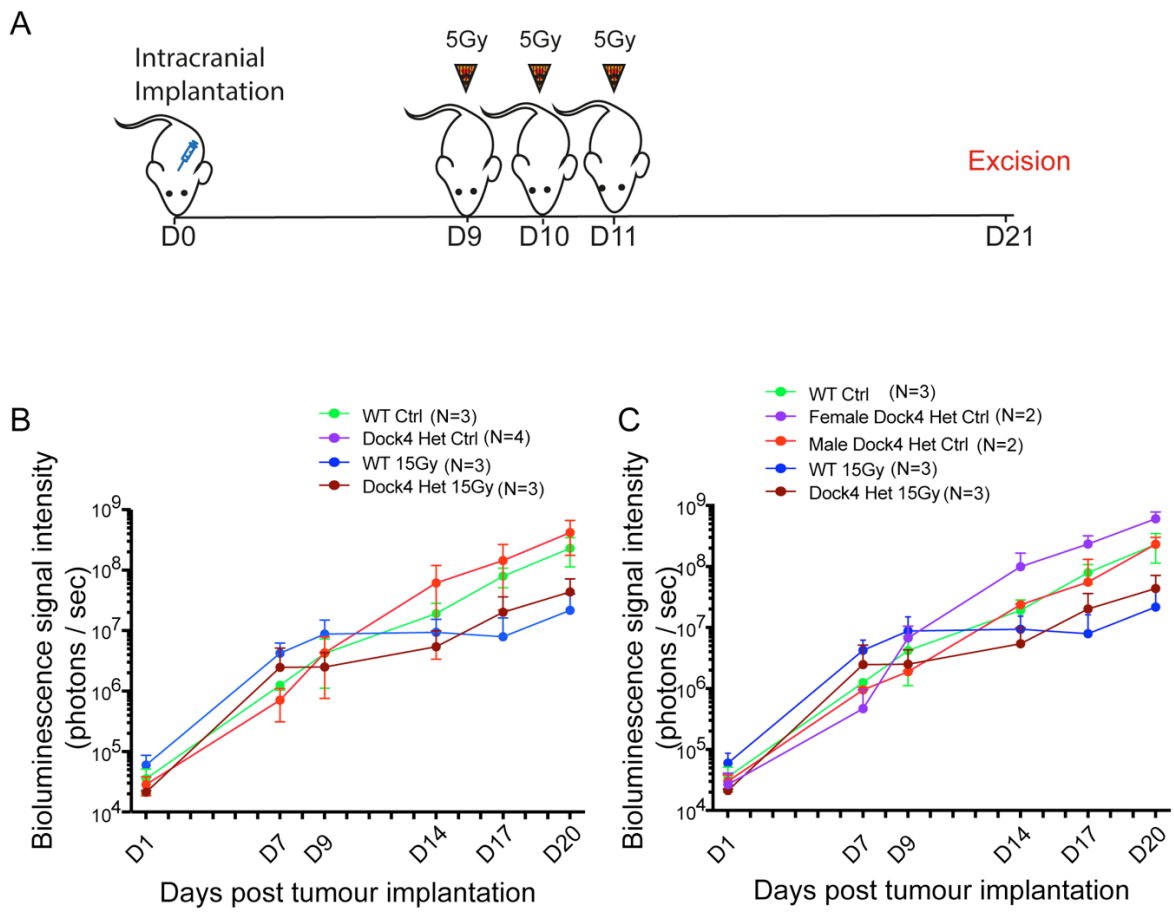

Figure 4.3 CT2A tumour growth in C57BL/6J wild type and Dock4 heterozygous mice treated with an irradiation dose of 15Gy

CT2A-Luc tumour cells ($1x10^5$) were injected intracranially into the striatum of C57BL/6 wild type and *Dock4* heterozygous mice. Tumour growth was monitored by IVIS and after 9 days radiation (5Gy) was delivered for 3 consecutive days using the RAD X-Ray irradiator.

(A) Schematic diagram of irradiation schedule and time of excision. WT (N=3) and Dock4 het mice (N=4) received a total of 15Gy (5Gy/day) whole brain irradiation using RAD X-Ray irradiator. Mice were sacrificed at 21 days post intracranial injection following development of neurological symptoms in the first mouse.

(B) Graphs depict tumour growth determined by IVIS bioluminescence photons count. Left-hand graph shows the growth of the entire cohort with mixed sex for *Dock4* het control: WT control (male), Dock4 control (2 males and 2 females), WT 15Gy (male) and Dock4 het 15Gy (male). Right-hand graph shows separately the growth of the 2 male and 2 female Dock4 het mice. Note that following imaging, one WT control and one WT irradiated mouse were excluded from analysis due to their IVIS reading signal remaining low.

Having an excellent capability for detecting differences in soft tissue, MRI is widely used for diagnosis and the evaluation of the effects of therapy in brain tumours (McKnight 2004). Hence, in addition to IVIS imaging mice were scanned using the M7 Compact MRI available in our unit for the detection of brain tumours. The results of MR imaging were compared to gross observation and immunohistochemical analysis of tumour samples. Since there were some sex dependent effects on tumour growth identified by IVIS (Figure 4.3), male mice were chosen for MR scanning on Day 20 post tumour implantation. Those mice were subsequently sacrificed by terminal perfusion (Day 21), and gross lesions identified were compared with the MR scanned images. The MRI imaging showed that control mice (wild type and Dock4 het) had significantly larger tumour volumes compared to irradiated mice both by MRI and gross observation of macroscopic lesions (Figure 4.4). These data show clear corroboration between MRI and macroscopic findings. When mice were taken down on Day 21 following tumour implantation 7/8 control mice had developed neurological symptoms. However, none of the mice from the irradiated group had shown neurological symptoms at this timepoint (Appendix 4).

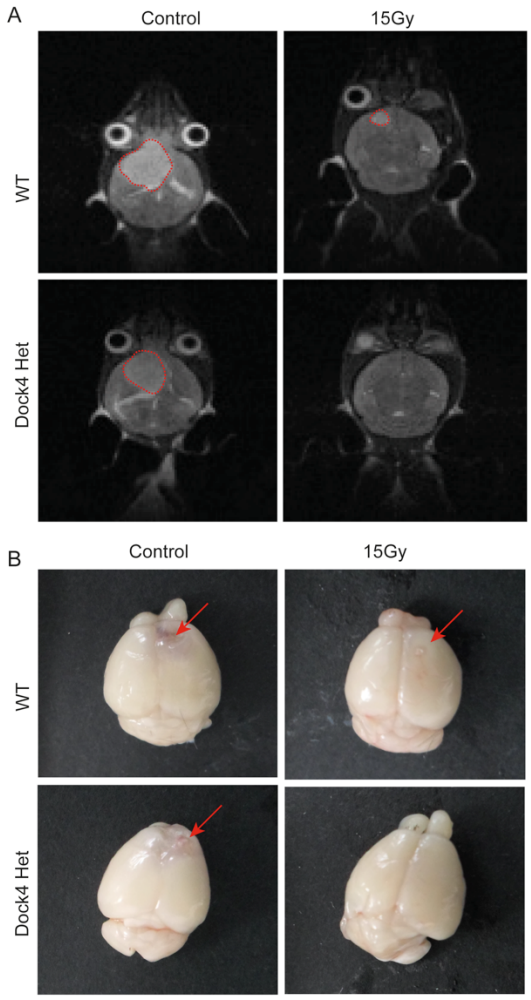

Figure 4.4 MR images of CT2A tumours growing in control and Dock4 heterozygous mice and corresponding gross lesions following terminal perfusion

CT2A-Luc tumour cells ($1x10^5$) injected intracranially into the striatum of wild type and Dock4 heterozygous mice were monitored by IVIS and after 9 days radiation (5Gy) was delivered for 3 consecutive days using the RAD X-Ray irradiator. Male mice with comparable IVIS readings on Day 9 were scanned coronally using M7 Compact Magnetic Resonance Imaging (MRI). Aspect imaging software was used to capture T2-Weighted MR images.

(A) Images show MR scans of control and irradiated tumours growing intracranially in wild type (WT) or Dock4 heterozygous (het) mice at 20 days post implantation. Presence of tumour is indicated as a white mass (dotted red circles).

(B) Images show gross macroscopic lesions (red arrows) in the same mice following terminal perfusion at 21 days post implantation. Note lack of tumour mass in the irradiated Dock4 het by both MRI and gross lesion observation.

Following tumour growth analysis by IVIS, MRI and gross lesion observation I sought to investigate tumour growth at the microscopic level. Tumour sections were compared following H&E staining (Figure 4.5). Overall, ionising irradiation reduced tumour volume significantly in accordance with the IVIS reading, MRI and macroscopic observation. However, there was no significant difference between the tumours growing in wild type and Dock4 heterozygous mice (Figure 4.5).

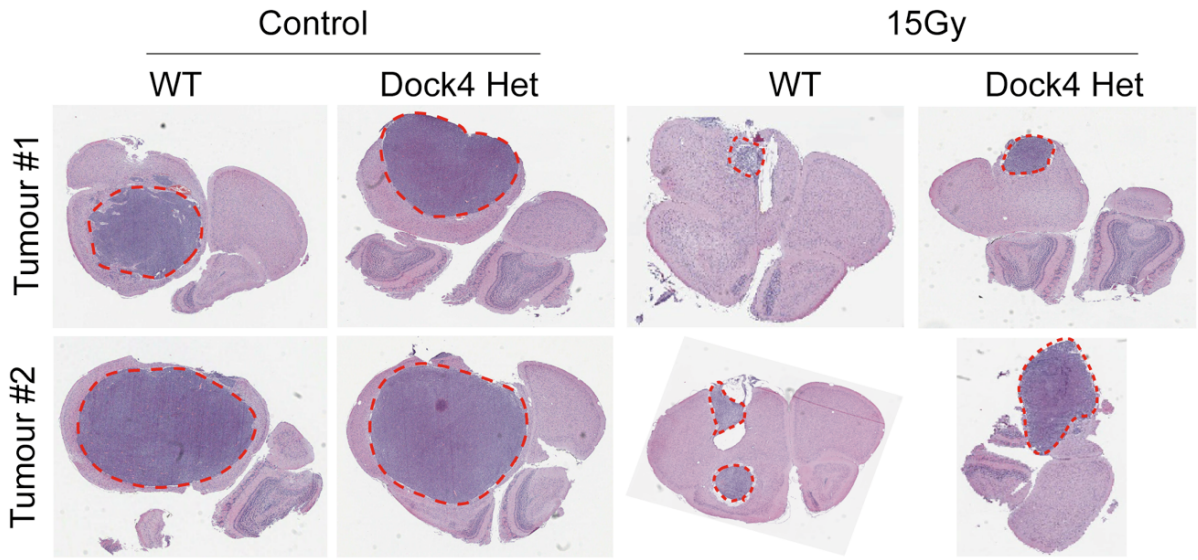

Figure 4.5 Immunohistochemical analysis of CT2A tumours growing in control and Dock4 het mice treated with an irradiation dose of 15Gy

Brain tissue samples from control and irradiated tumours growing in wild type (WT) or Dock4 heterozygous (het) mice were excised and paraffin embedded, sectioned at 4 µm thickness and H&E stained. Images depict two larger representative tumour mass (red dotted circles) from each group. Note that tumours shown were grown in male mice except for the control Dock4 het tumours which were from one male and one female mouse. Red dotted circles indicate tumour mass in each representative sample.

4.5 The effect of radiotherapy and heterozygous Dock4 deletion on blood vessel growth and lumenisation

Pilot immunohistochemical analysis of CT2A tumours suggested that the blood vessels of tumours growing in the Dock4 het mice may have smaller lumens compared to blood vessels in tumours growing in wild type mice. This observation is similar to that previously reported for EO771 intracranial tumours, a model of breast cancer brain metastases. I therefore set out to quantify blood vessel lumen size in these tumours as described in Materials and Methods Section 2.3.8. A total of 749 blood vessels were analysed in the 4 groups, of which 235 had a confidently detectable lumen ($\geq$ 10 μm).

Analysis showed that there was a trend of somewhat reduced number of blood vessels with heterozygous Dock4 deletion both in the presence and absence of radiation, although this was not statistically significant (Figure 4.6 B&C). The percentage of lumenised vessels was increased in response to irradiation from 28.1% and 24.7% to 34.5% and 34.6% in the wild type and Dock4 het groups, respectively (Figure 4.7A). Furthermore, analysis showed that there was no difference in tumour blood vessel lumen size between tumours growing in wild type (average lumen diameter 17.7μm) and Dock4 heterozygous mice (average lumen diameter 18.3) as shown in Figure 4.7B. Surprisingly, there was a trend for increased lumen size in response to irradiation (average lumen diameter 20.19 μm) in tumours growing in wild type mice, which was not statistically significant compared to controls (p=0.6). One probable reason for lack of a significant difference between control and irradiated groups could be due to the fact that relatively smaller sized tumours were analysed in the irradiated mice as they were sacrificed before developing neurological symptoms. This trend was reversed with Dock4 heterozygous deletion, as larger diameter lumens (>40 mm) observed in irradiated wild type tumours were not observed in the irradiated heterozygous Dock4 deletion group (Figure 4.7B).

In summary, 3 out of 4 Dock4 het mice developed tumour following irradiation and 3 out of 5 mice had a tumour in WT irradiated mice. It is possible that the high irradiation dose ablates tumour growth in both WT and Dock4 het mice and as a result the effect of heterozygous Dock4 deletion were masked (Appendix 4). Alternatively, tumour growth inhibition in response to irradiation delivered by the X-RAD was suboptimal. Hence, I decided to use a sub-curative radiation dose (10Gy) in the next experiments delivered by SARRP in order to understand whether Dock4 deletion improves the effect of radiotherapy.

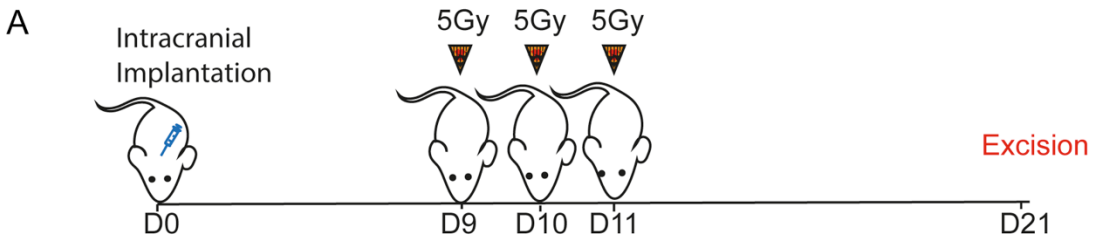
A
Intracranial
Implantation
5Gy
5Gy
5Gy
Excision
D0
D9
D10
D11
D21

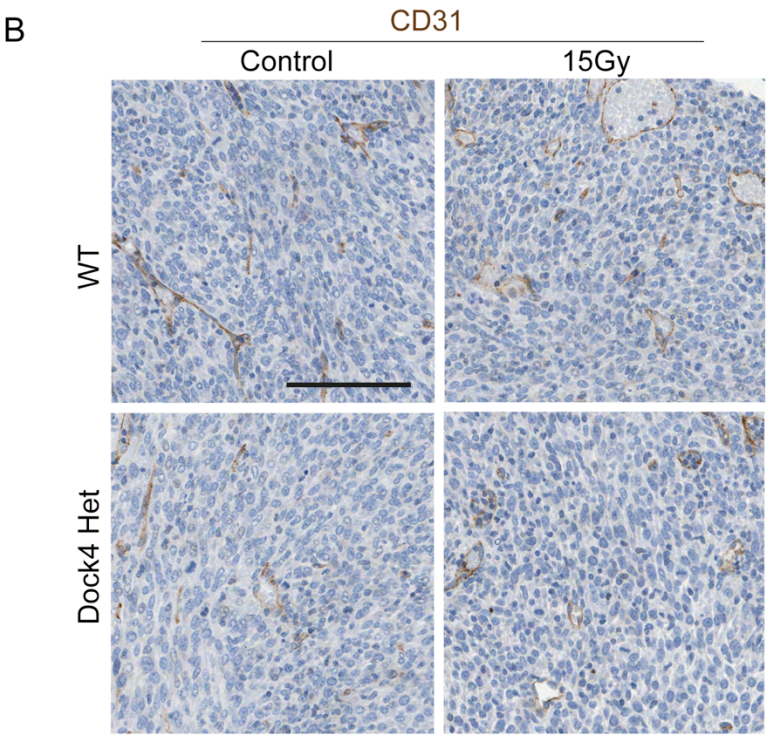
B
CD31
Control
15Gy
WT
Dock4 Het

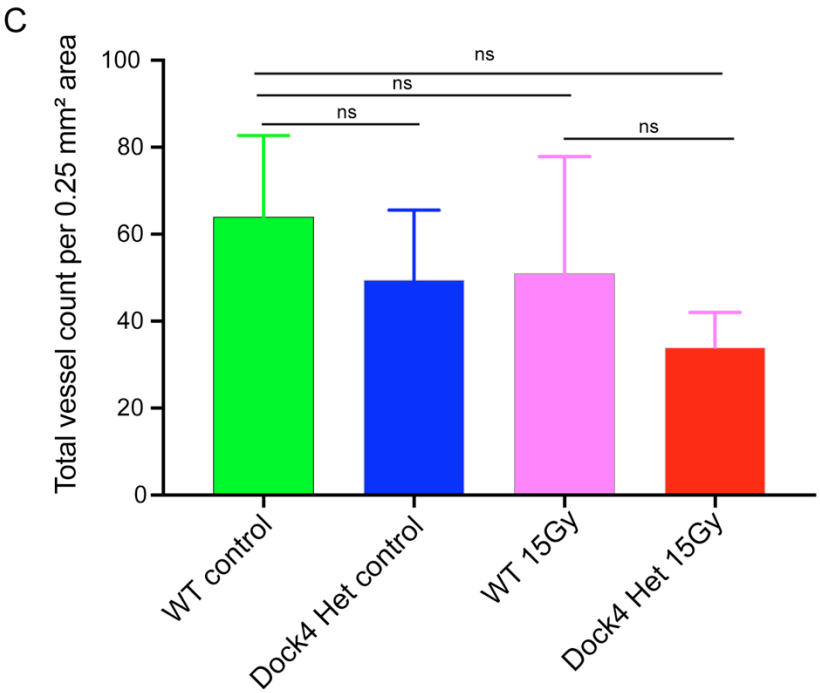
C
Total vessel count per 0.25 mm² area
100
80
60
40
20
0
ns
ns
ns
ns
WT control
Dock4 Het control
WT 15Gy
Dock4 Het 15Gy

Figure 4.6 Analysis of blood vessel growth in CT2A tumours growing in control and Dock4 heterozygous mice treated with irradiation

Brain tissue samples from control and irradiated tumours growing in wild type (WT) or Dock4 heterozygous (het) mice were sectioned at 4µm thickness, stained for CD31 and haematoxylin counterstained. The slides were scanned and blood vessel growth and lumenisation were quantified as described in Materials and Methods. A total of 235 blood vessels with lumen from 17 0.5x0.5mm^2 boxes were analysed (Appendix 2).

(A) Experimental schedule of intracranial implantation, irradiation and tumour excision.

(B) Representative images show increased tumour blood vessel lumen size and number of lumenised vessels in WT and Dock4 het mice in absence or presence of ionising radiation. Note more lumenised vessels in irradiated tumours compared to control and large lumen size blood vessels in irradiated WT mice.

(C) Graph shows total vessel count per 0.25 mm^2 area ± SD, N= number of 0.25 mm^2 area (WT control,4; Dock4 het control, 4; WT 15Gy, 3; and Dock4 het 15Gy, 3).

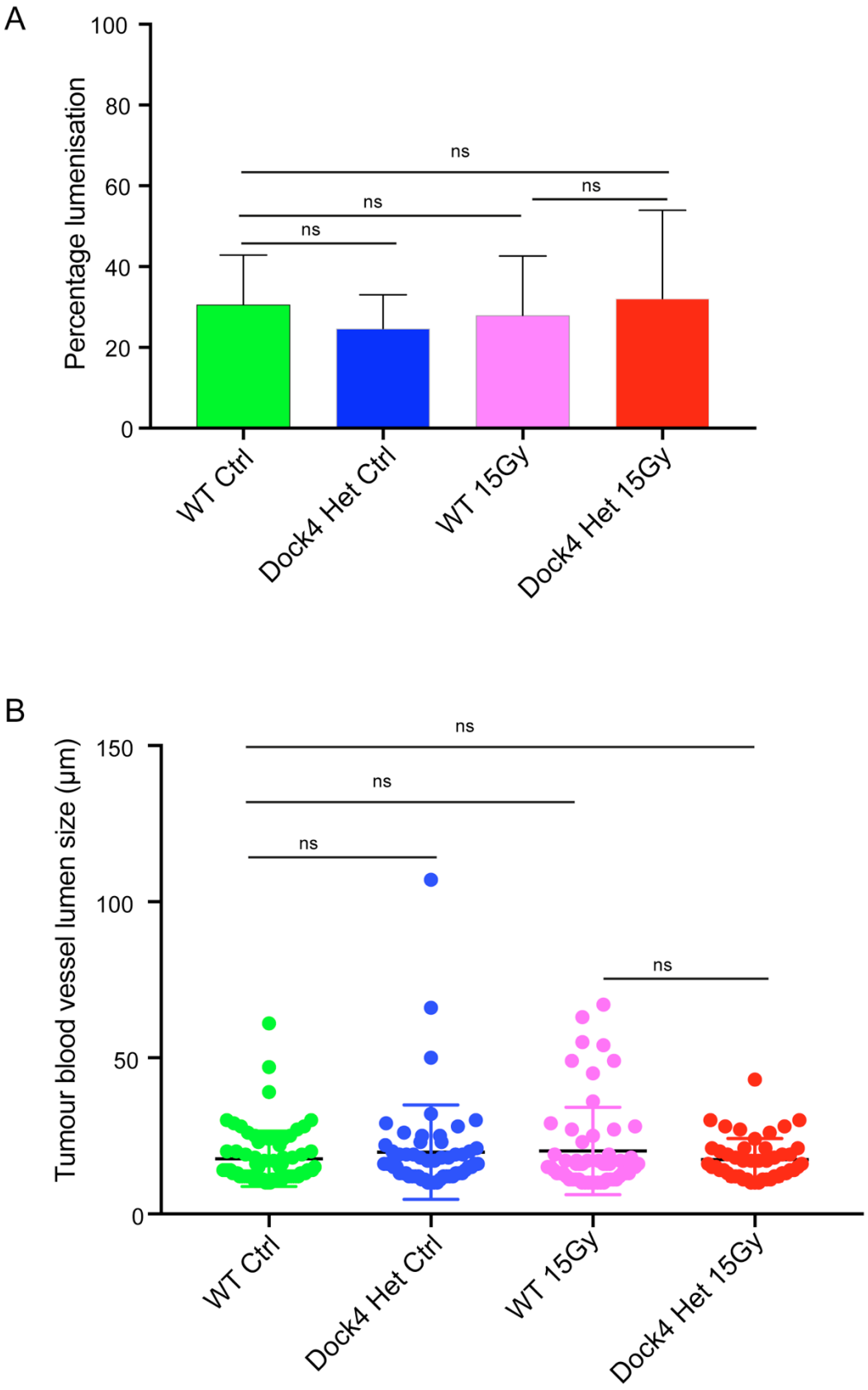
A
Percentage lumenisation
100
80
60
40
20
0
ns
ns
ns
ns
WT Ctrl
Dock4 Het Ctrl
WT 15Gy
Dock4 Het 15Gy
B
Tumour blood vessel lumen size (µm)
150
100
50
0
ns
ns
ns
ns
WT Ctrl
Dock4 Het Ctrl
WT 15Gy
Dock4 Het 15Gy

Figure 4.7 Analysis of blood vessel lumenisation in CT2A tumours growing in control and Dock4 heterozygous mice treated with irradiation

Brain tissue samples from control and irradiated tumours growing in wild type (WT) or Dock4 heterozygous (het) mice were sectioned at 4μm thickness, stained for CD31 and H&E counterstained. The slides were scanned and blood vessel growth and lumenisation were quantified as described in Materials and Methods. A total of 235 blood vessels with lumen from 17 0.5x0.5mm^2 boxes were analysed (Appendix 4).

(A) Graph shows percentage lumenised blood vessels (≥ 10 μm) ± SD, N= number of 0.5x0.5mm^2 areas (WT control, 4; Dock4 het control, 5; WT 15Gy, 3 and Dock4 het 15Gy, 3).

(B) Graph shows blood vessel lumen size ± SD, N= number of blood vessels with lumen (WT control, 72; Dock4 het control, 56; WT 15Gy, 59 and Dock4 het 15Gy, 47).

4.6 The effect of heterozygous Dock4 deletion on the efficacy of irradiation delivered by SARRP

Previously an irradiation dose of 10Gy had been shown to reduce but not ablate tumour growth (Kegelman et al. 2017 and Zhang et al. 2017). In an irradiation experiment carried out using SARRP a total of 52 female mice were injected $1x10^5$ CT2A-luc cells intracranially into the striatum of the right hemisphere of the brain. Mice were sacrificed at two different timepoints: early, at 11 days post tumour implantation; and late, upon development of neurological symptoms (Figure 4.8A). Tumour growth was assessed using bioluminescence IVIS imaging and measurements showed a strong tumour growth signal in control mice and weak signal in irradiated mice. In agreement with the IVIS reading tumours in control mice showed a bigger tumour volume on MRI scans when compared with irradiated mice. Irradiation significantly reduced tumour growth ($p<0.0001$) in both WT treated and Dock4 treated mice compared to control groups (Figure 4.8B). I then looked into the effect of irradiation on overall survival and whether combination of heterozygous Dock4 deletion and radiotherapy improved survival. Although there was significant increase ($p<0.0001$) in survival for mice that received radiotherapy (Figure 4.8C), there was no significant difference between control WT and Dock4 het or between the two irradiated groups. Tumour growth appeared somewhat increased in Dock4 het mice compared to WT controls, however, this was not statistically significant. These results showed lack of an overall benefit from global heterozygous Dock4 deletion pertaining to survival following lower irradiation dose delivered by SARRP.

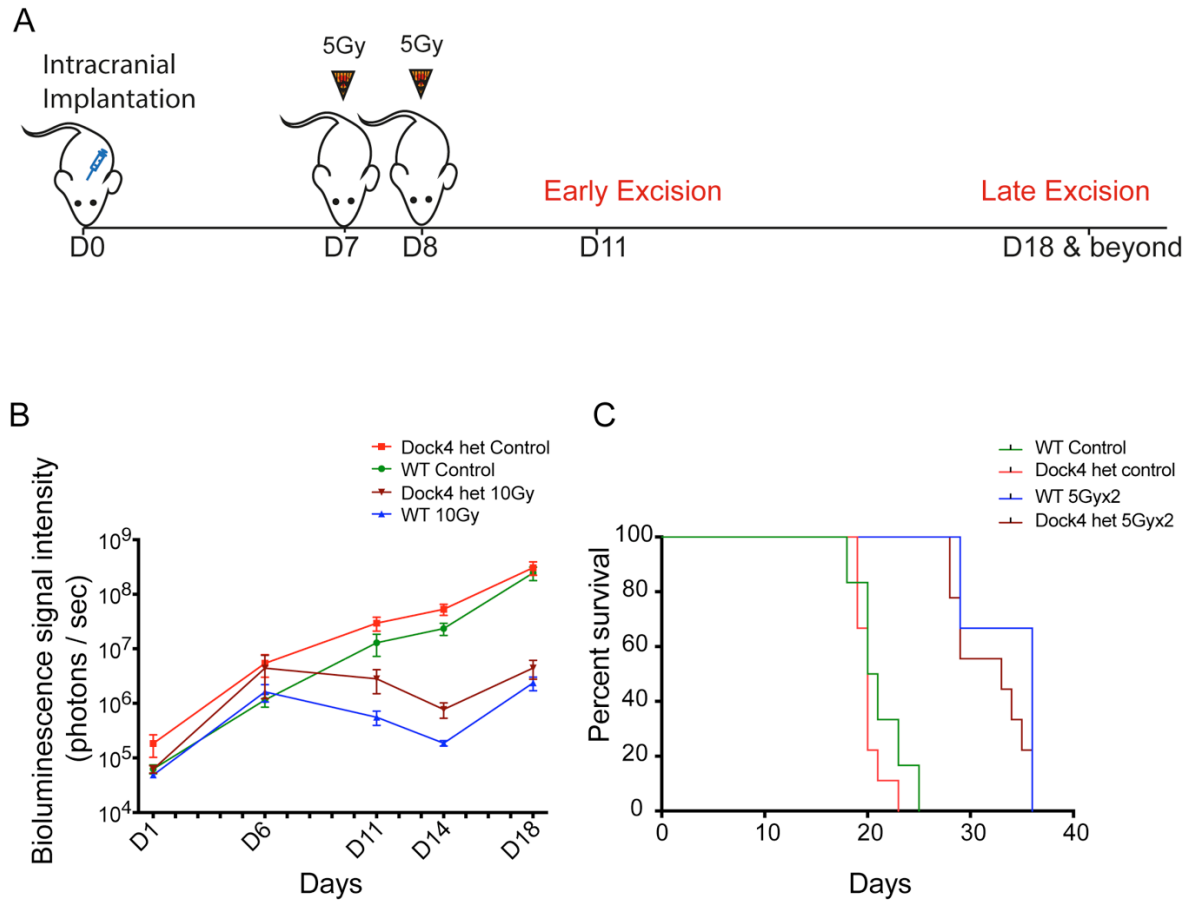

CT2A tumour growth and survival in wild type and Dock4 heterozygous mice treated with an irradiation dose of 10Gy delivered by SARRP

CT2A-Luc tumour cells (1x10^5) were injected intracranially into the striatum of C57BL/6J wild type and Dock4 heterozygous mice. Tumour growth was monitored by IVIS and after 7 days radiation (5Gy) was delivered for 2 consecutive days using SARRP.

(A) Experimental schedule for early and late excision of CT2A tumours. WT control mice (N=6), Dock4 het control mice (N=9), WT mice received 10Gy (N=3) and Dock4 het mice received 10Gy (N=9) whole brain irradiation using SARRP. Mice were sacrificed at two points: early, Day 11 post tumour implantation and late, upon development of neurological symptoms.

(B) Growth curve - Graphs depict tumour growth determined by IVIS bioluminescence signal intensity from late timepoint analysis. N= number of mice (WT control, 6; Dock4 control, 9; WT 15Gy, 3 and Dock4 het 15Gy, 9).

(C) Survival curve – the graph shows number of mice sacrificed following development of neurological symptoms and overall survival were analysed per group. N=number of mice (WT control, 6; Dock4 control, 9; WT 15Gy, 3 and Dock4 het 15Gy, 9).

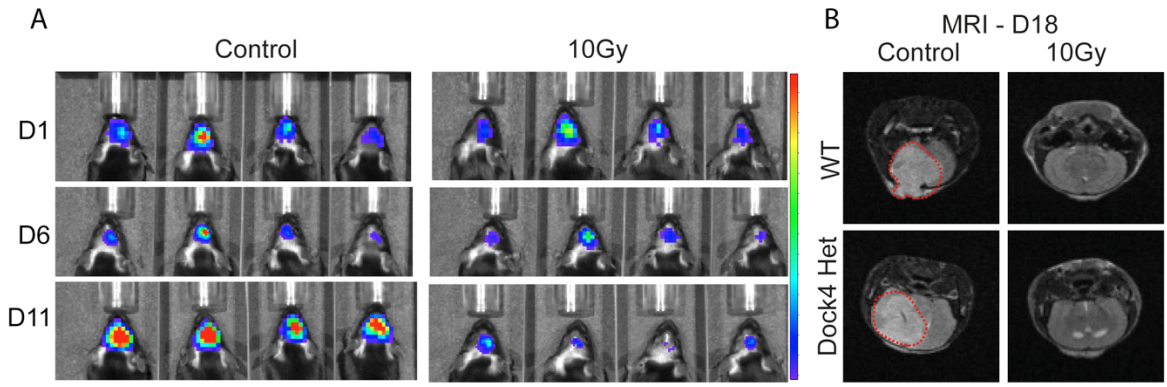

Figure 4.9 IVIS and MR imaging of CT2A tumours growing in control and Dock4 heterozygous mice treated with an irradiation dose of 10Gy delivered by SARRP

CT2A-Luc tumour cells ($1x10^5$) injected intracranially into the striatum of wild type and Dock4 heterozygous mice were monitored by IVIS and after 7 days radiation (5Gy) was delivered for 2 consecutive days using SARRP. Three mice/group which had a maximum IVIS reading on Day 18 post tumour implantation were scanned coronally using M7 Compact Magnetic Resonance Imaging (MRI). Aspect imaging software was used to capture T2-Weighted MR images.

(A) A total of 52 mice were grouped into 4 groups; 26 mice (13 WT and 13 Dock4 het) received a total of 10Gy whole brain irradiation dose over two consecutive days (D7 and D8 post implantation) using SARRP and 26 mice (13 WT and 13 Dock4 het) were control. Tumour growth was assessed regularly using bioluminescence IVIS imaging following subcutaneous injection of luciferin.

(B) Images show MR scans of control and irradiated tumours growing intracranially in wild type (WT) or Dock4 heterozygous (het) mice at 18 days post implantation. Presence of tumour is indicated as a white mass (dotted red circles).

4.7 The effect of low dose radiotherapy and heterozygous Dock4 deletion on blood vessel growth and lumenisation early after irradiation delivered by SARRP

I sought to examine the effects of irradiation on the tumour vasculature first at an early timepoint following treatment, 3 days after irradiation. For this analysis brain tumours from 12 mice (3 mice per group) were excised on D11 following intracranial implantation (Figure 4.10A). Staining of available CT2A tumour samples (Appendix 5) with CD31 showed the presence of blood vessels with smaller lumen size in irradiated tumours compared to controls (Figure 4.10B). The total number of vessels count per 0.25mm^2 area significantly increased in WT irradiated tumours compared to WT control and decreased in Dock4 het irradiated compared to WT irradiated (Figure 4.10C). Interestingly, heterozygous Dock4 deletion significantly decreased the abundance of lumenised blood vessels in the presence of irradiation but not in its absence (Figure 4.11A). Blood vessel lumen size was significantly decreased with Dock4 deletion, and further more in the presence of irradiation (Figure 4.11B). Hence, combination of radiotherapy and heterozygous Dock4 decreased the overall number of lumenised blood vessels and the average lumen size. Altogether, the analysis of the vasculature early after irradiation showed effects on the percentage of blood vessels with detectable lumens which was more pronounced in tumours with Dock4 heterozygous deletion. However, Dock4 deletion did not affect tumour growth either in the absence, or presence of irradiation. Analysis of the late tumour samples, by A. Widiyadari, showed a significantly increased lumen size in WT mice following irradiation (Appendix 6). These opposing effects of irradiation on the vasculature at earlier and later timepoints may account for the absence of measurable differences in overall survival between tumours growing in wild type and Dock4 heterozygous mice.

A

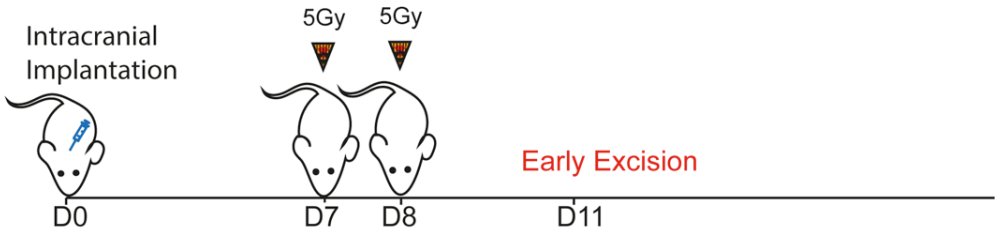
Intracranial
Implantation
5Gy
5Gy
Early Excision
D0
D7
D8
D11

B

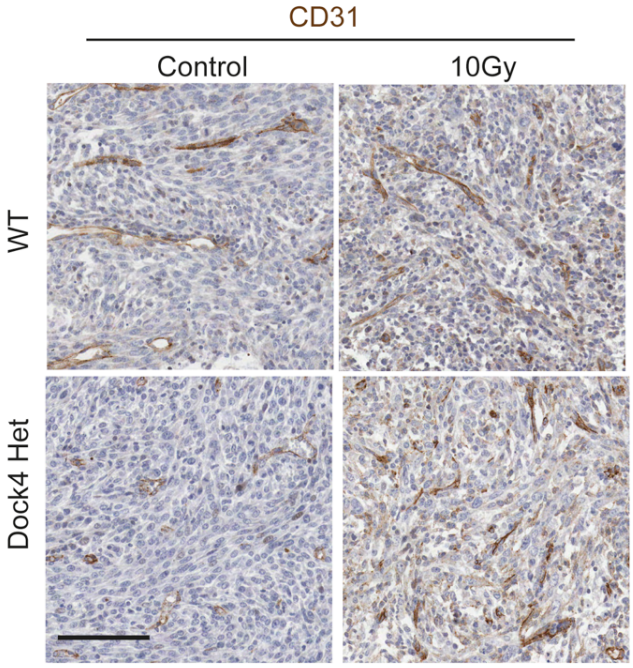
CD31
Control
10Gy
WT
Dock4 Het

C

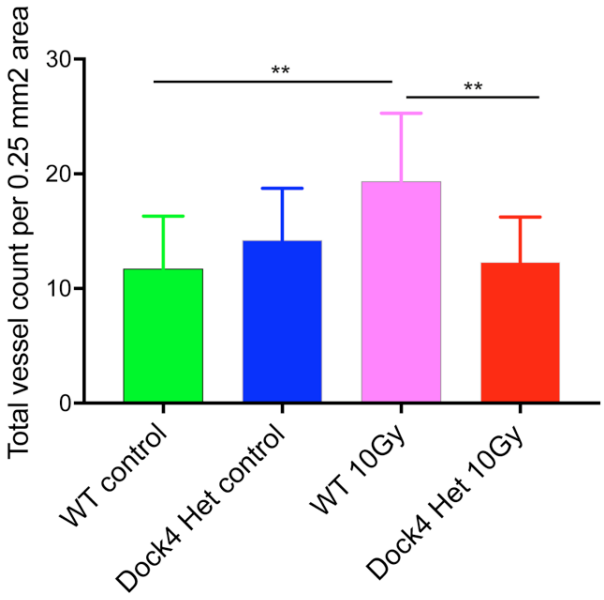
Total vessel count per 0.25 mm2 area
30
20
10
0
**
**
WT control
Dock4 Het control
WT 10Gy
Dock4 Het 10Gy

Figure 4.10 Analysis of blood vessel growth of CT2A tumours growing in control and Dock4 heterozygous mice treated with an irradiation dose of 10Gy delivered by SARRP

Brain tissue samples from control and irradiated tumours growing in wild type (WT) or Dock4 heterozygous (het) mice were sectioned at 4µm thickness, stained for CD31 and haematoxylin counterstained. The slides were scanned and blood vessel growth and lumenisation were quantified as described in Materials and Methods. A total of 76 blood vessels with lumen from 32 0.5x0.5mm^2 areas were analysed.

(A) Experimental schedule of intracranial implantation, irradiation and tumour excision.

(B) Representative images of sections from excised tumours.

(C) Graph shows total vessel count per 0.25 mm^2 area ± SD, N= number of 0.25 mm^2 areas (WT control, 11; Dock4 het control, 18; WT 15Gy, 6; and Dock4 het 15Gy, 16).

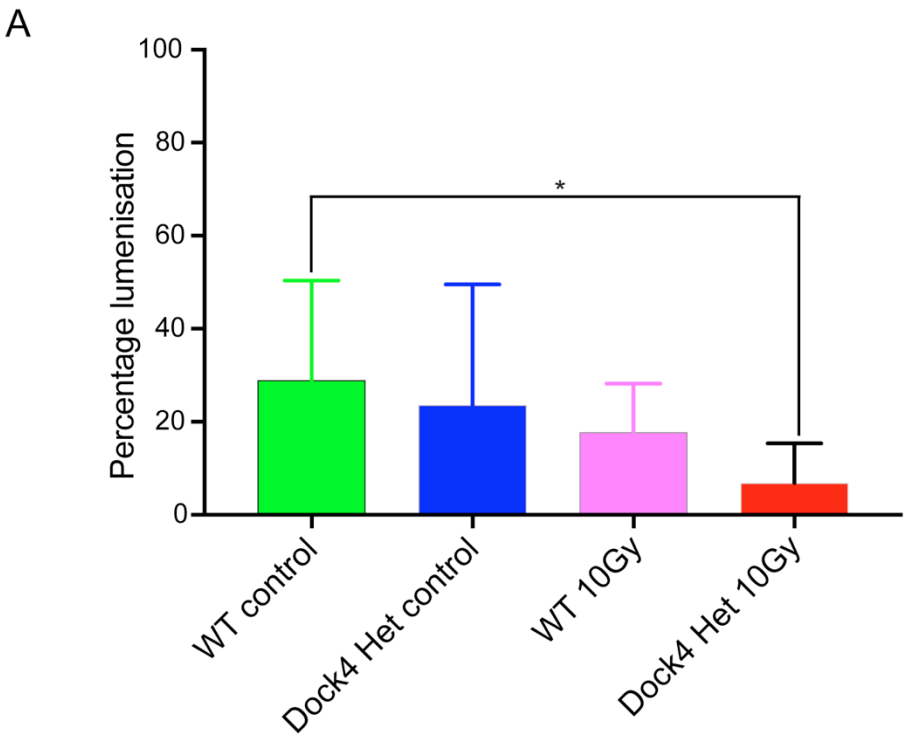
A
Percentage lumenisation
100
80
60
40
20
0
*
WT control
Dock4 Het control
WT 10Gy
Dock4 Het 10Gy

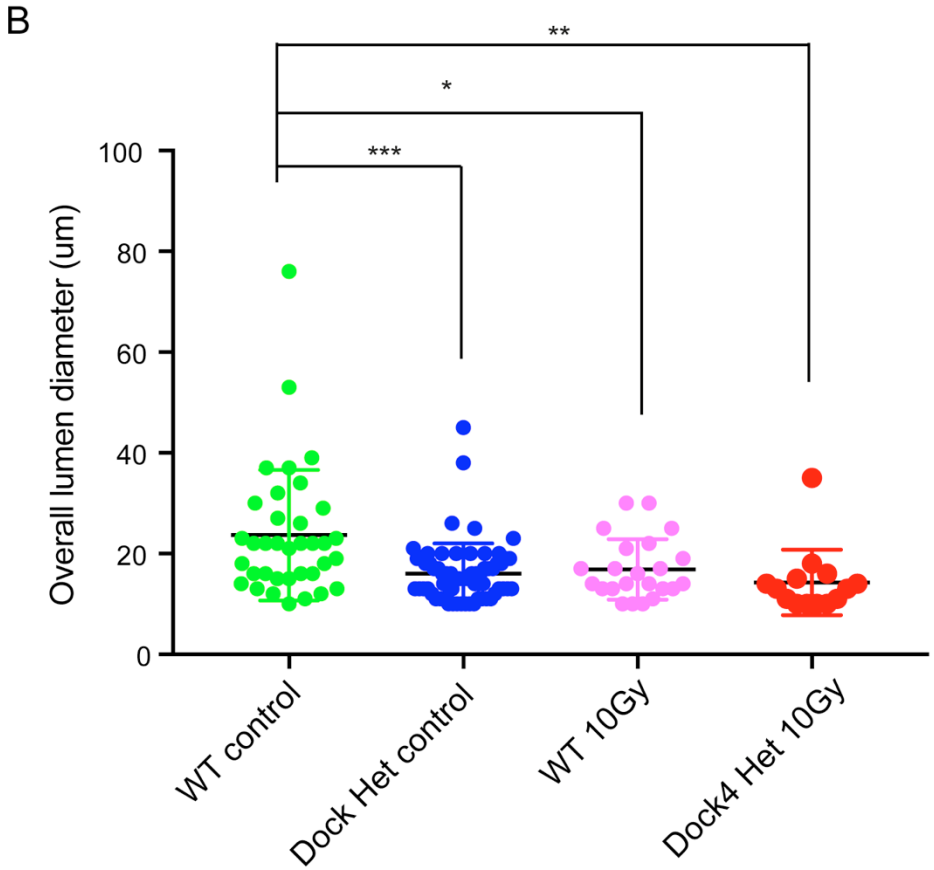
B
Overall lumen diameter (um)
100
80
60
40
20
0
**
*
***
WT control
Dock Het control
WT 10Gy
Dock4 Het 10Gy

Figure 4.11 Analysis of blood vessel lumenisation of CT2A tumours growing in control and Dock4 heterozygous mice treated with an irradiation dose of 10Gy delivered by SARRP

Brain tissue samples from control and irradiated tumours growing in wild type (WT) or Dock4 heterozygous (het) mice were sectioned at 4μm thickness, stained for CD31 and H&E counterstained. The slides were scanned and blood vessel growth and lumenisation were quantified as described in Materials and Methods. A total of 76 blood vessels with lumen from 32 0.5x0.5mm^2 boxes were analysed.

(A) Graph shows percentage lumenised blood vessels (≥ 10 μm) ± SD, N= number of 0.5x0.5mm^2 areas (WT control, 11; Dock4 het control, 18; WT 15Gy, 6 and Dock4 het 15Gy, 16).

(B) Graph shows blood vessel lumen size ± SD, N= number of blood vessels with lumen (WT control, 72; Dock4 het control, 56; WT 15Gy, 59 and Dock4 het 15Gy, 47). * $p<0.05$; ** $p<0.01$ and ** $p<0.001$.

4.8 Effects of irradiation on blood vessel α-SMA expression

Following the increased finding of SMA positivity and its direct association with nestin expression in patient samples, I investigated whether α-SMA positivity increased in irradiated CT2A tumours recapitulating the phenotype of the recurrent patient GBM tumours. Serial sections of CT2A tumours were stained for endothelial marker CD31 and the SMC marker α-SMA. Overall, α-SMA failed to stain the majority of blood vessels in untreated CT2A tumours, particularly small blood vessels growing in either wild type or heterozygous Dock4 mice (Figure 4.12). However, we can clearly see large blood vessels, particularly those in the edge region of irradiated tumour tissue, positive for α-SMA (red arrows) although this is very low compared to matured blood vessels in normal brain (black arrows). This shows that the aberrant blood vessels which showed high α-SMA positivity in recurrent patient tumours could, at least partly result from irradiation. In addition to increased SMA positivity in the irradiated tumour tissue following irradiation, there was also an increased presence of F4/80 positive macrophages/ microglia. Apoptosis and DNA damage markers caspase-3 and γ-H2AX, respectively were also slightly increased (Appendix 7).

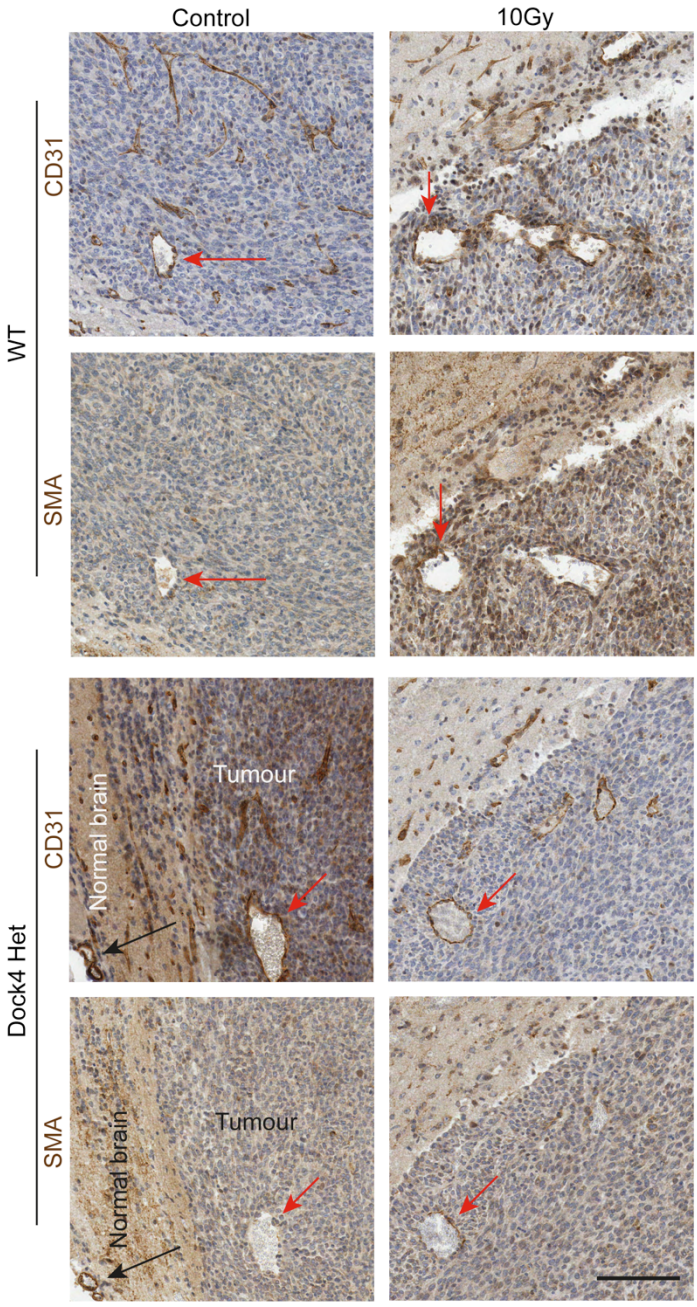

Figure 4.12 α-SMA positivity in CT2A tumours

CT2A tumours were paraffin embedded, sectioned serially (4 µm) and stained using antibodies against CD31 and α-SMA. Red arrows point to CD31 positive blood vessels in control and irradiated tumour tissues with their respective serial sections showing presence or absence of α-SMA positivity. Black arrows point to blood vessels in the normal brain parenchyma showing positivity for both CD31 and α-SMA. Scale bar, 100 µm.

4.9 Optimisation of deletion of Dock4 f/f using Cre/loxP system and confirmation by tdTomato reporter gene

Initially, *in vivo* experiments to address the role of Dock4 were performed using mice with global heterozygous Dock4 allele knockout as homozygous Dock4 deletion was embryonically lethal beyond E7.5. In our work, although the findings showed decreased tumour blood vessel lumen size following Dock4 heterozygous deletion there was no overall survival benefit for CT2A tumour bearing mice. Then, I hypothesised that deletion of both alleles of Dock4 from ECs could improve the overall survival of mice. The use of combined Dock4 conditional knockout and radiotherapy was beyond the remit of this thesis. I used a conditional Dock4 knockout mice generated by Ozgene using a Cre/loxP; FLP-FRT systems to delete Dock4 in adult mice (Appendix 8A). The VEcad-iCreERT and TdTomato reporter gene (both from Beatson Institute of Cancer research) were employed to achieve inducible Dock4 genetic deletion and to confirm the activity of VEcad-iCreERT. Hence, Dock4f/f mice were crossed with the line VE-CadiCreERT2-mice in our animal facility and genotyped by Transnetyx. The genotyping results confirmed the genotype of each mouse as homozygous or heterozygous or wild type for Dock4, TdTomato and Cre genes (Appendix 8B).

Following confirmation of mice genotype, tamoxifen was injected intraperitoneally and CT2A tumour cells were injected intracranially. Staining of tumour samples confirmed Cre recombinase activity using the TdTomato reporter gene. Using Red Fluorescent Protein (RFP) antibody staining successfully detected deletion of the floxed STOP codon of TdTomato allowing its expression upon induction with tamoxifen (Figure 4.13A). Interestingly, in addition to reduced expression of DOCK4 in endothelial cells in VEcad-iCre+ve; Dock4f/f mice compared to VEcad-iCre-ve; Dock4f/f mice upon induction with tamoxifen (Figure 4.13B), there was also reduced DOCK4 expression in CT2A cells potentially indicating a possible role of endothelial Dock4 in the regulation of DOCK4 expression in cancer cells.

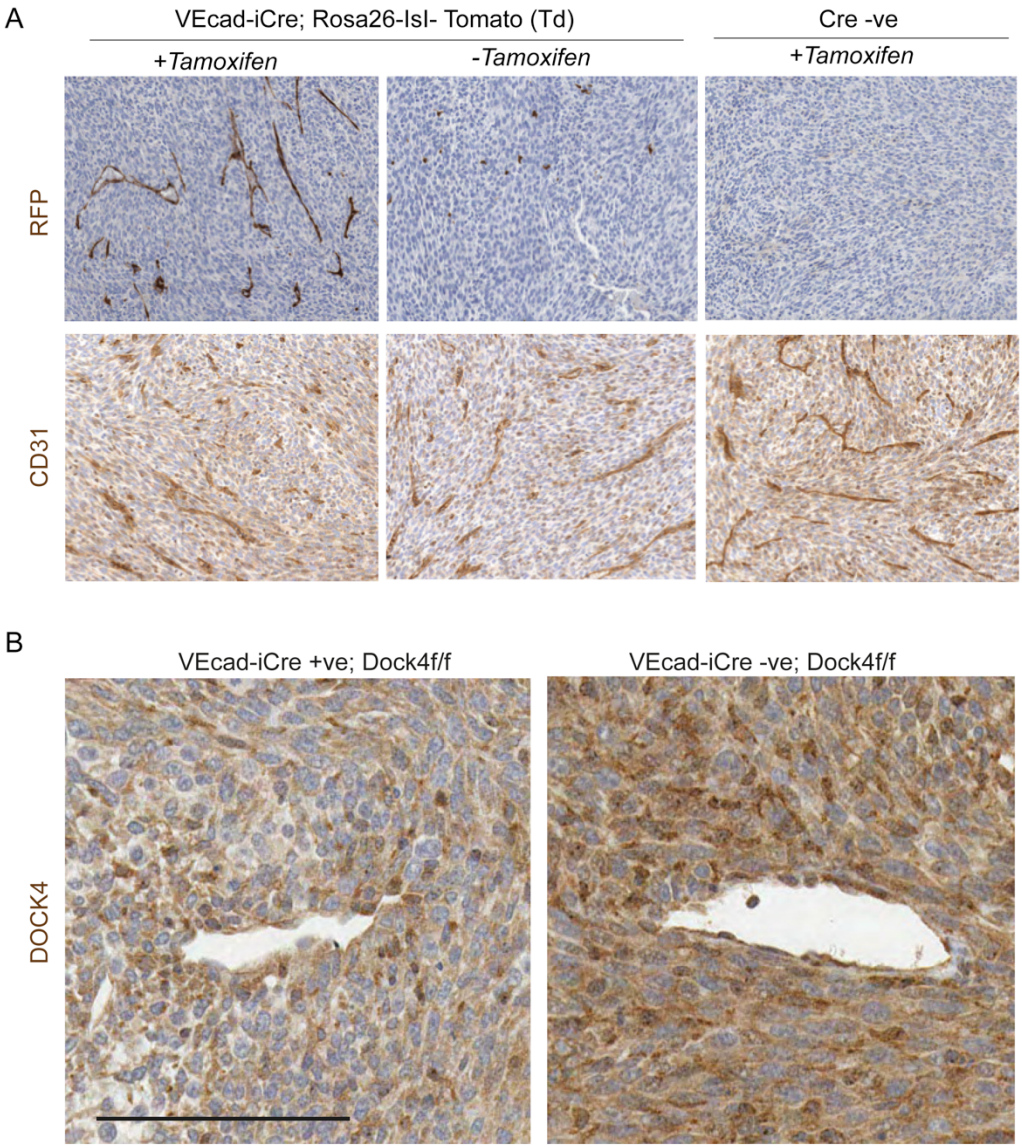

Figure 4.13 Optimisation of Cre activity using the TdTomato reporter

(A) Mice were injected with tamoxifen intraperitoneally at a dose of 2mg/mouse/day for 5 consecutive days and implanted with CT2A tumour cells intracranially. CT2A brain tumours were excised, sectioned and stained for CD31 and TdTomato using an antibody against RFP.

(B) DOCK4 staining of sections from CT2A tumours growing in VEcad-iCre+ve; Dock4f/f and VEcad-iCre-ve; Dock4f/f mice. Scale bar, 100 µm.

4.10 Pilot analysis of CT2A blood vessels in the conditional Dock4 knockout model in the absence of irradiation

The experiments performed in the Dock4 heterozygous mice showed increased tumour blood vessel lumen size following irradiation. On the other hand, it was noticed from both early and late stage Dock4 het tumour vasculature analysis that there was a trend of normalisation of tumour vessel lumen size with heterozygous Dock4 deletion. In this pilot study I hypothesised that deletion of both alleles from endothelial cells could result in further blood vessel normalization improving chemo- and radiotherapy. Analysis of tumour blood vessel lumen size was performed at early and late stages post tumour implantation, either at 10 days or upon development of neurological symptoms from day 14 onwards (Figure 4.14A).

For analysis early after intracranial injection a total of 126 blood vessels from 4 Cre negative and 64 blood vessels from 3 Cre positive mice were analysed. Tumours from Cre positive and Cre negative mice had an average of 36% and 14% lumenised vessels, respectively, showing that surpisingly, endothelial Dock4 deletion increased blood vessel lumenisation (Figure 4.14B). Similarly, the late timepoint analysis, when mice were taken down following development of neurological symptoms, showed a higher percentage of lumenised blood vessels in tumour samples from Cre positive mice 20% of a total of 324 blood vessels, compared to Cre negative mice, 12% from a total of 303 vessels (Figure 4.14C). However, despite the consistent trend, the differences were not statistically significant for either the early and late timepoints. Again, analysis of blood vessel lumen size from Cre positive and Cre negative mice showed no significant differences between control tumours and tumours with endothelial Dock4 deletion at early ($p=0.34$) or late ($p=0.35$) timepoints (Figure 4.15A, B).

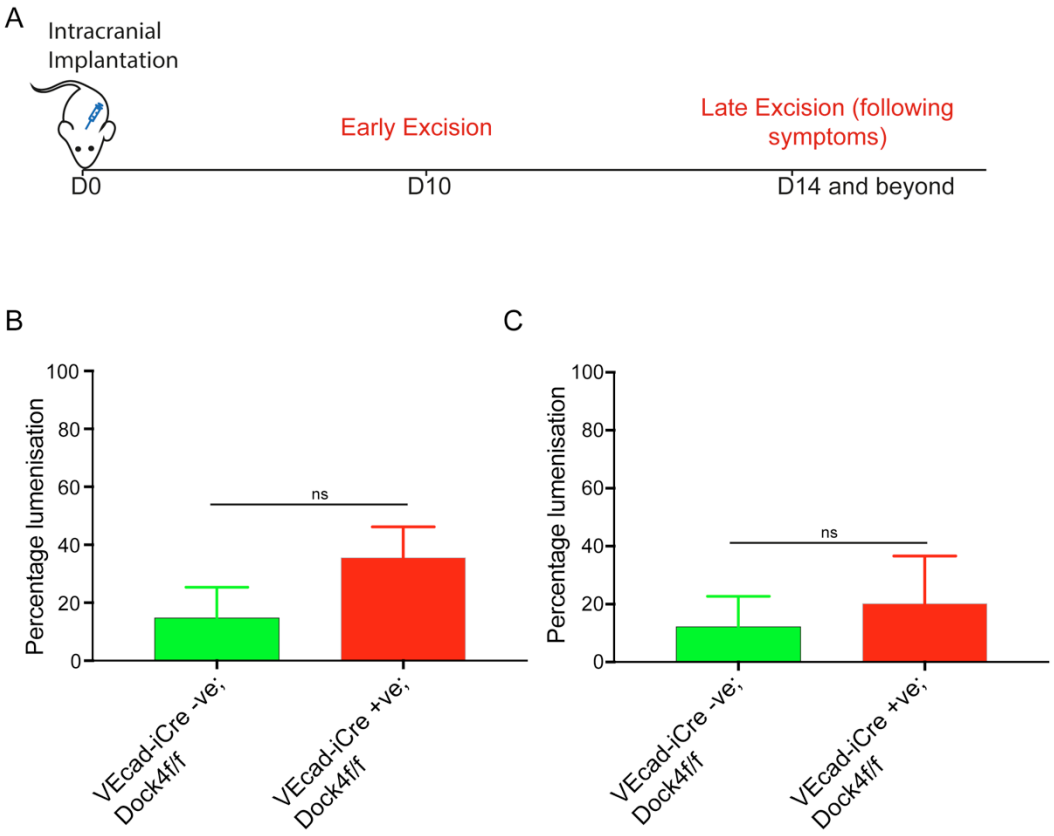

Figure 4.14 Analysis of blood vessel lumenisation of CT2A tumours growing in VEcad-iCre; Dock4f/f mice

Brain tissue samples from control from 6 VEcad-iCre positive Dock4f/f and 8 VEcad-iCre negative Dock4f/f mice were sectioned at 4µm thickness, stained for CD31 and H&E counterstained. The slides were scanned and percentage blood vessel lumenisation was quantified. A total of 188 and 625 blood vessels with lumen (≥ 10 µm) from early and late analysis, respectively were analysed.

(A) Experimental schedule of intracranial implantation and tumour excision at Early and Late timepoints.

(B) Graph shows Early percentage lumenisation of blood vessels ± SD, N= number of tumour samples (VEcad-iCre negative Dock4f/f, 4 and VEcad-iCre positive Dock4f/f, 3).

(C) Graph shows late percentage lumenisation of blood vessels ± SD, N= number of samples (VEcad-iCre -ve; Dock4f/f, 4 and VEcad-iCre +ve; Dock4f/f, 3).

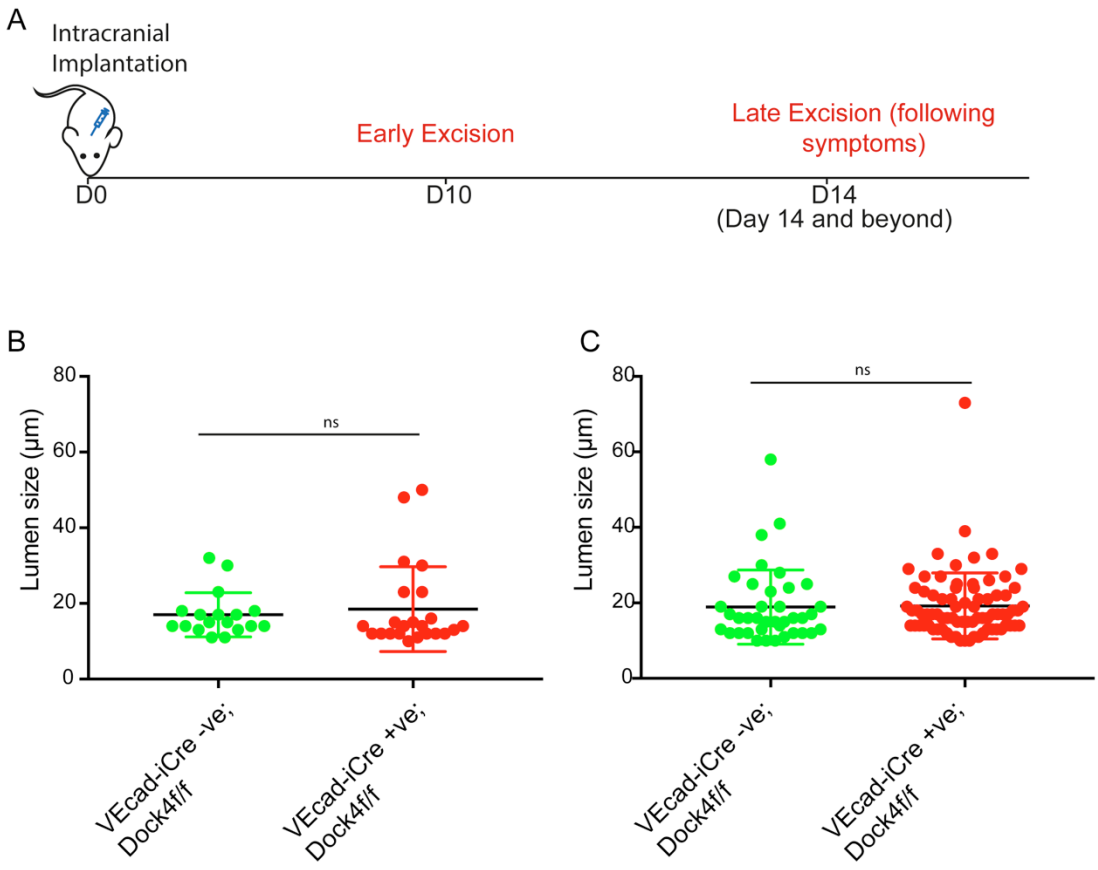

Figure 4.15 Analysis of blood vessel growth of CT2A tumours growing in VEcad-iCre; Dock4f/f mice

CT2A cells ($1x10^5$) were intracranially injected into the striatum of 6 VEcad-iCre positive Dock4f/f and 8 VEcad-iCre negative Dock4f/f mice and brain tissue samples were sectioned at 4µm thickness, stained for CD31 and H&E counterstained. The slides were scanned and blood vessel lumen sizes were quantified as described in Materials and Methods. A total of 188 and 625 blood vessels with lumens from Early and Late tumours respectively were analysed.

(A) Experimental schedule of intracranial implantation and tumour excision at Early and Late timepoints.

(B) Graph shows Early blood vessel lumen size ± SD, N= number of blood vessels with lumen (VEcad-iCre -ve; Dock4f/f, 18 and VEcad-iCre +ve Dock4f/f, 23).

(C) Graph shows late blood vessel lumen size ± SD, N= number of blood vessels with lumen (VEcad-iCre; Dock4f/f negative, 38 and VEcad-iCre; Dock4f/f positive, 78).

4.11 Conclusions

The dedicator of cytokinesis (DOCK) 4 is a GEF for the small Rho GTPase Rac1, which has been shown previously to regulate filopodia formation in organotypic angiogenesis assays, and lumen formation in organotypic assays and in the brain *in vivo* through control of the endothelial actin cytoskeleton. Blood vessels play a vital role in tumour growth and understanding the molecular mechanisms by which cancer cells manipulate blood vessels to their advantage can provide key approaches to cancer therapies. In this part of the study, I first established in the lab and characterised the mouse GBM tumour model CT2A for experiments to elucidate the control of tumour vascularisation in GBM. Compared to the commonly employed GL261 model, the CT2A tumour model was found to be more angiogenic, co-optive and to recapitulate better the invasive cancer cell behaviour seen in human GBM tumours. Using the Dock4 heterozygous global deletion model previously developed in our lab I grew CT2A tumours orthotopically and assessed changes in tumour vascularisation and growth. Analysis showed that there are no significant differences in the vasculature of tumours growing in Dock4 het mice compared to tumours growing in wild type controls except at early day analysis where there is a significant reduction of lumen size in Dock4 het mice. Consistently, no changes in tumour growth were observed in tumours growing in the Dock4 het mice compared to controls. Analysis of tumour growth in Dock4 het and litter mate WT mice showed no significant difference as measured using IVIS and also confirmed by MRI.

In addition, I optimised a protocol in which initial tumour regression could be observed in response to irradiation of CT2A tumours, followed by tumour regrowth (Figure 4.8) recapitulating the response of patient GBM tumours to radiotherapy. As most GBM patients receive radiotherapy as part of the standard therapy I had hypothesised that radiotherapy may play a role in the changes observed in the vasculature of patient recurrent tumours, namely increased vessel size and pericyte coverage. I found that in tumours excised early after irradiation there was a significant decrease rather than anticipated increase in blood vessel lumen size and percentage lumenisation. However, in the late CT2A tumour sample analysis performed by A. Widiyadari in our team, it was found that there is indeed increased blood vessel lumen size following irradiation (Appendix 6), although that vascular change was not accompanied by a change in tumour growth.

The irradiated tumours growing in Dock4 het mice showed significantly smaller lumen size blood vessels compared to irradiated tumours growing in wild type mice in the early timepoint analysis at 3 days after irradiation. Further, the increase in lumen size observed in response to irradiation at the late timepoint analysis was reversed by Dock4 heterozygous deletion. In addition, as observed in

recurrent patient GBM samples, α-SMA positivity appeared increased following treatment of ionizing radiation, particularly in larger blood vessels at the late timepoint analysis, but not in the early timepoint. Therefore, there are different and sometimes opposing effects of irradiation on the vasculature at different timepoints, which may explain the lack of observed differences in tumour growth. Dock4 could therefore play a significant role in normalisation of blood vessels following radiotherapy by regulating blood vessel lumen size. However, what appeared to be normalisation in tumour blood vessel by decreasing lumen size did not affect survival suggesting that either the reduction of DOCK4 is not adequate, and/ or longer term growth effects could not be captured in these short-term tumour growth experiments. One typical cellular effect of radiotherapy in early samples was the increased infiltration of macrophage/microglia which could had accounted for blood vessel abnormality at the late timepoint.

Pilot analysis of CT2A tumour blood vessel lumen size in conditional Dock4 knockout mice, where Dock4 deletion of both alleles takes place specifically in endothelial cells upon tamoxifen treatment, showed no significant difference of tumours with Dock4 deletion compared with control mice, and lack of survival benefit. Further experiments in the future will be necessary to determine the precise response, particularly in combination with radiotherapy.

Chapter 5

The role of DOCK4 in glioblastoma cancer cell invasion

5.1 Introduction

One characteristic feature of GBM is its diffuse infiltrative growth into the normal brain parenchyma by destroying the neuronal cells. This results in loss of neurological and cognitive ability and subsequently patients' death. Although the use of radiotherapy to treat such infiltrative cancer is widespread some cells remain resistant after such treatments and the cells become more invasive and ends up with local or distance recurrence (Edalat et al. 2016 and Wild-Bode et al. 2001). Blood vessels in cancer microenvironment play an important role as a scaffold for the invasion of such cancers in addition to providing oxygen and nutrients (Cuddapah et al. 2014). The fact that DOCK4, a GEF for Rac1, controls both cell-cell adhesion and migration make it both promotor and suppressor of some diseases (Gadea and Blangy 2014). For instance, it was reported to have a tumour suppressor property and DOCK4 mutations have been observed in some human cancer cell lines (Hiramoto, Negishi, and Katoh 2006 and Yajnik et al. 2003). Rac1 also plays a central role in GBM cells growth and progression in association with other cell surface receptors (Tajiri et al. 2017; Ueda et al. 2008 and Aoki, Nakamura, and Matsuda 2004).

The role of Rac in cell migration and invasion has been controversial and reported to depend on cell type. For instance, in rat glioma cells Rac knockdown increased cell migration and this migration was even more increased with irradiation (Hwang et al. 2006). Different studies demonstrated increased cancer cell invasion following ionising radiation in an *in vitro* model. For instance, ionising radiation increased migration and invasion of neuroblastoma cells in spheroid and Matrigel assays by increasing expression of MMP-9, VEGF and uPA (Jadhav and Mohanam 2006). The work of Dong et al. showed that ionising radiation increased U87 cells invasion in Matrigel assays by inducing nuclear translocation of ß-catenin (Dong et al. 2014). In this part of the study, I set out to investigate the role of DOCK4 in glioblastoma invasion and in addition, the effect of the combination of radiotherapy and DOCK4 knockdown on tumour invasion. I next employed lentiviral shRNA knockdown of DOCK4 in cancer cells to investigate the effects in tumour invasion in spheroid assays. Using the U251 glioblastoma cell line, which is the most widely used GBM cell line and the patient-derived GBM cells, GBM1, to knockdown DOCK4, I investigate the effect of DOCK4 knockdown on GBM cell invasion. In order to recapitulate the tumour microenvironment a co-culture experiment using endothelial cells (ECs) and cancer cells was used in which tumour invasion was analysed.

5.2 DOCK4 expression in glioblastoma cancer cells

Previous studies showed that DOCK4 was expressed differently in normal brain and glioblastoma. While DOCK4 expression in glioblastoma is significantly higher than that of the neural stem cells,

analysis of 547 glioblastoma and 10 normal brain samples from The Cancer Genome Atlas (TCGA) data showed no significant differences between normal brain and glioblastoma samples in DOCK4 expression. However, there is a lack of clarity as to which region of normal brain was used as a reference as different brain regions express different levels of DOCK4. For instance, DOCK4 is highly expressed in grey matter compared to white matter in a normal brain and within the brain, the highest expression of DOCK4 was detected in caudate, hippocampus, and cerebral cortex. In this study double immunostaining of normal brain tissue sections for DOCK4/CD31 was conducted. Intriguingly, the immunohistochemical staining showed a higher expression of DOCK4 in grey matter, the highest expression being in the neurons, and almost none in the white matter (Appendix 9). Hence, this result clearly showed that the neuronal cells are the ones expressing DOCK4 in normal brain. Following this finding, I investigated whether DOCK4 expression in GBM was different from normal brain and whether there was any variation among different patient GBM tumour samples.

Following optimisation of DOCK4 staining on normal tissue I then investigated the level of DOCK4 expression in different GBM samples. For this I first determined how to score DOCK4 expression in these tumours and adopted DOCK4 expression intensity and fractions of stained cells using different GBM tissues based on the Human Protein Atlas (HPA) scoring system (Appendix 10). Accordingly, 4 different levels of DOCK4 expression were identified depending on intensity and fractions of DOCK4 expressing cells; None, Low, Moderate and High (Appendix 11). Accordingly, a total of 12 primary patient-derived GBM tumour samples and one control normal brain tissues were sectioned and stained for DOCK4/CD31 and analysed for DOCK4 medium/high expression level (Figure 5.1). Because it is known that cancer cells invade along blood vessels and I also observed a relatively higher DOCK4 expression around blood vessels, I decided to score DOCK4 expression level around blood vessels.

Overall, a total of 3, 473 tumour blood vessels from 12 primary GBM patient samples were assessed for DOCK4 expression of cancer cells around perivascular regions. The result showed a heterogenous expression of DOCK4 in different glioblastoma tumour samples (Figure 5.1A) and the most angiogenic regions of the tumour had the highest DOCK4 expression and this expression was more common in aberrant blood vessel morphologies such as nestin positive and glomeruloid types compared to normal-like blood vessels.

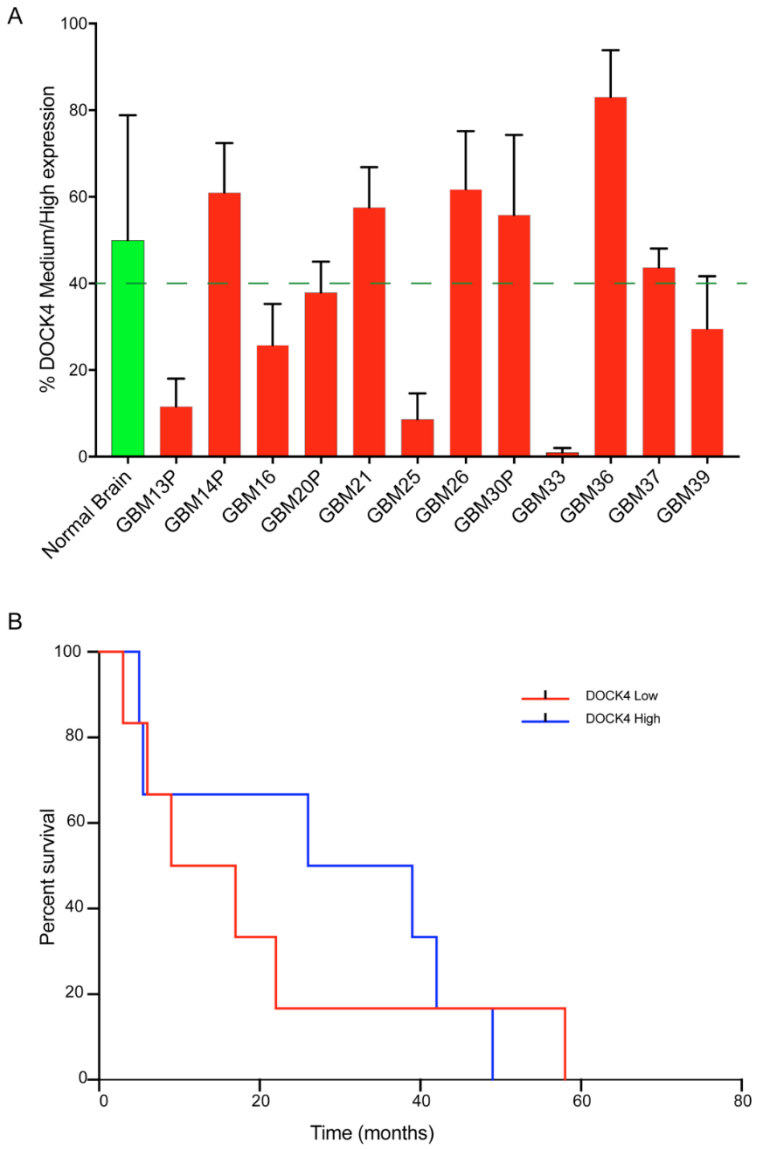

Figure 5.1 DOCK4 expression levels in patient-derived GBM and its association with survival

(A) Histogram shows average % of cancer cells expressing high and medium level of DOCK4 expression in patient-derived GBM samples along blood vessels as scored using HPA scoring guideline. Cancer cells around blood vessels were scored as low (Score 0 &1) and high (score 2&3) (Appendix 11). Up to two layers of cells along each blood vessel were scored for DOCK4 expression. An average of 25 blood vessels, minimum 7 and maximum 57, were analysed per box. A total of 12 GBM tumour tissue samples were analysed for cancer cell DOCK4 expression level: Values represent average expression ± SEM; N= Number of 1mm^2 areas (Normal Brain, 4; GBM13P, 15; GBM14P, 11; GBM16, 9; GBM20P, 10; GBM21, 11; GBM25, 13; GBM26, 9; GBM30P, 4; GBM33, 10; GBM36, 9; GBM 37, 12 and GBM39, 13).

(B) Graph showing survival curve for patients with high, as defined high DOCK4 expression in > 40% cells. N= number of GBM patients (Low, 6 and High, 6).

Previously, Debruyne and co-workers found a better survival for GBM patients with high DOCK4 expression compared to those with low expression using a median cut-off 30% (Debruyne et al. 2018). In this study, as the median DOCK4 expression of 12 primary GBM samples was 41% I examined whether there is a link between DOCK4 expression and overall patient survival using a cut-off 40% (Figure 5.1B). The result showed that although there was a trend of high DOCK4 expression in favour of a better overall survival this was not statistically significant (p=0.8). In agreement with this finding the analysis of 122 glioblastoma patient samples from Human Protein Atlas data showed lack of significant difference between high and low Dock4 mRNA expression and patients' overall survival (Appendix 12). The findings of heterogenous DOCK4 expression in primary patient-derived GBM samples prompted me to investigate whether expression level would be increased in recurrences as observed in irradiated mouse CT2A tumour samples. Intriguingly, I found that in all four tumours there was a tendency of increased DOCK4 expression in recurrent tumours compared to primary tumours (Figure 5.2) but not statistically significant. However, the degree of such increment varied. For instance, while in GBM13 DOCK4 expression increased from 12% to 21%, in GBM14 it increased from 61% to 67% as tumour progressed from primary to recurrent.

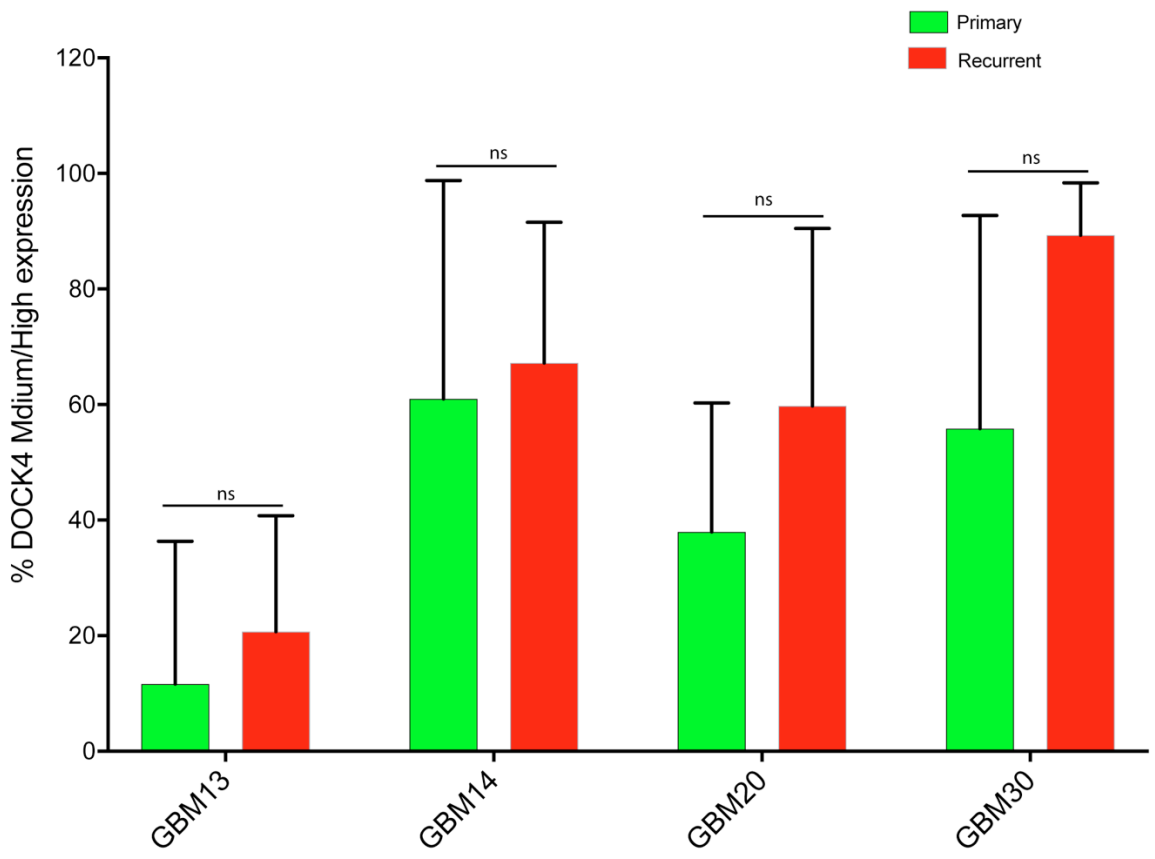

Figure 5.2 DOCK4 expression in primary versus recurrent patient GBM samples

Four pairs of patients GBM tissue samples were immunostained using DOCK4/CD31 and % Medium/High DOCK4 expression of cancer cells along blood vessels were assessed using HPA protein expression scoring system (Appendix 10). A total of 1,266 areas were scored around blood vessels from primary GBM and 377 areas from recurrent GBM and analysed % DOCK4 expression. N= % of medium/high DOCK4 expression per 1mm^2 area ± SEM: Number of N for primary tumours as shown in Figure 5.1 and for Recurrent (GBM13R, 9; GBM14R, 9; GBM20R, 9 and GBM30R, 5).

5.3 DOCK4 knockdown in the U251 cell line inhibits invasion

Since I found high levels of DOCK4 expression in half of the GBM patient samples analysed while DOCK4 has been shown to play a role in invasion and metastasis in lung cancer (Yu et al. 2015), this led me to ask whether DOCK4 knockdown in glioblastoma cancer cells would inhibit invasion. In order to investigate this, I used the commonly used cell line U251 (Cheng et al., 2015,) (Cockle et al. 2015) (Polson, 2018 #180) to assess cancer cell invasion in 3D spheroid assays. Firstly, I tested whether U251 cancer cells migrate in collagen and I found that they do invade into the surrounding collagen matrix (Figure 5.3). Invasion was determined using Migration Index (MI) as previously described by Cockle and co-workers (Cockle et al. 2015; see also section 2.1.10 in Materials and Methods). Following knockdown of DOCK4 from U251 cells using shRNA a spheroid assay was conducted. There was clear reduction of cancer cell invasion into the surrounding collagen matrix when DOCK4 was knocked down in U251 cancer cells compared to control U251 cells. In particular, DOCK4 knockdown significantly ($p<0.01$) reduced tumour invasion 3 days after addition of collagen (Figure 5.4). However, measurements of cancer cell invasion at later timepoints showed lack of significant differences between control in U251 cancer cells and U251 cells with DOCK4 knockdown from day 7 onwards (Figure 5.5). A potential reason for loss of the inhibitory effect with longer term culture could be a compensatory mechanism by other Dock180 family members in the absence of DOCK4.

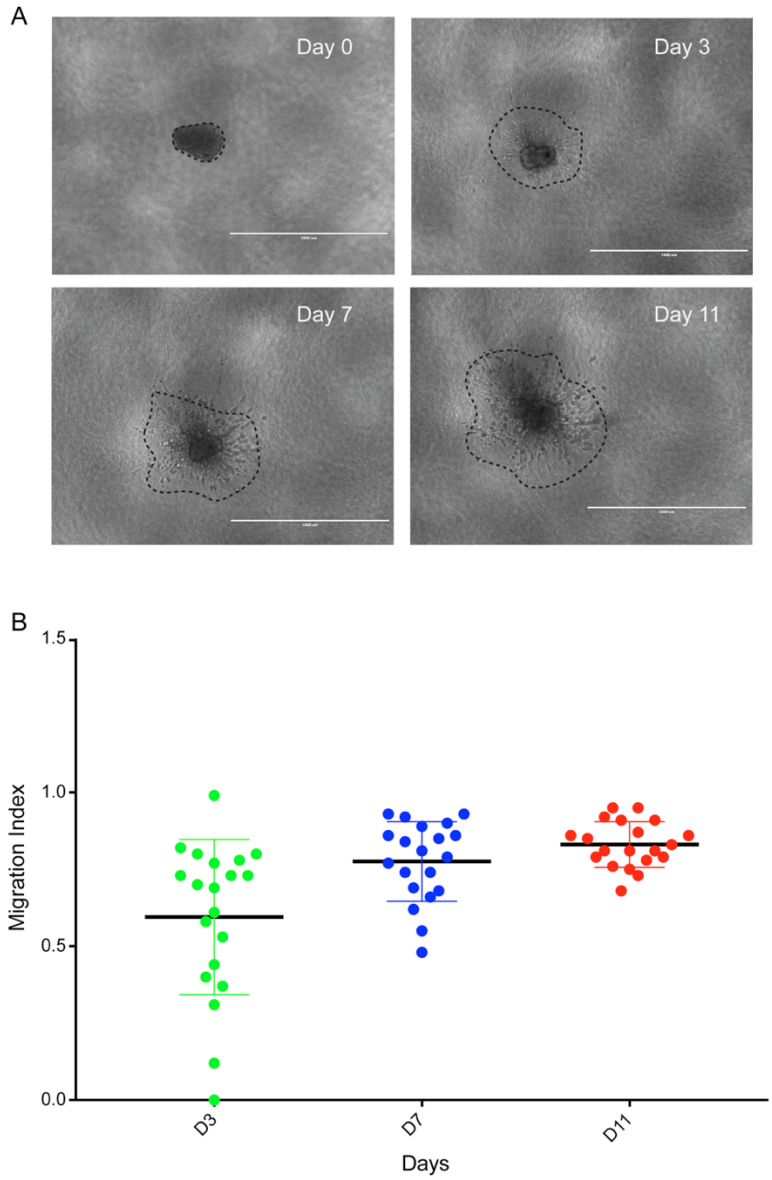

Figure 5.3 Invasion of U251 cancer cells over time in spheroid assays

U251 cancer cells ($1x10^3$) were seeded in a low adherent and round bottom 96-well plate in 200 µl 5xDMEM medium. After 3 days when a sphere was formed, supernatants were removed and 100µl collagen was added per well at 6.8 : 1 ratio of Collagen to 5xDMEM and neutralised by 0.7% 1M NaOH. Finally, 100µl 5xDMEM was added to each well and the plate was incubated at 37° and 5% CO_2. Cancer cell invasion was measured at Days 0, 3, 7, and 11 following the addition of collagen using EVOS at 4x magnification.

(A) Images depict spheroids formed by cancer cells and their invasion into the surrounding collagen matrix. Black dotted circles show area of invasion.

(B) Dot plot shows invasion area of U251 cells. Mean ± SD, N= number of wells (20 wells).

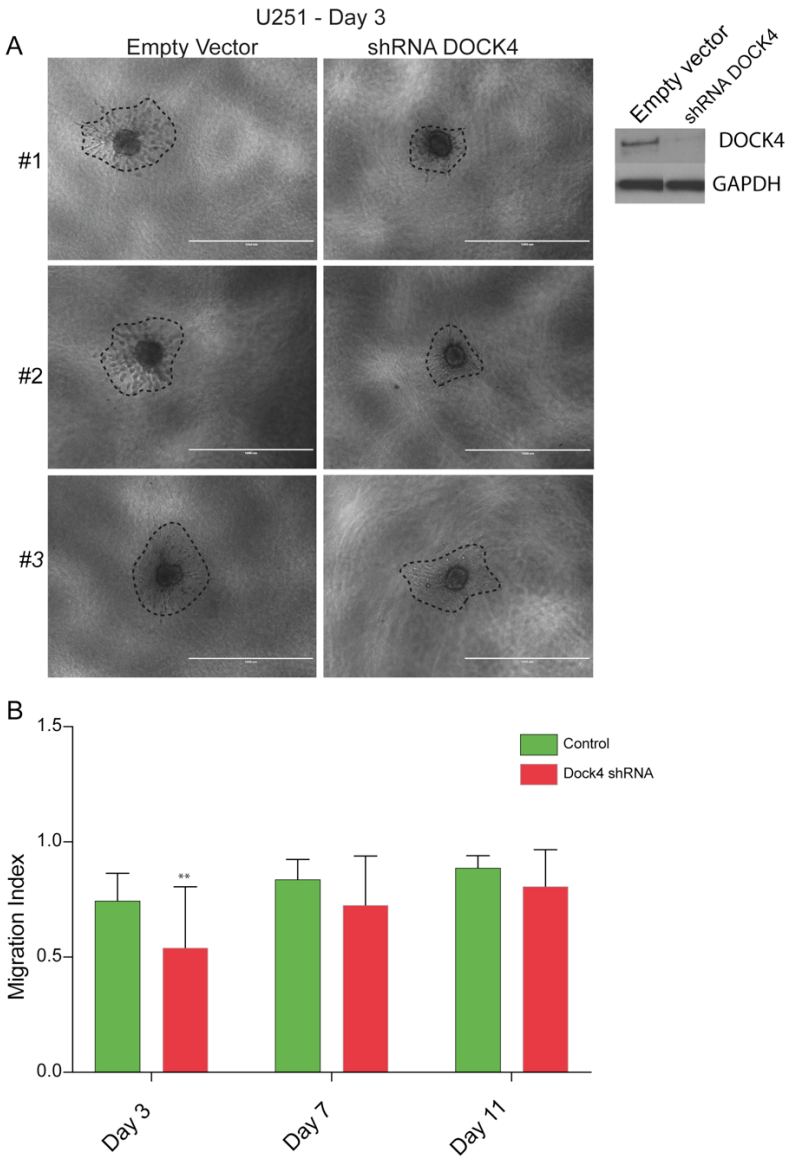

Figure 5.4 Effect of DOCK4 knockdown in U251 cells on invasion in spheroid assays

U251 cancer cells ($2x10^3$) transduced with either empty vector or DOCK4 shRNA were seeded in a low adherent round bottom 96-well plate in 200µl neurobasal medium. After 3 days when a sphere was formed, supernatants were removed and 100µl collagen was added per well at 6.8 : 1 ratio of collagen to 5xDMEM, and neutralised by 0.7% 1M NaOH. Finally, 100 µl 5xDMEM medium was added to each well and the plate was incubated at 37° and 5% CO_2. Cancer cell invasion was measured at Days 0, 3, 7, and 11 following the addition of collagen using EVOS at 4x magnification. N= number of wells (EV, 23; DOCK4 shRNA, 20). EV, Empty vector.

(A) Images depict spheroids formed by cancer cells transduced with lentiviruses harbouring EV or DOCK4 shRNAs. Black dotted circles show area of invasion.

(B) Bar chart shows invasion area of U251 cells transduced with EV and DOCK4 shRNA measured using ImageJ. ** $p<0.01$.

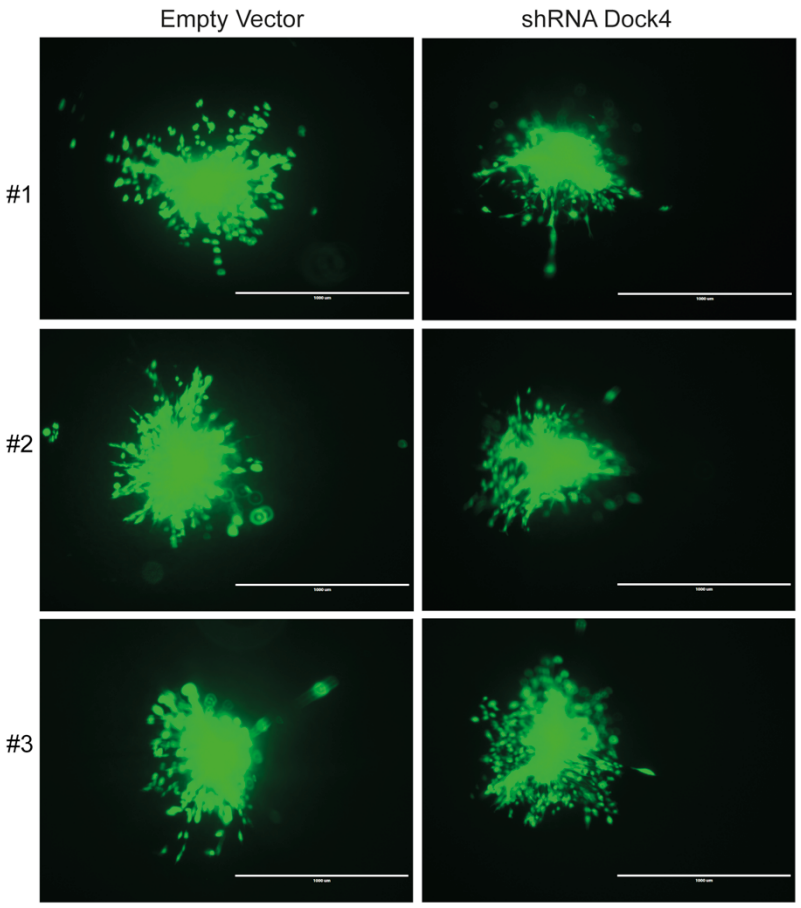

Figure 5.5 Effect of DOCK4 knockdown on U251 cancer cell invasion following transfection in spheroid assays

U251 cancer cells ($2x10^3$) transfected with either empty vector or DOCK4 shRNA were seeded in a low adherent round bottom 96-well plate in 200µl neurobasal medium. After 3 days when a sphere was formed, supernatants were removed and 100µl collagen was added per well at 6.8 : 1 ratio of collagen to 5xDMEM, and neutralised by 0.7% 1M NaOH. Finally, 100 µl 5xDMEM medium was added to each well and the plate was incubated at 37° and 5% CO_2. Cancer cell invasion was measured at Days 0, 3, 7, and 11 following the addition of collagen using EVOS at 4x magnification. Images depict invasion of EV or DOCK4 shRNAs transfected U251 cancer cells into the surrounding collagen matrix on Day 7. N= number of wells (EV, 23; DOCK4 shRNA, 20). EV, Empty vector.

5.4 DOCK4 knockdown in patient-derived cancer cells inhibits invasion

Following the observation of reduced invasion in DOCK4 knockdown from U251 cancer cells on Day3 I sought to check if knockdown of DOCK4 from patient-derived GBM cancer cells also decrease invasion. However, before trying to do this experiment I established whether patient-derived cells grow in a 3-D sphere model (Appendix 13) as they normally grow in neurobasal medium. The result showed that GBM1 cells could grow in neurobasal based medium in a spheroid assay although at a slower rate compared to the U251 cancer cell line which grows well in 5x Dulbecco's Modified Eagle Media (5xDMEM). When either empty vector or DOCK4 shRNA transfected GBM1 cancer cells were seeded in 96-well plates there was a significant ($p<0.05$) reduction in cancer cell invasion into the surrounding collagen in DOCK4 knockdown GBM1 cells on Day 8 post collagen addition, unlike the early effect observed on Day 3 in U251 cells, probably due to the fact that the latter grow faster than GBM1 cells (Figure 5.6).

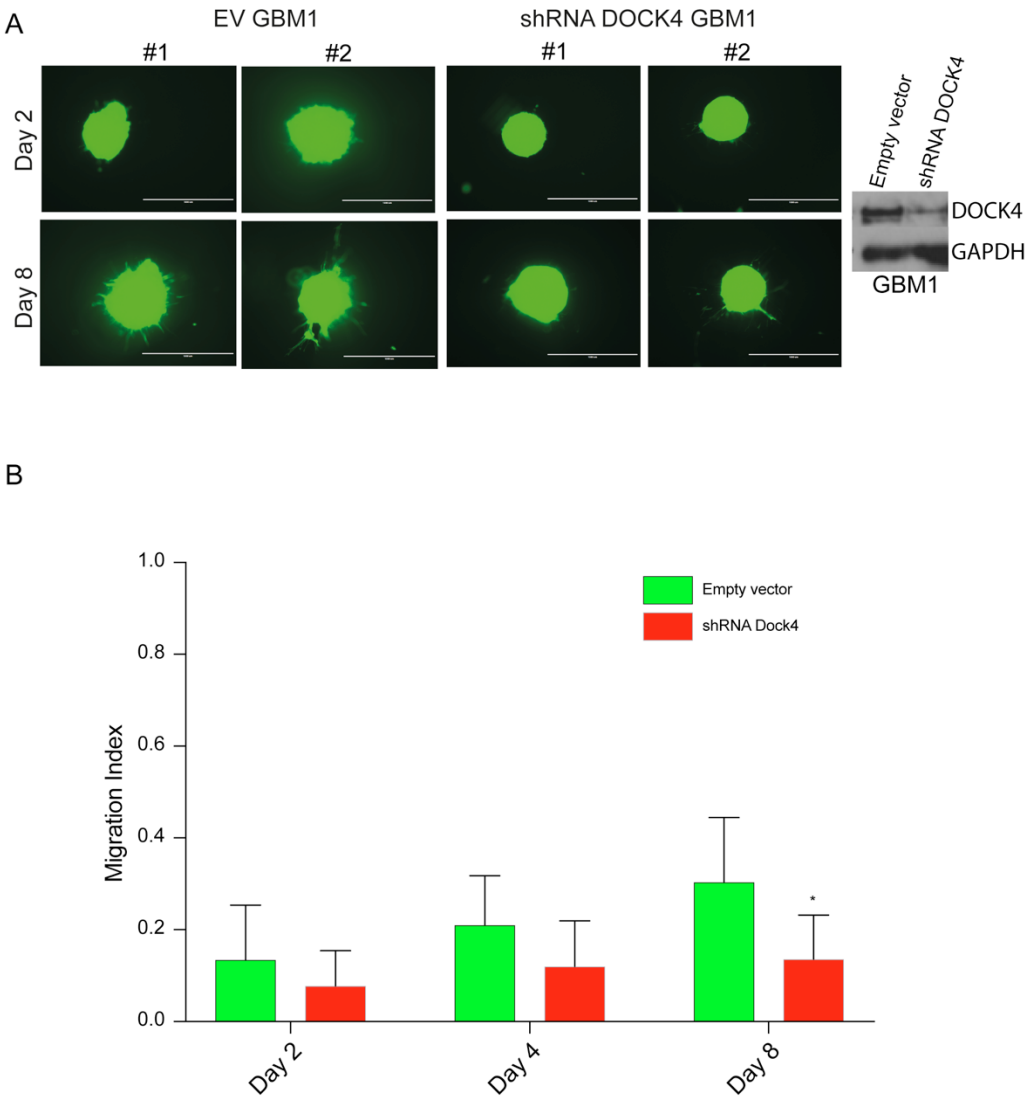

Figure 5.6 Effect of DOCK4 knockdown in patient-derived GBM1 cancer cell invasion in spheroid assays

GBM1 cancer cells ($2x10^3$) transfected with either empty vector or DOCK4 shRNA were seeded in a low adherent round bottom 96-well plate in 200µl neurobasal medium. After 5 days when a sphere was formed, supernatants were removed and 100µl collagen was added per well at 6.8 : 1 ratio of collagen to 5xDMEM, and neutralised by 0.7% 1M NaOH. Finally, 100 µl neurobasal medium was added to each well and the plate was incubated at 37° and 5% CO_2. Cancer cell invasion was measured at Days 0, 2, 4, and 8 following the addition of collagen using EVOS at 4x magnification. N= number of wells (EV, 15; DOCK4 shRNA, 5). EV, Empty vector.

(A) Images depict spheroids formed by cancer cells infected with lentiviruses harbouring EV or DOCK4 shRNAs.

(B) Bar chart shows invasion area of U251 cells transfected with EV and DOCK4 shRNA measured using ImageJ.

5.5 Establishing collagen based 3-D co-culture assays of glioblastoma cancer cells and HUVEC

In order to investigate the effect of DOCK4 knockdown in glioblastoma cancer cells under a condition which better recapitulates the GBM microenvironment I used a co-culture model of glioblastoma cancer cells and ECs instead of the simple monoculture assay. Firstly, I tested the growth and invasion of cancer cells in this co-culture model using U251 cell line. When cancer cell invasion into the surrounding collagen matrix was assessed under EVOS (Figure 5.7A) there were more invading cells in the presence of ECs compared to U251 only cells. Intriguingly, the quantification result showed a significant increase in invasion of cancer cells compared to monoculture (Figure 5.7B). Secondly, as most U251 cell lines lack both heterogeneity and drug resistance (Patrizii et al. 2018) and do not recapitulate the exact nature of patient-derived tumours I decided to use patient-derived GBM cells. GBM cells were co-cultured with HUVEC in a 1:1 ratio using neurobasal medium and Human Large Vessel Endothelial Cell Basal (HLVEC) medium in a spheroid assay. The result clearly showed a significant increase in invasion of cancer cells into the surrounding collagen matrix in the presence of ECs (Figure 5.8). Compared to U251 cancer cell line GBM1 cells invaded less, both in the presence and absence of ECs. However, comparing the two glioblastoma models the presence of ECs significantly increased tumour invasion in GBM1 than in U251 cancer cells.

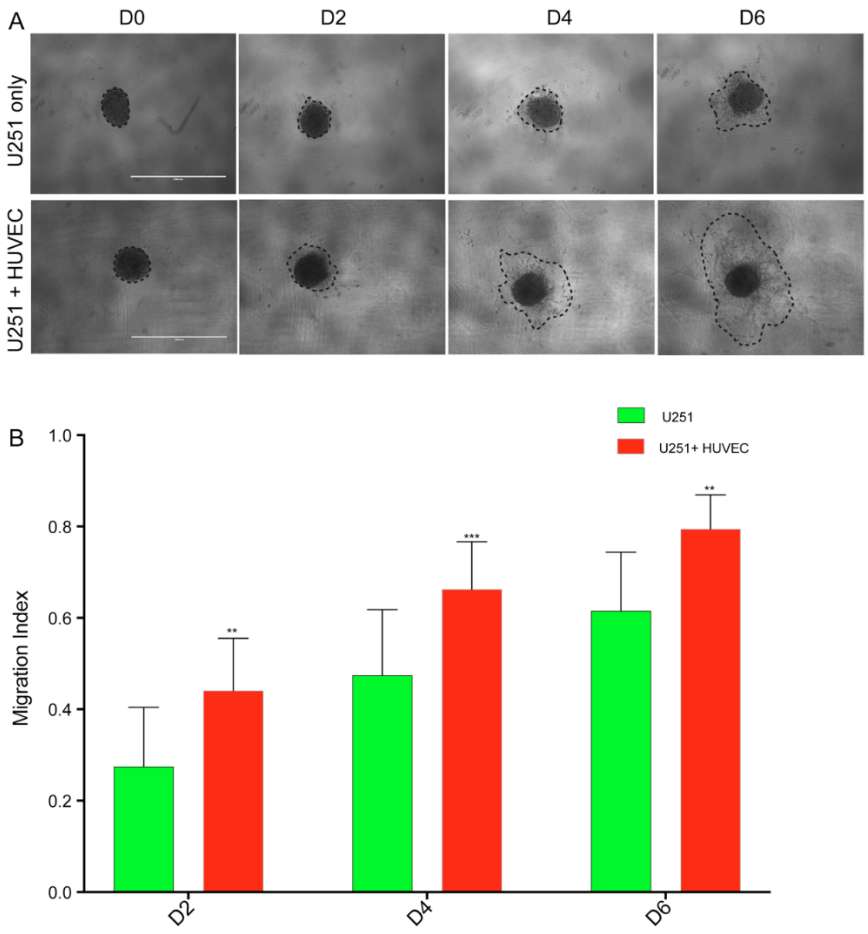

Figure 5.7 Establishment of co-culture of U251 cancer cells and HUVEC in collagen based spheroid assays

U251 cancer cells ($2x10^3$), or $2x10^3$ U251 cancer cells mixed with $2x10^3$ HUVEC were seeded in a low adherent and round bottom 96-well plates in a 1:1 ratio of 100 µl 5xDMEM and 100µl HLVEC medium. After 3 days when a sphere was formed, supernatants were removed and 100µl collagen was added per well at 6.8 : 1 ratio of collagen to medium (equal mix of 5xDMEM and Human Large Vessel Endothelial Cell Basal (HLVEC) medium), and neutralised by 0.7% 1M NaOH. Finally, 100 µl of the mix medium was added to each well and the plate was incubated at 37° and 5% CO_2. Cancer cell invasion was measured at Days 0, 2, 4, and 6 following the addition of collagen using EVOS at 4x magnification. N= number of wells (U251 cells, 13 and U251 + HUVEC, 11).

(A) Images depict spheroids formed by cancer cells and HUVEC and their invasion into the surrounding collagen matrix. Black dotted circles show area of invasion.

(B) Bar chart shows invasion area of U251 cancer cells and HUVEC.

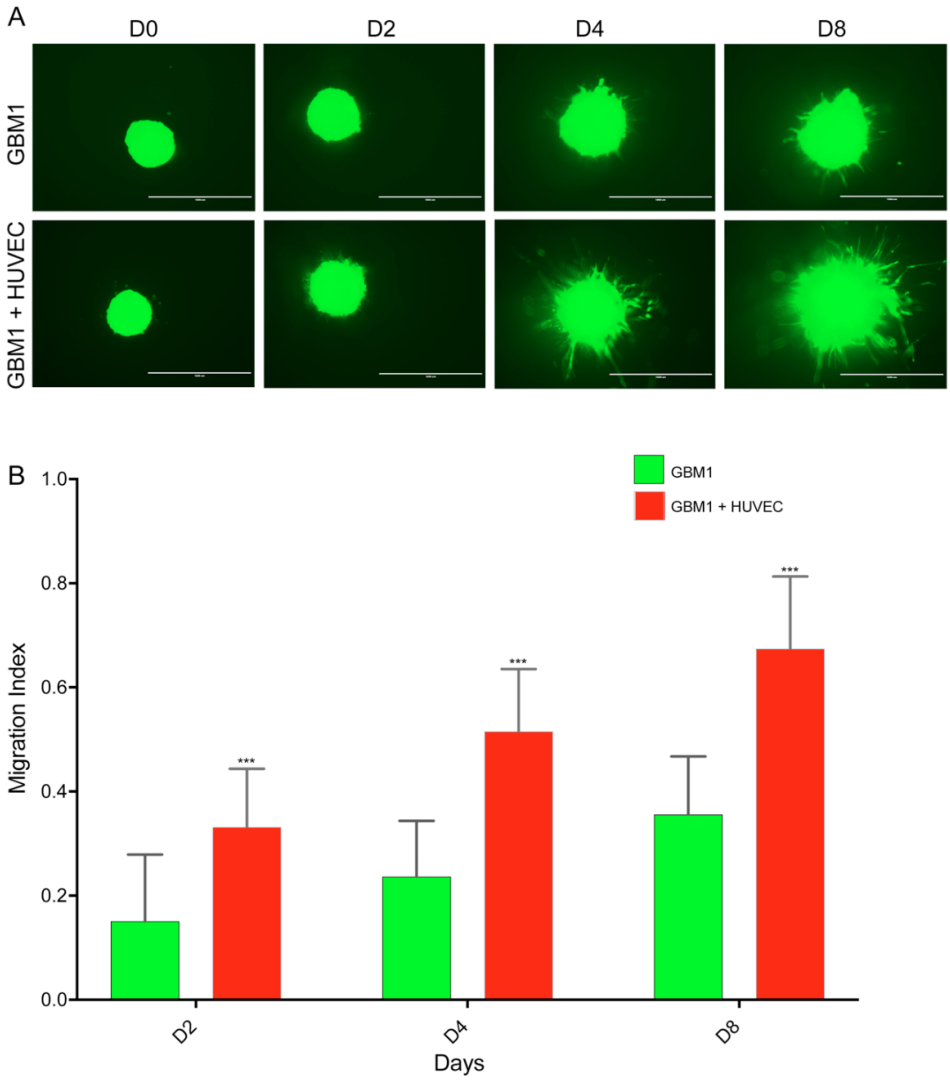

Figure 5.8 Establishment of co-culture of GBM1 cancer cells and HUVEC in collagen based spheroid assays

GBM1 cancer cells ($2x10^3$), or $2x10^3$ GBM1 cancer cells mixed with $2x10^3$ HUVEC were seeded in a low adherent and round bottom 96-well plates in a 1:1 ratio of 100 µl neurobasal medium and 100µl HLVEC medium. After 5 days when a sphere was formed, supernatants were removed and 100µl collagen was added per well at 6.8 : 1 ratio of collagen to medium (equal mix of neurobasal and HLVEC medium), and neutralised by 0.7% 1M NaOH. Finally, 100 µl of the mix medium was added to each well and the plate was incubated at 37° and 5% CO_2. Cancer cell invasion was measured at Day 0, 2, 4, and 8 following the addition of collagen using EVOS at 4x magnification. N=Number of wells (GBM1 cells, 12 and GBM1 + HUVEC, 16). D=Day.

(A) Images depict spheroids formed by cancer cells and HUVEC and their invasion into the surrounding collagen matrix.

(B) Bar chart shows invasion area of GBM1 cancer cells in the presence and absence of HUVEC.

5.6 Glioblastoma cells but not ECs invade into the surrounding collagen matrix

Following the increased invasion observed in a co-culture spheroid assay experiment using cancer cells and ECs I asked whether this increased invasiveness came from cancer cells or ECs. Hence, in order to investigate this, I used green labelled cancer cells with unlabelled ECs and vice-versa. The result showed that when green U251 cells were co-cultured with unlabelled ECs the green cancer cells invaded into the collagen matrix as observed and measured using the GFP channel of the EVOS (Figure 5.9, upper panel). On the other hand, when green ECs were co-cultured with unlabelled U251 cancer cells the green ECs remained at the centre of the sphere and there was no spreading away of green ECs at all. Further, in order to see if there was any spread of the unlabelled cancer cells present in the sphere where green labelled ECs remained at the centre of the sphere I used a phase contrast images to demonstrate that the invading cells were indeed cancer cells (Figure 5.9, lower panel). A similar approach confirmed that the invading cells were cancer cells not ECs using patient-derived GBM1 cancer cells co-cultured with HUVEC (Figure 5.10). This clearly indicates that cancer cells but not ECs are invading into the surrounding normal tissue and ECs play a crucial role in glioblastoma invasion.

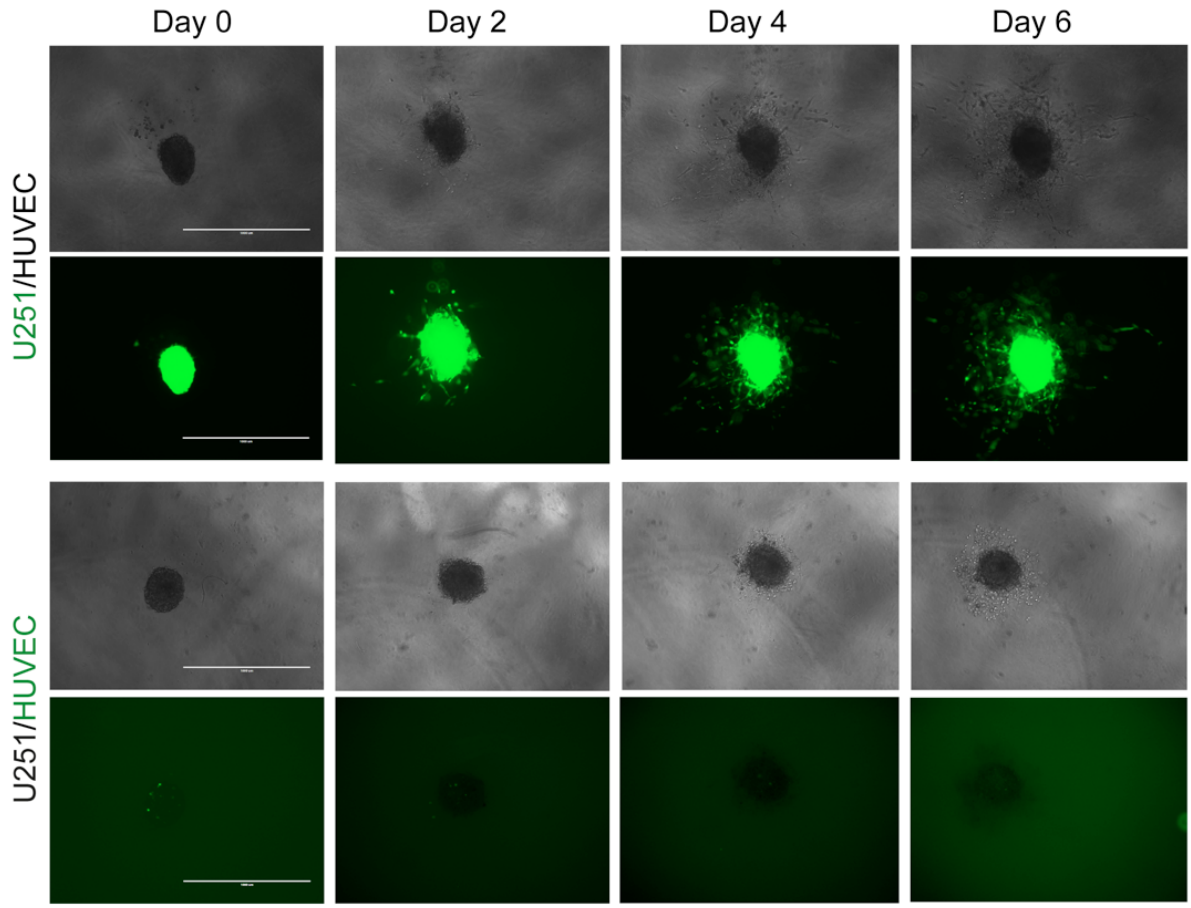

Figure 5.9 U251 cancer cells but not endothelial cells invade into collagen matrix in spheroid co-cultures

Green labelled U251 cancer cells ($2x10^3$) and $2x10^3$ unlabelled HUVEC, and vice versa, were seeded in a low adherent and round bottom 96-well plates in a 1:1 ratio of 100 µl DMEM and 100µl HLVEC medium. After 3 days when a sphere was formed, supernatants were removed and 100µl collagen was added per well at 6.8 : 1 ratio of collagen to medium (equal mix of 5xDMEM and HLVEC medium), and neutralised by 0.7% 1M NaOH. Finally, 100 µl of the mix medium was added to each well and the plate was incubated at 37^o and 5% CO_2. Cancer cell invasion was measured at Days 0, 2, 4, and 6 following the addition of collagen using EVOS at 4x magnification. GFP and phase contrast images depict spheroids formed by cancer cells and HUVEC and their invasion into the surrounding collagen matrix. N= number of wells (green U251 cells co-cultured with unlabelled HUVEC, 9 and unlabelled U251 cancer cells co-cultured with green HUVEC, 13).

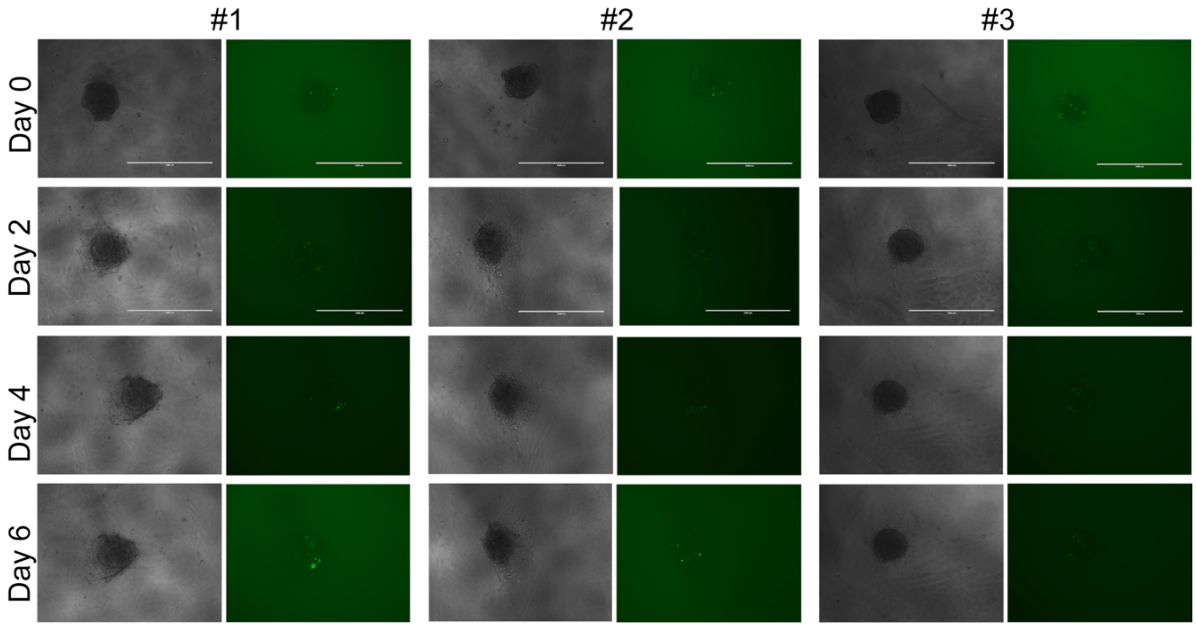

Figure 5.10 GBM1 cancer cells but not endothelial cells invade into collagen matrix in spheroid co-cultures

Green labelled HUVEC ($2x10^3$) and $2x10^3$ unlabelled GBM1 cancer cells were seeded in a low adherent and round bottom 96-well plates in a 1:1 ratio of 100 μl neurobasal medium and 100μl HLVEC medium. After 5 days when a sphere was formed, supernatants were removed and 100μl collagen was added per well at 6.8 : 1 ratio of collagen to medium (equal mix of neurobasal and HLVEC medium), and neutralised by 0.7% 1M NaOH. Finally, 100 μl of the mix medium was added to each well and the plate was incubated at 37° and 5% CO_2. Cancer cell invasion was measured at Days 0, 2, 4, and 8 following the addition of collagen using EVOS at 4x magnification. GFP and phase contrast images depict the growth and invasion of spheroids into the surrounding collagen matrix. N= number of wells (7 wells).

5.7 The presence of both cancer cell and endothelial cell growth medium is important for invasion

Following the findings of increased glioblastoma cancer cells invasion in the presence of endothelial cells, I asked whether the growth medium in which the cancer cells and ECs were seeded affected most the degree of cancer cell invasion. The result of this experiment showed that for glioblastoma invasion the presence of both cancer and ECs growth medium were equally important, particularly the growth factors and supplements used during seeding the cells. While on average only 3/12 spheres (wells) managed to grow and invade into the surrounding collagen matrix when seeded in neurobasal medium only, this number increased to over 8 in the presence of both neurobasal and HLVEC medium, suggesting that the addition of HLVEC medium doubled the invasion of cancer cells into the surrounding collagen matrix in a spheroid assay co-culture (Figure 5.11).

Further, when the medium mixed with collagen or added at the final stage was compared it was observed that the medium without supplement didn't support the formation and growth of spheres very well compared to the complete medium with supplement. This implies the important role of growth factors such as vascular endothelial growth factor (VEGF), epidermal growth factor (EGF), basic fibroblast growth factor (bFGF) and others which are normally added to the medium to grow these cancer cells. It was also noticed that rather than the medium used with collagen after sphere formation the medium used during the initial seeding stage was more vital for cancer cells to form spheres, growth and invasion. Accordingly, while GBM1 and HUVEC co-culture in a 1:1 ratio of complete neurobasal medium and HLVEC medium with supplement performed better than those cells seeded in neurobasal medium only. In particular, cancer cells invaded better when collagen was added with either complete neurobasal medium (Figure 5.11E) or HLVEC medium with supplement (Figure 5.11G). However, cells which received neurobasal medium without growth factors and supplements with collagen to the spheres formed at the bottom of the 96-well plate had the least invasion. This leads to a conclusion that it is highly likely that the growth factors, which are normally produced by either cancer cells or stroma, play an essential role in cancer cell invasion.

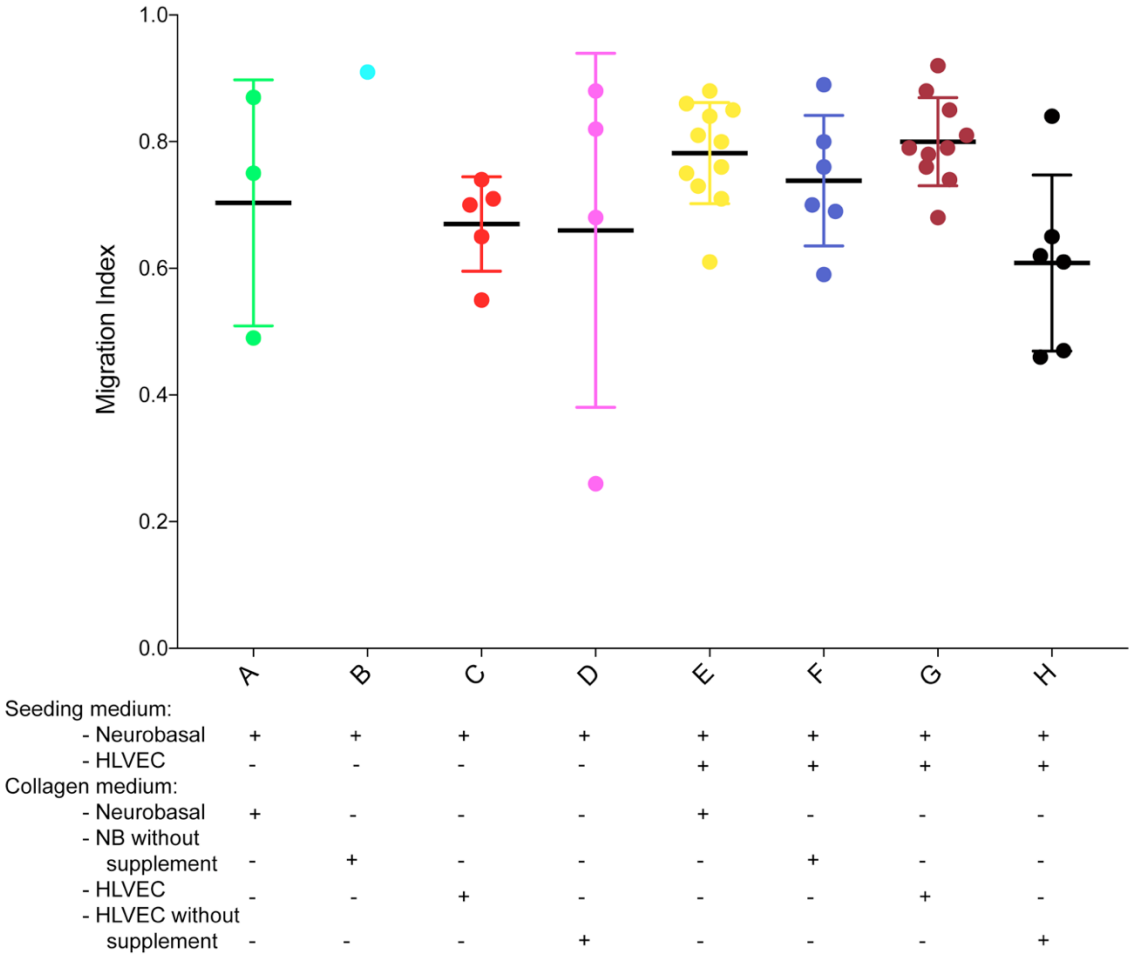

Figure 5.11 The impact of different growth factors and supplements on cancer cell invasion

GBM1 cancer cells ($2x10^3$) were co-cultured with $2x10^3$ HUVEC cells in a low adherent and round bottom 96-well plate in either 200µl neurobasal (NB) medium only (A-D) or in 200µl medium containing a 1:1 ratio of neurobasal medium and HLVEC medium (Row E-H). After 5 days when a sphere was formed, supernatants were removed and 100µl collagen was added per well at 6.8 : 1 ratio of collagen to neurobasal medium only (A&E), neurobasal without supplement (B&F), HLVEC medium (C&G) or HLVEC medium without supplement (D&H) and then neutralised by 0.7% 1M NaOH. Finally, 100µl of NB (A&E), NB without supplement (B&F), HLVEC medium only (C&G) and HLVEC without supplement (D&H) were added, respectively and the plate was incubated at 37° and 5% CO_2. Cancer cell invasion was measured on Days 0, 2, 4 and 8 following the addition of collagen using EVOS at 4x magnification. Complete neurobasal medium contains EGF and bFGF growth factors and complete HLVEC contains at least VEGF, and Insulin-like growth factor (IGF) or EGF growth factors. N= number of wells (A, 3; B, 1; C, 5; D, 4; E, 11; F, 6; G, 10 and H, 6). A-H represents the 96-well plate's rows.

5.8 DOCK4 knockdown in glioblastoma cancer cells does not affect invasion in the presence of endothelial cells

Following the observation of increased cancer cell invasion into the surround collagen matrix in the presence of ECs using a spheroid assay, I asked whether knockdown of DOCK4 from such cancer cells under co-culture condition could actually reduce or stop their invasiveness. Using U251 cancer cells and ECs co-culture in a spheroid assay model I assessed the effect of DOCK4 knockdown from U251 cancer cells. Surprisingly, despite a slight trend of decrease following DOCK4 knockdown, there was no significant difference between empty vector (EV) control and DOCK4 shRNA in invasion of U251 cancer cells in a co-culture spheroid assay model. Both EV and DOCK4 shRNA U251 cancer cells in a co-culture condition invaded greater than U251 cancer cells in a monoculture condition (Figure 5.12). This shows that the significantly reduced effect of cancer cell invasion observed following knockdown of DOCK4 from U251 cells under monoculture condition failed to repeat in the presence of ECs, a model which better recapitulate the normal tumour microenvironment in patients.

Then, I investigated the effect of DOCK4 knockdown from patient-derived GBM cells on cancer cell invasion in the presence of ECs. Unsurprisingly, just like U251 cell line there was no significant difference between control GBM1 cells and DOCK4 shRNA GBM1 cells both co-cultured with HUVEC (Figure 5.13). However, compared to U251 cell line there was a slightly increased invasion in GBM1 cancer cells when DOCK4 was deleted compared to control GBM1 implying that deleting DOCK4 could have a negative consequence. In conclusion, the use of both glioblastoma cancer cell models showed lack of significant difference in cancer cell invasion between DOCK4 knockdown and control in the presence of ECs co-culture unlike the significant difference observed in a monoculture scenario.

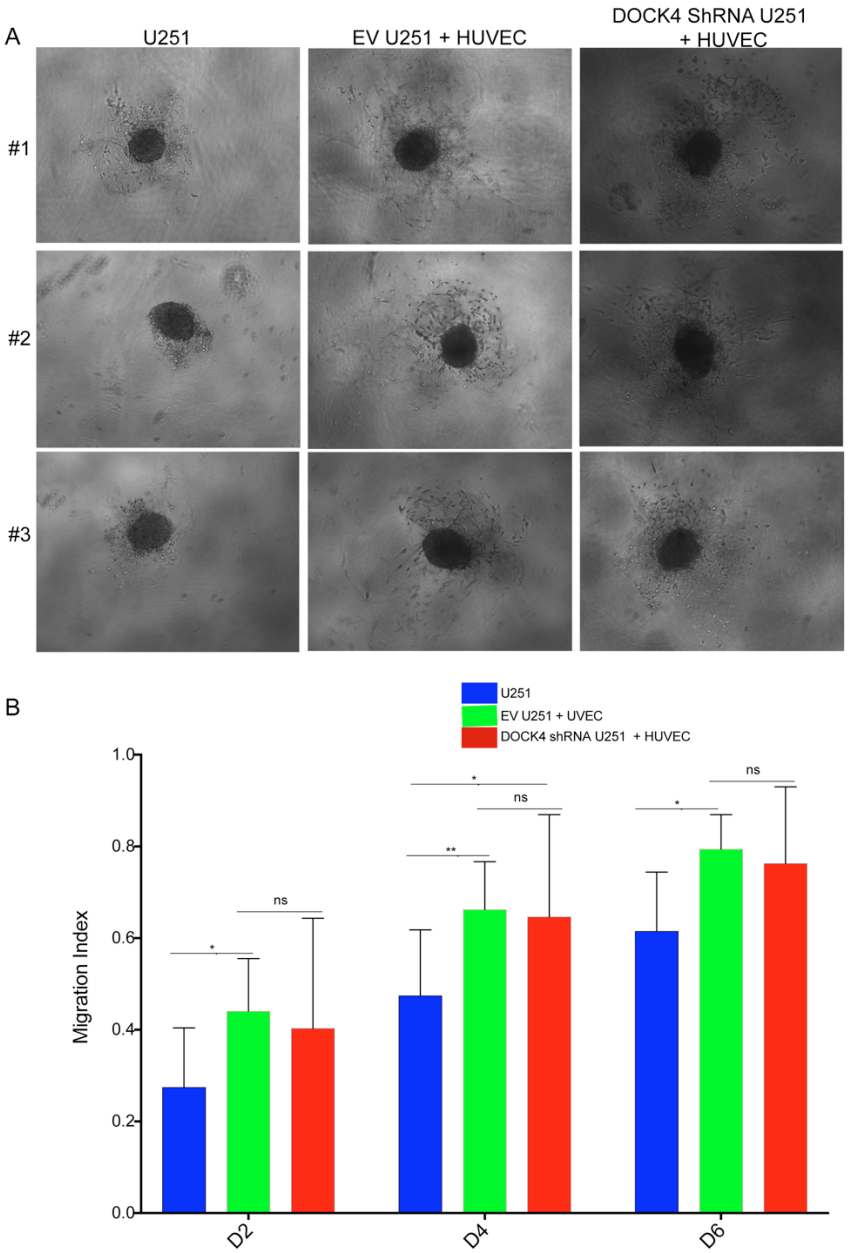

Figure 5.12 Effect of DOCK4 knockdown on U251 cancer cell invasion in the presence of HUVEC

U251 cancer cells ($2x10^3$) as monoculture or a co-culture of EV or DOCK4 knockdown $2x10^3$ U251 cancer cells with with HUVEC were seeded in a low adherent round bottom 96-well plate in a 1:1 ratio of 100 µl 5xDMEM and 100µl HLVEC medium. After 3 days when a sphere was formed, supernatants were removed and 100µl collagen was added per well at 6.8 : 1 ratio of collagen to medium (equal mix of 5xDMEM and HLVEC medium), and neutralised by 0.7% 1M NaOH. Finally, 100 µl of the mix medium was added to each well and the plate was incubated at 37° and 5% CO_2. Cancer cell invasion was measured at Days 0, 2, 4, and 6 following the addition of collagen using EVOS at 4x magnification. N= number of wells (U251 cells, 13; EV + HUVEC, 11 and DOCK4 shRNA + HUVEC, 9).

(A) Images depict invasion of cancer cells into collagen matrix, 3 representative images from D6.

(B) Bar chart shows invasion area of U251 cancer cells and HUVEC.

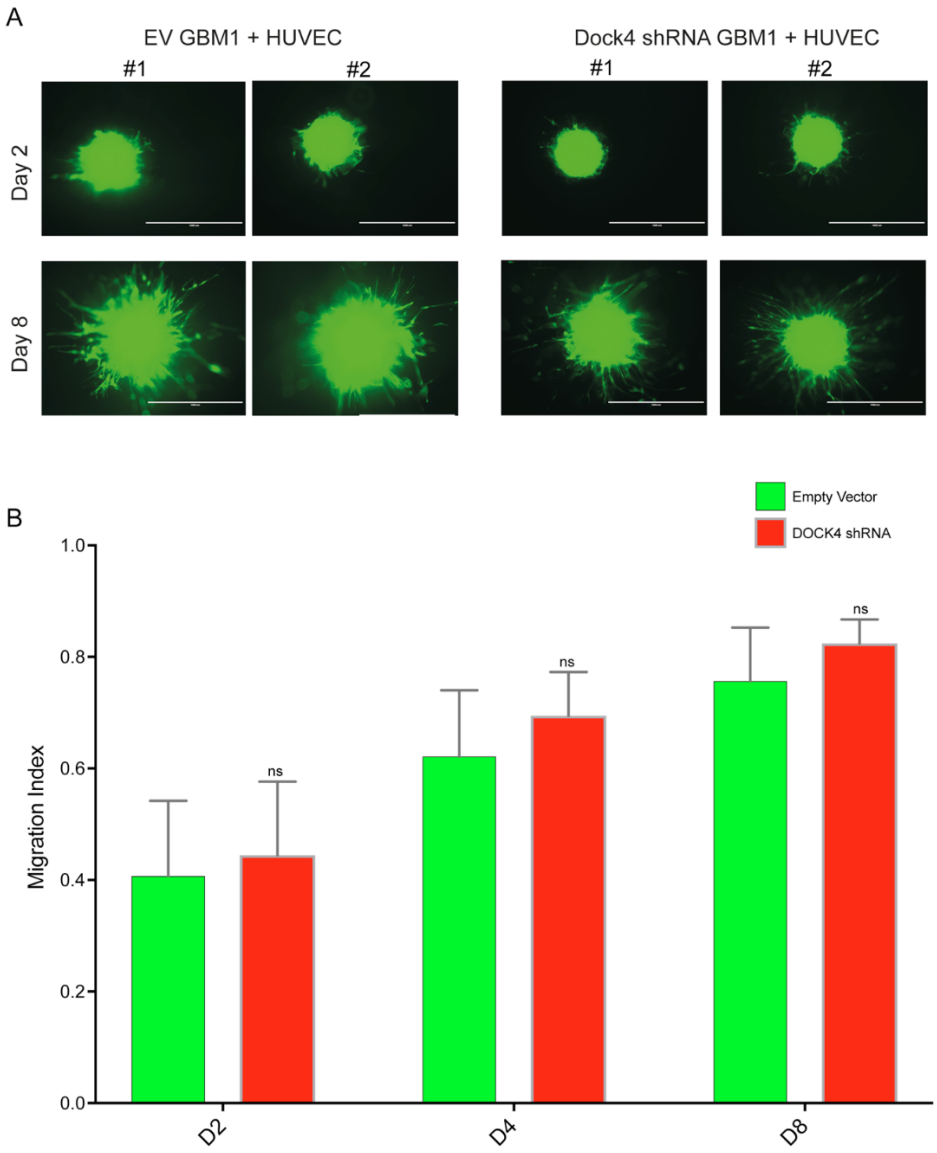

Figure 5.13 Effect of DOCK4 knockdown on GBM1 cancer cell invasion in the presence of HUVEC

GBM1 cancer cells ($2x10^3$) or $2x10^3$ GBM1 cancer cells with DOCK4 knockdown were seeded in a low adherent round bottom 96-well plate in a 1:1 ratio of 100 µl neurobasal medium and 100µl HLVEC medium. After 5 days when a sphere was formed, supernatants were removed and 100µl collagen was added per well at 6.8 : 1 ratio of collagen to medium (equal mix of neurobasal medium and HLVEC medium), and neutralised by 0.7% 1M NaOH. Finally, 100 µl of the mix medium was added to each well and the plate was incubated at 37° and 5% CO_2. Cancer cell invasion was measured at Days 0, 2, 4, and 8 following the addition of collagen using EVOS at 4x magnification. N= number of wells (Empty Vector, 17 and DOCK4 shRNA, 9).

(A) Images depict invasion of cancer cells into collagen matrix.

(B) Bar chart shows invasion area of U251 cancer cells and HUVEC.

5.9 Effect of ionising radiation on cancer cell invasion in the presence of endothelial cells

Radiotherapy is widely used for treatment of cancer patients. Despite its wide spread use in cancer treatment, ionising radiation also cause aggressive invasion in several tumours including breast, brain, and lung tissues by increasing production of MMPs from both cancer and the microenvironment (Artacho-Cordon et al. 2012). Many other studies also have shown that the use of ionising radiation increased cancer cell invasion in a spheroid assay. Here, following the observation of increased cancer cells invasion in a co-culture of cancer cells and ECs, I hypothesised that irradiation could potentially decrease such invasion in the absence of ECs and increases invasion in the presence of ECs as ECs could potentially play a protective role. In order to investigate this, I used the U251 cancer cell line in a spheroid assay with or without HUVEC and treated the cells using irradiation dose of 10Gy. To my surprise, I observed an opposite effect of my initial hypothesis. Simply, the U251 cells showed a sign of resistance on their own and susceptibility to irradiation when co-cultured with HVEC (Figure 5.14). Although there was no significant difference in invasion at any timepoint between control and irradiated cancer cells in a monoculture, I observed a significant reduction of cancer cell invasion following irradiation at Day 6 post collagen addition to the spheroid assay in the case of cancer cell and HUVEC co-culture.

Then I asked whether sensitivity to irradiation is cell type dependent and used the mouse glioblastoma CT2A (Appendix 14) and patient-derived GBM20 cancer cells (Appendix 15). When a monoculture of CT2A cancer cells were irradiated using either 5Gy or 10Gy doses of ionising irradiation, the spheres became smaller in size as opposed to control CT2A spheres which became elongated and expanded without invading into the surrounding collagen matrix. However, under co-culture condition, only CT2A cells seeded with Human Cerebral Microvascular Endothelial Cells (HCMEC) but not HUVEC invaded into the matrix and co-culturing CT2A cancer cells with HUVEC made them sensitive to irradiation as observed in the U251 cancer cells. When I tested the effect of irradiation on patient-derived GBM samples using GBM20, unlike that of U251 cells, I found a total sensitivity of cancer cells to irradiation in absence of ECs and a significant increase in cancer cell invasion following irradiation doses 5Gy and 10Gy when GBM cancer cells were co-cultured with either HCMEC or HUVEC (Appendix 15). Further, the patient-derived GBM20 cells failed to grow and spread in the absence of ECs. Overall, the results of ionising radiation in a spheroid assay showed how cancer cells' radioresistance depends on both cell type and presence or absence of different cells in the tumour microenvironment like ECs.

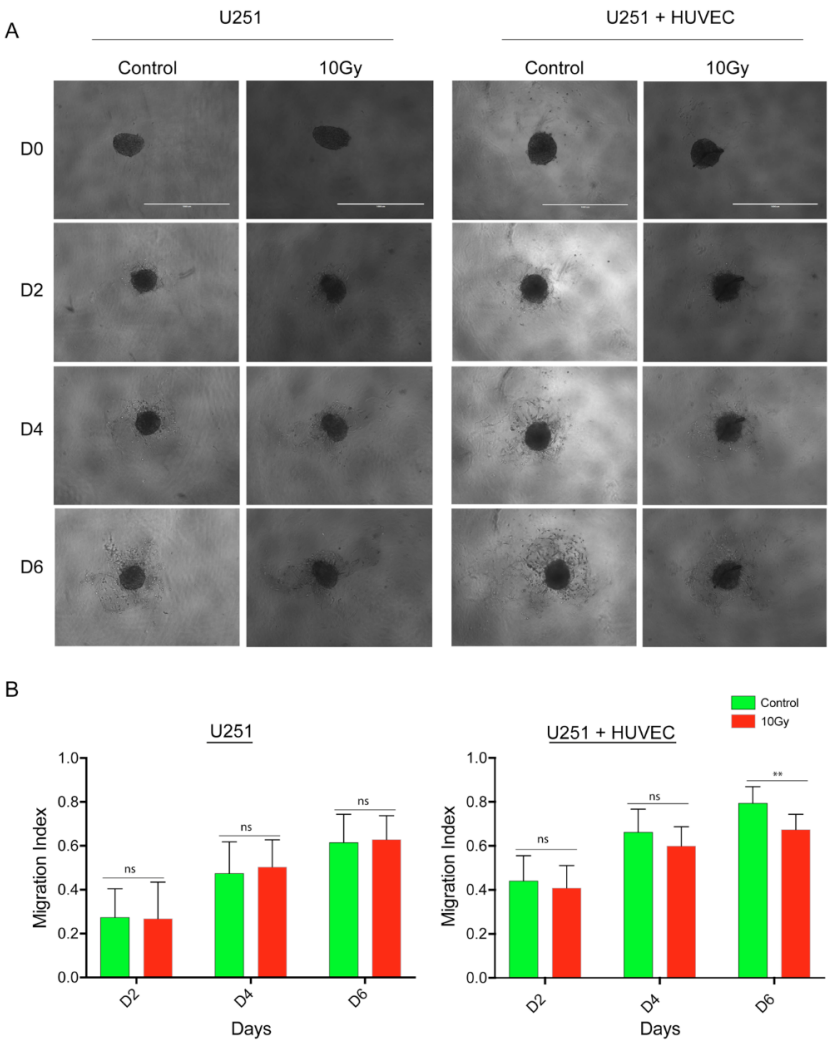

Figure 5.14 Effect of ionising radiation on U251 cancer cell invasion in the presence or absence of HUVEC

U251 cancer cells ($2x10^3$), or $2x10^3$ U251 cancer cells mixed with $2x10^3$ HUVEC were seeded in a low adherent and round bottom 96-well plates in a 1:1 ratio of 100 µl 5xDMEM and 100µl HLVEC medium. After 3 days when a sphere was formed, supernatants were removed and 100µl collagen was added per well at 6.8 : 1 ratio of collagen to medium (equal mix of 5xDMEM and HLVEC) medium, and neutralised by 0.7% 1M NaOH. Finally, 100 µl of the mix medium was added to each well and the plate was incubated at 37° and 5% CO_2. Next day 10Gy irradiation dose was delivered using RAD 2000 at a rate of 2Gy/minute. Cancer cell invasion was measured at Days 0, 2, 4, and 6 following the addition of collagen using EVOS at 4x magnification. N= number of wells (U251 control, 13; U251 10Gy, 21; U251 + HUVEC Control, 11 and U251 +HUVEC 10Gy, 16 wells).

(A) Images depict spheroids formed by cancer cells monoculture and co-culture of cancer cells and HUVEC, and their consequent invasion into the surrounding collagen matrix.

(B) Bar chart shows invasion area following irradiation under monoculture and co-culture conditions.

5.10 Effect of combined DOCK4 knockdown and irradiation on cancer cell invasion

Following the demonstration of a slight decrease in U251 cells invasion following irradiation in the presence of endothelial cells I hypothesised that a combination of irradiation and DOCK4 knockdown in the presence of ECs could lead to further reduction of U251 cancer cells invasion. Unfortunately, except the slight trend of decrease observed following irradiation there was no significant difference between control and irradiated tumours in the presence of ECs (Figure 5.15). This could imply that DOCK4 knockdown from glioblastoma cells may not significantly decrease or have no synergistic effect at least in U251 cancer cell invasion in the presence of endothelial cells, which better recapitulates the brain tumour microenvironment. Hence, a combination therapy of DOCK4 knockdown and irradiation showed no overall significant benefit in decreasing invasion of glioblastoma cancer cells in a spheroid assay. To sum up, although there was no difference between control and irradiated U251 cells in cancer cells monoculture, U251 cancer cell invasion significantly ($p<0.01$) reduced in a co-culture assay with ECs on Day 6 following 10Gy irradiation probably implying that ECs made these particular cancer cells susceptible to irradiation although presence of ECs had an opposite effect on GBM20 leading to radioresistance. However, combination therapy using both DOCK4 knockdown and irradiation failed to reduce cancer cell invasion in the presence of ECs.

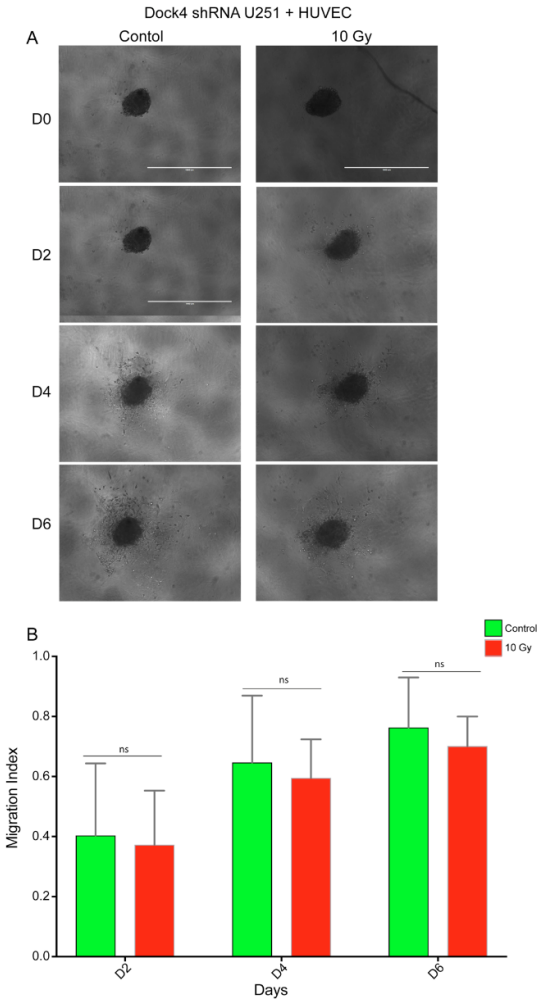

Figure 5.15 Effect of ionising radiation and DOCK4 deletion on U251 cancer cell invasion in the presence of HUVEC

U251 cancer cells ($2x10^3$), or $2x10^3$ U251 cancer cells mixed with $2x10^3$ HUVEC were seeded in a low adherent and round bottom 96-well plates in a 1:1 ratio of 100 µl 5xDMEM and 100µl HLVEC medium. After 3 days when a sphere was formed, supernatants were removed and 100µl collagen was added per well at 6.8 : 1 ratio of collagen to medium (equal mix of 5xDMEM and HLVEC) medium, and neutralised by 0.7% 1M NaOH. Finally, 100 µl of the mix medium was added to each well and the plate was incubated at 37° and 5% CO_2. Next day, an irradiation dose of 10Gy was delivered using RAD 2000 at a rate of 2Gy/minute. Cancer cell invasion was measured at Days 0, 2, 4, and 6 following the addition of collagen using EVOS at 4x magnification. N= number of wells (DOCK4 shRNA U251 control, 9 and DOCK4 shRNA U251 10Gy, 21 wells).

(A) Images depict spheroids formed by cancer cells monoculture and co-culture of cancer cells and HUVEC, and their consequent invasion into the surrounding collagen matrix.

(B) Bar chart shows invasion area following irradiation under monoculture and co-culture conditions.

5.11 Conclusions

DOCK4 protein is upregulated in normal brain, particularly in grey matter. However, the overall analysis of DOCK4 expression in this thesis showed that there is no difference in DOCK4 expression in samples from a normal brain and glioblastoma tumour tissue samples. Over the course of this study Debruyne and co-workers showed that DOCK4 expressing cells are differentiated cancer cells and had low stem cell marker OLIG2 expression and such cells were non-mitotic and such increased DOCK4 expression in GBM samples had been associated with better patient's outcome (Debruyne et al. 2018). The finding of this thesis showed no significant overall survival benefit between patients with high and low DOCK4 expression although there was a trend of association between high DOCK4 expression and better overall survival (OS). Nevertheless, there were some patients with low DOCK4 expression but had a longer duration of OS.

Knockdown of DOCK4 from both U251 and GBM1 glioblastoma cancer cells significantly reduced invasion in a spheroid assay using a monoculture model. However, under a co-culture model of glioblastoma cells with ECs cancer cell invasion significantly increased regardless of DOCK4 knockdown. Hence, unlike the results observed in monoculture model, in a co-culture model knocking down DOCK4 did not reduce cancer cell invasion in both U251 and GBM1 cancer cells. Further, the investigation as to whether the increased invasion of cancer cells in the presence of ECs was due to ECs or cancer cells themselves using both U251 and GBM1 cancer cells clearly demonstrated that those invading cells are indeed cancer cells.

Finally, the investigation of the effect of radiotherapy on cancer cell invasion showed that when U251 cancer cells were cultured with or without HUVEC in a spheroid assay and irradiated using 10Gy irradiation dose cancer cells became sensitive to ionising radiation in the presence of ECs. Further, there was no overall significant benefit from a combination therapy of DOCK4 knockdown and radiotherapy using U251 cancer cells and ECs co-culture in a spheroid assay. Although the same effect was seen using CT2A cancer cells co-cultured with ECs, the use of irradiation in a co-culture of GBM20 cancer cells and ECs increased cancer cell invasion. This shows that the effect of ionising radiation on cancer cell invasion is probably cell type dependent.

Chapter 6

Discussion

6.1 Introduction

Microvascular proliferation is a hallmark of GBM and plays an important role in the growth and progression of these brain tumours. Tumour blood vessels are inherently abnormal and this abnormality ranges from large vessel diameter, leakiness and chaotic organisation to glomeruloid structures (Carmeliet and Jain 2011). Aberrantly dilated, hyperpermeable and tortuous blood vessels in tumours are the result of an imbalance between proangiogenic and anti-angiogenic signaling factors leading to temporal and spatial blood flow and oxygenation heterogeneity within a tumour tissue (Goel et al. 2011). Vascular endothelial growth factor (VEGF), particularly VEGF-A (Roodink et al. 2006), is highly expressed in glioblastoma (Huang et al. 2005) and is primarily responsible for aberrant tumour angiogenesis through activation of its receptor VEGFR2 (Xu, Wu, and Zhu 2013). Despite its initial promise of increased progression-free survival the anti-VEGF drug Bevacizumab (Avastin) failed to improve the overall survival advantage of glioblastoma patients (Wick et al. 2017). The failure of Bevacizumab in the clinic for GBM clearly implicate the presence of VEGF independent alternative mechanisms in GBM neovascularisation (Kumar and Arbab 2013). Transdifferentiation has been described as one of the reasons for the unresponsive nature of GBM to anti-angiogenic drugs (Soda et al. 2011). Bergers and co-workers emphasised the presence of mature blood vessels in tumours that are refractory to Avastin, also known as Bevacizumab, treatment (Bergers et al. 2003 and Nagy et al. 2009).

Therefore, understanding the mechanisms of neovascularisation and nature of blood vessels in GBM is vital. Here, I investigated the cellular composition of the perivascular niche in glioblastoma using immunohistochemical staining of patient-derived GBM tissue samples and characterised the type and prevalence of blood vessel morphologies and their respective lumen sizes in GBM. The result of GBM blood vessel characterisation at baseline, following therapy in recurrent patients and in the experimental *in vivo* CT2A model showed an increased prevalence of abnormal morphologies and blood vessels with large diameter in recurrent and/or irradiated tumour tissue. Furthermore, global heterozygous deletion of Dock4 from stromal cells in mice reduced tumour blood vessel size when combined with radiotherapy. However, this was not reflected on the overall survival of mice. Furthermore, DOCK4 deletion from GBM cancer cells reduced invasion in a spheroid assays, however, when cancer cells were co-cultured with ECs the effect of DOCK4 deletion was not observed, implying that DOCK4 may not control cancer cells invasion within the PVN.

6.2 Characterisation of the glioblastoma vasculature

Glioblastoma is characterised by aberrant blood vessels, the diagnostic and prognostic value of which has not yet been fully exploited due to several limiting factors. Although most previous studies characterised GBM blood vessels using microvascular density (MVD), this approach had a number of drawbacks. For instance, researchers used different types of characterisation methods and cell markers (Korkolopoulou et al. 2002 and Chen et al. 2015). Furthermore, the inherent problems of intratumoural variation (Kalkan 2015; Schiffer et al. 2015 and Takeuchi et al. 2010) and inter-observer variability (Preusser et al. 2006) enormously affected its reliability. This current study also clearly showed that there is a significant difference between the MVD of primary and recurrent tumours as the number of blood vessels (MVD) dramatically decreased in recurrences.

Using positivity of GBM blood vessels for the stem cell marker Nestin (Suzuki et al. 2010) this study identified 5 different types of GBM blood vessel morphologies by immunohistochemistry staining: Single perivascular, Multi perivascular, Nestin +ve, Glomeruloid Nestin –ve and Glomeruloid Nestin +ve morphologies. While the first two morphologies are referred to as 'normal-like' as they are also found in normal brain tissue, the latter three morphologies are abnormal and only found in GBM tumour tissue samples. The analysis of blood vessel morphologies in primary GBM tumour tissue samples from both Leeds and Imperial College samples showed that patients present with heterogeneous blood vessel morphologies. This finding is in accordance with that of Chen et al who also reported 4 different types of microvascular patterns in primary GBM samples using immunofluorescence staining. In their study they identified microvascular sprouting (MS), vascular cluster (VC), vascular garland (VG) and glomeruloid vascular proliferation (GVP), and reported that the level of CD34, CD133 and Nestin expression was significantly higher in VG and GVP (Chen et al. 2017). Earlier, Briner et al had examined vascular patterns in 114 primary glioblastomas and had first described the presence of unevenly distributed 'glomeruloid/ garland-like/clustered vascular formations' and evenly distributed 'capillary-like vessels', the latter potentially arising at least partly from classic angiogenesis based on expression of the neoangiogenic markers CD105 and Id-1 (Birner et al. 2003). Patients with high proportion of aberrant blood vessels, particularly Nestin positive Glomeruloids showed a trend for poorer overall survival compared to patients with higher proportion of normal-like blood vessels although this was not statistically significant, presumably due to the relatively small number of patient samples.

Analysis of paired samples from two independent data sets from Leeds and Imperial College demonstrated that recurrent tumours had more aberrant blood vessel morphologies compared to primary tumours. Out of a total of 15 paired primary and recurrent GBM samples analysed 80% had a

decrease in normal-like tumour blood vessel morphologies, and an accompanied increase in abnormal morphologies upon recurrence. The identification of more normal-like blood vessels in primary tumours compared to recurrent tumours in this study showed that normal-like blood vessels may indicate an earlier stage of progression within the glioblastoma diagnosis. On the other hand, the increased abundance of Nestin positive and glomeruloid networks of aberrant blood vessel morphologies in recurrent tumours could be an indication of either progression or the effects of therapy.

A novel approach of this study is the use of Nestin positivity to define the boundary between cancer cells and stroma. One characteristic feature of the Nestin positive cells lining the glioblastoma blood vessel channels was their shape. Generally, unlike the spindle shaped ECs in normal brain vasculature the ECs lining the GBM vasculature were found to be round and plump just like some cancer cells. Hence, these cells were observed in some tumours and seemed to be 'replacement' of normal endothelial cells by cancer-like Nestin positive cells. Chang (Chang et al. 2000) and Tomaso (di Tomaso et al. 2005) and their co-workers had previously reported the presence of mosaic type of blood vessels in tumours where round and plump shaped cells lined tumour blood vessels. However, in this current study I found intact CD31 positivity in all blood vessels analysed in GBM from a total of 26 primary and 15 paired GBM patients and therefore it can be concluded that normal ECs line the GBM blood vessels. Although some GBM blood vessels stained positive for both stem cell marker Nestin and endothelial cell marker CD31 using Nestin/ CD31 double immunostaining, IF staining clearly showed that Nestin positive cells are distinct from CD31 positive cells although the Nestin positive cells were located in close association with the CD31 positive ECs.

The identity of Nestin positive cells forming or surrounding GBM blood vessels has been controversial and has led to different theories by which glioblastoma tumours derive their blood supply. The detection of CD31 and Nestin positive cells in GBM blood vessels prompted me to further investigate their identity and whether these cells could be cancer cells, astrocytes, immune cells or pericytes/SMCs. Some previous studies have indicated that vascular abnormalities in tumours could be due to other cells forming blood vessels. For instance, the work of Ricci-Vitiani and colleagues (Ricci-Vitiani et al. 2010) and Soda and co-workers (Soda et al. 2011) suggested that cancer stem cells transdifferentiated into ECs and form the blood vessel lumen lining of the glioblastoma. However, this raised controversy and other studies argued that ECs positivity for mutant IDH1 and EGFR amplification in GBM blood vessels is a truly rare event, and if there at all it accounts for less than 1% of the lining of blood vessels in samples (Rodriguez et al. 2012) as opposed to 60% GSCs to EC

transdifferentiation claimed by Ricci-Vitiani and colleagues (Ricci-Vitiani et al. 2010). Furthermore, El Halluin and co-workers also found that only a small fraction of ECs expressed EGFR amplification in GBM tissue samples and in *in vitro* experiment cancer cells only became positive for EC marker in the presence of co-culture of cancer cells and ECs (El Hallani et al. 2014). However, the analysis of De Pascalis and colleagues showed more CD31 positive ECs showing a EGFR/CEP7 amplification in recurrent tumours compared to primary GBM tumours (De Pascalis et al. 2018).

When stem cell marker SOX2 and OLIG2 staining was performed in this study none of the blood vessels in primary and recurrent GBM tumours stained positive, again arguing against nestin positive perivascular cells being cancer cell derived. The astrocytes and differentiated cancer cell marker GFAP, and immune cell markers CD45 and CD68 were also negative in the Nestin positive cells. However, using IHC, 68.2% of these Nestin positive cells were positive for pericyte/SMCs markers α-SMA and PDGFRβ. This was confirmed using IF showing that Nestin positive cells co-expressed α-SMA and PDGFRβ markers but not cancer cell, astrocyte and immune cell markers. Jain described these perivascular pericytes as morphologically abnormal and have a weak contact with both ECs and the matrix (Jain 2003). Bergers and Benjamin associated increased tumour blood vessel lumen size with increased proliferation of blood vessel wall (Bergers and Benjamin 2003) and lack of pericytes consequently leading to vessel enlargement, leakage, and tumour metastasis (Carmeliet and Jain 2011). However, large calibre blood vessels identified in this study by means of nestin positivity were mature blood vessels lined by PDGFRβ and α-SMA perivascular cells.

In future studies it will be interesting to find out whether the α-SMA/Nestin positive perivascular cells are resident stem cells or bone-marrow derived mesenchymal stem cells. In an *in vivo* experiment using Nestin-GFP transgenic mice Klein and colleagues showed that Nestin positive cells around melanoma tumour blood vessels originated from resident cells, but not from the bone-marrow (Klein et al. 2014). On the other hand, in an *in vitro* study, bone-marrow derived human mesenchymal stem cells (hMSCs) which had been cultured in tumour conditioned medium became positive for Nestin, α-SMA, NG2, CD151 and desmin but not for vWF and smooth myosin indicating that they are pericyte-like cells but not ECs or SMCs (Birnbaum et al. 2011). Furthermore, pericytes themselves have a mesenchymal stem cell (MSC) potential (Appaix et al. 2014).

This study showed that Nestin/α-SMA positive aberrant blood vessels are commonly located near areas of necrosis and near regions of tumour hypoxia compared to the peripheral region of a tumour tissue where more of normal-like blood vessel morphologies are commonly located. This probably

implies that hypoxia could potentially be a contributing factor to the formation of these aberrant blood vessels in GBM. In recurrent tumours Nestin positive and glomeruloid Nestin positive blood vessels supported lower hypoxia levels compared to blood vessels with normal-like morphology and/or occluded blood vessels which were associated with the highest hypoxia levels. Using a glioblastoma xenograft ear model Sundberg found that glomeruloid blood vessels form at the very late stage of tumour development following necrosis and hypoxia (Sundberg et al. 2001). Importantly, the presence of blood vessels with large lumen size and Nestin positive aberrant morphologies in recurrent GBM could be a consequence of radiotherapy and/or chemotherapy normally administered post-surgery. Radiotherapy causes destruction of immature blood vessels leading to hypoxia (Barker et al. 2015). Hence, it is highly likely that the increased changes in blood vessel morphology, Nestin positivity and functionality in GBM following recurrence could represent a therapy induced phenotype.

6.3 The role of DOCK4 in blood vessel growth and tumour progression in GBM

Tumour blood vessels are inherently aberrant and have a larger lumen size. Mostly, uneven and abnormal blood vessel lumen diameter follows compression of immature blood vessels by tumour mass (Jain 2003) and normalising them through the restoration of the pro- and anti-angiogenic cytokines can make solid tumours more sensitive to both chemo- and radiotherapy (Jain 2003 and Carmeliet and Jain 2011). Following establishment and characterisation of the experimental CT2A model I investigated whether Dock4 deletion would normalise the aberrant tumour blood vessels using mice with Dock4 heterozygous deletion, as homozygous Dock4 deletion is embryonically lethal (Abraham et al. 2015). The CT2A tumour model appeared to recapitulate the invasive and co-optive nature of patient GBM than the GL261 tumour model. Furthermore, a previous study also showed that just like patient-derived GBM samples murine glioblastoma tumour model CT2A express a stem cell markers nestin, CD133, OCT4 and is proliferative and invasive both in *in vitro* and *in vivo* (Binello et al. 2012). DOCK4 is a GEF for a small GTPase Rac1 which plays an important role in sprouting angiogenesis (Abraham et al. 2015). Nohata and co-workers demonstrated the importance of Rac1 for angiogenesis and blood vessel integrity in postnatal vascular network and vessel sprouting in retinal angiogenesis (Nohata et al. 2016). Our lab also showed that Dock4 regulates blood vessel lumen size in EO771 breast cancer brain met model when injected intracranially into Dock4 heterozygous mice (Abraham et al. 2015). Here, the effects of heterozygous Dock4 deletion were assessed in the presence or absence of irradiation.

The main effect of ionising radiation on tumour vasculature includes increased EC permeability, detachment from basement membrane and apoptosis (Heckmann et al. 1998). For instance, the use of a total dose of 40Gy (8Gy/ fraction) increased BBB permeability 5 days following irradiation in rats orthotopically injected with C6 glioma (Zawaski et al. 2012). Radiation treatment has acute, subacute or late effects on brain tissue with major injuries to blood vessels characterised by vasodilation, oedema and vascular lesion, respectively (Walker et al. 2014). Early effects of radiation therapy include DNA damage, recruitment of inflammatory cells and death of ECs, while late effects include collagen deposition (fibrosis), hypoxia and atherosclerosis (Barker et al. 2015). Hence, radiation appears to have different effects on the tumour microenvironment at different time points. In this study using two different doses (10Gy or 15Gy) and sources (SARRP or X-RAD) radiation significantly decreased tumour growth with a better response at 10Gy delivered by SARRP leading to tumour regression followed by regrowth, thus mimicking patient GBM response to radiotherapy. In order to assess the effect of global heterozygous Dock4 deletion on CT2A blood vessels in the presence of irradiation I performed analysis at early (3 days) and late (over 21 days on presentation of neurological symptoms) time points post irradiation. Early analysis showed a trend of decreased lumenisation with irradiation, which was further enhanced by Dock4 heterozygous deletion leading to a significant decrease in vessel size with combination of radiotherapy and DOCK4 reduction. At later time point (21 days post irradiation) there was a significant increase in blood vessel size which was reversed by heterozygous Dock4 deletion.

Immunohistochemical staining of early CT2A tumour samples showed increased expression of apoptosis marker Caspase-3, DNA double-strand break marker γH2Ax and immune cell marker F4/80 following irradiation. The finding of high expression of F4/80, although not quantified, agrees with previous findings. Morganti and co-workers showed that a single fraction of 10Gy irradiation dose increased the infiltration of $F4/80^{+}$ peripheral macrophages into the brain without affecting the integrity of the BBB (Morganti et al. 2014). Furthermore, in an orthotopic *in vivo* experiment using GBM cell line and murine glioblastoma cells, Kioi and co-workers found an increased recruitment of bone marrow-derived cells (BMDCs) following irradiation through secretion of HIF-1 (Kioi et al. 2010). Overall, radiotherapy

increases M2-like macrophages in GBM which are more radioresistant than M1-like macrophages and the non-polarised M0 macrophages (Leblond et al. 2017). Hence, secretes of macrophages and the angiogenic factors (Martin 2013) could be involved in late response to irradiation of blood vessel growth.

Previous studies used radiotherapy in combination with other treatments such as anti-angiogenic and chemotherapy to normalise blood vessels through reduction of hyperpermeability, increased pericyte coverage, normalised basement membrane and reduced hypoxia which eventually contributed to efficacy of therapy and improved patient survival (Goel et al. 2011). In future studies it will be interesting to determine the effects of Dock4 deletion on pericyte coverage, permeability, basement membrane characteristics and tumour hypoxia. As seen in the recurrent GBM patient tumour tissue samples, preliminary analysis showed that there was increased α-SMA expression in irradiated CT2A tumours. This may suggest that these cells play an important role in the progression of GBM post radiotherapy. Hosono and co-workers who reported desmin positive pericytes in rat RG2 glioma model using immunohistochemical staining showed that pericytes contribute to increased tumour angiogenesis through formation of basement membrane (Hosono et al. 2017).

6.4. The role of DOCK4 in glioblastoma cancer cell invasion

The current standard of therapy in glioblastoma failed to stop the infiltrative cancer stem cells which are the underlying cause of tumour recurrence, resistance and poor patients' outcome. Hence, targeting the molecular mechanisms behind the advancement of such cells is crucial. Invading glioblastoma cells highly express Rac1 and Cdc42 at the leading edge (Hirata et al. 2012), and while Rac1 regulates lamellipodia, Cdc42 regulates filopodia (Etienne-Manneville and Hall 2002). DOCK4 is a GEF which transforms a small Rho GTPase molecule Rac1 from inactive state to active state. In breast cancer cell line MDA-MB-231 the C-terminal proline-rich region of DOCK4 interacts with SH3YL1 region of Rac1 and increase cancer cell migration (Kobayashi et al. 2014). Westbrook et al. reported a higher DOCK4 expression in bone homing MDA-MB-231 compared to parental control and high DOCK4 was found to be a risk factor for bone metastasis (Westbrook et al. 2018). Furthermore, Yu and colleagues also showed that

high DOCK4 in lung ADC increases tumour cell extravasation and metastasis through TGF-β/Smad signaling pathway (Yu et al. 2015).

Using immunohistochemical staining of 12 primary patient derived GBM samples for DOCK4 this study found a heterogeneous level of DOCK4 expression in patient-derived GBM tumour tissue samples. High DOCK4 expression was detected along blood vessels, particularly along the nestin positive and glomeruloid aberrant blood vessel morphologies. Although there was no significant correlation between patients' OS and the level of DOCK4 expression from this small sample size it was observed that there was a trend of association between high DOCK4 expression and better patients' outcome. This is in agreement with the findings of Debruyne and colleagues who showed high Dock4 expression in GBM with better patients' outcome (Debruyne et al. 2018). The analysis of TCGA data also showed that patients with high DOCK expression had a trend of better outcome compared to those with low DOCK4 expression.

Therefore, in order to understand the role of DOCK4 in cancer cell invasion U251 cell line, which fundamentally lacks heterogeneity and drug resistance (Patrizii et al. 2018) and patient derived GBM1 were used. Knockdown of DOCK4 protein from these glioblastoma cancer cells initially reduced cancer cell invasion in a spheroid assays on Day 3 and Day 8 post collagen addition, respectively. Nonetheless, this difference gradually disappeared at a later time points. Then, using a co-culture model which better recapitulates the tumour microenvironment in patients I observed a significantly increased invasion of cancer cells in the presence of ECs in both U251 and GBM1. Calabrese and co-workers showed that endothelial cells play an important role in the tumour environment. For instance, brain tumour ECs serve as self-renewal and maintenance of glioma stem cells and their depletion stopped tumour growth in in vivo experiment using mice (Calabrese et al. 2007).

Unsurprisingly, under such co-culture model knockdown of DOCK4 from both U251 and GBM1 failed to decrease cancer cell invasion in the presence of ECs. The fact that deleting DOCK4 from cancer cells in this experiment failed to decrease the overall cancer cell invasion in the presence of ECs in co-culture spheroid assays probably indicate that DOCK4 plays a cancer suppressor role. In a recent study, silencing DOCK4 from differentiated glioblastoma cancer cells using siRNA showed suppression of the nuclear translocation of β-catenin and

consequent tumour growth. Subsequently, over expression of DOCK4 increased nuclear translocation of β-catenin and decreased GBM cancer cell stemness and proliferation in differentiated GBM cancer cells implying the importance of DOCK4 in cancer cells (Debruyne et al. 2018). This shows that DOCK4 plays contradicting roles in different cell types. Therefore, ECs in co-culture assays play an important role in tumour growth and aggressiveness. When Yan et al co-cultured U251 cells with HUVEC the level of CD133 positivity and invasiveness increased in a co-culture model compared to U251 cells only (Yan et al. 2014).

Radiotherapy induces DNA double strand breaks and stops tumour growth, however, the development of radioresistance is very common (Lim et al. 2018). Both in vitro and in vivo studies showed that ionising radiation increase VEGF secretion by cancer cells which in turn leads to invasion of cancer cells and radioresistance (Scaringi, Enrici, and Minniti 2013). Borovski et al showed that the tumour ECs play an important role in maintaining cancer cell proliferation and protection of such cancer cells from chemotherapy and radiotherapy probably through regulation of MGMT gene (Borovski et al. 2013). Here, in a co-culture of cancer cells and HUVEC a single dose of 10Gy ionising radiation significantly reduced invasion of U251 cancer cells into the surrounding collagen matrix on Day 6, implying that the presence of ECs probably made U251 cancer cells susceptible to radiation. However, when murine model CT2A and patient-derived GBM cancer cells were irradiated in the presence of ECs their invasion increased showing variation in cell types. Although combination therapy using irradiation and Rac1 inhibition reduced radioresistance in breast cancer cell lines MCF-7 and T47D in *in vitro* assay (Hein et al. 2016) such combination therapy failed to reduce invasion in glioblastoma cell line U251 when DOCK4 deletion and a single dose of 10Gy ionising radiation were concurrently used.

6.5 Concluding remarks

Characterisation of patient derived GBM samples using Nestin/CD31 double immunostaining showed that GBM patients present with heterogenous blood vessel morphologies as well as blood vessel lumen size. There is a strong indication that high nestin positivity of GBM blood vessels, particularly glomeruloid morphology, is associated with poor patients' outcome. Analysis of these nestin positive blood vessels showed that they are less likely to be cancer cells as previously thought but the fact that they are positive for pericyte and SMC markers

indicate that stroma cells could be their ancestral origin. Furthermore, these nestin positivity significantly increased in recurrent tumour samples which are more hypoxic than primary tumours implying that hypoxia could be a factor for the formation of such aberrant blood vessels. In addition to nestin, different patient derived GBM tumours also expressed DOCK4 and there is a strong correlation between the level of DOCK4 and Nestin expression. Overall, this study concludes that there is an inverse correlation between DOCK4 between expression of hypoxia and Dock4 in most GBM patient samples and low DOCK4 expression was associated with a poor overall survival.

DOCK4, a GEF for Rac1, regulates blood vessel morphogenesis and lumen size through actin cytoskeleton (Abraham et al. 2015). An orthotopic implantation of CT2A cancer cells in mice with Dock4 heterozygous global deletion showed a reduced blood vessel lumen size in Dock4 heterozygous compared to control mice. When tumour blood vessel lumen size was analysed following irradiation the blood vessel lumen size was increased in irradiated WT mice compared to control mice. However, a combination of radiotherapy and Dock4 heterozygous deletion reduced such large blood vessels implying normalisation of glioblastoma blood vessels. Nonetheless, such combination did not reflect on the overall survival of mice.

Using a spheroid assay I demonstrated that cancer cell invasion into the surrounding collagen matrix was reduced in both U251 and GBM1 cancer cells. However, when such cancer cells were co-cultured with endothelial cells there was no significant difference between DOCK4 knockdown and control glioblastoma cancer cells. Furthermore, while radiotherapy reduced cancer cell invasion in a co-culture of U251 cancer cells and HUVEC there was no significant difference between irradiated and control U251 cells in the absence of ECs. However, a combination of DOCK4 knockout and radiotherapy did not reduce tumour invasion at least in U251 cancer cells in a spheroid assay. To sum up, the analysis of both patient GBM tissue samples and *in vivo* experiment showed increased tumour blood vessel lumen size and SMA positivity in recurrent/irradiated samples. The fact that deletion of DOCK4 from stroma and cancer cells increased tumour growth and invasion, respectively, might imply that DOCK4 molecule could rather play an important tumour suppressor role in GBM and may not be directly responsible for the increased aberrant blood vessels in GBM.

Appendices

Appendix 1

ID	Patient		GBM Grade	Location	1st operation date	Recurre-nce date	Treatment			MGMT Methylation	1DH1/2 mutation	Molecular subtype	Date of death	OS
	Gender	Age					Surgery	RT	Chemotherapy post surgery					
GBM 13	Female	79	GBM IV	Left frontal lobe	13.10.12	6.1.14	Yes	Yes 2012		Not detected	No	Proneural	31.8.14	22
GBM 14	Male	58	Giant cell GBM IV	Right cerebral lobe	29.3.11	28.1.13	Yes	Yes 2011	Temozolomide	Moderate	No	Proneural (Mesenchymal)	16.5.14	39
GBM 16	Female	63	GBM IV	Left posterior parietal lobe	4.4.13		Yes	post surgery	n/a		No		2.7.13	3
GBM 20	Male	50	GBM IV	Right temporal region	28.8.12	22.7.13	Yes	Sep -Nov 2012	Temozolomide and IMA950 post primary surgery. PCV post second surgery	Not detected	No	Proneural (Mesenchymal)	14.1.14	17
GBM 21	Male	72	GBM IV	Left temporal lobe	19.08.13		Yes	Post surgery		Methylated	No		3.2.14	5
GBM 25	Female	38	GBM IV (60%) arising in a background of diffuse astrocytoma.	Left frontal craniotomy	30.9.13	17.7.18	Yes	Post surgery	Temozolamide	Methylated	Detected		25.10.18	58
GBM26	Male	63	GBM IV	Right temporal craniotomy	21.10.13		Yes	Post surgery	Temozolamide	Not detected	No		7.4.14	5.5
GBM 30	Female	50	GBM IV	Right frontal lobe	3.2.14	15.1.16	Yes	Post surgery	Temozolamide, PCV and Avastin	Not detected	No	Classical	20.4.16	26
GBM 33	Male	42	GBM IV	Right hemisphere	25.4.14		Yes		Temozolamide		No		4.1.15	9
GBM 36	Male	64	GBM IV	Left parieto-occipital lobe	2.6.14		Yes	Post surgery	Temozolomide + Lomustine		No		7.12.17	42
GBM 37	Female	61	GBM IV	Right frontal lobe	6.6.14	13.5.17/ 14.8.17/ 20.4.18	Yes	Post surgery	Temozolamide		No		12.8.18	49
GBM 39	Male	47	GBM IV	Right frontal lobe	8.7.14		Yes	post surgery	Temozolamide	Not detected	No		20.1.15	6
GBM 46	Male	66	GBM IV	Right parietal lobe	6.3.15		Yes	Post surgery			No		11.1.16	10
GBM47	Male	52	GBM IV	Left frontal lobe	13.3.15		Yes	Post surgery	Temozolamide		No		2.12.16	21
GBM52	Male	56	GBM IV	Right occipital lobe	15.5.15		Yes	Post surgery	Temozolamide		No	Classical	21.2.16	9
GBM63	Male	57	GBM IV	Left Parietal lobe	11.1.16	11.11.16	Yes	Post surgery	Temozolamide, PCV, and Avastin		No	Classical	2.4.17	15

Leeds Teaching Hospitals NHS Trust clinical data

GBM tissue samples were collected from Leeds Teaching Hospital (LTH) theatre through a research nurse from patients who were admitted to Leeds General Infirmary Hospital for brain tumour surgery and consented for their samples to be used for research. In addition, ethical approval was obtained from the University of Leeds Ethical Committee in order to use patient samples and their clinical data in anonymized way. The samples were fixed in 4% PFA and paraffin embedded following collection. Out of a total of 64 patients diagnosed with GBM over a period of 5 years 52 FFPE blocks were available for analysis. After excluding samples with inadequate amount of material 21 FFPE blocks (16 primary and 5 recurrent) were available and presented in this table with their clinical data.

Appendix 2

Imperial College GBM patients' data						
Laboratory nomenclature	**Gender**	**Age**	**GBM Grade**	**Surgery**	**Tumour Location**	
GBM1	F	53	GBM IV	Debulking	Right parietal	Right parietal
GBM2	F	59	GBM IV	Debulking	Right frontal	Right frontal
GBM3	M	52	GBM IV	Debulking	Right temporo-parietal	Right temporo-parietal
GBM4	F	43	GBM IV	Biopsy	Right parietal	Right parietal
GBM5	M	48	GBM IV	Debulking	Left frontal	Left frontal
GBM6	M	47	GBM IV	debulking	Left parietal	Left frontal
GBM7	F	70	GBM IV	Debulking	Right fronto-temporal	Right fronto-temporal
GBM8	M	50	GBM IV	Debulking	Right parietal	Right parietal
GBM9	F	49	GBM IV	Debulking	Right frontal	Right frontal
GBM10	F	38	GBM IV	Debulking	Left parietal	Left parietal

Imperial College Healthcare NHS Trust clinical data

Imperial College GBM FFPE blocks were obtained following application to Brain UK. Imperial College patient data was incomplete hence analysis of overall survival was not possible.

Appendix 3

Leeds samples			Imperial samples		
Normal brain/ GBM	**No. of boxes analysed**	**No. of blood vessels characterised**	**GBM**	**No. of boxes**	**No. of blood vessels characterised**
Normal brain	4	147	GBM1	7	183
GBM13P	16	670	GBM1R	8	71
GBM13R	9	61	GBM2	10	252
GBM14P	10	150	GBM2R	9	160
GBM14R	9	43	GBM3	8	216
GBM20P	10	152	GBM3R	10	139
GBM20R	9	46	GBM4	8	145
GBM30P	3	91	GBM4R	9	112
GBM30R	5	32	GBM5	10	761
GBM63P	2	34	GBM5R	7	221
GBM63R	2	118	GBM6	8	144
GBM16	9	177	GBM6R	6	39
GBM21	11	73	GBM7	8	150
GBM25	13	324	GBM7R	8	92
GBM26	6	151	GBM8	9	349
GBM33	6	89	GBM8R	10	87
GBM36	9	255	GBM9	9	282
GBM37	11	129	GBM9R	8	151
GBM39	13	254	GBM10	8	131
GBM46	2	28	GBM10R	8	126
GBM47	7	131			
GBM52	7	120			
Total (Excluding normal brain)	**169**	**3128**	**Total**	**168**	**3811**

Total number of areas and blood vessels scored in Leeds and Imperial patient samples

Table shows number of 1mm^2 areas (boxes) analysed per patient sample. Boxes were placed on viable parts of the GBM tissue samples excluding necrotic zones.

Appendix 4

	WT control	Dock4 Het control	WT 15Gy	Dock4 Het 15Gy
No. of mice injected	4	4	5	4
No. of mice with symptoms	3	4	0	0
No. of mice with gross lesion	3	4	2	1
Microscopic lesion	3	4	3	3
No. of tumours used for IHC	2	3	3	3
No. of areas analysed	4	5	4	4

Number of mice, symptoms, lesions, staining and areas examined in the RAD-irradiator experiment

A total of 17 mice were intracranially injected $1x10^5$ CT2A-Luc cancer cells into the striatum of right brain hemisphere. Following injection mice were monitored for tumour growth using IVIS imaging and randomised into four treatment groups as shown in the table above. A total of 15Gy ionising radiation was delivered using RAD X-Ray irradiator for 3 consecutive days starting from Day 9–11 post tumour implantation. Mice were taken down on Day 21 post tumour implantation by terminal perfusion upon development of neurological symptoms in one mouse. Tumour tissue samples were collected, fixed in 4% PFA, paraffin embedded, sectioned at 4 μm and stained using EC marker CD31 antibody, and counterstained using haematoxylin. The stained tissue slides were scanned and 0.5mm x 0.5mm boxes were placed over different tumour tissue regions and blood vessels lumen size ≥10 μm were analysed using ImageScope.

Appendix 5

	Normal brain	WT control	Dock4 het control	WT 10Gy	Dock4 het 10Gy
No. of mice	1	3	3	3	3
No. of tumour samples available	1	2	2	3	3
No. of levels analysed	2	5	6	8	8
No. of vessels with lumen (≧10) μm	4	36	65	23	14

Number of mice, levels and vessels analysed in early irradiation effects analysis

A total of 52 mice intracranially injected $1x10^5$ CT2A-Luc cancer cells into the striatum of right brain hemisphere. Mice were monitored for tumour growth and randomised into 4 different treatment groups based on their IVIS reading signal the day before radiotherapy. Mice which were in the treatment group received 2 consecutive doses of 5Gy ionising radiation using SARRP on Day 7 and Day 8. In order to see the early effect of radiation on tumour vasculature 3 mice/group were taken down by terminal perfusion on Day 11 following tumour implantation. One WT control and one Dock4 Het control did not develop tumour and both were excluded from analysis. However, one normal brain was included for reference. Tumour tissue samples were collected, fixed in 4% PFA, paraffin embedded, sectioned at 4 μm thickness at different levels and stained using EC marker CD31 antibody, and counterstained using haematoxylin. The stained tissue slides were scanned and a 0.5mm x 0.5mm boxes were placed over different tumour tissue regions and blood vessels lumen size ≥10 μm were analysed using ImageScope.

Appendix 6

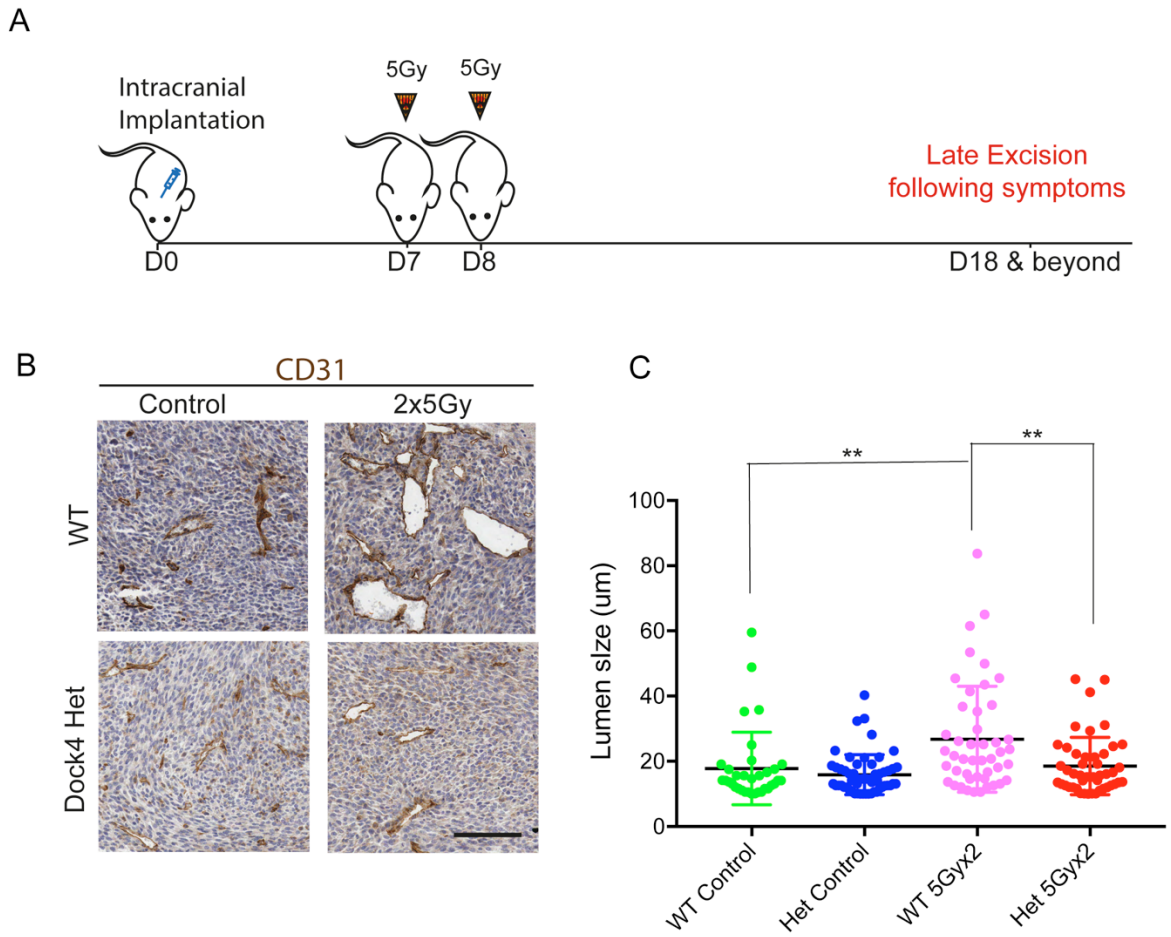

Analysis of CT2A samples at late timepoints following irradiation (performed by A. Widyadari)

(A) Schematic diagram depicting CT2A tumour implantation, irradiation and late excision upon development of neurological symptoms. Mice were taken down from D18 onwards by terminal perfusion.

(B) CT2A tumour tissue samples were paraffin embedded, sectioned and stained using EC marker CD31. Representative images from different groups show differences in blood vessel lumen size. Scale bar 100, μm.

(C) Quantification of lumen size. Boxes (0.5x0.5mm^2) were placed on scanned CT2A tumour tissue samples and blood vessels with lumens were analysed using ImageScope. N= number of blood vessels with detectable lumen (≥10 μm); WT control, 34; Dock4 het control, 57; WT irradiated, 46; Dock4 het irradiated, 46). ** $p<0.01$ and ** $p<0.001$. D, Day

Appendix 7

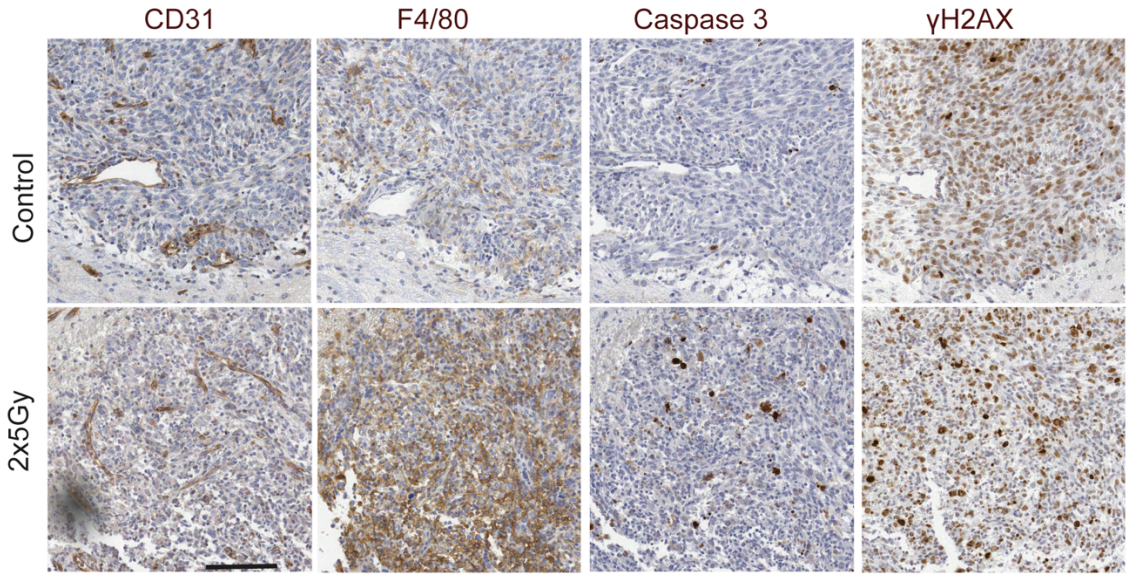

Staining of irradiated tumour samples for markers of immune cells, apoptosis and DNA damage

The images show a marked increase in F4/80 immune cells following irradiation, and a modest increase in apoptosis was also observed through staining for Caspase 3. The γH2AX staining show the expected effects of irradiation on DNA damage 3 days following irradiation. Mice received irradiation using SARRP 7 days after intracranial injection of CT2A cells as described in Figure 4.8.

Appendix 8

A

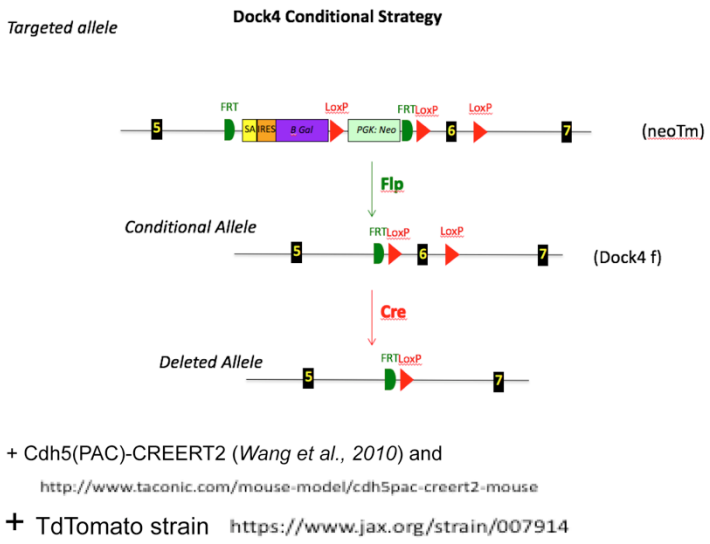

+ Cdh5(PAC)-CREERT2 (*Wang et al., 2010*) and
http://www.taconic.com/mouse-model/cdh5pac-creert2-mouse

+ TdTomato strain https://www.jax.org/strain/007914

B

Ear biopsy genotyping result					
Mouse ID	Dock4f/f	Dock4 WT	TdTomato	TdTomato WT	Cre
153	+	-	+	+	+
154	+	-	+	+	+
155	+	-	+	+	-
156	+	-	+	+	-
157	+	-	+	+	+
158	+	-	+	+	+
159	+	-	+	+	-
160	+	-	+	+	+

Conditional Dock4 knockout model generated by Ozgene (A) and typical genotyping (B)

(A) Dock4 conditional knockout model generated by Ozgene. Dock4f/f mice were crossed with VE-cadERT2-CreTd tomato gene carrying mice. In order to confirm how well Cre delete the stop codon and allow Td to be expressed iVE-Cre;Rosa26Td mice were first injected tamoxifen intraperitoneally followed by intracranial injection of CT2A tumours. Upon development of neurological symptoms mice were taken down and tumour tissue samples were stained using RFP antibody which appeared red in the presence of Cre gene as shown in Figure 4.13.

Both Cre and FLP recombinase enzymes were used in order to recognise and delete Dock4 gene specifically from ECs with the help of LoxP and FRT sites, respectively. Litters with TdVEcadCre^{+};Dock4f/f genes or control litter mates with TdVEcadCre^{-};Dock4f/f genotype were injected tamoxifen intraperitoneally before intracranial injection of CT2A cancer cells.

(B) Typical example of genotyping of ear biopsies performed by Transnetyx.

Appendix 9

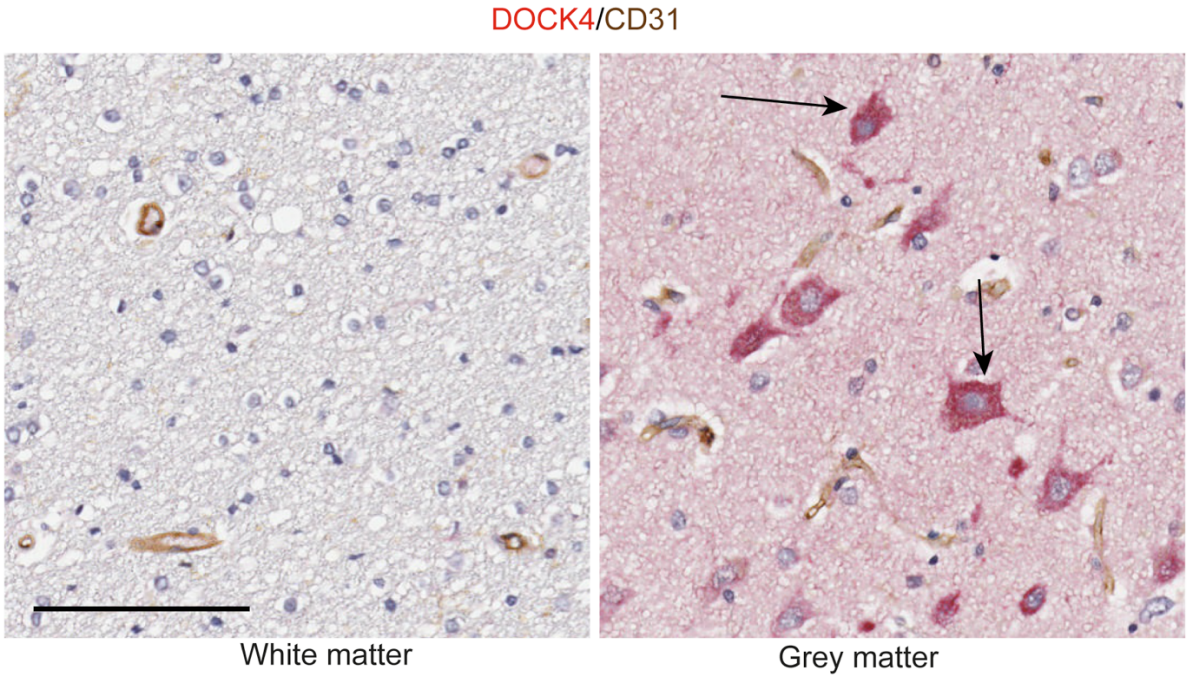

DOCK4 expression level of white matter and grey matter in a normal brain

Normal brain tissue sample was formalin fixed, paraffin embedded and sectioned at 4 µm. Double immunostaining of DOCK4 and CD31 primary antibodies on normal brain tissue were followed by secondary antibodies and counterstained using DAB. Low or no DOCK4 expression in white matter (left) and increased DOCK4 positivity in neurons (arrow) in grey matter (right). Scale bar, 100 µm.

Appendix 10

HPA Scoring Method		
Staining Intensity	**Fraction of Stained Cells**	**Combination of the Two**
Negative	(-)	Not detected
	<25% weak	
Weak	25-75% or 75% low	Low
	<25% moderate	
Moderate	25-75% or 75% medium	Medium
	<25% strong	
Strong	25-75% or 75% high	High

Quantification of protein expression level by different cells was scored based on The Human Protein Atlas (HPA) method

For quantification of the level of protein expression in different cell types used in this thesis the combination of both Staining Intensity (Appendix 11) and Fraction of Stained Cells were used based on the Human Protein Atlas (HPA) scoring method.

Appendix 11

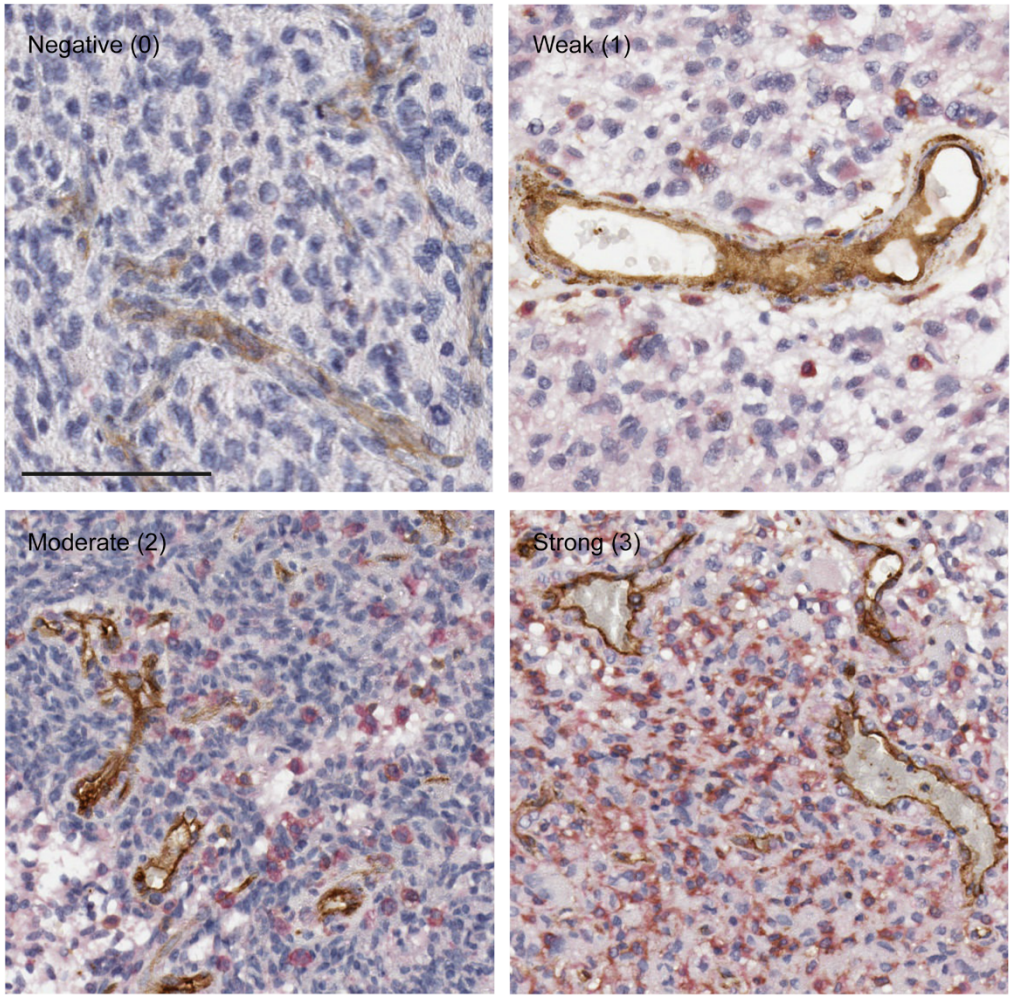

Scoring DOCK4 expression level in patient GBM samples

GBM tissues samples were paraffin embedded, sectioned at 4 μm and stained using DOCK4/CD31 primary antibodies followed by secondary antibodies and counterstained using DAB. GBM patient samples were classified into four groups based on their DOCK4 expression intensity and fraction of stained cells (Appendix 10): 'negative' DOCK4 expression (0); 'weak' expression (1), 'moderate' expression (2) and 'strong' expression (3). Scale bar, 100 μm.

Appendix 12

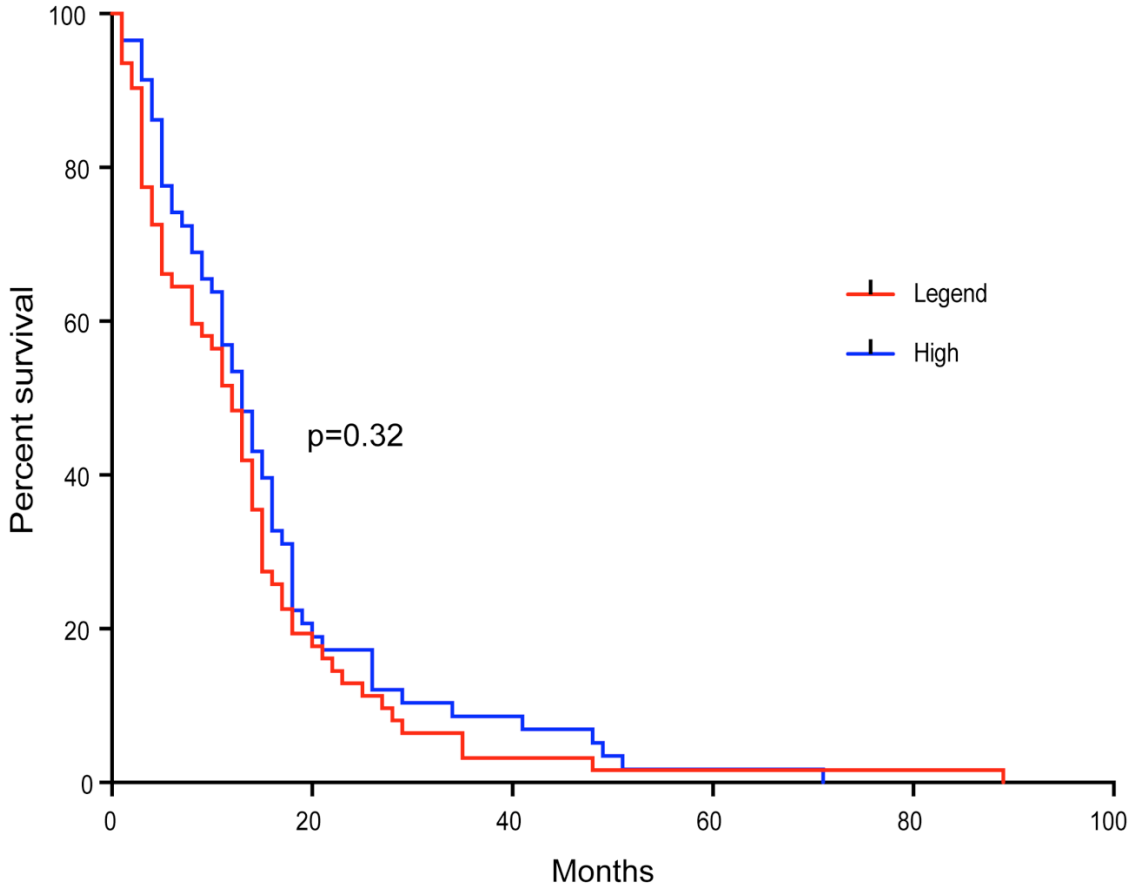

High and low DOCK4 mRNA expression in patient glioblastoma samples and their overall survival

A total of 122 patient glioblastoma samples from The Cancer Genome Atlas (TCGA) was analysed for DOCK high and low expression using fragments per kilobase of transcript per million reads (FPKM) mRNA. Using an average cut-off 5.9 FPKM as high and low DOCK4 mRNA expression there was no significant difference in patient's overall survival between the two groups. N = Number of patients ± SD (Low, 56 and High, 66 samples).

Appendix 13

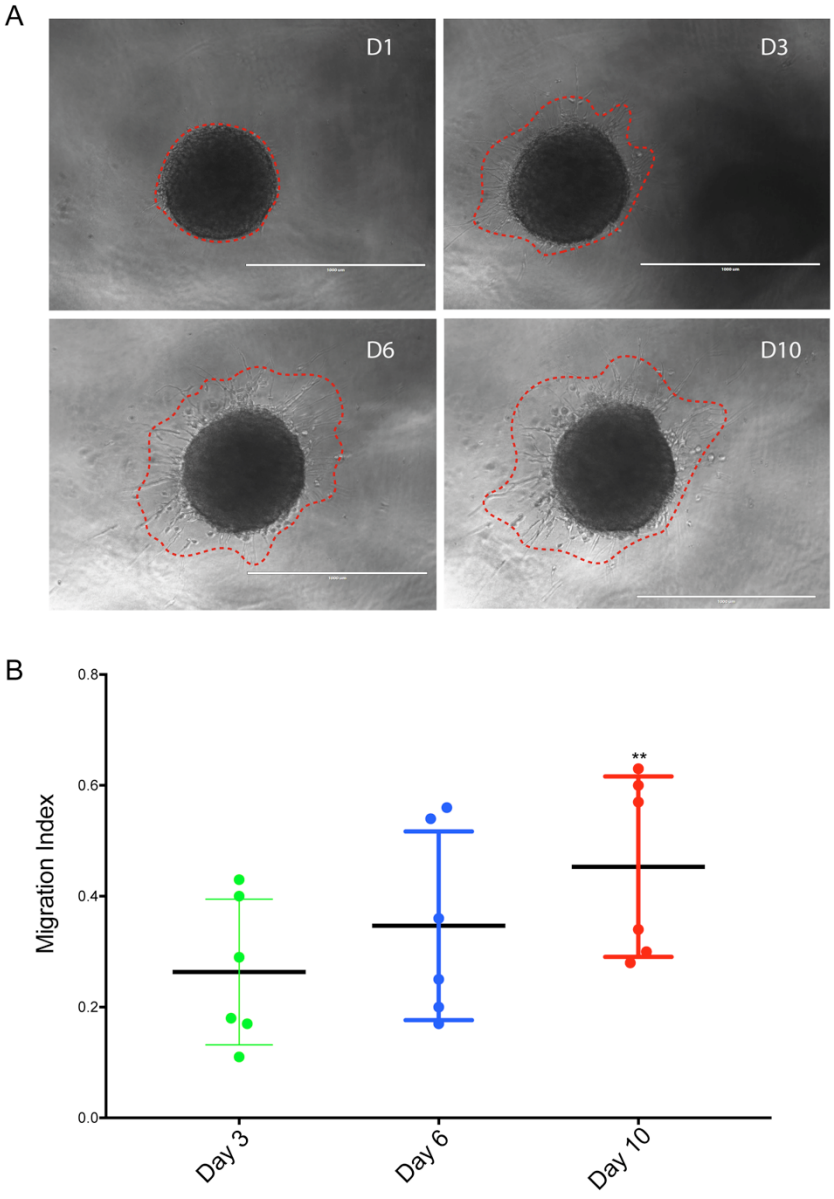

Optimisation of patient derived GBM cancer cells in collagen based spheroid assay

GBM1 cancer cells ($1x10^3$) were seeded in a low adherent and round bottom 96-well plates in 200 µl neurobasal medium. After 5 days when a sphere was formed, supernatants were removed and 100µl collagen was added per well at 6.8 : 1 ratio of collagen to neurobasal medium and neutralised by 0.7% 1M NaOH. Finally, 100 µl of neurobasal medium was added to each well and the plate was incubated at 37^o and 5% CO_2. Cancer cell invasion was measured at Day 0, 3, 6 and 10 following the addition of collagen using EVOS at 4x magnification. N=Number of wells = 6 wells.

Appendix 14

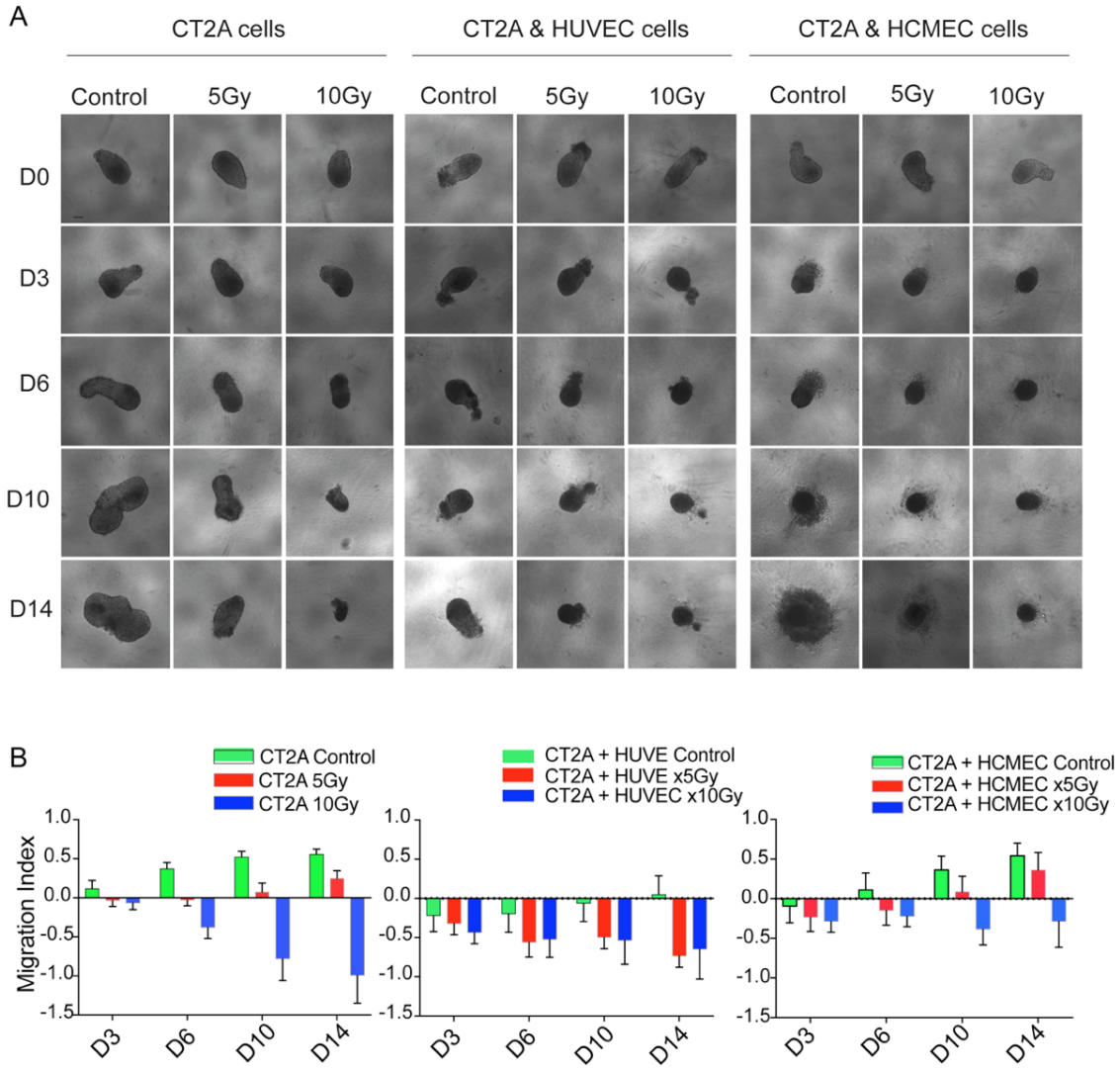
A
CT2A cells
CT2A & HUVEC cells
CT2A & HCMEC cells
Control
5Gy
10Gy
D0
D3
D6
D10
D14
B
CT2A Control
CT2A 5Gy
CT2A 10Gy
CT2A + HUVE Control
CT2A + HUVE x5Gy
CT2A + HUVEC x10Gy
CT2A + HCMEC Control
CT2A + HCMEC x5Gy
CT2A + HCMEC x10Gy
Migration Index
1.0
0.5
0.0
-0.5
-1.0
-1.5
D3
D6
D10
D14

Effect of ionising radiation on CT2A cancer cell invasion in a spheroid assay in the presence and absence of endothelial cells

CT2A cancer cells ($2x10^3$), or $2x10^3$ CT2A cancer cells mixed with $2x10^3$ HUVEC or HCMEC were seeded in a low adherent and round bottom 96-well plates in a 1:1 ratio of 100 μl neurobasal medium and 100μl HLVEC medium. After 5 days when a sphere was formed, supernatants were removed and 100μl collagen was added per well at 6.8 : 1 ratio of collagen to medium (equal mix of neurobasal and HLVEC medium), and neutralised by 0.7% 1M NaOH. Finally, 100 μl of the mix medium was added to each well and the plate was incubated at 37^o and 5% CO_2. In a treatment groups either 5Gy or 10Gy irradiation doses were applied at a rate of 2Gy/minute using RAD irradiator. Cancer cell invasion was measured at Day 0, 3, 6, 10 and 14 following the addition of collagen using EVOS at 4x magnification. N=Number of wells (Control CT2A, 15; Control CT2A + HUVEC, 14; Control CT2A + HCMEC, 12; 5Gy & 10Gy CT2A, 16; 5Gy & 10Gy CT2A + UVEC, 8; and 5Gy & 10Gy CT2A + HCMEC, 8 wells). D=Day; HCMEC, Human Cerebral Microvascular Endothelial Cells

(A) Images depict spheroids formed by cancer cells or their co-culture with HUVEC or HCMEC and their invasion into the surrounding collagen matrix .

(B) Bar chart shows invasion area of CT2A cancer cells in the presence and absence of HUVEC or HCMEC.

Appendix 15

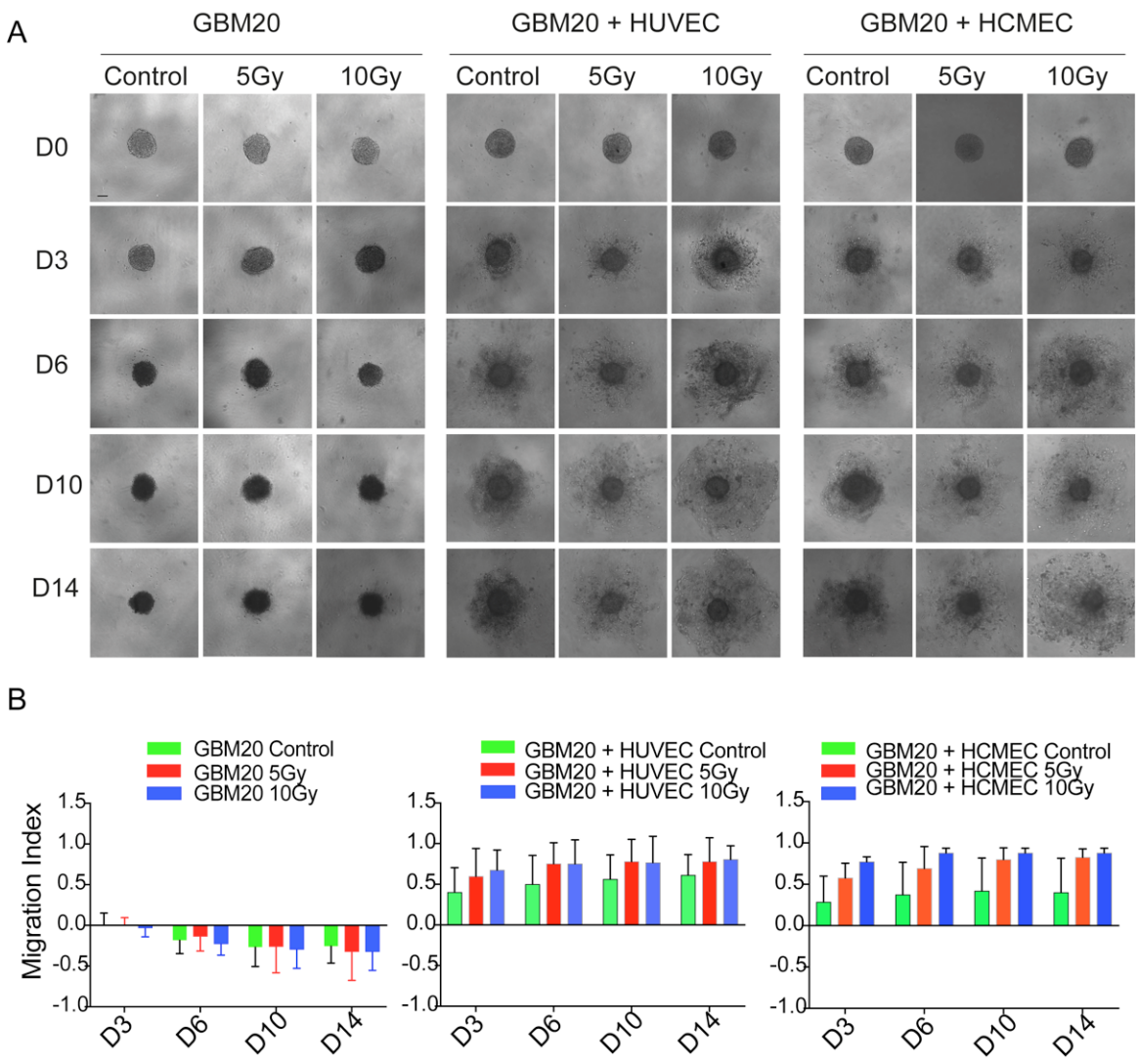
A
GBM20
GBM20 + HUVEC
GBM20 + HCMEC
Control
5Gy
10Gy
D0
D3
D6
D10
D14
B
GBM20 Control
GBM20 5Gy
GBM20 10Gy
GBM20 + HUVEC Control
GBM20 + HUVEC 5Gy
GBM20 + HUVEC 10Gy
GBM20 + HCMEC Control
GBM20 + HCMEC 5Gy
GBM20 + HCMEC 10Gy
Migration Index
1.5
1.0
0.5
0.0
-0.5
-1.0
D3
D6
D10
D14

Effect of ionising radiation on GBM20 cancer cell invasion in a spheroid assay in the presence and absence of endothelial cells

GBM20 cancer cells ($2x10^3$), or $2x10^3$ GBM20 cancer cells mixed with $2x10^3$ HUVEC or HCMEC were seeded in a low adherent and round bottom 96-well plates in a 1:1 ratio of 100 μl neurobasal medium and 100μl HLVEC medium. After 5 days when a sphere was formed, supernatants were removed and 100μl collagen was added per well at 6.8 : 1 ratio of collagen to medium (equal mix of neurobasal and HLVEC medium), and neutralised by 0.7% 1M NaOH. Finally, 100 μl of the mix medium was added to each well and the plate was incubated at 37^o and 5% CO_2. In a treatment groups either 5Gy or 10Gy irradiation doses were applied at a rate of 2Gy/minute using RAD irradiator. Cancer cell invasion was measured at Day 0, 3, 6, 10 and 14 following the addition of collagen using EVOS at 4x magnification. N=Number of wells (Control GBM20, 14; Control GBM20 + HUVEC, 16; Control GBM20 + HCMEC, 15; 5Gy & 10Gy GBM20, 16; 5Gy & 10Gy GBM20 + HUVEC, 13; 5Gy GBM20 + HCMEC, 13 and 10Gy GBM20 + HCMEC , 15). D=Day; HCMEC, Human Cerebral Microvascular Endothelial Cells

(A) Images depict spheroids formed by cancer cells or their co-culture with HUVEC or HCMEC and their invasion into the surrounding collagen matrix.

(B) Bar chart shows invasion area of GBM20 cancer cells in the presence and absence of HUVEC or HCMEC.

References

Abraham, S., M. Scarcia, R. D. Bagshaw, K. McMahon, G. Grant, T. Harvey, M. Yeo, F. O. Esteves, H. H. Thygesen, P. F. Jones, V. Speirs, A. M. Hanby, P. J. Selby, M. Lorger, T. N. Dear, T. Pawson, C. J. Marshall, and G. Mavria. 2015. 'A Rac/Cdc42 exchange factor complex promotes formation of lateral filopodia and blood vessel lumen morphogenesis', *Nat Commun*, 6: 7286.

Adams, R. H., and K. Alitalo. 2007. 'Molecular regulation of angiogenesis and lymphangiogenesis', *Nat Rev Mol Cell Biol*, 8: 464-78.

Anderson, J. C., B. C. McFarland, and C. L. Gladson. 2008. 'New molecular targets in angiogenic vessels of glioblastoma tumours', *Expert Rev Mol Med*, 10: e23.

Andor, N., J. V. Harness, S. Muller, H. W. Mewes, and C. Petritsch. 2014. 'EXPANDS: expanding ploidy and allele frequency on nested subpopulations', *Bioinformatics*, 30: 50-60.

Aoki, K., T. Nakamura, and M. Matsuda. 2004. 'Spatio-temporal regulation of Rac1 and Cdc42 activity during nerve growth factor-induced neurite outgrowth in PC12 cells', *J Biol Chem*, 279: 713-9.

Aonuma, M., Y. Saeki, T. Akimoto, Y. Nakayama, C. Hattori, Y. Yoshitake, K. Nishikawa, M. Shibuya, and N. G. Tanaka. 1999. 'Vascular endothelial growth factor overproduced by tumour cells acts predominantly as a potent angiogenic factor contributing to malignant progression', *Int J Exp Pathol*, 80: 271-81.

Appaix, F., M. F. Nissou, B. van der Sanden, M. Dreyfus, F. Berger, J. P. Issartel, and D. Wion. 2014. 'Brain mesenchymal stem cells: The other stem cells of the brain?', *World J Stem Cells*, 6: 134-43.

Armulik, A., G. Genove, and C. Betsholtz. 2011. 'Pericytes: developmental, physiological, and pathological perspectives, problems, and promises', *Dev Cell*, 21: 193-215.

Armulik, A., G. Genove, M. Mae, M. H. Nisancioglu, E. Wallgard, C. Niaudet, L. He, J. Norlin, P. Lindblom, K. Strittmatter, B. R. Johansson, and C. Betsholtz. 2010. 'Pericytes regulate the blood-brain barrier', *Nature*, 468: 557-61.

Artacho-Cordon, F., S. Rios-Arrabal, P. C. Lara, A. Artacho-Cordon, I. Calvente, and M. I. Nunez. 2012. 'Matrix metalloproteinases: potential therapy to prevent the development of second malignancies after breast radiotherapy', *Surg Oncol*, 21: e143-51.

Badiga, A. V., C. Chetty, D. Kesanakurti, D. Are, M. Gujrati, J. D. Klopfenstein, D. H. Dinh, and J. S. Rao. 2011. 'MMP-2 siRNA inhibits radiation-enhanced invasiveness in glioma cells', *PLoS One*, 6: e20614.

Bao, S., Q. Wu, R. E. McLendon, Y. Hao, Q. Shi, A. B. Hjelmeland, M. W. Dewhirst, D. D. Bigner, and J. N. Rich. 2006. 'Glioma stem cells promote radioresistance by preferential activation of the DNA damage response', *Nature*, 444: 756-60.

Barker, H. E., J. T. Paget, A. A. Khan, and K. J. Harrington. 2015. 'The tumour microenvironment after radiotherapy: mechanisms of resistance and recurrence', *Nat Rev Cancer*, 15: 409-25.

Baskar, R., J. Dai, N. Wenlong, R. Yeo, and K. W. Yeoh. 2014. 'Biological response of cancer cells to radiation treatment', *Front Mol Biosci*, 1: 24.

Basu-Roy, U., N. S. Bayin, K. Rattanakorn, E. Han, D. G. Placantonakis, A. Mansukhani, and C. Basilico. 2015. 'Sox2 antagonizes the Hippo pathway to maintain stemness in cancer cells', *Nat Commun*, 6: 6411.

Bayin, N. S., J. D. Frenster, R. Sen, S. Si, A. S. Modrek, N. Galifianakis, I. Dolgalev, V. Ortenzi, I. Illa-Bochaca, A. Khahera, J. Serrano, L. Chiriboga, D. Zagzag, J. G. Golfinos, W. Doyle, A. Tsirigos, A. Heguy, M. Chesler, M. H. Barcellos-Hoff, M. Snuderl, and D. G. Placantonakis. 2017. 'Notch signaling regulates metabolic heterogeneity in glioblastoma stem cells', *Oncotarget*, 8: 64932-53.

Beatty, G. L., and W. L. Gladney. 2015. 'Immune escape mechanisms as a guide for cancer immunotherapy', *Clin Cancer Res*, 21: 687-92.

Benjamin, L. E., D. Golijanin, A. Itin, D. Pode, and E. Keshet. 1999. 'Selective ablation of immature blood vessels in established human tumors follows vascular endothelial growth factor withdrawal', *J Clin Invest*, 103: 159-65.

Berezovsky, A. D., L. M. Poisson, D. Cherba, C. P. Webb, A. D. Transou, N. W. Lemke, X. Hong, L. A. Hasselbach, S. M. Irtenkauf, T. Mikkelsen, and A. C. deCarvalho. 2014. 'Sox2 promotes malignancy in glioblastoma by regulating plasticity and astrocytic differentiation', *Neoplasia*, 16: 193-206, 06 e19-25.

Bergers, G., and L. E. Benjamin. 2003. 'Tumorigenesis and the angiogenic switch', *Nat Rev Cancer*, 3: 401-10.

Bergers, G., and S. Song. 2005. 'The role of pericytes in blood-vessel formation and maintenance', *Neuro Oncol*, 7: 452-64.

Bergers, G., S. Song, N. Meyer-Morse, E. Bergsland, and D. Hanahan. 2003. 'Benefits of targeting both pericytes and endothelial cells in the tumor vasculature with kinase inhibitors', *J Clin Invest*, 111: 1287-95.

Berthiaume, A. A., R. I. Grant, K. P. McDowell, R. G. Underly, D. A. Hartmann, M. Levy, N. R. Bhat, and A. Y. Shih. 2018. 'Dynamic Remodeling of Pericytes In Vivo Maintains Capillary Coverage in the Adult Mouse Brain', *Cell Rep*, 22: 8-16.

Binello, E., Z. A. Qadeer, H. P. Kothari, L. Emdad, and I. M. Germano. 2012. 'Stemness of the CT-2A Immunocompetent Mouse Brain Tumor Model: Characterization In Vitro', *J Cancer*, 3: 166-74.

Birnbaum, T., J. Hildebrandt, G. Nuebling, P. Sostak, and A. Straube. 2011. 'Glioblastoma-dependent differentiation and angiogenic potential of human mesenchymal stem cells in vitro', *J Neurooncol*, 105: 57-65.

Birner, P., M. Piribauer, I. Fischer, B. Gatterbauer, C. Marosi, P. F. Ambros, I. M. Ambros, M. Bredel, G. Oberhuber, K. Rossler, H. Budka, A. L. Harris, and J. A. Hainfellner. 2003. 'Vascular patterns in

glioblastoma influence clinical outcome and associate with variable expression of angiogenic proteins: evidence for distinct angiogenic subtypes', *Brain Pathol*, 13: 133-43.

Bjarnegard, M., M. Enge, J. Norlin, S. Gustafsdottir, S. Fredriksson, A. Abramsson, M. Takemoto, E. Gustafsson, R. Fassler, and C. Betsholtz. 2004. 'Endothelium-specific ablation of PDGFB leads to pericyte loss and glomerular, cardiac and placental abnormalities', *Development*, 131: 1847-57.

Blaes, J., C. M. Thome, P. N. Pfenning, P. Rubmann, F. Sahm, A. Wick, T. Bunse, T. Schmenger, J. Sykora, A. von Deimling, B. Wiestler, C. Merz, M. Jugold, U. Haberkorn, A. Abdollahi, J. Debus, C. Gieffers, C. Kunz, M. Bendszus, M. Kluge, M. Platten, H. Fricke, W. Wick, and D. Lemke. 2018. 'Inhibition of CD95/CD95L (FAS/FASLG) Signaling with APG101 Prevents Invasion and Enhances Radiation Therapy for Glioblastoma', *Mol Cancer Res*, 16: 767-76.

Bonacquisti, E. E., and J. Nguyen. 2019. 'Connexin 43 (Cx43) in cancer: Implications for therapeutic approaches via gap junctions', *Cancer Lett*, 442: 439-44.

Borovski, T., P. Beke, O. van Tellingen, H. M. Rodermond, J. J. Verhoeff, V. Lascano, J. B. Daalhuisen, J. P. Medema, and M. R. Sprick. 2013. 'Therapy-resistant tumor microvascular endothelial cells contribute to treatment failure in glioblastoma multiforme', *Oncogene*, 32: 1539-48.

Bradley, J. D., Y. Kataoka, S. Advani, S. M. Chung, R. B. Arani, G. Y. Gillespie, R. J. Whitley, J. M. Markert, B. Roizman, and R. R. Weichselbaum. 1999. 'Ionizing radiation improves survival in mice bearing intracranial high-grade gliomas injected with genetically modified herpes simplex virus', *Clin Cancer Res*, 5: 1517-22.

Bradshaw, A., A. Wickremsekera, S. T. Tan, L. Peng, P. F. Davis, and T. Itinteang. 2016. 'Cancer Stem Cell Hierarchy in Glioblastoma Multiforme', *Front Surg*, 3: 21.

Brat, D. J., and E. G. Van Meir. 2001. 'Glomeruloid microvascular proliferation orchestrated by VPF/VEGF: a new world of angiogenesis research', *Am J Pathol*, 158: 789-96.

Brooks, M. D., R. Sengupta, S. C. Snyder, and J. B. Rubin. 2013. 'Hitting Them Where They Live: Targeting the Glioblastoma Perivascular Stem Cell Niche', *Curr Pathobiol Rep*, 1: 101-10.

Brown, D. V., G. Filiz, P. M. Daniel, F. Hollande, S. Dworkin, S. Amiridis, N. Kountouri, W. Ng, A. P. Morokoff, and T. Mantamadiotis. 2017. 'Expression of CD133 and CD44 in glioblastoma stem cells correlates with cell proliferation, phenotype stability and intra-tumor heterogeneity', *PLoS One*, 12: e0172791.

Brown, J. M., and A. J. Giaccia. 1998. 'The unique physiology of solid tumors: opportunities (and problems) for cancer therapy', *Cancer Res*, 58: 1408-16.

Bustelo, X. R., V. Sauzeau, and I. M. Berenjeno. 2007. 'GTP-binding proteins of the Rho/Rac family: regulation, effectors and functions in vivo', *Bioessays*, 29: 356-70.

Cabezas, R., M. Avila, J. Gonzalez, R. S. El-Bacha, E. Baez, L. M. Garcia-Segura, J. C. Jurado Coronel, F. Capani, G. P. Cardona-Gomez, and G. E. Barreto. 2014. 'Astrocytic modulation of blood brain barrier: perspectives on Parkinson's disease', *Front Cell Neurosci*, 8: 211.

Calabrese, C., H. Poppleton, M. Kocak, T. L. Hogg, C. Fuller, B. Hamner, E. Y. Oh, M. W. Gaber, D. Finklestein, M. Allen, A. Frank, I. T. Bayazitov, S. S. Zakharenko, A. Gajjar, A. Davidoff, and R. J. Gilbertson. 2007. 'A perivascular niche for brain tumor stem cells', *Cancer Cell*, 11: 69-82.

Campos, B., L. R. Olsen, T. Urup, and H. S. Poulsen. 2016. 'A comprehensive profile of recurrent glioblastoma', *Oncogene*, 35: 5819-25.

Carmeliet, P., and R. K. Jain. 2011. 'Principles and mechanisms of vessel normalization for cancer and other angiogenic diseases', *Nat Rev Drug Discov*, 10: 417-27.

Cea, V., C. Sala, and C. Verpelli. 2012. 'Antiangiogenic therapy for glioma', *J Signal Transduct*, 2012: 483040.

Ceccarelli, M., F. P. Barthel, T. M. Malta, T. S. Sabedot, S. R. Salama, B. A. Murray, O. Morozova, Y. Newton, A. Radenbaugh, S. M. Pagnotta, S. Anjum, J. Wang, G. Manyam, P. Zoppoli, S. Ling, A. A. Rao, M. Grifford, A. D. Cherniack, H. Zhang, L. Poisson, C. G. Carlotti, Jr., D. P. Tirapelli, A. Rao, T. Mikkelsen, C. C. Lau, W. K. Yung, R. Rabadan, J. Huse, D. J. Brat, N. L. Lehman, J. S. Barnholtz-Sloan, S. Zheng, K. Hess, G. Rao, M. Meyerson, R. Beroukhim, L. Cooper, R. Akbani, M. Wrensch, D. Haussler, K. D. Aldape, P. W. Laird, D. H. Gutmann, Tcga Research Network, H. Noushmehr, A. Iavarone, and R. G. Verhaak. 2016. 'Molecular Profiling Reveals Biologically Discrete Subsets and Pathways of Progression in Diffuse Glioma', *Cell*, 164: 550-63.

Chang, Y. S., E. di Tomaso, D. M. McDonald, R. Jones, R. K. Jain, and L. L. Munn. 2000. 'Mosaic blood vessels in tumors: frequency of cancer cells in contact with flowing blood', *Proc Natl Acad Sci U S A*, 97: 14608-13.

Charalambous, C., T. C. Chen, and F. M. Hofman. 2006. 'Characteristics of tumor-associated endothelial cells derived from glioblastoma multiforme', *Neurosurg Focus*, 20: E22.

Charles, N., and E. C. Holland. 2010. 'The perivascular niche microenvironment in brain tumor progression', *Cell Cycle*, 9: 3012-21.

Chen, H. Y., L. T. Lin, M. L. Wang, B. Laurent, C. H. Hsu, C. M. Pan, W. R. Jiang, P. Y. Chen, H. I. Ma, Y. W. Chen, P. I. Huang, A. Chiou, and S. H. Chiou. 2017. 'Musashi-1 Enhances Glioblastoma Cell Migration and Cytoskeletal Dynamics through Translational Inhibition of Tensin3', *Sci Rep*, 7: 8710.

Chen, J., S. Mao, H. Li, M. Zheng, L. Yi, J. M. Lin, and Z. X. Lin. 2017. 'The pathological structure of the perivascular niche in different microvascular patterns of glioblastoma', *PLoS One*, 12: e0182183.

Chen, L., Z. X. Lin, G. S. Lin, C. F. Zhou, Y. P. Chen, X. F. Wang, and Z. Q. Zheng. 2015. 'Classification of microvascular patterns via cluster analysis reveals their prognostic significance in glioblastoma', *Hum Pathol*, 46: 120-8.

Cheng, L., Z. Huang, W. Zhou, Q. Wu, S. Donnola, J. K. Liu, X. Fang, A. E. Sloan, Y. Mao, J. D. Lathia, W. Min, R. E. McLendon, J. N. Rich, and S. Bao. 2013. 'Glioblastoma stem cells generate vascular pericytes to support vessel function and tumor growth', *Cell*, 153: 139-52.

Cheng, V., F. Esteves, A. Chakrabarty, J. Cockle, S. Short, and A. Bruning-Richardson. 2015. 'High-content analysis of tumour cell invasion in three-dimensional spheroid assays', *Oncoscience*, 2: 596-606.

Choi, J., S. Y. Park, F. Costantini, E. H. Jho, and C. K. Joo. 2004. 'Adenomatous polyposis coli is down-regulated by the ubiquitin-proteasome pathway in a process facilitated by Axin', *J Biol Chem*, 279: 49188-98.

Chung, A. S., and N. Ferrara. 2011. 'Developmental and pathological angiogenesis', *Annu Rev Cell Dev Biol*, 27: 563-84.

Clement, V., P. Sanchez, N. de Tribolet, I. Radovanovic, and A. Ruiz i Altaba. 2007. 'HEDGEHOG-GLI1 signaling regulates human glioma growth, cancer stem cell self-renewal, and tumorigenicity', *Curr Biol*, 17: 165-72.

Cloughesy, T. F., W. K. Cavenee, and P. S. Mischel. 2014. 'Glioblastoma: from molecular pathology to targeted treatment', *Annu Rev Pathol*, 9: 1-25.

Cockle, J. V., S. Picton, J. Levesley, E. Ilett, A. M. Carcaboso, S. Short, L. P. Steel, A. Melcher, S. E. Lawler, and A. Bruning-Richardson. 2015. 'Cell migration in paediatric glioma; characterisation and potential therapeutic targeting', *Br J Cancer*, 112: 693-703.

Codrici, E., A. M. Enciu, I. D. Popescu, S. Mihai, and C. Tanase. 2016. 'Glioma Stem Cells and Their Microenvironments: Providers of Challenging Therapeutic Targets', *Stem Cells Int*, 2016: 5728438.

Coelho, A. L., M. P. Gomes, R. J. Catarino, C. Rolfo, A. M. Lopes, R. M. Medeiros, and A. M. Araujo. 2017. 'Angiogenesis in NSCLC: is vessel co-option the trunk that sustains the branches?', *Oncotarget*, 8: 39795-804.

Cote, J. F., and K. Vuori. 2002. 'Identification of an evolutionarily conserved superfamily of DOCK180-related proteins with guanine nucleotide exchange activity', *J Cell Sci*, 115: 4901-13.

Cuddapah, V. A., S. Robel, S. Watkins, and H. Sontheimer. 2014. 'A neurocentric perspective on glioma invasion', *Nat Rev Neurosci*, 15: 455-65.

Dahlrot, R. H., S. Hansen, S. S. Jensen, H. D. Schroder, J. Hjelmborg, and B. W. Kristensen. 2014. 'Clinical value of CD133 and nestin in patients with glioma: a population-based study', *Int J Clin Exp Pathol*, 7: 3739-51.

Daneman, R., L. Zhou, A. A. Kebede, and B. A. Barres. 2010. 'Pericytes are required for blood-brain barrier integrity during embryogenesis', *Nature*, 468: 562-6.

De Bacco, F., P. Luraghi, E. Medico, G. Reato, F. Girolami, T. Perera, P. Gabriele, P. M. Comoglio, and C. Boccaccio. 2011. 'Induction of MET by ionizing radiation and its role in radioresistance and invasive growth of cancer', *J Natl Cancer Inst*, 103: 645-61.

De Pascalis, I., L. Morgante, S. Pacioni, Q. G. D'Alessandris, S. Giannetti, M. Martini, L. Ricci-Vitiani, M. Malinverno, E. Dejana, L. M. Larocca, and R. Pallini. 2018. 'Endothelial trans-differentiation in glioblastoma recurring after radiotherapy', *Mod Pathol*, 31: 1361-66.

Deb, S., J. Wenjun Zhang, and P. E. Gottschall. 2003. 'Beta-amyloid induces the production of active, matrix-degrading proteases in cultured rat astrocytes', *Brain Res*, 970: 205-13.

Debruyne, D. N., L. Turchi, F. Burel-Vandenbos, M. Fareh, F. Almairac, V. Virolle, D. Figarella-Branger, N. Baeza-Kallee, P. Lagadec, V. Kubiniek, P. Paquis, D. Fontaine, M. P. Junier, H. Chneiweiss, and T. Virolle. 2018. 'DOCK4 promotes loss of proliferation in glioblastoma progenitor cells through nuclear beta-catenin accumulation and subsequent miR-302-367 cluster expression', *Oncogene*, 37: 241-54.

Demou, Z. N., and M. J. Hendrix. 2008. 'Microgenomics profile the endogenous angiogenic phenotype in subpopulations of aggressive melanoma', *J Cell Biochem*, 105: 562-73.

di Tomaso, E., D. Capen, A. Haskell, J. Hart, J. J. Logie, R. K. Jain, D. M. McDonald, R. Jones, and L. L. Munn. 2005. 'Mosaic tumor vessels: cellular basis and ultrastructure of focal regions lacking endothelial cell markers', *Cancer Res*, 65: 5740-9.

Dome, B., J. Timar, and S. Paku. 2003. 'A novel concept of glomeruloid body formation in experimental cerebral metastases', *J Neuropathol Exp Neurol*, 62: 655-61.

Dong, Z., L. Zhou, N. Han, M. Zhang, and X. Lyu. 2015. 'Wnt/beta-catenin pathway involvement in ionizing radiation-induced invasion of U87 glioblastoma cells', *Strahlenther Onkol*, 191: 672-80.

Donnem, T., A. R. Reynolds, E. A. Kuczynski, K. Gatter, P. B. Vermeulen, R. S. Kerbel, A. L. Harris, and F. Pezzella. 2018. 'Non-angiogenic tumours and their influence on cancer biology', *Nat Rev Cancer*, 18: 323-36.

Du, R., K. V. Lu, C. Petritsch, P. Liu, R. Ganss, E. Passegue, H. Song, S. Vandenberg, R. S. Johnson, Z. Werb, and G. Bergers. 2008. 'HIF1alpha induces the recruitment of bone marrow-derived vascular modulatory cells to regulate tumor angiogenesis and invasion', *Cancer Cell*, 13: 206-20.

Edalat, L., B. Stegen, L. Klumpp, E. Haehl, K. Schilbach, R. Lukowski, M. Kuhnle, G. Bernhardt, A. Buschauer, D. Zips, P. Ruth, and S. M. Huber. 2016. 'BK K+ channel blockade inhibits radiation-induced migration/brain infiltration of glioblastoma cells', *Oncotarget*, 7: 14259-78.

Eilken, H. M., and R. H. Adams. 2010. 'Dynamics of endothelial cell behavior in sprouting angiogenesis', *Curr Opin Cell Biol*, 22: 617-25.

Eilken, H. M., R. Dieguez-Hurtado, I. Schmidt, M. Nakayama, H. W. Jeong, H. Arf, S. Adams, N. Ferrara, and R. H. Adams. 2017. 'Pericytes regulate VEGF-induced endothelial sprouting through VEGFR1', *Nat Commun*, 8: 1574.

El Hallani, S., C. Colin, Y. El Houfi, A. Idbaih, B. Boisselier, Y. Marie, P. Ravassard, M. Labussiere, K. Mokhtari, J. L. Thomas, J. Y. Delattre, A. Eichmann, and M. Sanson. 2014. 'Tumor and endothelial cell hybrids participate in glioblastoma vasculature', *Biomed Res Int*, 2014: 827327.

Ellis, L. M., and D. J. Hicklin. 2008. 'VEGF-targeted therapy: mechanisms of anti-tumour activity', *Nat Rev Cancer*, 8: 579-91.

Etienne-Manneville, S., and A. Hall. 2002. 'Rho GTPases in cell biology', *Nature*, 420: 629-35.

Francescone, R., S. Scully, B. Bentley, W. Yan, S. L. Taylor, D. Oh, L. Moral, and R. Shao. 2012. 'Glioblastoma-derived tumor cells induce vasculogenic mimicry through Flk-1 protein activation', *J Biol Chem*, 287: 24821-31.

Friedl, P., and D. Gilmour. 2009. 'Collective cell migration in morphogenesis, regeneration and cancer', *Nat Rev Mol Cell Biol*, 10: 445-57.

Fujita, M., Y. Otsuka, S. Yamada, M. Iwakawa, and T. Imai. 2011. 'X-ray irradiation and Rho-kinase inhibitor additively induce invasiveness of the cells of the pancreatic cancer line, MIAPaCa-2, which exhibits mesenchymal and amoeboid motility', *Cancer Sci*, 102: 792-8.

Gadea, G., and A. Blangy. 2014. 'Dock-family exchange factors in cell migration and disease', *Eur J Cell Biol*, 93: 466-77.

Gerstner, E. R., P. J. Chen, P. Y. Wen, R. K. Jain, T. T. Batchelor, and G. Sorensen. 2010. 'Infiltrative patterns of glioblastoma spread detected via diffusion MRI after treatment with cediranib', *Neuro Oncol*, 12: 466-72.

Gialeli, C., A. D. Theocharis, and N. K. Karamanos. 2011. 'Roles of matrix metalloproteinases in cancer progression and their pharmacological targeting', *FEBS J*, 278: 16-27.

Gilbertson, R. J., and J. N. Rich. 2007. 'Making a tumour's bed: glioblastoma stem cells and the vascular niche', *Nat Rev Cancer*, 7: 733-6.

Gill, B. J., D. J. Pisapia, H. R. Malone, H. Goldstein, L. Lei, A. Sonabend, J. Yun, J. Samanamud, J. S. Sims, M. Banu, A. Dovas, A. F. Teich, S. A. Sheth, G. M. McKhann, M. B. Sisti, J. N. Bruce, P. A. Sims, and P. Canoll. 2014. 'MRI-localized biopsies reveal subtype-specific differences in molecular and cellular composition at the margins of glioblastoma', *Proc Natl Acad Sci U S A*, 111: 12550-5.

Goel, S., D. G. Duda, L. Xu, L. L. Munn, Y. Boucher, D. Fukumura, and R. K. Jain. 2011. 'Normalization of the vasculature for treatment of cancer and other diseases', *Physiol Rev*, 91: 1071-121.

Goffart, N., A. Lombard, F. Lallemand, J. Kroonen, J. Nassen, E. Di Valentin, S. Berendsen, M. Dedobbeleer, E. Willems, P. Robe, V. Bours, D. Martin, P. Martinive, P. Maquet, and B. Rogister. 2017. 'CXCL12 mediates glioblastoma resistance to radiotherapy in the subventricular zone', *Neuro Oncol*, 19: 66-77.

Gogineni, V. R., O. Kargiotis, J. D. Klopfenstein, M. Gujrati, D. H. Dinh, and J. S. Rao. 2009. 'RNAi-mediated downregulation of radiation-induced MMP-9 leads to apoptosis via activation of ERK and Akt in IOMM-Lee cells', *Int J Oncol*, 34: 209-18.

Goldman, S. A., and Z. Chen. 2011. 'Perivascular instruction of cell genesis and fate in the adult brain', *Nat Neurosci*, 14: 1382-9.

Gritsenko, P., W. Leenders, and P. Friedl. 2017. 'Recapitulating in vivo-like plasticity of glioma cell invasion along blood vessels and in astrocyte-rich stroma', *Histochem Cell Biol*, 148: 395-406.

Hambardzumyan, D., O. J. Becher, M. K. Rosenblum, P. P. Pandolfi, K. Manova-Todorova, and E. C. Holland. 2008. 'PI3K pathway regulates survival of cancer stem cells residing in the perivascular niche following radiation in medulloblastoma in vivo', *Genes Dev*, 22: 436-48.

Hambardzumyan, D., and G. Bergers. 2015. 'Glioblastoma: Defining Tumor Niches', *Trends Cancer*, 1: 252-65.

Hambardzumyan, D., D. H. Gutmann, and H. Kettenmann. 2016. 'The role of microglia and macrophages in glioma maintenance and progression', *Nat Neurosci*, 19: 20-7.

Hanahan, D., and R. A. Weinberg. 2011. 'Hallmarks of cancer: the next generation', *Cell*, 144: 646-74.

Hara, A., M. Hashimura, K. Tsutsumi, M. Akiya, M. Inukai, Y. Ohta, and M. Saegusa. 2016. 'The role of FilGAP, a Rac-specific Rho-GTPase-activating protein, in tumor progression and behavior of astrocytomas', *Cancer Med*, 5: 3412-25.

Harada, H., M. Inoue, S. Itasaka, K. Hirota, A. Morinibu, K. Shinomiya, L. Zeng, G. Ou, Y. Zhu, M. Yoshimura, W. G. McKenna, R. J. Muschel, and M. Hiraoka. 2012. 'Cancer cells that survive radiation therapy acquire HIF-1 activity and translocate towards tumour blood vessels', *Nat Commun*, 3: 783.

Hardee, M. E., and D. Zagzag. 2012. 'Mechanisms of glioma-associated neovascularization', *Am J Pathol*, 181: 1126-41.

He, H., C. S. Niu, and M. W. Li. 2012. 'Correlation between glioblastoma stem-like cells and tumor vascularization', *Oncol Rep*, 27: 45-50.

Heasman, S. J., and A. J. Ridley. 2008. 'Mammalian Rho GTPases: new insights into their functions from in vivo studies', *Nat Rev Mol Cell Biol*, 9: 690-701.

Heckmann, M., K. Douwes, R. Peter, and K. Degitz. 1998. 'Vascular activation of adhesion molecule mRNA and cell surface expression by ionizing radiation', *Exp Cell Res*, 238: 148-54.

Hegi, M. E., A. C. Diserens, T. Gorlia, M. F. Hamou, N. de Tribolet, M. Weller, J. M. Kros, J. A. Hainfellner, W. Mason, L. Mariani, J. E. Bromberg, P. Hau, R. O. Mirimanoff, J. G. Cairncross, R. C. Janzer, and R. Stupp. 2005. 'MGMT gene silencing and benefit from temozolomide in glioblastoma', *N Engl J Med*, 352: 997-1003.

Hein, A. L., C. M. Post, Y. M. Sheinin, I. Lakshmanan, A. Natarajan, C. A. Enke, S. K. Batra, M. M. Ouellette, and Y. Yan. 2016. 'RAC1 GTPase promotes the survival of breast cancer cells in response to hyper-fractionated radiation treatment', *Oncogene*, 35: 6319-29.

Helm, A., R. Lee, M. Durante, and S. Ritter. 2016. 'The Influence of C-Ions and X-rays on Human Umbilical Vein Endothelial Cells', *Front Oncol*, 6: 5.

Hendrix, M. J., E. A. Seftor, R. E. Seftor, J. T. Chao, D. S. Chien, and Y. W. Chu. 2016. 'Tumor cell vascular mimicry: Novel targeting opportunity in melanoma', *Pharmacol Ther*, 159: 83-92.

Herbert, S. P., and D. Y. Stainier. 2011. 'Molecular control of endothelial cell behaviour during blood vessel morphogenesis', *Nat Rev Mol Cell Biol*, 12: 551-64.

Hill, R. A., L. Tong, P. Yuan, S. Murikinati, S. Gupta, and J. Grutzendler. 2015. 'Regional Blood Flow in the Normal and Ischemic Brain Is Controlled by Arteriolar Smooth Muscle Cell Contractility and Not by Capillary Pericytes', *Neuron*, 87: 95-110.

Hiramoto, K., M. Negishi, and H. Katoh. 2006. 'Dock4 is regulated by RhoG and promotes Rac-dependent cell migration', *Exp Cell Res*, 312: 4205-16.

Hirata, E., H. Yukinaga, Y. Kamioka, Y. Arakawa, S. Miyamoto, T. Okada, E. Sahai, and M. Matsuda. 2012. 'In vivo fluorescence resonance energy transfer imaging reveals differential activation of Rho-family GTPases in glioblastoma cell invasion', *J Cell Sci*, 125: 858-68.

Ho, I. A. W., and W. S. N. Shim. 2017. 'Contribution of the Microenvironmental Niche to Glioblastoma Heterogeneity', *Biomed Res Int*, 2017: 9634172.

Hobson, B., and J. Denekamp. 1984. 'Endothelial proliferation in tumours and normal tissues: continuous labelling studies', *Br J Cancer*, 49: 405-13.

Hol, E. M., and M. Pekny. 2015. 'Glial fibrillary acidic protein (GFAP) and the astrocyte intermediate filament system in diseases of the central nervous system', *Curr Opin Cell Biol*, 32: 121-30.

Holash, J., P. C. Maisonpierre, D. Compton, P. Boland, C. R. Alexander, D. Zagzag, G. D. Yancopoulos, and S. J. Wiegand. 1999. 'Vessel cooption, regression, and growth in tumors mediated by angiopoietins and VEGF', *Science*, 284: 1994-8.

Holmes, K., O. L. Roberts, A. M. Thomas, and M. J. Cross. 2007. 'Vascular endothelial growth factor receptor-2: structure, function, intracellular signaling and therapeutic inhibition', *Cell Signal*, 19: 2003-12.

Hosono, J., S. Morikawa, T. Ezaki, T. Kawamata, and Y. Okada. 2017. 'Pericytes promote abnormal tumor angiogenesis in a rat RG2 glioma model', *Brain Tumor Pathol*, 34: 120-29.

Hovinga, K. E., F. Shimizu, R. Wang, G. Panagiotakos, M. Van Der Heijden, H. Moayedpardazi, A. S. Correia, D. Soulet, T. Major, J. Menon, and V. Tabar. 2010. 'Inhibition of notch signaling in glioblastoma targets cancer stem cells via an endothelial cell intermediate', *Stem Cells*, 28: 1019-29.

Huang, H., J. Held-Feindt, R. Buhl, H. M. Mehdorn, and R. Mentlein. 2005. 'Expression of VEGF and its receptors in different brain tumors', *Neurol Res*, 27: 371-7.

Huang, Q., F. Li, X. Liu, W. Li, W. Shi, F. F. Liu, B. O'Sullivan, Z. He, Y. Peng, A. C. Tan, L. Zhou, J. Shen, G. Han, X. J. Wang, J. Thorburn, A. Thorburn, A. Jimeno, D. Raben, J. S. Bedford, and C. Y. Li. 2011. 'Caspase 3-mediated stimulation of tumor cell repopulation during cancer radiotherapy', *Nat Med*, 17: 860-6.

Hubert, C. G., M. Rivera, L. C. Spangler, Q. Wu, S. C. Mack, B. C. Prager, M. Couce, R. E. McLendon, A. E. Sloan, and J. N. Rich. 2016. 'A Three-Dimensional Organoid Culture System Derived from Human Glioblastomas Recapitulates the Hypoxic Gradients and Cancer Stem Cell Heterogeneity of Tumors Found In Vivo', *Cancer Res*, 76: 2465-77.

Hwang, S. Y., J. W. Jung, J. S. Jeong, Y. J. Kim, E. S. Oh, T. H. Kim, J. Y. Kim, K. H. Cho, and I. O. Han. 2006. 'Dominant-negative Rac increases both inherent and ionizing radiation-induced cell migration in C6 rat glioma cells', *Int J Cancer*, 118: 2056-63.

Jadhav, U., and S. Mohanam. 2006. 'Response of neuroblastoma cells to ionizing radiation: modulation of in vitro invasiveness and angiogenesis of human microvascular endothelial cells', *Int J Oncol*, 29: 1525-31.

Jain, R. K. 2003. 'Molecular regulation of vessel maturation', *Nat Med*, 9: 685-93.

Jain, R. K., E. di Tomaso, D. G. Duda, J. S. Loeffler, A. G. Sorensen, and T. T. Batchelor. 2007. 'Angiogenesis in brain tumours', *Nat Rev Neurosci*, 8: 610-22.

Jakobsson, L., C. A. Franco, K. Bentley, R. T. Collins, B. Ponsioen, I. M. Aspalter, I. Rosewell, M. Busse, G. Thurston, A. Medvinsky, S. Schulte-Merker, and H. Gerhardt. 2010. 'Endothelial cells dynamically compete for the tip cell position during angiogenic sprouting', *Nat Cell Biol*, 12: 943-53.

Joseph, J. V., V. Balasubramaniyan, A. Walenkamp, and F. A. Kruyt. 2013. 'TGF-beta as a therapeutic target in high grade gliomas - promises and challenges', *Biochem Pharmacol*, 85: 478-85.

Kalkan, R. 2015. 'Glioblastoma Stem Cells as a New Therapeutic Target for Glioblastoma', *Clin Med Insights Oncol*, 9: 95-103.

Kaur, B., F. W. Khwaja, E. A. Severson, S. L. Matheny, D. J. Brat, and E. G. Van Meir. 2005. 'Hypoxia and the hypoxia-inducible-factor pathway in glioma growth and angiogenesis', *Neuro Oncol*, 7: 134-53.

Kegelman, T. P., B. Wu, S. K. Das, S. Talukdar, J. M. Beckta, B. Hu, L. Emdad, K. Valerie, D. Sarkar, F. B. Furnari, W. K. Cavenee, J. Wei, A. Purves, S. K. De, M. Pellecchia, and P. B. Fisher. 2017. 'Inhibition of radiation-induced glioblastoma invasion by genetic and pharmacological targeting of MDA-9/Syntenin', *Proc Natl Acad Sci U S A*, 114: 370-75.

Kienast, Y., L. von Baumgarten, M. Fuhrmann, W. E. Klinkert, R. Goldbrunner, J. Herms, and F. Winkler. 2010. 'Real-time imaging reveals the single steps of brain metastasis formation', *Nat Med*, 16: 116-22.

Kim, C. S., S. Jung, T. Y. Jung, W. Y. Jang, H. S. Sun, and H. H. Ryu. 2011. 'Characterization of invading glioma cells using molecular analysis of leading-edge tissue', *J Korean Neurosurg Soc*, 50: 157-65.

Kioi, M., H. Vogel, G. Schultz, R. M. Hoffman, G. R. Harsh, and J. M. Brown. 2010. 'Inhibition of vasculogenesis, but not angiogenesis, prevents the recurrence of glioblastoma after irradiation in mice', *J Clin Invest*, 120: 694-705.

Klein, D., N. Meissner, V. Kleff, H. Jastrow, M. Yamaguchi, S. Ergun, and V. Jendrossek. 2014. 'Nestin(+) tissue-resident multipotent stem cells contribute to tumor progression by differentiating into pericytes and smooth muscle cells resulting in blood vessel remodeling', *Front Oncol*, 4: 169.

Kobayashi, M., K. Harada, M. Negishi, and H. Katoh. 2014. 'Dock4 forms a complex with SH3YL1 and regulates cancer cell migration', *Cell Signal*, 26: 1082-8.

Korkolopoulou, P., E. Patsouris, N. Kavantzas, A. E. Konstantinidou, P. Christodoulou, E. Thomas-Tsagli, A. Pananikolaou, C. Eftychiadis, P. M. Pavlopoulos, D. Angelidakis, D. Rologis, and P. Davaris. 2002. 'Prognostic implications of microvessel morphometry in diffuse astrocytic neoplasms', *Neuropathol Appl Neurobiol*, 28: 57-66.

Kuczynski, E. A., M. Yin, A. Bar-Zion, C. R. Lee, H. Butz, S. Man, F. Daley, P. B. Vermeulen, G. M. Yousef, F. S. Foster, A. R. Reynolds, and R. S. Kerbel. 2016. 'Co-option of Liver Vessels and Not Sprouting Angiogenesis Drives Acquired Sorafenib Resistance in Hepatocellular Carcinoma', *J Natl Cancer Inst*, 108.

Kuhnert, F., M. R. Mancuso, J. Hampton, K. Stankunas, T. Asano, C. Z. Chen, and C. J. Kuo. 2008. 'Attribution of vascular phenotypes of the murine Egfl7 locus to the microRNA miR-126', *Development*, 135: 3989-93.

Kumar, S., and A. S. Arbab. 2013. 'Neovascularization in Glioblastoma: Current Pitfall in Anti-angiogenic therapy', *Zhong Liu Za Zhi*, 1: 16-19.

Kuo, K. T., B. Guan, Y. Feng, T. L. Mao, X. Chen, N. Jinawath, Y. Wang, R. J. Kurman, M. Shih Ie, and T. L. Wang. 2009. 'Analysis of DNA copy number alterations in ovarian serous tumors identifies new molecular genetic changes in low-grade and high-grade carcinomas', *Cancer Res*, 69: 4036-42.

Lapa, C., T. Linsenmann, K. Luckerath, S. Samnick, K. Herrmann, C. Stoffer, R. I. Ernestus, A. K. Buck, M. Lohr, and C. M. Monoranu. 2015. 'Tumor-associated macrophages in glioblastoma multiforme-a suitable target for somatostatin receptor-based imaging and therapy?', *PLoS One*, 10: e0122269.

Leblond, M. M., E. A. Peres, C. Helaine, A. N. Gerault, D. Moulin, C. Anfray, D. Divoux, E. Petit, M. Bernaudin, and S. Valable. 2017. 'M2 macrophages are more resistant than M1 macrophages following radiation therapy in the context of glioblastoma', *Oncotarget*, 8: 72597-612.

Lee, Y., J. K. Lee, S. H. Ahn, J. Lee, and D. H. Nam. 2016. 'WNT signaling in glioblastoma and therapeutic opportunities', *Lab Invest*, 96: 137-50.

Leiss, L., E. Mutlu, A. Oyan, T. Yan, O. Tsinkalovsky, L. Sleire, K. Petersen, M. A. Rahman, M. Johannessen, S. S. Mitra, H. K. Jacobsen, K. M. Talasila, H. Miletic, I. Jonassen, X. Li, N. H. Brons, K. H. Kalland, J. Wang, and P. O. Enger. 2017. 'Tumour-associated glial host cells display a stem-like phenotype with a distinct gene expression profile and promote growth of GBM xenografts', *BMC Cancer*, 17: 108.

Li, B., W. Feng, O. Luo, T. Xu, Y. Cao, H. Wu, D. Yu, and Y. Ding. 2017. 'Development and Validation of a Three-gene Prognostic Signature for Patients with Hepatocellular Carcinoma', *Sci Rep*, 7: 5517.

Li, Q., X. Wei, Z. W. Zhou, S. N. Wang, H. Jin, K. J. Chen, J. Luo, K. D. Westover, J. M. Wang, D. Wang, C. X. Xu, and J. L. Shan. 2018. 'GADD45alpha sensitizes cervical cancer cells to radiotherapy via increasing cytoplasmic APE1 level', *Cell Death Dis*, 9: 524.

Li, R., X. Chen, Y. You, X. Wang, Y. Liu, Q. Hu, and W. Yan. 2015. 'Comprehensive portrait of recurrent glioblastoma multiforme in molecular and clinical characteristics', *Oncotarget*, 6: 30968-74.

Liang, Z. W., Z. Wang, H. Chen, C. Li, T. Zhou, Z. Yang, X. Yang, Y. Yang, G. Gao, and W. Cai. 2015. 'Nestin-mediated cytoskeletal remodeling in endothelial cells: novel mechanistic insight into VEGF-induced cell migration in angiogenesis', *Am J Physiol Cell Physiol*, 308: C349-58.

Lim, Y. C., H. Quek, C. Offenhauser, S. Fazry, A. Boyd, M. Lavin, T. Roberts, and B. Day. 2018. 'ATM inhibition prevents interleukin-6 from contributing to the proliferation of glioblastoma cells after ionizing radiation', *J Neurooncol*, 138: 509-18.

Lin, Q., K. Balasubramanian, D. Fan, S. J. Kim, L. Guo, H. Wang, M. Bar-Eli, K. D. Aldape, and I. J. Fidler. 2010. 'Reactive astrocytes protect melanoma cells from chemotherapy by sequestering intracellular calcium through gap junction communication channels', *Neoplasia*, 12: 748-54.

Lin, Q., Z. Liu, F. Ling, and G. Xu. 2016. 'Astrocytes protect glioma cells from chemotherapy and upregulate survival genes via gap junctional communication', *Mol Med Rep*, 13: 1329-35.

Liu, J., X. Ji, Z. Li, H. Zheng, W. Zheng, J. Jia, H. Shen, Q. Zhang, and J. An. 2015. 'Nestin overexpression promotes the embryonic development of heart and brain through the regulation of cell proliferation', *Brain Res*, 1610: 1-11.

Liu, S. C., R. Alomran, S. B. Chernikova, F. Lartey, J. Stafford, T. Jang, M. Merchant, D. Zboralski, S. Zollner, A. Kruschinski, S. Klussmann, L. Recht, and J. M. Brown. 2014. 'Blockade of SDF-1 after irradiation inhibits tumor recurrences of autochthonous brain tumors in rats', *Neuro Oncol*, 16: 21-8.

Loeffler, J. S., E. Alexander, 3rd, F. H. Hochberg, P. Y. Wen, J. H. Morris, W. C. Schoene, R. L. Siddon, R. H. Morse, and P. M. Black. 1990. 'Clinical patterns of failure following stereotactic interstitial irradiation for malignant gliomas', *Int J Radiat Oncol Biol Phys*, 19: 1455-62.

Lorger, M., J. S. Krueger, M. O'Neal, K. Staflin, and B. Felding-Habermann. 2009. 'Activation of tumor cell integrin alphavbeta3 controls angiogenesis and metastatic growth in the brain', *Proc Natl Acad Sci U S A*, 106: 10666-71.

Lorger, M. 2012. 'Tumor microenvironment in the brain', *Cancers (Basel)*, 4: 218-43.

Louis, D. N., H. Ohgaki, O. D. Wiestler, W. K. Cavenee, P. C. Burger, A. Jouvet, B. W. Scheithauer, and P. Kleihues. 2007. 'The 2007 WHO classification of tumours of the central nervous system', *Acta Neuropathol*, 114: 97-109.

Louis, D. N., A. Perry, G. Reifenberger, A. von Deimling, D. Figarella-Branger, W. K. Cavenee, H. Ohgaki, O. D. Wiestler, P. Kleihues, and D. W. Ellison. 2016. 'The 2016 World Health Organization Classification of Tumors of the Central Nervous System: a summary', *Acta Neuropathol*, 131: 803-20.

Lu, Y., J. Kwintkiewicz, Y. Liu, K. Tech, L. N. Frady, Y. T. Su, W. Bautista, S. I. Moon, J. MacDonald, M. G. Ewend, M. R. Gilbert, C. Yang, and J. Wu. 2017. 'Chemosensitivity of IDH1-Mutated Gliomas Due to an Impairment in PARP1-Mediated DNA Repair', *Cancer Res*, 77: 1709-18.

Luca, M., S. Huang, J. E. Gershenwald, R. K. Singh, R. Reich, and M. Bar-Eli. 1997. 'Expression of interleukin-8 by human melanoma cells up-regulates MMP-2 activity and increases tumor growth and metastasis', *Am J Pathol*, 151: 1105-13.

Manini, I., F. Caponnetto, A. Bartolini, T. Ius, L. Mariuzzi, C. Di Loreto, A. P. Beltrami, and D. Cesselli. 2018. 'Role of Microenvironment in Glioma Invasion: What We Learned from In Vitro Models', *Int J Mol Sci*, 19.

Maniotis, A. J., R. Folberg, A. Hess, E. A. Seftor, L. M. Gardner, J. Pe'er, J. M. Trent, P. S. Meltzer, and M. J. Hendrix. 1999. 'Vascular channel formation by human melanoma cells in vivo and in vitro: vasculogenic mimicry', *Am J Pathol*, 155: 739-52.

Marampon, F., G. L. Gravina, B. M. Zani, V. M. Popov, A. Fratticci, M. Cerasani, D. Di Genova, M. Mancini, C. Ciccarelli, C. Ficorella, E. Di Cesare, and C. Festuccia. 2014. 'Hypoxia sustains glioblastoma radioresistance through ERKs/DNA-PKcs/HIF-1alpha functional interplay', *Int J Oncol*, 44: 2121-31.

Markovic, D. S., R. Glass, M. Synowitz, Nv Rooijen, and H. Kettenmann. 2005. 'Microglia stimulate the invasiveness of glioma cells by increasing the activity of metalloprotease-2', *J Neuropathol Exp Neurol*, 64: 754-62.

Martin, B. J. 2013. 'Inhibiting vasculogenesis after radiation: a new paradigm to improve local control by radiotherapy', *Semin Radiat Oncol*, 23: 281-7.

Martinez-Murillo, R., and A. Martinez. 2007. 'Standardization of an orthotopic mouse brain tumor model following transplantation of CT-2A astrocytoma cells', *Histol Histopathol*, 22: 1309-26.

McKnight, T. R. 2004. 'Proton magnetic resonance spectroscopic evaluation of brain tumor metabolism', *Semin Oncol*, 31: 605-17.

Moeller, B. J., Y. Cao, C. Y. Li, and M. W. Dewhirst. 2004. 'Radiation activates HIF-1 to regulate vascular radiosensitivity in tumors: role of reoxygenation, free radicals, and stress granules', *Cancer Cell*, 5: 429-41.

Mooney, K. L., W. Choy, S. Sidhu, P. Pelargos, T. T. Bui, B. Voth, N. Barnette, and I. Yang. 2016. 'The role of CD44 in glioblastoma multiforme', *J Clin Neurosci*, 34: 1-5.

Morantz, R. A., G. W. Wood, M. Foster, M. Clark, and K. Gollahon. 1979. 'Macrophages in experimental and human brain tumors. Part 2: studies of the macrophage content of human brain tumors', *J Neurosurg*, 50: 305-11.

Morganti, J. M., T. D. Jopson, S. Liu, N. Gupta, and S. Rosi. 2014. 'Cranial irradiation alters the brain's microenvironment and permits CCR2+ macrophage infiltration', *PLoS One*, 9: e93650.

Muto, J., T. Imai, D. Ogawa, Y. Nishimoto, Y. Okada, Y. Mabuchi, T. Kawase, A. Iwanami, P. S. Mischel, H. Saya, K. Yoshida, Y. Matsuzaki, and H. Okano. 2012. 'RNA-binding protein Musashi1 modulates glioma cell growth through the post-transcriptional regulation of Notch and PI3 kinase/Akt signaling pathways', *PLoS One*, 7: e33431.

Nagy, J. A., S. H. Chang, A. M. Dvorak, and H. F. Dvorak. 2009. 'Why are tumour blood vessels abnormal and why is it important to know?', *Br J Cancer*, 100: 865-9.

Neilsen, B. K., R. Sleightholm, R. McComb, S. H. Ramkissoon, J. S. Ross, R. J. Corona, V. A. Miller, M. Cooke, and M. R. Aizenberg. 2018. 'Comprehensive genetic alteration profiling in primary and recurrent glioblastoma', *J Neurooncol*.

Neradil, J., and R. Veselska. 2015. 'Nestin as a marker of cancer stem cells', *Cancer Sci*, 106: 803-11.

Neufeld, S., L. Planas-Paz, and E. Lammert. 2014. 'Blood and lymphatic vascular tube formation in mouse', *Semin Cell Dev Biol*, 31: 115-23.

Newcomb, E. W., Y. Lukyanov, N. Kawashima, M. Alonso-Basanta, S. C. Wang, M. Liu, M. Jure-Kunkel, D. Zagzag, S. Demaria, and S. C. Formenti. 2010. 'Radiotherapy enhances antitumor effect of anti-CD137 therapy in a mouse Glioma model', *Radiat Res*, 173: 426-32.

Nijaguna, M. B., V. Patil, S. Urbach, S. D. Shwetha, K. Sravani, A. S. Hegde, B. A. Chandramouli, A. Arivazhagan, P. Marin, V. Santosh, and K. Somasundaram. 2015. 'Glioblastoma-derived Macrophage Colony-stimulating Factor (MCSF) Induces Microglial Release of Insulin-like Growth Factor-binding Protein 1 (IGFBP1) to Promote Angiogenesis', *J Biol Chem*, 290: 23401-15.

Nobes, C. D., and A. Hall. 1995. 'Rho, rac, and cdc42 GTPases regulate the assembly of multimolecular focal complexes associated with actin stress fibers, lamellipodia, and filopodia', *Cell*, 81: 53-62.

Nohata, N., Y. Uchida, A. N. Stratman, R. H. Adams, Y. Zheng, B. M. Weinstein, Y. S. Mukouyama, and J. S. Gutkind. 2016. 'Temporal-specific roles of Rac1 during vascular development and retinal angiogenesis', *Dev Biol*, 411: 183-94.

Obermeier, B., R. Daneman, and R. M. Ransohoff. 2013. 'Development, maintenance and disruption of the blood-brain barrier', *Nat Med*, 19: 1584-96.

Oh, M., and J. E. Nor. 2015. 'The Perivascular Niche and Self-Renewal of Stem Cells', *Front Physiol*, 6: 367.

Okamoto, O. K., A. C. Carvalho, L. C. Marti, R. Z. Vencio, and C. A. Moreira-Filho. 2007. 'Common molecular pathways involved in human CD133+/CD34+ progenitor cell expansion and cancer', *Cancer Cell Int*, 7: 11.

Oki, K., N. Kaneko, H. Kanki, T. Imai, N. Suzuki, K. Sawamoto, and H. Okano. 2010. 'Musashi1 as a marker of reactive astrocytes after transient focal brain ischemia', *Neurosci Res*, 66: 390-5.

Pankov, R., Y. Endo, S. Even-Ram, M. Araki, K. Clark, E. Cukierman, K. Matsumoto, and K. M. Yamada. 2005. 'A Rac switch regulates random versus directionally persistent cell migration', *J Cell Biol*, 170: 793-802.

Park, H. J., R. J. Griffin, S. Hui, S. H. Levitt, and C. W. Song. 2012. 'Radiation-induced vascular damage in tumors: implications of vascular damage in ablative hypofractionated radiotherapy (SBRT and SRS)', *Radiat Res*, 177: 311-27.

Patel-Hett, S., and P. A. D'Amore. 2011. 'Signal transduction in vasculogenesis and developmental angiogenesis', *Int J Dev Biol*, 55: 353-63.

Patrizii, M., M. Bartucci, S. R. Pine, and H. E. Sabaawy. 2018. 'Utility of Glioblastoma Patient-Derived Orthotopic Xenografts in Drug Discovery and Personalized Therapy', *Front Oncol*, 8: 23.

Pekny, M., and M. Nilsson. 2005. 'Astrocyte activation and reactive gliosis', *Glia*, 50: 427-34.

Petzelbauer, P., T. Halama, and M. Groger. 2000. 'Endothelial adherens junctions', *J Investig Dermatol Symp Proc*, 5: 10-3.

Phi, J. H., S. H. Park, S. K. Kim, S. H. Paek, J. H. Kim, Y. J. Lee, B. K. Cho, C. K. Park, D. H. Lee, and K. C. Wang. 2008. 'Sox2 expression in brain tumors: a reflection of the neuroglial differentiation pathway', *Am J Surg Pathol*, 32: 103-12.

Phillips, H. S., S. Kharbanda, R. Chen, W. F. Forrest, R. H. Soriano, T. D. Wu, A. Misra, J. M. Nigro, H. Colman, L. Soroceanu, P. M. Williams, Z. Modrusan, B. G. Feuerstein, and K. Aldape. 2006. 'Molecular subclasses of high-grade glioma predict prognosis, delineate a pattern of disease progression, and resemble stages in neurogenesis', *Cancer Cell*, 9: 157-73.

Polson, E. S., V. B. Kuchler, C. Abbosh, E. M. Ross, R. K. Mathew, H. A. Beard, B. da Silva, A. N. Holding, S. Ballereau, E. Chuntharpursat-Bon, J. Williams, H. B. S. Griffiths, H. Shao, A. Patel, A. J. Davies, A. Droop, P. Chumas, S. C. Short, M. Lorger, J. E. Gestwicki, L. D. Roberts, R. S. Bon, S. J. Allison, S. Zhu, F. Markowetz, and H. Wurdak. 2018. 'KHS101 disrupts energy metabolism in human glioblastoma cells and reduces tumor growth in mice', *Sci Transl Med*, 10.

Potiron, V. A., R. Abderrahmani, K. Clement-Colmou, S. Marionneau-Lambot, T. Oullier, F. Paris, and S. Supiot. 2013. 'Improved functionality of the vasculature during conventionally fractionated radiation therapy of prostate cancer', *PLoS One*, 8: e84076.

Preusser, M., H. Heinzl, E. Gelpi, K. Schonegger, C. Haberler, P. Birner, C. Marosi, M. Hegi, T. Gorlia, J. A. Hainfellner, Research European Organization for, and Group Treatment of Cancer Brain Tumor. 2006. 'Histopathologic assessment of hot-spot microvessel density and vascular patterns in glioblastoma: Poor observer agreement limits clinical utility as prognostic factors: a translational research project of the European Organization for Research and Treatment of Cancer Brain Tumor Group', *Cancer*, 107: 162-70.

Pu, P., Z. Xia, S. Yu, and Q. Huang. 2004. 'Altered expression of Cx43 in astrocytic tumors', *Clin Neurol Neurosurg*, 107: 49-54.

Qian, C. N. 2013. 'Hijacking the vasculature in ccRCC--co-option, remodelling and angiogenesis', *Nat Rev Urol*, 10: 300-4.

Ricci-Vitiani, L., R. Pallini, M. Biffoni, M. Todaro, G. Invernici, T. Cenci, G. Maira, E. A. Parati, G. Stassi, L. M. Larocca, and R. De Maria. 2010. 'Tumour vascularization via endothelial differentiation of glioblastoma stem-like cells', *Nature*, 468: 824-8.

Ridley, A. J. 2012. 'Historical overview of Rho GTPases', *Methods Mol Biol*, 827: 3-12.

Rodda, D. J., J. L. Chew, L. H. Lim, Y. H. Loh, B. Wang, H. H. Ng, and P. Robson. 2005. 'Transcriptional regulation of nanog by OCT4 and SOX2', *J Biol Chem*, 280: 24731-7.

Rodriguez, F. J., B. A. Orr, K. L. Ligon, and C. G. Eberhart. 2012. 'Neoplastic cells are a rare component in human glioblastoma microvasculature', *Oncotarget*, 3: 98-106.

Roggendorf, W., S. Strupp, and W. Paulus. 1996. 'Distribution and characterization of microglia/macrophages in human brain tumors', *Acta Neuropathol*, 92: 288-93.

Rojiani, A. M., and K. Dorovini-Zis. 1996. 'Glomeruloid vascular structures in glioblastoma multiforme: an immunohistochemical and ultrastructural study', *J Neurosurg*, 85: 1078-84.

Roodink, I., J. van der Laak, B. Kusters, P. Wesseling, K. Verrijp, R. de Waal, and W. Leenders. 2006. 'Development of the tumor vascular bed in response to hypoxia-induced VEGF-A differs from that in tumors with constitutive VEGF-A expression', *Int J Cancer*, 119: 2054-62.

Rooj, A. K., A. Bronisz, and J. Godlewski. 2016. 'The role of octamer binding transcription factors in glioblastoma multiforme', *Biochim Biophys Acta*, 1859: 805-11.

Sambade, M. J., E. C. Peters, N. E. Thomas, W. K. Kaufmann, R. J. Kimple, and J. M. Shields. 2011. 'Melanoma cells show a heterogeneous range of sensitivity to ionizing radiation and are radiosensitized by inhibition of B-RAF with PLX-4032', *Radiother Oncol*, 98: 394-9.

Scaringi, C., R. M. Enrici, and G. Minniti. 2013. 'Combining molecular targeted agents with radiation therapy for malignant gliomas', *Onco Targets Ther*, 6: 1079-95.

Schiffer, D., L. Annovazzi, M. Mazzucco, and M. Mellai. 2015. 'The Microenvironment in Gliomas: Phenotypic Expressions', *Cancers (Basel)*, 7: 2352-9.

Scully, S., R. Francescone, M. Faibish, B. Bentley, S. L. Taylor, D. Oh, R. Schapiro, L. Moral, W. Yan, and R. Shao. 2012. 'Transdifferentiation of glioblastoma stem-like cells into mural cells drives vasculogenic mimicry in glioblastomas', *J Neurosci*, 32: 12950-60.

Sharma, A., and A. Shiras. 2016. 'Cancer stem cell-vascular endothelial cell interactions in glioblastoma', *Biochem Biophys Res Commun*, 473: 688-92.

Shmelkov, S. V., J. M. Butler, A. T. Hooper, A. Hormigo, J. Kushner, T. Milde, R. St Clair, M. Baljevic, I. White, D. K. Jin, A. Chadburn, A. J. Murphy, D. M. Valenzuela, N. W. Gale, G. Thurston, G. D. Yancopoulos, M. D'Angelica, N. Kemeny, D. Lyden, and S. Rafii. 2008. 'CD133 expression is not restricted to stem cells, and both CD133+ and CD133- metastatic colon cancer cells initiate tumors', *J Clin Invest*, 118: 2111-20.

Shmelkov, S. V., R. St Clair, D. Lyden, and S. Rafii. 2005. 'AC133/CD133/Prominin-1', *Int J Biochem Cell Biol*, 37: 715-9.

Simons, M., K. Alitalo, B. H. Annex, H. G. Augustin, C. Beam, B. C. Berk, T. Byzova, P. Carmeliet, W. Chilian, J. P. Cooke, G. E. Davis, A. Eichmann, M. L. Iruela-Arispe, E. Keshet, A. J. Sinusas, C. Ruhrberg, Y. J. Woo, S. Dimmeler, Sciences American Heart Association Council on Basic Cardiovascular, Surgery Council on Cardiovascular, and Anesthesia. 2015. 'State-of-the-Art Methods for Evaluation of Angiogenesis and Tissue Vascularization: A Scientific Statement From the American Heart Association', *Circ Res*, 116: e99-132.

Simons, M., E. Gordon, and L. Claesson-Welsh. 2016. 'Mechanisms and regulation of endothelial VEGF receptor signaling', *Nat Rev Mol Cell Biol*, 17: 611-25.

Sin, W. C., Q. Aftab, J. F. Bechberger, J. H. Leung, H. Chen, and C. C. Naus. 2016. 'Astrocytes promote glioma invasion via the gap junction protein connexin43', *Oncogene*, 35: 1504-16.

Singh, S. K., C. Hawkins, I. D. Clarke, J. A. Squire, J. Bayani, T. Hide, R. M. Henkelman, M. D. Cusimano, and P. B. Dirks. 2004. 'Identification of human brain tumour initiating cells', *Nature*, 432: 396-401.

Smith, A. W., M. P. Mehta, and A. G. Wernicke. 2016. 'Neural stem cells, the subventricular zone and radiotherapy: implications for treating glioblastoma', *J Neurooncol*, 128: 207-16.

Soda, Y., T. Marumoto, D. Friedmann-Morvinski, M. Soda, F. Liu, H. Michiue, S. Pastorino, M. Yang, R. M. Hoffman, S. Kesari, and I. M. Verma. 2011. 'Transdifferentiation of glioblastoma cells into vascular endothelial cells', *Proc Natl Acad Sci U S A*, 108: 4274-80.

Soda, Y., C. Myskiw, A. Rommel, and I. M. Verma. 2013. 'Mechanisms of neovascularization and resistance to anti-angiogenic therapies in glioblastoma multiforme', *J Mol Med (Berl)*, 91: 439-48.

Sormendi, S., and B. Wielockx. 2018. 'Hypoxia Pathway Proteins As Central Mediators of Metabolism in the Tumor Cells and Their Microenvironment', *Front Immunol*, 9: 40.

Stanzani, E., F. Martinez-Soler, T. M. Mateos, N. Vidal, A. Villanueva, M. A. Pujana, J. Serra-Musach, N. de la Iglesia, P. Gimenez-Bonafe, and A. Tortosa. 2017. 'Radioresistance of mesenchymal glioblastoma initiating cells correlates with patient outcome and is associated with activation of inflammatory program', *Oncotarget*, 8: 73640-53.

Sun, H., D. Guo, Y. Su, D. Yu, Q. Wang, T. Wang, Q. Zhou, X. Ran, and Z. Zou. 2014. 'Hyperplasia of pericytes is one of the main characteristics of microvascular architecture in malignant glioma', *PLoS One*, 9: e114246.

Sundaravel, S., R. Duggan, T. Bhagat, D. L. Ebenezer, H. Liu, Y. Yu, M. Bartenstein, M. Unnikrishnan, S. Karmakar, T. C. Liu, I. Torregroza, T. Quenon, J. Anastasi, K. L. McGraw, A. Pellagatti, J. Boultwood, V. Yajnik, A. Artz, M. M. Le Beau, U. Steidl, A. F. List, T. Evans, A. Verma, and A. Wickrema. 2015. 'Reduced DOCK4 expression leads to erythroid dysplasia in myelodysplastic syndromes', *Proc Natl Acad Sci U S A*, 112: E6359-68.

Sundberg, C., J. A. Nagy, L. F. Brown, D. Feng, I. A. Eckelhoefer, E. J. Manseau, A. M. Dvorak, and H. F. Dvorak. 2001. 'Glomeruloid microvascular proliferation follows adenoviral vascular permeability factor/vascular endothelial growth factor-164 gene delivery', *Am J Pathol*, 158: 1145-60.

Suzuki, S., J. Namiki, S. Shibata, Y. Mastuzaki, and H. Okano. 2010. 'The neural stem/progenitor cell marker nestin is expressed in proliferative endothelial cells, but not in mature vasculature', *J Histochem Cytochem*, 58: 721-30.

Szatmari, T., K. Lumniczky, S. Desaknai, S. Trajcevski, E. J. Hidvegi, H. Hamada, and G. Safrany. 2006. 'Detailed characterization of the mouse glioma 261 tumor model for experimental glioblastoma therapy', *Cancer Sci*, 97: 546-53.

Tabatabaei, P., E. Visse, P. Bergstrom, T. Brannstrom, P. Siesjo, and A. T. Bergenheim. 2017. 'Radiotherapy induces an immediate inflammatory reaction in malignant glioma: a clinical microdialysis study', *J Neurooncol*, 131: 83-92.

Tajiri, H., T. Uruno, T. Shirai, D. Takaya, S. Matsunaga, D. Setoyama, M. Watanabe, M. Kukimoto-Niino, K. Oisaki, M. Ushijima, F. Sanematsu, T. Honma, T. Terada, E. Oki, S. Shirasawa, Y. Maehara, D. Kang, J. F. Cote, S. Yokoyama, M. Kanai, and Y. Fukui. 2017. 'Targeting Ras-Driven Cancer Cell Survival and Invasion through Selective Inhibition of DOCK1', *Cell Rep*, 19: 969-80.

Takeuchi, H., N. Hashimoto, R. Kitai, T. Kubota, and K. Kikuta. 2010. 'Proliferation of vascular smooth muscle cells in glioblastoma multiforme', *J Neurosurg*, 113: 218-24.

Tan, W., T. R. Palmby, J. Gavard, P. Amornphimoltham, Y. Zheng, and J. S. Gutkind. 2008. 'An essential role for Rac1 in endothelial cell function and vascular development', *FASEB J*, 22: 1829-38.

Thon, N., S. Kreth, and F. W. Kreth. 2013. 'Personalized treatment strategies in glioblastoma: MGMT promoter methylation status', *Onco Targets Ther*, 6: 1363-72.

Tsai, J. H., S. Makonnen, M. Feldman, C. M. Sehgal, A. Maity, and W. M. Lee. 2005. 'Ionizing radiation inhibits tumor neovascularization by inducing ineffective angiogenesis', *Cancer Biol Ther*, 4: 1395-400.

Tsigelny, I. F., V. L. Kouznetsova, N. Lian, and S. Kesari. 2016. 'Molecular mechanisms of OLIG2 transcription factor in brain cancer', *Oncotarget*, 7: 53074-101.

Tsukamoto, H., K. Shibata, H. Kajiyama, M. Terauchi, A. Nawa, and F. Kikkawa. 2007. 'Irradiation-induced epithelial-mesenchymal transition (EMT) related to invasive potential in endometrial carcinoma cells', *Gynecol Oncol*, 107: 500-4.

Ueda, S., S. Fujimoto, K. Hiramoto, M. Negishi, and H. Katoh. 2008. 'Dock4 regulates dendritic development in hippocampal neurons', *J Neurosci Res*, 86: 3052-61.

Upadhyay, G., W. Goessling, T. E. North, R. Xavier, L. I. Zon, and V. Yajnik. 2008. 'Molecular association between beta-catenin degradation complex and Rac guanine exchange factor DOCK4 is essential for Wnt/beta-catenin signaling', *Oncogene*, 27: 5845-55.

Verhaak, R. G., K. A. Hoadley, E. Purdom, V. Wang, Y. Qi, M. D. Wilkerson, C. R. Miller, L. Ding, T. Golub, J. P. Mesirov, G. Alexe, M. Lawrence, M. O'Kelly, P. Tamayo, B. A. Weir, S. Gabriel, W. Winckler, S. Gupta, L. Jakkula, H. S. Feiler, J. G. Hodgson, C. D. James, J. N. Sarkaria, C. Brennan, A. Kahn, P. T. Spellman, R. K. Wilson, T. P. Speed, J. W. Gray, M. Meyerson, G. Getz, C. M. Perou, D. N. Hayes, and Network Cancer Genome Atlas Research. 2010. 'Integrated genomic analysis identifies clinically relevant subtypes of glioblastoma characterized by abnormalities in PDGFRA, IDH1, EGFR, and NF1', *Cancer Cell*, 17: 98-110.

Viallard, C., and B. Larrivee. 2017. 'Tumor angiogenesis and vascular normalization: alternative therapeutic targets', *Angiogenesis*, 20: 409-26.

Wacker, A., and H. Gerhardt. 2011. 'Endothelial development taking shape', *Curr Opin Cell Biol*, 23: 676-85.

Walker, A. J., J. Ruzevick, A. A. Malayeri, D. Rigamonti, M. Lim, K. J. Redmond, and L. Kleinberg. 2014. 'Postradiation imaging changes in the CNS: how can we differentiate between treatment effect and disease progression?', *Future Oncol*, 10: 1277-97.

Walters, M. J., K. Ebsworth, R. D. Berahovich, M. E. Penfold, S. C. Liu, R. Al Omran, M. Kioi, S. B. Chernikova, D. Tseng, E. E. Mulkearns-Hubert, M. Sinyuk, R. M. Ransohoff, J. D. Lathia, J. Karamchandani, H. E. Kohrt, P. Zhang, J. P. Powers, J. C. Jaen, T. J. Schall, M. Merchant, L. Recht, and J. M. Brown. 2014. 'Inhibition of CXCR7 extends survival following irradiation of brain tumours in mice and rats', *Br J Cancer*, 110: 1179-88.

Wang, J., E. Cazzato, E. Ladewig, V. Frattini, D. I. Rosenbloom, S. Zairis, F. Abate, Z. Liu, O. Elliott, Y. J. Shin, J. K. Lee, I. H. Lee, W. Y. Park, M. Eoli, A. J. Blumberg, A. Lasorella, D. H. Nam, G. Finocchiaro, A. Iavarone, and R. Rabadan. 2016. 'Clonal evolution of glioblastoma under therapy', *Nat Genet*, 48: 768-76.

Wang, L., L. Zhang, W. Shen, Y. Liu, and Y. Luo. 2016. 'High expression of VEGF and PI3K in glioma stem cells provides new criteria for the grading of gliomas', *Exp Ther Med*, 11: 571-76.

Wang, Q., Z. He, M. Huang, T. Liu, Y. Wang, H. Xu, H. Duan, P. Ma, L. Zhang, S. S. Zamvil, J. Hidalgo, Z. Zhang, D. M. O'Rourke, N. Dahmane, S. Brem, Y. Mou, Y. Gong, and Y. Fan. 2018. 'Vascular niche IL-6 induces alternative macrophage activation in glioblastoma through HIF-2alpha', *Nat Commun*, 9: 559.

Wang, R., K. Chadalavada, J. Wilshire, U. Kowalik, K. E. Hovinga, A. Geber, B. Fligelman, M. Leversha, C. Brennan, and V. Tabar. 2010. 'Glioblastoma stem-like cells give rise to tumour endothelium', *Nature*, 468: 829-33.

Wang, S. Y., Y. Q. Ke, G. H. Lu, Z. H. Song, L. Yu, S. Xiao, X. L. Sun, X. D. Jiang, Z. L. Yang, and C. C. Hu. 2013. 'Vasculogenic mimicry is a prognostic factor for postoperative survival in patients with glioblastoma', *J Neurooncol*, 112: 339-45.

Watkins, S., S. Robel, I. F. Kimbrough, S. M. Robert, G. Ellis-Davies, and H. Sontheimer. 2014. 'Disruption of astrocyte-vascular coupling and the blood-brain barrier by invading glioma cells', *Nat Commun*, 5: 4196.

Westbrook, J. A., S. L. Wood, D. A. Cairns, K. McMahon, R. Gahlaut, H. Thygesen, M. Shires, S. Roberts, H. Marshall, M. R. Oliva, M. J. Dunning, A. M. Hanby, P. J. Selby, V. Speirs, G. Mavria, R. E. Coleman, and J. E. Brown. 2018. 'Identification and validation of DOCK4 as a potential biomarker for risk of bone metastasis development in patients with early breast cancer', *J Pathol*.

Wick, W., T. Gorlia, M. Bendszus, M. Taphoorn, F. Sahm, I. Harting, A. A. Brandes, W. Taal, J. Domont, A. Idbaih, M. Campone, P. M. Clement, R. Stupp, M. Fabbro, E. Le Rhun, F. Dubois, M. Weller, A. von Deimling, V. Golfinopoulos, J. C. Bromberg, M. Platten, M. Klein, and M. J. van den Bent. 2017. 'Lomustine and Bevacizumab in Progressive Glioblastoma', *N Engl J Med*, 377: 1954-63.

Wild-Bode, C., M. Weller, A. Rimner, J. Dichgans, and W. Wick. 2001. 'Sublethal irradiation promotes migration and invasiveness of glioma cells: implications for radiotherapy of human glioblastoma', *Cancer Res*, 61: 2744-50.

Winkler, F., Y. Kienast, M. Fuhrmann, L. Von Baumgarten, S. Burgold, G. Mitteregger, H. Kretzschmar, and J. Herms. 2009. 'Imaging glioma cell invasion in vivo reveals mechanisms of dissemination and peritumoral angiogenesis', *Glia*, 57: 1306-15.

Wykoff, C. C., N. J. Beasley, P. H. Watson, K. J. Turner, J. Pastorek, A. Sibtain, G. D. Wilson, H. Turley, K. L. Talks, P. H. Maxwell, C. W. Pugh, P. J. Ratcliffe, and A. L. Harris. 2000. 'Hypoxia-inducible expression of tumor-associated carbonic anhydrases', *Cancer Res*, 60: 7075-83.

Xiao, Y., Y. Peng, J. Wan, G. Tang, Y. Chen, J. Tang, W. C. Ye, N. Y. Ip, and L. Shi. 2013. 'The atypical guanine nucleotide exchange factor Dock4 regulates neurite differentiation through modulation of Rac1 GTPase and actin dynamics', *J Biol Chem*, 288: 20034-45.

Xie, Y., T. Bergstrom, Y. Jiang, P. Johansson, V. D. Marinescu, N. Lindberg, A. Segerman, G. Wicher, M. Niklasson, S. Baskaran, S. Sreedharan, I. Everlien, M. Kastemar, A. Hermansson, L. Elfineh, S. Libard, E. C. Holland, G. Hesselager, I. Alafuzoff, B. Westermark, S. Nelander, K. Forsberg-Nilsson, and L. Uhrbom. 2015. 'The Human Glioblastoma Cell Culture Resource: Validated Cell Models Representing All Molecular Subtypes', *EBioMedicine*, 2: 1351-63.

Xiong, B., A. Li, Y. Lou, S. Chen, B. Long, J. Peng, Z. Yang, T. Xu, X. Yang, X. Li, T. Jiang, Q. Luo, and H. Gong. 2017. 'Precise Cerebral Vascular Atlas in Stereotaxic Coordinates of Whole Mouse Brain', *Front Neuroanat*, 11: 128.

Xu, C., X. Wu, and J. Zhu. 2013. 'VEGF promotes proliferation of human glioblastoma multiforme stem-like cells through VEGF receptor 2', *ScientificWorldJournal*, 2013: 417413.

Xu, Y., I. Stamenkovic, and Q. Yu. 2010. 'CD44 attenuates activation of the hippo signaling pathway and is a prime therapeutic target for glioblastoma', *Cancer Res*, 70: 2455-64.

Xue, X. J., and X. B. Yuan. 2010. 'Nestin is essential for mitogen-stimulated proliferation of neural progenitor cells', *Mol Cell Neurosci*, 45: 26-36.

Yadav, V. N., D. Zamler, G. J. Baker, P. Kadiyala, A. Erdreich-Epstein, A. C. DeCarvalho, T. Mikkelsen, M. G. Castro, and P. R. Lowenstein. 2016. 'CXCR4 increases in-vivo glioma perivascular invasion, and reduces radiation induced apoptosis: A genetic knockdown study', *Oncotarget*, 7: 83701-19.

Yajnik, V., C. Paulding, R. Sordella, A. I. McClatchey, M. Saito, D. C. Wahrer, P. Reynolds, D. W. Bell, R. Lake, S. van den Heuvel, J. Settleman, and D. A. Haber. 2003. 'DOCK4, a GTPase activator, is disrupted during tumorigenesis', *Cell*, 112: 673-84.

Yan, G. N., L. Yang, Y. F. Lv, Y. Shi, L. L. Shen, X. H. Yao, Q. N. Guo, P. Zhang, Y. H. Cui, X. Zhang, X. W. Bian, and D. Y. Guo. 2014. 'Endothelial cells promote stem-like phenotype of glioma cells through activating the Hedgehog pathway', *J Pathol*, 234: 11-22.

Yan, S., P. Li, Y. Wang, W. Yu, A. Qin, M. Liu, A. P. Xiang, W. Zhang, and W. Li. 2016. 'Nestin regulates neural stem cell migration via controlling the cell contractility', *Int J Biochem Cell Biol*, 78: 349-60.

Yang, H., D. Ye, K. L. Guan, and Y. Xiong. 2012. 'IDH1 and IDH2 mutations in tumorigenesis: mechanistic insights and clinical perspectives', *Clin Cancer Res*, 18: 5562-71.

Yi, L., H. Xiao, M. Xu, X. Ye, J. Hu, F. Li, M. Li, C. Luo, S. Yu, X. Bian, and H. Feng. 2011. 'Glioma-initiating cells: a predominant role in microglia/macrophages tropism to glioma', *J Neuroimmunol*, 232: 75-82.

Yi, Y., I. Y. Hsieh, X. Huang, J. Li, and W. Zhao. 2016. 'Glioblastoma Stem-Like Cells: Characteristics, Microenvironment, and Therapy', *Front Pharmacol*, 7: 477.

Yu, J. R., Y. Tai, Y. Jin, M. C. Hammell, J. E. Wilkinson, J. S. Roe, C. R. Vakoc, and L. Van Aelst. 2015. 'TGF-beta/Smad signaling through DOCK4 facilitates lung adenocarcinoma metastasis', *Genes Dev*, 29: 250-61.

Zawaski, J. A., M. W. Gaber, O. M. Sabek, C. M. Wilson, C. D. Duntsch, and T. E. Merchant. 2012. 'Effects of irradiation on brain vasculature using an in situ tumor model', *Int J Radiat Oncol Biol Phys*, 82: 1075-82.

Zbinden, M., A. Duquet, A. Lorente-Trigos, S. N. Ngwabyt, I. Borges, and A. Ruiz i Altaba. 2010. 'NANOG regulates glioma stem cells and is essential in vivo acting in a cross-functional network with GLI1 and p53', *EMBO J*, 29: 2659-74.

Zhang, M., T. Song, L. Yang, R. Chen, L. Wu, Z. Yang, and J. Fang. 2008. 'Nestin and CD133: valuable stem cell-specific markers for determining clinical outcome of glioma patients', *J Exp Clin Cancer Res*, 27: 85.

Zhang, Y., F. Chen, G. Tai, J. Wang, J. Shang, B. Zhang, P. Wang, B. Huang, J. Du, J. Yu, H. Zhang, and F. Liu. 2017. 'TIGAR knockdown radiosensitizes TrxR1-overexpressing glioma in vitro and in vivo via inhibiting Trx1 nuclear transport', *Sci Rep*, 7: 42928.

Zhou, W., C. Chen, Y. Shi, Q. Wu, R. C. Gimple, X. Fang, Z. Huang, K. Zhai, S. Q. Ke, Y. F. Ping, H. Feng, J. N. Rich, J. S. Yu, S. Bao, and X. W. Bian. 2017. 'Targeting Glioma Stem Cell-Derived Pericytes Disrupts the Blood-Tumor Barrier and Improves Chemotherapeutic Efficacy', *Cell Stem Cell*, 21: 591-603 e4.

Zinn, P. O., R. R. Colen, E. M. Kasper, and J. K. Burkhardt. 2013. 'Extent of resection and radiotherapy in GBM: A 1973 to 2007 surveillance, epidemiology and end results analysis of 21,783 patients', *Int J Oncol*, 42: 929-34.